



THE UNIVERSITY *of* EDINBURGH

This thesis has been submitted in fulfilment of the requirements for a postgraduate degree (e.g. PhD, MPhil, DClinPsychol) at the University of Edinburgh. Please note the following terms and conditions of use:

- This work is protected by copyright and other intellectual property rights, which are retained by the thesis author, unless otherwise stated.
- A copy can be downloaded for personal non-commercial research or study, without prior permission or charge.
- This thesis cannot be reproduced or quoted extensively from without first obtaining permission in writing from the author.
- The content must not be changed in any way or sold commercially in any format or medium without the formal permission of the author.
- When referring to this work, full bibliographic details including the author, title, awarding institution and date of the thesis must be given.

**Removal mechanisms of organic and
inorganic solutes in raw, upland
drinking water by nanofiltration:
Influence of solute-solute and
solute-membrane interactions**

Annalisa De Munari

A thesis submitted for the degree of Doctor of Philosophy

The University of Edinburgh

School of Engineering

2012



For Serge

Declaration

I declare that the thesis has been composed by myself and the work contained in it is my own, except where stated otherwise. Further, this work has not been submitted for any other degree or professional qualification except as specified.

Abstract

Nanofiltration (NF) membranes have been applied successfully for the removal of inorganic and organic pollutants, including micropollutants, from drinking water for the past two decades. However, a complete and quantitative understanding of NF removal mechanisms has yet to be achieved. Quantifying the factors governing solute transport and retention by NF is necessary in order to achieve higher treatment efficiency at a lower cost.

The aim of this research was to contribute to the current state of the knowledge of the mechanisms of solute retention and transport by NF membranes. The focus was on evaluating the contribution of solute-solute interactions and solute-membrane interactions on solute removal and transport mechanisms. To the knowledge of the author, at the start of this research there was a lack of understanding of the simultaneous impacts of both interactions on the performance of NF membranes, which renders this research novel.

To highlight challenges faced by modern membrane plants and identify inorganic and organic pollutants of interest, a study of water quality in Scotland was carried out. Experiments were performed in dead-end stirred cells using two commercial NF membranes, TFC-SR2 and TFC-SR3 provided by Koch, which were extensively characterized. Radiolabeled Endosulfan (ES, 10 $\mu\text{g/L}$), manganese (5-1,500 mg/L) and Humic Acids (HA, 5-250 mgC/L) were spiked in synthetic water with background electrolyte (1 mM NaHCO_3 and 20 mM NaCl). Calcium (Ca, 2.5 mM) was employed in fouling experiments.

The influence of the complexation of solutes with HA on solute retention by NF was for the first time quantified for the solute concentrations employed in this study. It was found that manganese retention was influenced by membrane pore size and charge (solute-membrane interactions) and solute speciation (solute-solute interactions). Complexation of manganese and HA (solute-solute interactions) occurred at alkaline conditions but did not enhance manganese retention. At high pH

manganese precipitated as solid MnCO_3 and these precipitates achieved high retention (99%), even without the presence of HA.

ES retention by NF membrane was controlled by size exclusion (solute-membrane interactions). For the tighter TFC-SR3, whose pore size are smaller than the size of ES, ES retention increased in the presence of HA, while for the looser TFC-SR2, whose pores are bigger than ES diameter, ES retention decreased in the presence of HA. For TFC-SR3 increase of ES retention in the presence of HA was due to size exclusion (solute-membrane interactions) and formation of ES-HA complexes (solute-solute interactions). For TFC-SR2 HA-membrane interactions were dominant with respect to solute-solute interactions, increasing membrane molecular weight cut-off (MWCO) and in turn passage of ES.

The influence of pressure (5-15 bar) on ES retention in the presence of HA was systematically investigated. Results showed that ES transport through TFC-SR2 and TFC-SR3 was dominated by convection. For the tighter TFC-SR3 lower permeate flux was responsible for the increase of retention with pressure, while for the looser TFC-SR2 higher permeate flux increased concentration polarisation, decreasing retention with pressure. The presence of HA lowered the permeate flux, resulting in a less pronounced variation of retention with pressure for TFC-SR2 and in constant retention for TFC-SR3.

The impact of manganese scaling on the performance of NF membranes was investigated at neutral pH. The effects of inorganic precipitates on flux and solute retention by NF have been so far scarcely studied and the impact of inorganic scaling on micropollutant retention by NF is unknown. Findings from this research indicated that manganese deposits did not foul the membranes but on the contrary enhanced their flux and prevented fouling by HA and Ca. The retention of ES, manganese and HA by membranes through which manganese was previously filtered was found to decrease with respect to solute retention by virgin membranes. Manganese filtration was shown to increase membrane MWCO and hydrophilicity. It was proposed that manganese-membrane interactions caused swelling of the membrane active layer by

increasing the membrane free volume. The findings of this research indicated the importance of investigating simultaneously the impacts of solute-solute interactions and solute-membrane interactions to understand and explain transport and removal mechanisms of organic and inorganic contaminants by NF.

Acknowledgements

This thesis would not have been possible without the vision and the financial sponsorship of the late Drinking Water Quality Regulator of Scotland, Colin McLaren. Colin offered me the opportunity to work in his team for two months and to participate to a conference in Malawi, wonderful experiences that greatly contributed to my personal and professional growth.

Professor Andrea Schäfer is thanked for giving me the opportunity to undertake this PhD, for providing financial support for this work and for feedback and comments on the papers submitted. Dr. Blanca Antizar-Ladislao is thanked for her support in the final part of this work and for her useful and timely comments on the thesis. Blanca, thank you for jeopardising your Easter holidays to allow me to submit. Professor Jose Torero is very much thanked for the support, advice and help he provided during the PhD, especially in the final and most stressful part. Jose, you are a fantastic educator and mentor and I learnt tremendously from you. You shaped my character and my way of thinking, greatly contributing to the person I am now.

Matthew Bower (DWQR) is thanked for all his support and help throughout this work. Thank you for being a fantastic industrial sponsor and juggling amazingly well among crazy academics!

Prof. Asif Usmani, Prof David Ingram and Prof. Alan Murray are thanked for their crucial support and advice.

My deepest gratitude goes to the past and present fellow students that shared the joys and burdens of the PhD life. Dr. Andrea Semiao is thanked for assistance with the TOC instrument, especially when it did not work at 10 pm, for help with thesis and paper proof reading and for all the interesting and stimulating scientific discussions we had. Ime Akanayeti is thanked for thesis proof reading, help in the lab and for giving me a home in the last stretch of my PhD. Dr. Helfrid Rossiter is thanked for assistance with the ICP-OES and for explaining me the most obscure concepts of

chemistry. Dr. Peta Neale is thanked for useful discussion on the SPME method and paper proof-reading. Dr. Laura Banasiak is thanked for the information about Endosulfan. Dr. Laura Richards is thanked for paper proof reading and for allowing me to stay in her desk at Heriot-Watt University. Helen Cope is thanked for thesis proof reading and for her hilarious stories. Molly Patrick is thanked for being a fun flatmate and good friend. Raquel Garcia is thanked for her help, without you and Ioan I would have never been able to finish experiments and at the same time move house. Morgan Letellier, Dr. Gavin Park and Dalila Capão are thanked for valuable help with the work at Heriot-Watt University. Thank you all for being there and making my PhD experience special.

Colette Kellie, David Grzybowski, Philip Anderson and Victoria MacDougall (DWQR) are thanked for welcoming me in their team. It has been a pleasure and an honour to work with you all. Colette Kellie is specially thanked for being a great travel companion in Malawi and for constant support during and after the PhD. Aaron Mapsere (Ministry of Water Development, Malawi) is thanked for his hospitality in Malawi and organising the visit to the water treatment plant.

Several people contributed to the work presented in this thesis. Flamina Gallo is specially thanked for carrying out the experiments in Chapter 9 and for membrane analysis at ITM-CNR, Italy. Flaminia, it has been great fun working with you, you really brought much needed sunshine from the south of Italy, other than amazing food. BEng students John Knight, Kristin Mcgaff and MEng students Nick Gardener and Rachel Wood are thanked for visiting the membrane plants, collecting the data and providing the photos used in Appendix 1, it has been fun supervising you all. Some of the data in Appendix 1 were submitted, albeit in different formats, in their final year dissertations. Prof Bryce Richard is thanked for enabling the work carried out at Heriot-Watt University (Appendix 4). The system design, construction, experimental design and data collection for the Australian experiments described in Appendix 4 were performed by Prof. Andrea Schäfer, Prof. Bryce Richards and students Andrea Broeckmann, Kai Ratte, Thomas Kruttschnitt and Philip Sausele, while Dalila Capão (Heriot-Watt University) helped with data analysis. The design

of the wind turbine simulator and of the wind experiments carried out in Appendix 4 was performed by Dr. Gavin Park (Heriot-Watt University). David Grzybowski (DWQR) provided Figure 3-4 in Chapter 3. The design of the stirred cells used in this thesis was performed by Prof. Andrea Schäfer and Dr. Peta Neale. Ime Akanayeti performed the AFM measurements of the membranes presented in Section A.2.6. Dr. Silvia Simone (ITM-CNR, Italy) performed contact angle and SEM analysis and Dr. Gianluca di Profio (ITM-CNR, Italy) carried out ATR-FTIR analysis on the fouled membranes reported in Appendix 3.

Steve Gourlay, Pamela Beattie, Dr. Lorna Eades, Bobby Hog, Bill Leaslie, Derek Jardine, Douglas Carmichael, Dr. Peter Anderson and Dr. Alan Simm are thanked for their valuable support in the laboratory. Ronald Miller, Curtis Abbott and Cameron Smith are thanked for their support during the work at Heriot-Watt University. Kathy Moore is thanked for her efficiency in making everything run smoothly from the backstage.

Several people at Scottish Water enabled the outcomes of this thesis. Richard Allen, George Ponton, Catrina Attwood, Peter Jones and Simon West are thanked for support and data provision. Richard MacLennan, Alan Taylor and Allan Lain are thanked for assistance during site visits of membrane plants. Chris Stewart and Ross Fleming are thanked for facilitating the water collection and the operators of the plant are thanked for precious help in collecting the raw water.

I had several valuable discussions with various people throughout my PhD. Dr Alberto Figoli and Dr Gianluca Di Profio (ITM-CNR, Italy) are thanked for useful discussion and scientific input on Chapter 9. Prof. Meny Elimelech (Yale University), Dr. Slava Freger (Ben Gurion University) and Professor Maria Norberta de Pinho (Instituto Superior Tecnico, Lisboa) are thanked for useful scientific discussions. Dr Richard Baker (Membrane Technology and Research Inc., USA) is thanked for the interesting talk we had in front of my poster at ICOM 2011. David Welch and Dr. Nic Booker (MottMcDonald) are thanked for useful information on Scottish membrane plants. Peter Moss and Martin Howard (Koch Membrane

System) are thanked for information on membranes and for organising a membrane plant visit in Norway. Ian Sadler, Alan Merry and Geoff Balko (PCI membranes) are thanked for information on PCI membranes used in Scottish plants. Professor Alexander Bismarck, Dr. Kingsley Ho, and Koonyang Lee (Imperial College, UK) are thanked for assistance with zeta potential and contact angle measurements and useful discussions on result interpretation. Dr. Arno Kraft (Heriot-Watt University) is thanked for scientific input on the design of the diffusion cells. A special thank goes to all participants and organisers of the NanoMemCourse at the University of Twente, where I met very bright researchers and I really felt part of a creative scientific community.

My PhD scholarship was funded by the DWQR of Scotland and the School of Engineering at the University of Edinburgh. Koch Membrane System is thanked for donating the membrane coupons and membrane modules used in the experiments. The Moray Endowment Fund (The University of Edinburgh) and George Ponton (Scottish Water) are thanked for providing funding for the laboratory experiments carried out in Appendix 4. GE Global Research is thanked for contributing financially to project material and donating the UF membranes used in the experiments in Appendix 4.

Finally, I would like to deeply thank my family. Mamma and papà, thank you for your unconditioned love and for supporting all my decisions. Your belief that I can achieve anything I want in life if I work hard pushed me to never been afraid of new challenges. Silvia, thank you for your Skype calls with Giosuè, his happiness, joy and laughters made many of my days.

Serge, this thesis is dedicated to you. This work would have not been possible without your constant support, understanding and love. Thank you for encouraging my decision of quitting my job and starting this adventure, even if this meant putting our life on hold for many years. Thank you for commuting Edinburgh-London on a weekly basis. Your drive, ambition and strength inspire me everyday. I am looking forward to starting a new chapter of our life together.

List of Publications

De Munari A, Capão DPS, Richards BS, Schäfer AI. Application of solar-powered desalination in a remote town in South Australia. *Desalination* 2009; 248: 72-82.

De Munari A, Schäfer AI. Impact of speciation on removal of manganese and organic matter by nanofiltration. *Journal of water supply: Research and Technology—AQUA* 2010; 59: 152-163.

De Munari A, Schäfer AI. Membrane plants for drinking water provision in remote Scottish communities: performance, costs and lessons learnt *Proceedings of "Membrane in Drinking and Industrial Water Conference", Trondheim, Norway, 2010.*

De Munari A, Bower M, McLaren C, Knight J, Schäfer AI. Water supply for remote communities using membrane technology: is it feasible in Africa? *Proceedings of "2nd All Africa Environmental Health Congress ", Lilongwe, Malawi, 2010.*

Table of Contents

Abstract	ii
Acknowledgements	v
List of Publications	ix
List of Figures	xvii
List of Tables	xxv
Abbreviations and symbols	xxviii
1. Introduction.....	1
1.1 Mechanisms of solute retention in nanofiltration.....	2
1.2 Aim and objectives of the thesis	3
1.3 Structure of the thesis.....	3
2. Literature Review.....	5
2.1 Introduction.....	5
2.2 Removal and transport of solutes by nanofiltration.....	6
2.2.1 <i>Nanofiltration principles</i>	6
2.2.2 <i>Retention mechanisms</i>	9
2.2.3 <i>Transport mechanisms</i>	13
2.2.4 <i>Fouling and scaling</i>	15
2.2.5 <i>Influence of operating conditions</i>	17
2.3 Solute-membrane and solute-solute interactions.....	19
2.3.1 <i>Solute-membrane interactions</i>	19
2.3.2 <i>Solute-solute interactions</i>	21
2.4 Conclusions	23

3. Contaminants of interest.....	25
3.1 Introduction.....	25
3.2 Water quality and treatment in Scotland.....	25
3.3 Membrane plants in Scotland	28
3.4 Occurrence and removal of organic and inorganic contaminants ..	31
3.4.1 Humic acids.....	33
3.4.2 Manganese.....	36
3.4.3 Endosulfan	40
3.5 Conclusions	43
4. Materials and Methods	45
4.1 Introduction.....	45
4.2 Chemicals and background solutions	45
4.3 Analytical Equipment	47
4.3.1 pH and conductivity meters	47
4.3.2 Inductively-coupled plasma optical emission spectroscopy....	47
4.3.3 Total organic carbon analyser	48
4.3.4 UV-visible spectrophotometer	48
4.3.5 Liquid scintillation counter	49
4.3.6 Contact angle measurement	50
4.3.7 Zeta potential measurement.....	51
4.3.8 Atomic force microscopy	53
4.3.9 Scanning electron microscopy.....	53
4.3.10 Infrared spectroscopy	55
4.4 Experimental equipment and protocol	55

4.4.1	<i>Stirred cells</i>	55
4.4.2	<i>Diffusion cells</i>	58
4.5	Speciation modelling.....	60
4.5.1	<i>Manganese speciation</i>	61
4.5.2	<i>Manganese and humic acids complexation</i>	62
4.6	Solid-phase micro-extraction	63
4.6.1	<i>Fibre calibration and determination of K_{fW}</i>	64
4.6.2	<i>Determination of K_{HA}</i>	65
4.7	Membrane characteristics.....	67
4.8	Quality assurance and quality control	68
5.	Transport models	72
5.1	Film theory.....	72
5.2	Hydrodynamic Model.....	74
5.3	Limitations of the Hydrodynamic Model	77
5.4	Sieving coefficients.....	78
6.	Manganese and humic acid removal mechanism	80
6.1	Introduction.....	80
6.2	Filtration protocol	82
6.3	Manganese and humic acids speciation	82
6.3.1	<i>Manganese speciation</i>	82
6.3.2	<i>Manganese and humic acids complexation</i>	85
6.4	Membrane flux.....	87
6.5	Manganese and humic acid retention	88
6.6	Mass deposited on the membranes.....	92

6.7	Manganese and humic acid retention in real Scottish water.....	93
6.8	Conclusions	95
7.	Endosulfan and humic acid removal mechanisms.....	97
7.1	Introduction.....	97
7.2	Filtration protocol	101
7.3	Formation of ES-HA complexes	102
7.3.1	<i>Fibre calibration and determination of K_{TW}.....</i>	<i>103</i>
7.3.2	<i>Determination of K_{HA} and percentage of ES bound to HA</i>	<i>106</i>
7.4	Influence of pH on ES retention.....	108
7.5	Influence of HA on ES retention	111
7.6	Estimation of ES removal in the presence of HA	114
7.7	Mechanisms of ES removal in the presence of HA.....	116
7.8	Conclusions	120
8.	Effects of pressure on solute retention	122
8.1	Introduction.....	122
8.2	Filtration protocol	126
8.3	Influence of transmembrane pressure on Mn removal.....	126
8.4	Influence of transmembrane pressure on ES removal.....	128
8.5	ES diffusion through NF membranes.....	132
8.6	Transport of ES through NF membranes.....	136
8.7	Transport of ES through NF membranes in the presence of HA .	143
8.8	Conclusions	145
9.	Effect of manganese scaling on NF performance.....	148
9.1	Introduction.....	148

9.2	Filtration protocol	150
9.3	Effect of manganese on membrane fouling	152
9.3.1	<i>Effect of manganese concentration and pressure</i>	<i>152</i>
9.3.2	<i>Comparison with fouling by other solutes</i>	<i>154</i>
9.4	Solute retention during manganese filtration	157
9.4.1	<i>Retention of manganese</i>	<i>157</i>
9.4.2	<i>Retention of sodium.....</i>	<i>159</i>
9.4.3	<i>Retention of humic acids</i>	<i>162</i>
9.5	Retention of pesticide Endosulfan	162
9.6	Effect of manganese deposits on membrane characteristics.....	166
9.6.1	<i>Visualization of deposits</i>	<i>166</i>
9.6.2	<i>Membrane chemical composition</i>	<i>168</i>
9.6.3	<i>Molecular weight cut-off.....</i>	<i>169</i>
9.6.4	<i>Contact angle</i>	<i>170</i>
9.6.5	<i>Surface charge</i>	<i>171</i>
9.7	Suggested mechanisms	173
9.8	Conclusions	174
10.	Conclusions and future work.....	175
10.1	Conclusions	175
10.2	Future work.....	178
	References.....	180
	Appendix 1 – Membrane plants in remote Scottish communities	213
A.1.1	Introduction	213
A.1.2	Case study A: small size plant on a Northern island	215

A.1.2.1 Plant Description	215
A.1.2.2 Operational parameters.....	216
A.1.2.3 Water quality	217
A.1.3 Case study B: micro-plant on a Western island	219
A.1.3.1 Plant Description	219
A.1.3.2 Operational parameters.....	220
A.1.3.3 Water quality	221
A.1.4 Energy requirements and costs	221
A.1.5 Conclusions	224
A.1.6 References.....	225
Appendix 2 – Membrane characterisation	227
A.2.1 Flux and Permeability.....	227
A.2.2 Molecular weight cut off	228
A.2.3 Pore size	229
A.2.4 Zeta potential	232
A.2.5 Contact angle.....	233
A.2.6 Roughness.....	234
A.2.7 Thickness.....	235
A.2.8 Functional groups	236
A.2.9 Salt retention.....	237
A.2.10 References.....	239
Appendix 3 – Characterisation of fouled membranes	240
A.3.1 SEM images.....	240
A.3.2 ATR-FTIR spectra.....	251

Appendix 4 – Solute removal using membranes powered by renewable energy	253
A.4.1 Introduction	253
A.4.2 Materials and methods	255
A.4.3 Experimental	258
<i>A.4.3.1 Australian field trial</i>	<i>258</i>
<i>A.4.3.2 Laboratory experiments.....</i>	<i>259</i>
A.4.4 Impact of real solar energy on conductivity removal	260
A.4.5 Impact of fluctuating energy on solute removal from real surface water	263
A.4.6 Conclusions	270
A.4.7 References.....	272

List of Figures

Figure 2-1 Application range of membrane processes compared with size of common contaminants and the contaminants used in this thesis (adapted from [19]).	6
Figure 2-2 Schematic of main factors affecting retention and transport mechanisms	10
Figure 3-1 Percentage of raw water samples that exceed their Prescribed Concentration Value, based on 300 samples collected at the inlet of water treatment works from 2006 to 2009 (Iron data available from 2008 and Aluminium data available for 2009 only)- Source: Drinking Water Quality Regulator of Scotland [184].	26
Figure 3-2 Number of samples collected at the outlet of water treatment works above their Prescribed Concentration Value, based on 400 samples collected from 2004 to 2006 Scottish-wide (Nitrite data available from 2005 only)- Source: Scottish Water [187].	27
Figure 3-3 (a) Number of membrane plants installed in Scotland from 1994 to 2010 (b) Cumulative frequency (%) versus capacity (m ³ /day) on logarithmic axis of Scottish membrane plants Source: Scottish Water [187].	29
Figure 3-4 Map of Scotland indicating remote rural areas (yellow areas) as categorised according to the Scottish Government 6-Fold Urban Classification [178] with location of membrane plants marked. Source: Drinking Water Quality Regulator of Scotland [184].	31
Figure 3-5 Proposed structure of HA. Adapted from [227].	33
Figure 3-6 Half life of α -ES and β -ES as a function of pH – from equations developed by [261].	42
Figure 4-1 TOC efficiency for HA.	48
Figure 4-2 Relationship between activity and ES concentration as a function of HA concentration.	50
Figure 4-3 Contact angle of nanofiltration membranes versus time	51
Figure 4-4 Stirred cell apparatus used for filtration experiments.....	56
Figure 4-5 Schematic of the stainless steel stirred cell used in this work. (not to scale)	57

Figure 4-6 Diffusion cells for pesticide ES diffusion experiments through NF membranes	58
Figure 4-7 Schematic of the diffusion cell used in this work. Not to scale.	58
Figure 4-8 Surface SEM images of (a) TFC-SR2 and (b) TFC-SR3 by SEM.....	67
Figure 5-1 Concentration polarisation according to the film theory (adapted from [19]).....	72
Figure 5-2 Sieving coefficients S_0 and S_a as a function of J_v according	79
Figure 6-1 Manganese speciation in absence of HA as logarithmic of the activity. Mn concentration: Mn concentration 5 mg/L, background electrolyte 1 mM NaHCO ₃ and 20 mM NaCl. Pressure: (a) 1.01 bar (b) 5 bar.....	83
Figure 6-2 Manganese speciation in absence of HA as percentage of total manganese concentration: Mn concentration 5 mg/L, background electrolyte 1 mM NaHCO ₃ and 20 mM NaCl, pressure 5 bar.	84
Figure 6-3 Manganese speciation in the presence of HA as logarithmic of the activity. Mn concentration: Mn concentration 5 mg/L, HA 5 mgC/L, background electrolyte 1 mM NaHCO ₃ and 20 mM NaCl. Pressure: (a) 1.01 bar (b) 5 bar.....	85
Figure 6-4 Manganese speciation in the presence of HA as percentage of total manganese concentration: Mn concentration 5 mg/L, HA 5 mgC/L, background electrolyte 1 mM NaHCO ₃ and 20 mM NaCl, pressure 5 bar.	86
Figure 6-5 (a) Ratio of pure water flux after (J) and before (J_0) experiments as a function of pH, (b) Permeability (J_v /pressure) of TFC-SR2 and TFC-SR3 as a function of pH. Mn concentration: 5 mg/L, HA concentration: 5 mgC/L, pressure: 5 bar, background electrolyte 1 mM NaHCO ₃ and 20 mM NaCl.....	88
Figure 6-6 Manganese and humic acid retention for (a) TFC-SR2 and (b) TFC-SR3 as a function of pH. Manganese concentration: 5 mg/L, HA concentration: 5 mgC/L, pressure: 5 bar, background electrolyte 1 mM NaHCO ₃ and 20 mM NaCl	90
Figure 6-7 Retention of aromatic fraction of HA for TFC-SR2 and TFC-SR3 as a function of pH. Manganese concentration: 5 mg/L, HA concentration: 5 mgC/L, pressure: 5 bar, background electrolyte 1 mM NaHCO ₃ and 20 mM NaCl	91
Figure 6-8 (a) Percentage of manganese deposit and (b) HA deposit on TFC-SR2 and TFC-SR3 as a function of pH. Manganese concentration: 5 mg/L, HA	

concentration: 5 mgC/L, pressure: 5 bar, background electrolyte 1 mM NaHCO ₃ and 20 mM NaCl.....	92
Figure 7-1 ES retention, feed and permeate concentration during ES filtration through (a) TFC-SR2 and (b) TFC-SR3, ES 10 µg/L, pressure: 5 bar, background electrolyte 1 mM NaHCO ₃ and 20 mM NaCl, pH 6. Values of the feed concentration that were not directly measured by sampling were calculated with a mass balance.	101
Figure 7-2 (a) Uptake of ES to PA* coated fibres as a function of time for pH 4 to 12 (b) ES concentration as function of time for pH 4 to 12 in the control samples, ES 10 µg/L, background electrolyte 1 mM NaHCO ₃ and 20 mM NaCl.	104
Figure 7-3 Mass of ES on the fibre for different ES concentrations and log K _{fw} values for ES as function of pH, background electrolyte 1 mM NaHCO ₃ and 20 mM NaCl.	105
Figure 7-4 (a) Uptake of ES by PA* fibre as a function of pH, HA 12.5 mgC/L (b) Humic Acid-water sorption isotherms for ES as a function of pH (c) uptake of ES by PA* fibre as a function of HA concentration (d) Humic Acid-water sorption isotherms for ES as a function of HA concentration, background electrolyte 1 mM NaHCO ₃ and 20 mM NaCl.....	107
Figure 7-5 (a) HA-water partition coefficient and fraction of ES bound to HA as a function of pH, HA 12.5 mgC/L and (b) as a function of HA concentration, ES 10 µg/L, background electrolyte 1 mM NaHCO ₃ and 20 mM NaCl.	108
Figure 7-6 Ratio of pure water flux after the experiments J and initial pure water flux J ₀ (dark symbols) and ratio of permeate flux J _v and initial pure water flux J ₀ (open symbols) for filtration of ES only and ES and HA as a function of pH for (a) TFC-SR2 (b) TFC-SR3. ES 10 µg/L, HA 12.5 mgC/L, pressure: 5 bar, background electrolyte 1 mM NaHCO ₃ and 20 mM NaCl (error bars not shown for clarity)	109
Figure 7-7 ES adsorption to the membranes with and without HA as a function of pH. ES 10 µg/L, HA 12.5 mgC/L, pressure: 5 bar, background electrolyte 1 mM NaHCO ₃ and 20 mM NaCl.	110
Figure 7-8 ES retention with and without HA as a function of pH for (a) TFC-SR2 (b) TFC-SR3. ES 10 µg/L, HA 12.5 mgC/L, pressure: 5 bar, background electrolyte	

1 mM NaHCO ₃ and 20 mM NaCl. Dotted lines indicate ES retention in the presence of HA estimated using the calculated partition coefficient K_{HA}	111
Figure 7-9 Ratio of pure water flux after the experiments J and initial pure water flux J_0 (dark symbols) and ratio of permeate flux J_v and initial pure water flux J_0 (open symbols) for filtration of ES as a function of HA concentration for (a) TFC-SR2 at pH 4 and pH 8 and (b) TFC-SR3. ES 10 µg/L, HA 5 - 250 mgC/L, pressure: 5 bar, background electrolyte 1 mM NaHCO ₃ and 20 mM NaCl.	112
Figure 7-10 ES adsorption to the membranes with and without HA as a function of pH. ES 10 µg/L, HA 5-250 mgC/L, pressure: 5 bar, background electrolyte 1 mM NaHCO ₃ and 20 mM NaCl.	113
Figure 7-11 ES retention as a function of HA concentration for TFC-SR2 at pH 4 and pH 8 and for TFC-SR3 at pH 4. ES 10 µg/L, HA 5- 250 mgC/L, pressure: 5 bar, background electrolyte 1 mM NaHCO ₃ and 20 mM NaCl. Dotted lines indicate ES retention in the presence of HA estimated using the calculated partition coefficient K_{HA}	114
Figure 7-12 Conceptual sketch of main retention mechanisms for freely dissolved ES and ES-HA complexes by TFC-SR2 and TFC-SR3 at (a) pH 4 and (b) pH 8...	120
Figure 8-1 (a) Ratio of pure water flux after the experiments J and initial pure water flux J_0 and J and (b) J_0 and J_v as a function of pressure for TFC-SR2 and TFC-SR3. Manganese 5 mg/L, background electrolyte 1 mM NaHCO ₃ and 20 mM NaCl, pH 7 (error bars not shown for clarity)	127
Figure 8-2 (a) Manganese retention and (b) manganese deposits as a function of pressure for TFC-SR2 and TFC-SR3. Manganese 5 mg/L, background electrolyte 1 mM NaHCO ₃ and 20 mM NaCl, pH 7	128
Figure 8-3 Ratio of pure water flux after the experiments J and initial pure water flux J_0 (dark symbols) and ratio of permeate flux J_v and initial pure water flux J_0 (open symbols) for filtration of ES only and ES and HA as a function of pressure for (a) TFC-SR2 (b) TFC-SR3. ES 10 µg/L, HA 12.5 mgC/L, pH 4, background electrolyte 1 mM NaHCO ₃ and 20 mM NaCl (error bars not shown for clarity)	129
Figure 8-4 ES adsorption to the membranes with and without HA as a function of pressure. ES 10 µg/L, HA 12.5 mgC/L, pH 4, background electrolyte 1 mM NaHCO ₃ and 20 mM NaCl.	130

Figure 8-5 (a) ES retention with and without HA as a function of pressure for TFC-SR2 and TFC-SR3 (b) ES flux with and without HA as a function of pressure for TFC-SR2 and TFC-SR3. ES 10 $\mu\text{g/L}$, HA 12.5 mgC/L , pH, 4, background electrolyte 1 mM NaHCO_3 and 20 mM NaCl	131
Figure 8-6 ES concentration in feed and permeate diffusion cells with time (a) TFC-SR2 and (b) TFC-SR3. ES 10-100 $\mu\text{g/L}$, pH 4.	132
Figure 8-7 Adsorption of ES to (a) TFC-SR2 and (b) TFC-SR3 during diffusion experiments. ES 10-100 $\mu\text{g/L}$, pH 4.....	134
Figure 8-8 ES flux through (a) TFC-SR2 and (b) TFC-SR3 during diffusion experiments (open symbols) and filtration experiments (dark symbols) as a function of the estimated concentration in the membrane boundary layer.	135
Figure 8-9 Observed sieving coefficients S_o and actual sieving coefficients S_a as a function of permeate flux J_v for TFC-SR2 and TFC-SR3. The continuous lines indicate (a) the purely steric hydrodynamic model (b) the hydrodynamic model with Φ fitted for TFC-SR2. The dotted lines indicate the hydrodynamic model with Φ and r_p fitted for TFC-SR3.	139
Figure 8-10 Observed sieving coefficients S_o and actual sieving coefficients S_a as a function of permeate flux J_v for TFC-SR2 and TFC-SR3. The continuous lines indicate the hydrodynamic model with Φ and λ fitted TFC-SR2 and the dotted lines indicate the hydrodynamic model with Φ and λ fitted for TFC-SR3.....	144
Figure 9-1 (a) TFC-SR2 and (b) TFC-SR3 after manganese filtration at neutral pH. Manganese concentration: 500 mg/L , pressure: 10 bar, background electrolyte 1 mM NaHCO_3 and 20 mM NaCl	153
Figure 9-2 (a,b) Pure water flux before experiments J_0 , permeate flux J_v and pure water flux after experiments J as a function of manganese concentration, pressure 10 bar, pH 7, background electrolyte 1 mM NaHCO_3 and 20 mM NaCl for TFC-SR2 and TFC-SR3 membranes (c,d) J_0 , J_v and J as a function of pressure, manganese 500 mg/L , pH 7, background electrolyte 1 mM NaHCO_3 and 20 mM NaCl for TFC-SR2 and TFC-SR3 membranes.....	154
Figure 9-3 Pure water flux before experiments J_0 , pure water flux after experiments J and permeate flux J_v during filtration of background electrolyte only, humic acids (HA), humic acids and calcium (HA+Ca), manganese (Mn), humic acids and	

manganese (HA+Mn), humic acid, manganese and calcium (HA+Mn+Ca) by (a) TFC-SR2 and (b) TFC-SR3; HA 12.5 mgC/L, CaCl ₂ 2.5 mM (278 mg/L of Ca), MnCl ₂ 500 mg/L as Mn, background electrolyte 1 mM NaHCO ₃ and 20 mM NaCl, pH 7, pressure 15 bar.	155
Figure 9-4 (a) Retention of sodium and (b, c) sodium flux during filtration of background electrolyte only, humic acids (HA), humic acids and calcium (HA+Ca), manganese (Mn), humic acids and manganese (HA+Mn), humic acid, manganese and calcium (HA+Mn+Ca) by TFC-SR2 and TFC-SR3 respectively. HA 12.5 mgC/L, CaCl ₂ 2.5 mM (278 mg/L of Ca), MnCl ₂ 500 mg/L as Mn, background electrolyte 1 mM NaHCO ₃ and 20 mM NaCl, pH 7, pressure 15 bar.....	161
Figure 9-5 (a) Retention of humic acids and (b, c) humic acids flux during filtration of humic acids (HA), humic acids and calcium (HA+Ca), humic acids and manganese (HA+Mn), humic acids, manganese and calcium (HA+Mn+Ca) by TFC-SR2 and TFC-SR3 respectively. HA 12.5 mgC/L, CaCl ₂ 2.5 mM (278 mg/L of Ca), MnCl ₂ 500 mg/L as Mn, background electrolyte 1 mM NaHCO ₃ and 20 mM NaCl, pH 7, pressure 15 bar.	163
Figure 9-6 (a) Retention of pesticide Endosulfan and (b, c) Endosulfan flux for TFC-SR2 and TFC-SR3. ES 10 µg/L, background electrolyte 1 mM NaHCO ₃ and 20 mM NaCl at 15 bar pH 7. Membrane previously filtered with humic acids (HA), humic acids and calcium (HA+Ca), humic acids and manganese (HA+Mn), humic acid, manganese and calcium (HA+Mn+Ca). HA 12.5 mgC/L, CaCl ₂ 2.5 mM (278 mg/L of Ca), MnCl ₂ 500 mg/L as Mn, background electrolyte 1 mM NaHCO ₃ and 20 mM NaCl, pH 7, pressure 15 bar.	165
Figure 9-7 Retention as function of molecular weight for (a) TFC-SR2 and (b) TFC-SR3, molecular weight at 90% retention shows membrane MWCO; concentration organic solutes 25mgC/L, pressure 15 bar, pH 6.5±0.5 (no pH adjustment); membranes previously filtered with HA 12.5 mgC/L, CaCl ₂ 2.5 mM (278 mg/L), Mn 500 mg/L, background electrolyte 1 mM NaHCO ₃ and 20 mM NaCl.	170
Figure 9-8 Contact angle of TFC-SR2 and TFC-SR3. Membranes previously filtered with HA 12.5 mgC/L, CaCl ₂ 2.5 mM (278 mg/L), Mn 500 mg/L, background electrolyte 1 mM NaHCO ₃ and 20 mM NaCl.	171

Figure 9-9 Zeta potential of (a) TFC-SR2 and (b) TFC-SR3. Virgin membranes and membranes previously filtered with Mn 500 mg/L and background electrolyte 1 mM NaHCO ₃ and 20 mM NaCl.	172
Figure A-1.1 Pictures of Plant A installed in a remote north island	215
Figure A-1.2 Typical schematic of the tubular membrane plants in Scotland.....	216
Figure A-1.3 Flux and pressure of Plant A from July 2009 to April 2010 (since installation of CA membranes)	217
Figure A-1.4 Water quality in raw and final water for Plant A; (a) turbidity , (b) colour, (c) iron, (d) pH, (e) manganese (f) aluminium [187]. Dotted lines indicated the Prescribed Concentration Value (PCV) of each parameter.....	218
Figure A-1.5 Pictures of Plant B located on the remote western island.....	219
Figure A-1.6 Flux and pressure of Plant B from January 2007 to January 2010 (since installation of CA membranes)	220
Figure A-1.7 Water quality in raw and final water for Plant B; (a) turbidity , (b) colour, (c) iron, (d) pH, (e) manganese (f) aluminium [187]. Dotted lines indicated the Prescribed Concentration Value (PCV) of each parameter.....	222
Figure A-2.1 Pure water flux during compaction at 8 bar and 15 bar for TFC-SR2 and TFC-SR3	227
Figure A-2.2 Pure water flux as a function of pressure for TFC-SR2 and TFC-SR3	228
Figure A-2.3 Determination of molecular weight cut-off (MWCO) for (a) TFC-SR2 and (b) TFC-SR3.....	229
Figure A-2.4 Observed retention R_0 and actual retention R_a of inert organics as a function of pressure for (a) TFC-SR2 and (b) TFC-SR3	230
Figure A-2.5 Observed sieving coefficient S_0 and actual sieving coefficient S_a as a function of J_v for the inert organics and fitted hydrodynamic model curves for (a) TFC-SR2 and (b) TFC-SR3	232
Figure A-2.6 Zeta potential as a function of pH for TFC-SR2 and TFC-SR3 (background electrolyte 1 mM NaHCO ₃ and 20 mM NaCl). Error bars represent the standard deviation of five repeated measurements, while the symbols represent the average of the five measurements.	233

Figure A-2.7 Photographs of water drops on (a) TFC-SR2 and (b) TFC-SR3 employed to measure contact angle	234
Figure A-2.8 Images of surface for (a) TFC-SR2 and (b) TFC-SR3 and three dimensional cross section for (c) TFC-SR2 and (d) TFC-SR3 obtained with AFM.	235
Figure A-2.9 Cross-section images of (a) TFC-SR2 and (b) TFC-SR3 by SEM with thickness measurements	236
Figure A-2.10 ATR-FTIR spectra of TFC-SR2 and TFC-SR3.....	236
Figure A-2.11 Membrane permeability (J_v /pressure) (a) and NaCl retention (b) as a function of pH for TFC-SR2 and TFC-SR3 Feed solution 20 mM NaCl and 1 mM NaHCO ₃ , pressure 5 bar.....	238
Figure A-2.12 NaCl retention as a function of pressure (pH not adjusted) for TFC-SR2 and TFC-SR3. Feed solution 0.1 mM NaCl.....	238
Figure A-4.1 Schematic of the RE-membrane system used in this study.....	256
Figure A-4.2 Performance of the PV-RO system tested on 26 October 2005 at Coober Pedy – Batch mode. EC is Electric Conductivity.....	262
Figure A-4.3 Performance of the PV-RO system tested on 27 October 2005 at Coober Pedy – Continuous mode. EC is Electric Conductivity.....	263
Figure A-4.4 Performance of the system in steady state conditions	265
Figure A-4.5 Performance of the system with simulated solar power	267
Figure A-4.6 Performance of the system with fluctuating energy- Average power 60W	268
Figure A-4.7 Performance of the system with fluctuating energy- Average power 60W	269
Figure A-4.8 Performance of the system with simulated wind energy.....	270

List of Tables

Table 3-1 Average, minimum and maximum water quality values detected in raw water at the inlet on water treatment plants based on 300 samples collected Scottish-wide in 2006-2009 - Source: Drinking Water Quality Regulator of Scotland [184].	28
Table 3-2 Elemental composition and inorganic impurities of Aldrich Humic Acids	34
Table 3-3 Crystal, Stokes and hydrated radii at 25 °C for Mn ²⁺ [70].....	37
Table 3-4 Summary of manganese (Mn) removal studies with MF and UF membranes	38
Table 3-5 Characteristics of Endosulfan isomers.....	41
Table 4-1 Formation constant and enthalpy constant used in the speciation modelling [294].....	61
Table 4-2 Characteristics of virgin TFC-SR2 and TFC-SR3 membranes.....	68
Table 4-3 Instrumental errors	69
Table 6-1 Quality parameter of well water collected in the Isle of Mull	93
Table 6-2 Retention of TFC-SR2 and TFC-SR3.....	94
Table 7-1 K _{oc} values for ES isomers determined for soils rich in organic matter...	102
Table 7-2 K _{fw} values for ES isomers (numbers in italics are calculated and numbers in normal font are published)	104
Table 7-3 Negligible depletion condition for PA* fibres at different pH values ...	105
Table 7-4 MWCO, contact angles and sodium retention for a clean TFC-SR2 and TFC-SR3 and membranes through which 12.5 mgC/L of HA and background electrolyte were filtered.....	118
Table 8-1 Diffusion coefficients for ES through TFC-SR2 and TFC-SR3 membranes determined by fitting Fick's equation with experimental data obtained with diffusion cells. The coefficient of determination r ² indicates the goodness of fitting. The membrane thickness Δδ _m was determined by SEM measurements.....	133
Table 8-2 Hydrodynamic model parameters and correlation coefficients between experimental and modelled values	140

Table 8-3 Diffusion coefficients and percentage of ES diffusive flux, estimated with diffusion experiments and the hydrodynamic model, with respect to the total ES flux during filtration.	141
Table 8-4 Hydrodynamic model parameters and correlation coefficients between experimental and modelled values	145
Table 9-1 Manganese retention, mass of manganese deposits and percentage of manganese deposits as a function of manganese concentration in the feed solution as a function of concentration of manganese in the feed. Pressure 10 bar, pH 7, background electrolyte 1 mM NaHCO ₃ and 20 mM NaCl.....	158
Table 9-2 Manganese retention, mass of manganese deposits and percentage of manganese deposits as a function of manganese concentration in the feed solution as a function of pressure. Manganese 500 mg/L, pH 7, background electrolyte 1 mM NaHCO ₃ and 20 mM NaCl.	158
Table 9-3 J_v/J_0 (ratio of permeate flux and pure water flux before experiments) and J/J_0 (ratio of pure water flux after experiments and pure water flux before experiments) for TFC-SR3 during experiments with pesticide Endosulfan. ES 10 µg/L, background electrolyte 1 mM NaHCO ₃ and 20 mM NaCl at 15 bar pH 7.....	164
Table A.1-1 Estimated operational and maintenance costs for small scale membrane plants	223
Table A.2-1 Solute characteristics and hydrodynamic conditions	231
Table A.2-2 Membrane characteristics determined by fitting the hydrodynamic model with sieving coefficient S_a obtained for the inert organics	232
Table A.2-3 Contact angle of TFC-SR2 and TFC-SR3	234
Table A.2-4 Average roughness R_a and root-mean square roughness R_q for TFC-SR2 and TFC-SR3	235
Table A.3-1 Surface SEM images (left side), SEM-BSE images (right side) and EDX spectra for TFC-SR2.....	241
Table A.3-2 Surface SEM images (left side), SEM-BSE images (right side) and EDX spectra for TFC-SR3	244
Table A.3-3 Cross-section SEM images (left side), SEM-BSE images (right side) for TFC-SR2	247

Table A.3-4 Cross-section SEM images (left side), SEM-BSE images (right side) for TFC-SR3	249
Table A.3-5 ATR-FTIR spectra of TFC-SR2 (left) and TFC-SR3 (right).....	251
Table A.4-1 Daily average results for pilot tests at Coober Pedy	261
Table A.4-2 Characteristic of Scottish surface water used in the experiments and removal by UF membranes	264
Table A.4-3 Average results for laboratory tests with Scottish surface water	266
Table A.4-4 Average solute retention obtained during laboratory tests with Scottish surface water	267

Abbreviations and symbols

List of abbreviations

(In alphabetical order)

AFM	Atomic Force Microscopy
ATR- FTIR	Attenuated Total Reflectance Fourier Transformed Infrared
BSE	Back Scattering Electron
CA	Cellulose Acetate
DL	Detection Limit
dpm	disintegrations per minute
DWQR	Drinking Water Quality Regulator (of Scotland)
EDS/EDX	Energy Dispersive X-ray Spectroscopy
ES	Endosulfan
GC	Gas Chromatography
HA	Humic Acids
HPLC	High-Performance Liquid Chromatography
ICP-OES	Inductively-Coupled Plasma Optical Emission Spectroscopy
MF	Microfiltration
MW	Molecular Weight
MWCO	Molecular Weight Cut-Off
nd-SPME	negligible-depletion Solid Phase Micro-Extraction
NF	Nanofiltration
NOM	Natural Organic Matter
NTU	Nephelometric Turbidity Units
PA	Polyamide
PA*	Polyacrylate
PCV	Prescribed Concentration Values
PDMS	Polydimethylsiloxane
PES	Polyethersulfone
POP	Persistent Organic Pollutant
PS	Polysulfone
PV	Photovoltaic

RE	Renewable Energy
RO	Reverse Osmosis
SEC	Specific Energy Consumption
SEM	Scanning Electro Microscopy
TFC	Thin Film Composite
TOC	Total Organic Carbon
TMP	Transmembrane Pressure
UF	Ultrafiltration
UV-Vis	Ultraviolet Visible
WHO	World Health Organization

List of symbols

(In alphabetical order)

A_m	Membrane area (m^2)
A_v	Area of voids (m^2)
c	Solute concentration at axial distance x from the membrane ($kg.L^{-1}$)
c_c	Solute concentration the concentrate ($kg.L^{-1}$)
c_f	Solute concentration in the bulk feed ($kg.L^{-1}$)
C_F	Solute concentration in the feed of diffusion cells ($kg.L^{-1}$)
C_{fb}	Concentration of ES in the fibre ($kg.L^{-1}$)
C_{HA}	Concentration of ES sorbed to HA ($kg.kg^{-1}$)
c_{imf}	Concentration inside the membrane at the feed side ($kg.L^{-1}$)
c_{imp}	Concentration inside the membrane at the permeate side ($kg.L^{-1}$)
c_{mf}	Solute concentration at the membrane surface on the feed side (in the boundary layer) ($kg.L^{-1}$)
c_{mp}	Concentration at the membrane surface on the permeate side ($kg.L^{-1}$)
c_p	Solute concentration in the permeate ($kg.L^{-1}$)
C_P	Solute concentration in the permeate of diffusion cells ($kg.L^{-1}$)
C_W	Concentration of freely dissolved ES in aqueous solution ($kg.L^{-1}$)
D_m	Diffusion coefficient in the membrane ($m^2.s^{-1}$)
D_∞	Diffusion coefficient of the solute in water ($m^2.s^{-1}$)
E	Error (%)

f_{HA}	Fraction of ES bound to HA (%)
H	Enthalpy constant (kJ.mol ⁻¹)
I	Ionic strength (mol.m ⁻³)
I_{pump}	Current of the pump (A)
J	Pure water flux after filtration experiments (L.m ⁻² .s ⁻¹)
J_o	Pure water flux before filtration experiments (L.m ⁻² .s ⁻¹)
J_s	Solute flux (kg.L ⁻¹)
J_v	Permeate flux (L.m ⁻² .s ⁻¹)
K	Formation constant for inorganic solutes (-)
K_1^*	Uptake rate (s ⁻¹)
K_2	Release rate (s ⁻¹)
k_b	Boltzmann constant (m ² .kg.s ⁻² .K ⁻¹)
K_c	Hindrance factor due to convection (-)
K_d	Hindrance factor due to diffusion (-)
k_f	Mass transfer coefficient (m.s ⁻¹)
K_{fw}	Fibre-water partitioning coefficient (-)
K_h	Hydrolysis rate (-)
K_{HA}	HA-water partitioning coefficient (-)
K_{oc}	Organic carbon – water partitioning coefficient (-)
K_{ow}	Octanol-water partition coefficient (-)
L	Active layer thickness (m)
m_d	Mass of solute deposited/adsorbed on the membrane (kg)
m_{DOM}	Mass of dissolved HA in solution (kg)
$m_{\text{ES-HA}}$	Mass of ES complexed to HA (kg)
$m_{\text{ES} \text{ tot}}$	Total mass of ES in solution (kg)
m_{fb}	Mass of ES on the fibre (kg)
m_{fES}	Mass of ES freely dissolved (kg)
m_{HA}	Mass of ES sorbed to HA (kg)
m_{TOT}	Mass of ES in solution (kg)
m_w	Mass of freely dissolved ES in aqueous solution (kg)
n_i	Slope of the linear regression (-)
p	Liquid permittivity (F.m ⁻¹)

p_c	Pressure of the concentrate (bar)
Pe	Peclet Number (-)
p_f	Pressure of the feed (bar)
pK_a	Acid dissociation constants (-)
p_o	Permittivity of the vacuum ($F.m^{-1}$)
p_p	Pressure of the permeate (bar)
$p\varepsilon$	Redox intensity (-)
q	Cross-sectional area of the channel in the zeta potential instrument (m^2)
Q_f	Feed flow ($L.h^{-1}$)
Q_p	Permeate flow ($L.s^{-1}$)
r	Recovery (-)
r	Electric resistance (Ω)
r^2	Coefficient of determination (m^2)
R_a	Membrane average roughness (m)
R_o	Observed retention (%)
r_p	Pore radius (m)
R_q	Membrane root-mean square roughness (m)
R_r	Real retention (%)
r_s	Stokes-Einstein radius (m)
r_{sc}	Stirred cell radius (m)
S_a	Actual (real) sieving coefficient (-)
S_o	Observed sieving coefficient (-)
t	Time (s)
T	Temperature (K)
$t_{1/2}$	Compound half time (s)
$TOTMn_{diss}$	Total dissolved manganese in solution ($kg.L^{-1}$)
U	Streaming pressure (Pa)
U_{pump}	Voltage of the pump (V)
V_c	Volume of concentrate (m^3)
V_f	Volume of feed (m^3)
V_F	Volume of the feed in the diffusion cells (L)

V_{fb}	Volume of the SPME fibre (m^3)
V_p	Volume of permeate (m^3)
V_w	Volume of the aqueous solution (L)
z_i	Charge of ion i (C)

List of Greek letters

α	Osmotic pressure coefficient ($Pa.kg^{-1}.L^{-1}$)
δ	Thickness of the boundary layer (m)
ΔG_i	Free (Gibbs) energy of interaction (J)
ΔP	Pressure gradient (Pa)
$\Delta \delta_m$	Membrane thickness (m)
$\Delta \pi$	Osmotic pressure gradient (Pa)
ε	Porosity (-)
ζ	Zeta potential (V)
η	Viscosity ($m^2.s^{-1}$)
κ	Specific conductivity of the electrolyte solution ($S.m^{-1}$)
λ	Ratio of solute radius and the membrane pore radius (-)
ν	Kinematic viscosity ($kg.m^{-2}.s^{-1}$)
ω	Stirring speed (s^{-1})
ℓ	Length of the channel in the zeta potential instrument (m)
Φ	Solute-membrane partitioning coefficient (-)

1. Introduction

Lack of access to clean, fresh water is one of the major challenges the humanity is facing worldwide and over 780 million people lack access to improved sources of drinking water [1]. About 1.2 million people live in water-stressed areas and about 1.5 million people live in developing countries where water scarcity is caused by lack of infrastructures to extract, deliver and treat water [2]. Population growth, climate change, industrialization and contamination of freshwater resources contribute to exacerbate the problem [3].

Groundwater and surface water are increasingly more contaminated with synthetic and geogenic pollutants: from traditional compounds such as metals and nutrients to “emerging contaminants”, that is organic micropollutants such as pesticides, pharmaceuticals and personal care products. Health and environmental concerns are driving the removal of these contaminants from drinking water [4-6].

Membrane processes have been employed successfully in the past two decades for the removal of inorganic and organic pollutants from drinking water [4, 7, 8]. Membrane plants are particularly suitable for small and remote communities, where the construction of traditional water treatment plants is not viable for technical and economical reasons [9]. Traditional treatments like coagulation, flocculation and sedimentation require large land areas, heavy civil works and high operation and maintenance resources, which make them convenient for serving towns and cities only. On the contrary, membrane plants are compact, modular, easily adapted to the scale of the process and can be partially automated. For these reasons, decentralised membrane plants have been considered as an alternative solution also in developing countries [10, 11].

Among the existing membrane processes, nanofiltration (NF) constitutes the preferred choice for the removal of inorganic and organic pollutants from surface water and groundwater [12]. Microfiltration (MF) and ultrafiltration (UF) have bigger pore size than NF, can remove viruses and bacteria but cannot remove many

solutes of interest, such as organic micropollutants, arsenic and fluoride, without dedicated pre- or post- treatments [13-16]. Reverse osmosis (RO) can successfully desalinate seawater and brackish water but it is not usually selected for the treatment of low salinity water. RO can remove the majority of the ions and post-mineralization is required to produce drinking water, since water lacking minerals such as magnesium and calcium can have adverse health effects [17]. Moreover, energy consumption for RO is higher than for NF due to the higher pressure required to produce water [3, 18]. Due to these advantages with respect to MF, UF and RO, NF is increasingly adopted worldwide for drinking water production [12] and for these reasons it was selected for this thesis.

1.1 Mechanisms of solute retention in nanofiltration

Given the huge potential for NF processes to tackle drinking water challenges, extensive research has been carried out to explain NF removal mechanisms [7, 19-21]. Understanding the factors governing solute retention by NF is necessary in order to achieve higher treatment efficiency, lower energy consumption and lower economic costs. Nevertheless, a complete and quantitative understanding of NF removal mechanisms has yet to be achieved [22, 23].

There is a lack of understanding of the simultaneous impact of all solute-membrane interactions and solute-solute interactions on solute retention and transport by NF in aqueous solutions. The consideration of all interactions is fundamental for elucidating retention and transport mechanisms of solutes through NF. Many solute-membrane interactions, such as size exclusion and electrostatic repulsion have been thoroughly studied [23-25]. Other solute-membrane interactions, such as hydrophobic-hydrophobic interactions between solutes and membranes, are not yet completely understood [26, 27]. Fouling, i.e. flux decline due to particle adsorption or deposition, is one of the main drawbacks in membrane applications [12, 21]. Studies on the interactions of specific foulants, especially inorganic scalants, with NF membranes (solute-membrane interactions) and their impact on membrane performance have been limited to a small number of solutes [28, 29]. Likewise, the impact of solute-solute interactions on solute retention by NF, in particular the

impact of the interactions between natural organic matter (NOM) and organic and inorganic solutes have not yet been entirely elucidated [23, 30, 31].

1.2 Aim and objectives of the thesis

The general aim of this study is to contribute to the knowledge and understanding of the mechanisms of solute retention and transport by NF membranes. The focus is on evaluating the contribution of solute-solute interactions and solute-membrane interactions on solute removal and transport mechanisms.

The objectives of the thesis are to:

- Elucidate the role of solute-NOM interactions in solute retention by NF. The contribution of solute-NOM complexation on solute removal by NF has never been quantified before. Studies on the impact of inorganic-NOM interactions on solute retention by NF are limited, while studies on the impact of micropollutant-NOM interactions on micropollutant removal show conflicting results [23, 30, 31], indicating the need for further investigations.
- Evaluate the role of solute-solute interactions and solute-membrane interactions in the influence of pressure on solute removal. The impact of pressure on micropollutant retention by NF is not well understood [7, 13] and it warrants a throughout analysis.
- Examine the effects of manganese precipitate on the performance of NF membranes (solute-membrane interactions) and the effects of scaling on micropollutant retention (solute-solute interactions). Studies investigating the influence of inorganic fouling on solute removal are limited and there are few investigations on the impact of scaling on micropollutant removal [32, 33].

1.3 Structure of the thesis

This thesis is organised in ten chapters. A comprehensive literature review presenting the main concepts in membrane technology and highlighting the gaps in knowledge at the time this work started is undertaken in Chapters 2. In order to achieve the thesis objectives within this research, the investigation was limited to specific solutes chosen as model contaminants: humic acids (HA), which constitute the largest

portion of NOM in upland source waters, manganese, selected as model inorganic solute and pesticide Endosulfan (ES), chosen as model micropollutant. The reasons for the choice of these contaminants are explained in Chapter 3, together with a description of their physicochemical characteristics and a review of their removal by traditional treatments and membrane processes. A detailed description of experimental methods, equipment and the two membranes selected in this work is presented in Chapter 4. Chapter 5 describes the theory behind the transport models employed in Chapter 8.

Chapter 6 investigates the impact of solute-solute interactions and solute-membrane interactions on the removal of manganese and HA. The impact of solute-solute interactions and solute-membrane interactions on transport and removal mechanisms of HA and ES are determined in Chapters 7 and 8. Chapter 7 investigates the impact of ES-HA interactions and HA-membrane interactions on ES removal by quantifying the contribution of complex formation on ES retention. Chapter 8 evaluates the influence of pressure on ES retention and elucidates the transport mechanisms of the solutes through NF membranes in the presence of HA. Finally, the effects of manganese-membrane interactions on membrane fouling and on the removal of ES are investigated in Chapter 9. In Chapter 10 the conclusions of the thesis are drawn and suggestions for future work are presented.

In Appendix 1, a study of the performance of two Scottish membrane plants is carried out to highlight challenges faced by the plants in terms of operational parameters, water quality, energy consumption and costs. Scotland was selected because of the high number of small membrane plants located in remote areas (Sections 3.2 and 3.3). Appendix 2 and 3 present the characterization of the membrane used in this work and of the fouled membranes used in Chapter 9, respectively. Appendix 4 describes the experiments carried out with a small battery-less membrane system powered by renewable energy in order to evaluate the impact of fluctuating energy on the system performance and on solute removal.

2. Literature Review

2.1 Introduction

Inorganic and organic solutes are present in groundwater and surface water both naturally and as a result of human activity. The main drivers behind the use of NF membranes for removing these solutes from drinking water are: (i) the development of highly sophisticated analytical instruments that has allowed for the detection of more compounds present in water at lower concentration levels than in the past; (ii) new awareness of the potential hazards to human health caused by exposure to chemical substances in drinking water [5, 34-38]; (iii) increasingly stringent guidelines that have been established to indicate the maximum allowable concentration of compounds in drinking water and ensure the provision of safe water supply [17, 39].

The effects of the above listed drivers on the choice of NF membranes as option for water treatment are exemplified in the removal of emerging micropollutants, such as pesticides, pharmaceuticals and personal care products, from drinking water. Organic micropollutants are increasingly detected around the world in groundwater and surface water [6, 40-42] and concerns is growing about their adverse effects on human health [5, 43-45]. NF membranes have been shown to provide effective micropollutant removal, resulting in increasing installation of NF plants worldwide [12, 13, 23, 46, 47]. Despite the widespread use of NF membranes, mechanisms of removal and transport are not completely understood and drawbacks to their operation, such as high energy consumption and fouling, have still to be resolved.

This chapter will describe NF principles and mechanisms, highlighting the importance of fouling, scaling and operational conditions (flux, pressure and recovery) on membrane performance. The role of solute-solute interactions and solute-membrane interactions on solute retention and transport will be elucidated.

2.2 Removal and transport of solutes by nanofiltration

2.2.1 Nanofiltration principles

NF is generally defined as “a process between UF and RO” with lower retention of monovalent salts with respect to RO and higher retention of divalent salts with respect to UF (Figure 2-1) [12, 19].

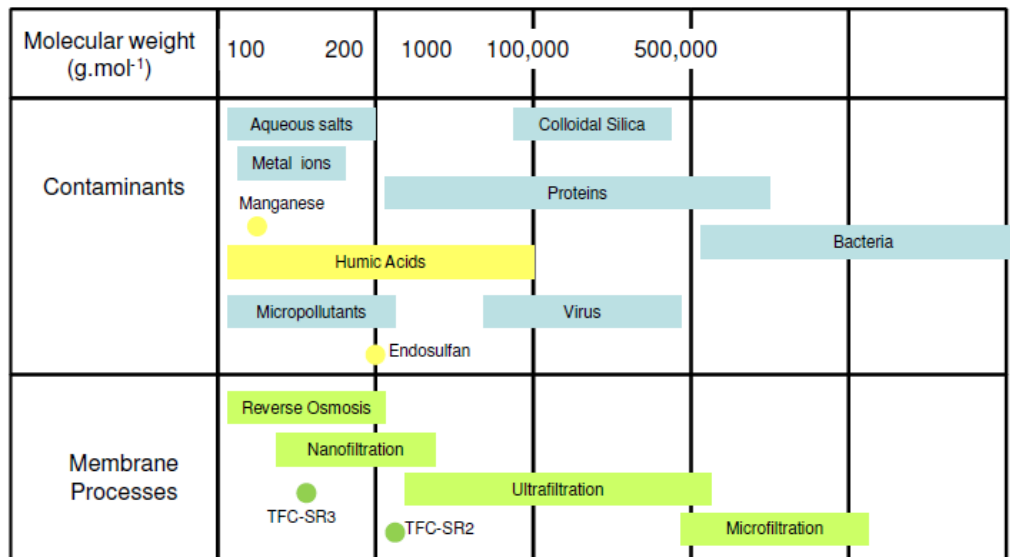


Figure 2-1 Application range of membrane processes compared with size of common contaminants and the contaminants used in this thesis (adapted from [19])

The above definition usually implies that the pore size of NF membranes is smaller than the pore size of UF membranes and bigger than the pore size of RO membranes. As a consequence, solute transport through NF is characterized by both solution diffusion, as for RO, and convection, as for UF (Section 2.2.3).

NF membranes are believed to be characterised by a pore size distribution [48] and the average pore size r_p can be used as membrane characteristic [49]. The existence of pores in NF membranes is a controversial topic. Some authors [50-53] discard the notion of pores and refer to “free volume” within the membrane layers. Free volume is defined as the volume in the membrane polymer not occupied by the polymer molecules, through which solutes can permeate. Free volume does not indicate any fixed pore and its size and location fluctuate with time [50]. The free volume theory

therefore allows for a less static representation of the voids within the membrane. In order to find an agreement between these views, the average pore radius r_p can be interpreted as the average pore radius of a “hypothetical” membrane whose hindrance to solute passage is equivalent to the hindrance experienced by the solute through the actual membrane [27, 54]. However, in contrast with the concept of membrane pores, the average pore radius r_p of the “hypothetical” membrane is not static but might change in time depending on solute-membrane interactions (i.e. the presence of charged solutes, variation in solution pH and conductivity) and on operations conditions (i.e. pressure).

Molecular weight cut-off (MWCO), which is the molecular weight (MW) of the compound that has 90% retention by the membrane, is also adopted as a measure of the pore size [25]. Pore size and MWCO are not the only parameters employed to characterize NF membranes, as membranes with similar pore size and MWCO can differ by type of material, thickness, porosity, charge, hydrophilicity and roughness.

Asymmetric thin film composite (TFC) NF membranes consist of a thin selective top layer, called the active layer, supported by a porous non-selective layer and a woven or non-woven fabric layer. The thickness of TFC NF membranes usually varies between 150 and 500 μm , with the active ultra-thin layer being at maximum a few μm thick. The most common materials for the support layer are polysulfone (PS) or polyethersulfone (PES) while the active layer can be made of polyamide (PA), cellulose acetate (CA) or piperazineamide [55]. The chemical composition of the active layer is related to other membrane characteristics [56]. Proprietary and unknown additives are usually added during manufacturing, altering membrane characteristics.

Membrane porosity ε is expressed as pore density or effective number of pores and it is defined as the percentage of membrane area occupied by voids

$$\varepsilon = \frac{A_v}{A_m} \tag{2.1}$$

with A_v the area of voids and A_m the membrane area.

Membranes acquire charge in contact with aqueous solution due to the dissociation of functional groups and the adsorption of ions or charged molecules. As a consequence, solution conditions influence membrane charge (Section 2.3.1). Solution pH induces the protonation/deprotonation of polymeric functional groups and PA membranes have been shown to acquire positive charge at low pH and negative charge at high pH [57]. The presence of divalent cations, such as calcium and magnesium (also responsible for hardness) has been shown to increase membrane positive charge, while membranes became more negative when NaCl was present in solution [57-59]. Furthermore, membrane charge has been shown to become less negative with increasing temperature of the solution [60].

Membrane charge is linked to the zeta potential of its surface and its pores. According to the electrical double layer theory [61, 62], a surface in contact with a liquid acquires two layers of charge, a layer of fixed charge (Stern layer), due to ions specifically adsorbed to the surface, and a diffusive layer (Gouy–Chapman layer), characterised by ions attracted by Coulomb interactions. The thickness of the two layers is denominated Debye length. The plane of shear defines the region at which the fluid becomes mobile and it is just beyond the Stern layer. The potential at the boundary between the Stern and diffusive layers is called Stern potential, while the potential at plane of shear is called zeta potential. According to the Gouy–Chapman equation, the electric charge in the diffusive layer is proportional to the Stern potential. Since the Stern potential can not be measured directly, while the zeta potential can be measured with several techniques (Section 4.3.7), the zeta potential is commonly employed as an indication of membrane charge [58].

Hydrophilicity is the characteristic of NF membranes to interact with water molecules allowing water to penetrate into the molecular structure of the polymer. Hydrophilicity can be estimated by measuring the contact angle (i.e. the wettability) of the membrane surface; the smaller the angle the higher the ability of the surface to interact with water and the higher the hydrophilicity [63-65].

The above described membrane characteristics have been shown to affect the performance of NF membranes and their determination is fundamental to the understanding of removal and transport mechanisms.

Membrane performance or efficiency is determined by two parameters: flux and retention [19]. Permeate flux J_v is defined by:

$$J_v = \frac{Q_p}{A_m} = \frac{1}{A_m} \frac{dV_p}{dt} \quad (2.2)$$

where Q_p is the permeate flow, i.e. the volume V_p of permeate produced in a determined time t and A_m is the membrane area.

Solute retention is expressed as

$$R_o = 1 - \frac{c_p}{c_f} \quad (2.3)$$

where c_p is the solute concentration in the permeate, c_f is the solute concentration in the bulk feed and R_o represents the (observed) retention.

In order to increase the understanding and prediction of membrane selectivity and flux, mechanisms of solute retention and transport through NF membranes have been thoroughly investigated. The following sections will present an overview of these mechanisms.

2.2.2 Retention mechanisms

Solutes are retained by NF membranes via the combined influence of (i) size exclusion, (ii) charge repulsion and (iii) adsorption/precipitation (Figure 2-2). Size exclusion depends on the ratio λ between the size of the solute and the membrane pores. If size exclusion is the only retention mechanism involved, the smaller the pores the higher the solute retention [46].

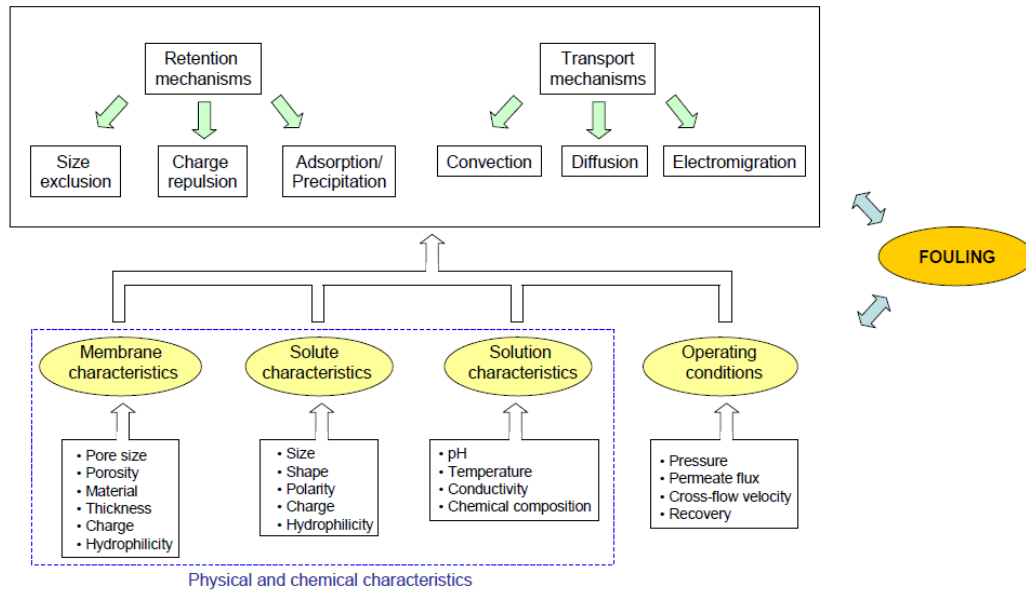


Figure 2-2 Schematic of main factors affecting retention and transport mechanisms

As the size of membrane pores is expressed by r_p and MWCO, the size of the solute can be expressed using the Stokes-Einstein radius r_s and the solute MW. In the case of ions, the hydrated radius has been shown to predict retention better than the Stokes-Einstein radius [66-69]. The hydrated radius depends on the ion charge and on the ion crystal radius: ions with smaller crystal radius have higher charge density and exhibit higher hydrated radius [70] so they are expected to be retained more. The strength of hydration energy has also been correlated with ion retention. Some ions have weak hydration energy and they are able to detach from their hydration layers and pass more easily through membrane pores. In particular, anions are believed to hold their hydration shells more strongly than cations [69] and as a consequence should be retained more by NF.

For organic compounds, in addition to the Stokes-Einstein radius the molecular width and the mean molecular size have also been employed as measures of molecular size [23, 71]. Some studies have suggested that the hydrated radius should be considered also for organics [22, 72, 73]. Since hydrophilic organic compounds are more solvated in water than hydrophobic ones, their retention might be higher even if their Stokes-Einstein radius is similar.

Solute retention by electrostatic repulsion depends on the charge of (i) the solute, (ii) the membrane surface and (iii) the membrane pores. In the case of salt retention, the Donnan charge exclusion mechanism applies. Charged membranes retain ions of the same charge (co-ions) and for electroneutrality their counter-ions are also retained. Retention is affected by ion charge density, ion concentration and by membrane shielding by ions in solution. Salts with higher valence co-ions and lower valence counter-ions will be better repelled, since in the first case charge density is higher while in the second case charge shielding is weaker. As a consequence, divalent co-ions are better retained than monovalent co-ions [25, 66, 67, 74].

Electrostatic repulsion is important for solutes that dissociate. Both organic and inorganic molecules can acquire charge at pH above their dissociation constants pK_a , if acid functional groups are present, and below their pK_a for basic groups; higher retention occurs for charged dissociated solutes [75-80]. The mechanism of charge repulsion applies also to neutral molecules that are highly polar. If the dipole moment of the solute is high, one side of the dipole will be attracted to the charged membrane while the other side will be repelled. The solute will assume an orientation perpendicular to the pores and its passage will be facilitated [76].

Precipitation and adsorption of solutes is the third mechanism influencing solute retention. Although precipitation and adsorption are based on very different chemical and physical phenomena they are determined with the same mass balance:

$$m_d = V_f c_f - \sum V_p c_p - V_c c_c \quad (2.4)$$

where m_d is the mass of solute deposited or adsorbed, V_f , V_p , and V_c are the volume of feed, permeate, and concentrate, respectively, and c_c is the solute concentration of the concentrate.

In the case of inorganic compounds, precipitation of solid species can occur on the membrane surface impacting solute retention [29, 74, 81]. Hybrid coagulation-NF processes exploit the precipitation of coagulants to remove solutes that adsorb onto them [82, 83]. However, the effects of inorganic precipitates on solute retention and permeate flux are, to date, scarcely studied [28, 29, 84, 85].

Adsorption of inorganic and organic solutes on the membranes also affects retention [26, 64, 73, 86-90]. In particular, hydrophobic organic micropollutants, whose octanol-water partition coefficient $\log K_{ow} > 2$, have been shown to adsorb to hydrophobic membranes and have an initial high retention which decreases with time until membrane saturation is reached [22, 91-93]. It has been shown that hydrophobic interactions between micropollutants and membranes become more important for solutes whose MW is lower than the membrane MWCO, while their role in retention decreases for bigger solutes [73]. Nevertheless, mechanisms of adsorptive interactions between solutes and membranes, such as hydrophobic-hydrophobic interactions, are to date not completely understood [23, 94].

The influence of solute precipitation and adsorption on retention is complicated by the occurrence of concentration polarisation, fouling and scaling. These phenomena will be discussed in detail in Sections 2.2.3 and 2.2.4.

In summary, retention mechanisms are influenced by the physical and chemical characteristics of membranes and solutes. Membrane characteristics (material, pore size, thickness, porosity, charge, hydrophilicity and roughness) and solute characteristics (size, shape, charge, polarity, and hydrophilicity) impact size exclusion, electrostatic interactions and solute precipitation/adsorption to the membrane. Solution characteristics, such as pH, temperature and conductivity and solution composition, such as the presence of multiple contaminants, also affect membrane and solute characteristics, influencing in turn retention (Figure 2-2). The impact of the feed composition on solute retention will be discussed in Section 2.3.2.

Operating conditions, such as pressure, flux, crossflow velocity and recovery are important parameters for retention and will be described in Section 2.2.5. Finally, the occurrence of fouling/scaling is another important factor impacting solute retention, as schematically represented in Figure 2-2, and will be examined in Section 2.2.4.

Retention mechanisms occur simultaneously during solute filtration, although some mechanisms can be stronger than others depending on the type of solute and

membrane, operating (hydrodynamic) conditions and solution characteristics. Retention mechanisms are well understood but it is important to evaluate their relative roles in solute retention by NF.

Numerous studies [7, 12, 23, 53, 66, 76, 92, 95-99] have elucidated the role of each mechanism in affecting retention of organic and inorganic solutes and have also related solute retention to the physicochemical properties of solutes and membranes and to the operating conditions. A thorough comprehension of retention mechanisms increases membrane efficiency by enabling the choice of optimum operating conditions for the removal of specific compounds [100].

2.2.3 Transport mechanisms

The study of transport mechanisms is fundamental in order to understand solute retention and evaluate membrane efficiency. Transport models include both models describing solute transport to the membrane surface and models describing the transport across the membrane [101].

Transport to the membrane surface is described by the film theory [19]: during solute filtration the solute can accumulate at the membrane surface and the concentration in the boundary layer becomes higher than the solute concentration in the bulk feed c_f . The accumulation of solute at the membrane surface is defined as concentration polarisation. As a result of concentration polarisation the real retention R_r is lower than the observed retention R_o . The film theory and the equations that describe the concentration polarisation phenomenon are presented in Section 5.1.

Transport of solutes across membranes has been described by several models [23, 102-105] that take into consideration the main mechanisms of solute transport, namely convection, diffusion and electromigration (Figure 2-2).

The solution diffusion model [102] predicts that solute separation by the membrane is achieved by dissolution of solute in the membrane and consequently diffusion to the permeate side. This model has been applied successfully to the transport of

inorganics and organic micropollutants through RO and NF membranes [106, 107], but it usually gives poor predictions for NF membranes, since solute transport by convection cannot be neglected [7, 23].

The thermodynamic model [104] and the hydrodynamic model [103] take both diffusion and convection into account and their application to the description of solute transport through NF is widespread [27, 67, 97, 101, 108-114]. Both models result in the same equation for solute retention when diffusion cannot be considered negligible [115].

In this work the hydrodynamic model was chosen because it describes the transport of solutes through membranes using variables with a well-defined physical meaning, while the thermodynamic model treats the membrane as a black box. Unknown parameters can be estimated from experimental data to gain information about the physical mechanisms behind the transport of solutes. The model has been used in previous studies in a non-predictive fashion to explain solute transport mechanisms [101, 111, 113]. The equations describing the hydrodynamic model are presented in Section 5.2.

The transport of charged solutes through NF membranes is described by the extended Nernst-Planck equation in which a transport term due to the electric field gradient is added to the equation of the hydrodynamic model [54, 105, 114].

According to the hydrodynamic model, solute transport through NF membranes is affected by solute and solution characteristics, membrane characteristics and operating conditions, as depicted in Figure 2-2. The investigation of transport mechanisms is fundamental for improving the efficiency of NF. Evaluating the role of the different mechanisms for specific solutes is crucial for optimising their removal [100, 110, 113, 116, 117].

2.2.4 Fouling and scaling

Fouling has been described as a loss of membrane performance due to solute adsorption or deposition on the membrane surface or within its pores resulting in irreversible flux decline [12]. Concentration polarisation, as described in Section 2.2.3, is not considered fouling since its effects are reversible, but it can contribute to worsen fouling.

Fouling remains one of the unresolved problems of NF [118, 119]. Numerous studies [29, 118, 120-129] have investigated fouling mechanisms, mainly focusing on the impact of fouling on solute retention and on the formation and characterisation of the fouling layer.

The main NF membrane foulants are considered to be organic molecules (especially NOM), colloids, biological solids and inorganics. Several studies obtained minimal flux decline when NOM alone were filtered and fouling was caused when divalent ions, such as calcium and magnesium, were present [125, 126, 129-131]. However, these results can not be generalised since NOM characteristics vary largely depending on the source (Section 3.4), so the type of NOM and its molecular weight distribution might play an important role.

Fouling caused by the precipitation of inorganics is referred to as scaling. While fouling mechanisms of NOM, colloids and proteins on NF and RO membranes have been thoroughly investigated in several studies [15, 112, 125-127, 129, 131-134], research on scaling caused by non-colloidal inorganics have been limited to a small number of solutes, such as iron hydroxide and calcium sulphate [28, 29, 84, 85, 119, 135]. There is a lack of investigation into the effect of non-colloidal inorganic scalants on the performance of NF and RO membranes.

The observed flux decline during membrane fouling is explained with the resistance in series model and with the cake-enhanced concentration polarisation model. According to the resistance in series model, the permeate flux is inversely proportional to the membrane resistance. Membrane resistance increases with the

presence of the fouling layer, therefore flux declines [19, 125]. According to the cake-enhanced concentration polarisation model, the fouling layer hinders the back diffusion of solutes during filtration, increasing concentration polarisation and the osmotic pressure near the membrane, resulting in turn in severe flux decline [128]. The first model has been shown to be valid for fouling caused by organics, while the second model has described satisfactorily fouling caused by colloids [128, 129, 132].

Membrane fouling not only causes flux decline but also impacts solute retention. It has been proposed that when fouling causes an increase of the membrane resistance (as in the case of organics) solute retention increases since the fouling layer behaves as a further barrier (an “active” membrane) to solute transport [129]. Conversely, when cake-enhanced concentration polarisation occurs (as for colloidal fouling), solute retention decreases since the solute concentration at the membrane increases and the diffusive transport of the solute to the permeate side increases too [128].

However, experimental results show that fouling mechanisms cannot be easily described with simple rules. Fouling caused by NOM and calcium, which according to the resistance in series model should increase solute retention, was shown to increase sodium and calcium retention but decrease NOM retention [135, 136]. Colloidal fouling, expected to decrease solute retention by cake-enhanced concentration polarisation, was shown to decrease retention of small MW inert organic solutes and hormones, but it did not affect retention of large MW inert organic solutes [129, 132].

Scaling was shown to reduce salt retention [29, 135] but studies investigating the influence of inorganic fouling on solute retention are limited. In particular, there are few investigations into the impact of scaling on micropollutant removal [32, 33].

The impact of fouling on retention is complicated by the simultaneous role played by the retention mechanisms (Figure 2-2). In the case of micropollutant retention by membranes fouled with NOM and calcium, it was inferred that the predominance of the resistance in series model and the cake-enhanced concentration polarisation

model might depend on the membrane pore size. Pore blocking, which improved retention by increasing membrane resistance, was predominant for loose membranes, while cake-enhanced concentration polarisation occurred for tighter membranes [134, 137].

The retention of pharmaceutically active compounds by membranes fouled by surface water was inferred to decrease due to cake-enhanced concentration polarisation and increase due to charge repulsion, as foulants increased the membrane negative charge [112].

In summary, fouling and scaling affect retention and transport mechanisms, as shown in Figure 2-2 and vice versa retention and transport mechanisms affect fouling, since solutes that are retained by the membrane accumulate on the boundary layer or adsorb to the membrane where they can contribute to flux decline. Finally, fouling and scaling can affect membrane characteristics (Figure 2-2), as discussed in more detail in Section 2.3.

Due to the complicated inter-relationships among all the parameters affecting and affected by fouling, the impact of fouling on membrane performance is a complex topic which still remains unclear [13].

2.2.5 Influence of operating conditions

Operating conditions, such as pressure, crossflow velocity and recovery, directly affect solute retention and transport by NF.

As described by the hydrodynamic model, crossflow velocity affects concentration polarisation and in turn solute retention (see equations 5.3, 5.5, 5.6 in Chapter 5). Pressure affects the permeate flux J_v and consequently solute flux J_s and solute retention (see equations 5.7, 5.12 and 5.13 in Chapter 5). The influence of pressure on retention of metals, ions and inorganic solutes has been thoroughly elucidated [54, 66, 138]. Retention of inorganic solutes increases with pressure and it can be effectively described by the solution-diffusion model. However, the influence of

pressure on micropollutant retention has shown conflicting results [7, 75, 91, 116, 139-142] and mechanisms are not well understood [7, 13].

Recovery r , which indicates the quantity of permeate produced with respect to the feed, is defined as:

$$r = \frac{Q_p}{Q_f} \quad (2.5)$$

where Q_p is the permeate flow and Q_f is the feed flow.

Membrane plants in drinking water are usually operated at 80% total recovery, which is obtained in two or three stages, each operating at 50-60% recovery [143]. High recovery is beneficial because it increases the drinking water production (permeate flow) and decreases the waste stream (concentrate flow). Increase in recovery has been shown to result in a decrease in flux, even when fouling does not occur [129], and recovery-flux relationships are membrane and solute dependent. Recovery impacts solute retention: increase in recovery was shown to increase retention of boron, arsenic and fluoride [14, 144] and decrease pesticide retention [145, 146].

Operating conditions can affect membrane characteristics, influencing in turn retention and transport mechanisms. Pressure has been shown to influence membrane pore size and porosity, although findings reported in the literature are contradictory [96, 108, 147]. Van der Bruggen and Vanecasteele [108] showed that pressure decreased membrane MWCO, while results obtained by Kiso *et al.* [148] indicated the pore radius slightly increased with pressure. Kosutic *et al.* [147] inferred that with increasing pressure the number of pores increased but the medium-sized pores shrunk to smaller dimensions.

Operating conditions also affect fouling [28]. High pressure and flux were shown to increase the rate of convective transport of solutes to the membrane and therefore their deposition, increasing fouling [84, 125, 127]. As a consequence, fouling can be avoided if the membrane is operated below the “critical flux” [122, 123, 126].

Crossflow velocity, which impacts the Reynolds number, affects fouling and scaling. High crossflow velocity was shown to increase the critical flux, in turn decreasing fouling [121, 149]. Change in crossflow velocity has been shown to disturb the fouling layer formed by deposited iron hydroxide particles, decreasing the rate of scaling [84].

Higher recovery increases solute concentration in the feed, increasing concentration polarisation and hence fouling potential. During NOM and calcium filtration, increase in recovery was shown to raise the resistance of the cake layer and reduce membrane flux [129]. Scaling by inorganic solutes was worsened by concentration polarisation enhanced by high recovery [143, 144].

2.3 Solute-membrane and solute-solute interactions

NF retention and transport mechanisms are related with physical and chemical characteristics of membranes, solutes and solution; operating conditions; and fouling; as described in the previous sections and illustrated in Figure 2-2. These relationships are controlled by the interactions between solutes and membranes and the interactions between the solutes themselves.

2.3.1 Solute-membrane interactions

The interactions between solutes and membranes are fundamental to the retention mechanisms of size exclusion, electrostatic repulsion and solute adsorption to the membrane described in Section 2.2.2. Therefore, the retention mechanisms have been classified as solute-membrane interactions [24, 32, 150].

Solute-membrane interactions not only regulate retention and transport mechanisms directly, but they also indirectly influence membrane performance through affecting membrane characteristics such as pore size, charge and hydrophilicity.

Solution pH affects charge of polymeric membranes since they are amphoteric, i.e. they have ionisable groups that protonate and deprotonate according to the pH [57]. Solution pH can affect membrane pore size and MWCO, which have been shown to

increase in alkaline conditions [151, 152]; it has been inferred that when membranes acquire charge their matrix is in a more expanded state due to intra-membrane electrostatic repulsion and their pore size increases [153].

Solution ionic strength and the presence of charged solutes, such as NOM and divalent cations, were shown to affect membrane charge, potentially influencing membrane pore size [24, 57, 77, 87, 98, 125, 133, 153, 154]. The Debye length, i.e. the thickness of the electrical double layer, decreases with increasing electrolyte concentration and increasing valence of the charged solutes [62], influencing the membrane zeta potential and in turn membrane charge. Decrease in glucose retention and in turn increase in membrane pore size were observed when salt ions were added to the solution [155].

Solutes adsorbed or deposited on the membranes can affect their hydrophilicity [65, 156, 157]. Membrane contact angle was shown to increase after filtration of HA and calcium [137]. Contact angle after filtration of secondary effluent water was shown to increase for hydrophilic membranes and decrease for hydrophobic ones, potentially indicating that the membranes acquired an intermediate hydrophobicity reflecting the organic deposit characteristics [133].

Fouling is regulated by solute-membrane interactions as fouling is caused by an interaction between the foulant and the membrane [158]. Contaminant characteristics have been shown to influence the rate of fouling. Contaminant size can affect fouling and particles whose radius was bigger than 5 μm were shown to minimally contribute to fouling [159].

Membrane characteristics can influence the rate of fouling. Roughness is considered the most influential membrane characteristic for colloidal fouling. Colloidal particles were shown to deposit preferentially on the “valleys” of rough membranes, while smooth membranes were fouled less [160]. Fouling seemed more severe for hydrophobic membranes due to the higher solute adsorption to the membrane surface

[131, 161]. Membranes with bigger pore size experienced higher fouling by NOM, probably due to the greater initial flux or to greater pore plugging [126, 134].

The fouling layer can affect membrane characteristics and in turn membrane performance. After fouling, the charge and hydrophilicity of the membrane surface have been shown to reflect those of the fouling layer [65, 112, 133, 161-163]. Membranes fouled by NOM were inferred to have an increased MWCO due to increased negative surface charge and consequent membrane swelling [87, 133].

The consideration of all solute-membrane interactions is fundamental for evaluating the retention and transport mechanisms of solutes through NF. The hydrodynamic model takes into account solute-membrane interactions by considering hindered diffusion and convection transport (Section 5.2). Recently developed expressions of the partition coefficient Φ for micropollutants have included solute adsorption to the membrane in the hydrodynamic model [27]. Nevertheless, other solute-membrane interactions, like fouling and scaling, have not yet been considered in the traditional transport models due to the limited understanding of their underlying mechanisms.

Some solute-membrane interactions, like sieving and electrostatic retention mechanisms, are fairly well understood [23]. However, other interactions, such as adsorptive interactions between some solutes and the membranes, fouling by specific solutes like inorganic scalants, and the effects of solutes on membrane characteristics, have not yet been completely elucidated. In this work particular stress will be placed on highlighting the influence of solute-membrane interactions on solute retention and transport across NF, and on investigating specific solute-membrane interactions whose mechanisms are to date unclear.

2.3.2 Solute-solute interactions

The interactions between solutes affect their retention and transport by NF, so studies investigating the impact of solute-solute interactions on solute retention and transport are fundamental to understand NF mechanisms. Unlike for solute-membrane interactions, the effects of solute-solute interactions are not included in transport

models such as the hydrodynamic model, where transport of only a single solute is described (see Chapter 5). Solute-solute interactions are exploited to increase solute retention by NF. For example, chelating agents, flocculants and adsorbents can be dosed to remove particular solutes by size exclusion [82, 83, 164-167].

The majority of the studies in the literature investigates the impact of the interactions between organic and inorganic solutes with NOM. NOM removal is an issue in water treatment since it is ubiquitously present in surface water and is a precursor of disinfection by-products, which are considered carcinogenic [36-38]. The influence of the interactions between NOM and organic and inorganic solutes on solute retention have been thoroughly examined in the case of UF [86, 168-170]. However, to the knowledge of the author, only a limited number of studies [95, 171] has investigated the influence of inorganic solutes-NOM interactions on solute removal by NF in non-fouling conditions.

Several studies investigated the impact of the presence of NOM on micropollutant retention by NF [31, 75, 87, 142, 172-175]. Nevertheless, obtained results and explanations of mechanisms are contradictory and these ambiguities have been attributed to the different types of micropollutants and organic matter used in the studies and to the complexity of the retention mechanisms [23, 30, 31]. There is an obvious need to further explore the role of solute-NOM interactions in solute removal by NF.

Solute-solute interactions are important because they can influence membrane fouling. The presence of divalent cations, such as calcium and magnesium, has been shown to increase membrane fouling by NOM. Increased fouling has been attributed to the formation of NOM-cation complexes [121, 126, 131, 149]. Cations are believed to interact with the membrane functional groups, and form “ionic bridges” between NOM and the membrane, increasing NOM adsorption on the membrane and consequent fouling. A recent study [131] has shown that a different mechanism could be responsible for increasing fouling: cations could promote NOM aggregation that could be the cause of fouling.

The presence of coagulants, such as alum sulphate, ferrous sulphate and ferric chloride has been shown not only to improve flux decline caused by HA, reducing fouling, but also to enhance permeate flux [82, 83]. Dosing of coagulants improves flux decline caused by NOM fouling for UF membranes, since the formation of flocs reduces the number of small particles responsible for fouling [176]. However, the enhancement of permeate flux when coagulants are dosed, as observed for NF membranes [82, 83] is a phenomenon that is still not understood and further investigations are required.

Solute-solute interactions can also influence the rate of fouling and the nature of the fouling layer. Solution pH influences formation of inorganic deposits and in turn scaling [29, 74, 84]. The deposition of HA and the consequent fouling was shown to be higher at low pH values when both membrane and HA were not charged [125, 126]. Ionic strength in the feed can impact fouling by influencing the solubility and configurations of foulants and in turn their fouling potential [177]. High ionic strength has been shown to increase fouling by organics as the presence of salts may enhance organic aggregation [121, 125, 126]. Ionic strength can impact fouling through increase of osmotic pressure, by contributing to flux decline and by influencing membrane-foulant interactions [177]. High ionic strength was shown to increase colloidal fouling as the repulsion of the electrostatic double layer between membrane and colloids was reduced [127].

Solute-solute interactions are fundamental to understanding solute retention mechanisms by NF. In particular, a better understanding of the role of inorganic-NOM interactions and micropollutant-NOM interactions in NF is required. This work will focus on elucidating the contribution of solute-solute interactions with respect to solute-membrane interactions in solute removal and transport.

2.4 Conclusions

This chapter has presented the principles governing NF membranes and highlighted the role of solute-solute interactions and solute-membrane interactions in influencing membrane efficiency. Despite the extensive research investigating the retention and

transport mechanisms of NF membranes, a complete understanding has yet to be achieved. There is a lack of investigations into the simultaneous impact of solute-membrane interactions and solute-solute interactions on solute retention and transport by NF.

While some solute-membrane interactions, like size exclusion and electrostatic retention mechanisms, are fairly well understood, other interactions have not been completely elucidated. Membrane fouling is a complex phenomenon, whose mechanisms are not fully explained. The effects of scaling by non-colloidal inorganics on membrane flux and solute removal, especially micropollutants, are unknown. Fouling reduction caused by inorganic solutes is an interesting effect that warrants detailed investigation. The effects of solutes and foulants on membrane characteristics (pore size, charge, and hydrophobicity) and in turn on membrane performance require further studies.

Studies exploring the impact of solute-solute interactions on NF membranes are scarce. In particular, given the ubiquity of NOM in water resources, there is a need to understand the role of solute-NOM interactions in solute removal by NF. The influence of the interactions between NOM and solutes, especially inorganics and micropollutants, on NF removal mechanisms is not completely understood.

This study will evaluate the role of solute-membrane and solute-solute interactions in the removal of a model inorganic contaminant and model micropollutant, in the presence of HA, chosen as NOM representatives (Section 3.4). Focus will be placed on investigating solute-membrane interactions whose mechanisms are to date unclear. The impact of scaling on membrane characteristics and performance (solute-membrane interactions) and on retention of salts, HA and micropollutants (solute-solute interactions) will be investigated. In the following chapter a review will be carried out to select the model organic and inorganic contaminants to be used in this study.

3. Contaminants of interest

3.1 Introduction

This chapter will describe the characteristics, occurrence and effects on human health and on the environment of the contaminants selected in this work. The removal of these contaminants by traditional treatment and membrane processes, as presented in the literature, will be reviewed.

Firstly, an overview of the principal contaminants in the water resources of Scotland will be carried out. Secondly, the choice of membrane plants to treat drinking water for Scottish remote communities will be discussed. The objective is to identify and select relevant compounds of interest for this study.

3.2 Water quality and treatment in Scotland

In Scotland the majority of the population lives in the major cities, while only 7% (about 350,000 people out of a total population of 5 millions) is scattered in remote rural areas that constitute the majority of its territory [178]. The areas of high population density coincide with the lowland areas, while remote rural areas are generally in the highlands and islands. Several small settlements, ranging from a few households up to 3,000 people, are located in sites that can be difficult to reach, often isolated due to adverse weather conditions and at times subjected to intermittent power supply [179]. This distribution of population influences the water quality, the type of drinking water sources and the choice of water treatment process.

Surface water from *lochs* (lakes) and *burns* (rivers) constitutes the principal source of drinking water, with groundwater making up only 7% of the public water supplies. However, the influence of groundwater is estimated to be much higher than 7% as groundwater naturally feeds into reservoirs and composes river baseflow [180]. Scottish water is “flashy” in nature due to snow melt and high intensity rains that cause large seasonal and daily fluctuations in the water quality [9, 181].

Surface water in the more populated lowland areas is more affected by anthropogenic pollution and large scale traditional water treatment plants serve the major cities. Surface water in highland areas is generally less polluted, although it has been facing increasing quality problems [182]. Surface water in Scotland is very soft, i.e. with low alkalinity and mineral content, and low bacteriological quality. It is characterised by a yellow-brown colour due to the presence of NOM, in particular humic and fulvic acids, caused by Scottish acidic peaty soil, and high concentrations of iron, manganese and aluminium [9].

In raw water bacteriological parameters (*Coliforms*, *E.coli*, and *Enterococci*) and colour are the components that most commonly exceed the Prescribed Concentration Values (PCV) established for drinking water in Scotland [183] (Figure 3-1). Unfortunately, data on Total Organic Carbon (TOC) in raw water is not available since TOC samples are collected at the point of supply only.

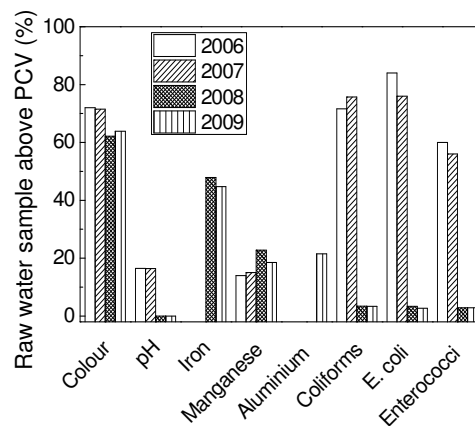


Figure 3-1 Percentage of raw water samples that exceed their Prescribed Concentration Value, based on 300 samples collected at the inlet of water treatment works from 2006 to 2009 (Iron data available from 2008 and Aluminium data available for 2009 only)- Source: Drinking Water Quality Regulator of Scotland [184]

Table 3-1 shows the average, minimum and maximum values for components of interest in Scottish raw water, together with their PCV and the World Health Organization (WHO) guidelines. Among the inorganic solutes, iron and manganese were the parameters with the highest average and maximum concentrations in raw

water with respect to their PCV. Concentrations of manganese in excess of its PCV are also found in Scottish groundwater [185].

Based on data collected from 2004 to 2006 at the outlets of water treatment plants throughout Scotland, manganese exceeded its regulatory limit more frequently than iron, aluminium and nitrite (Figure 3-2), indicating insufficient manganese removal to achieve the desired standard. The reason for the higher failure rates in 2004 is unknown. The number of raw water samples that exceeded 50 µg/L was only marginally higher in 2004 with respect to 2005 and 2006, probably due to the higher precipitation experienced in 2004 [186], and it can not fully explain the higher failure rates.

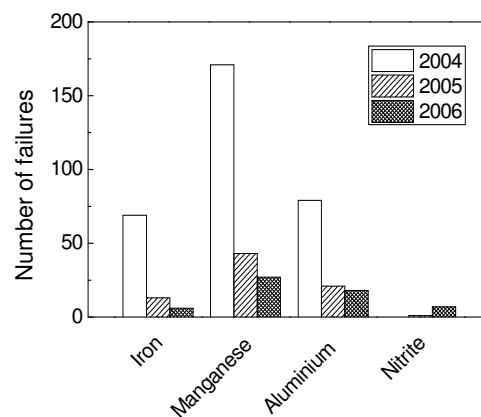


Figure 3-2 Number of samples collected at the outlet of water treatment works above their Prescribed Concentration Value, based on 400 samples collected from 2004 to 2006 Scottish-wide (Nitrite data available from 2005 only)- Source: Scottish Water [187]

Pesticides and herbicides are a not major problem in Scotland, although the reporting of their occurrence in raw water is increasing, probably due to lower instrumentation detection limits and increasing sampling frequency [180, 188, 189]. An area of particular concern is the east coast, where herbicides have been detected above the regulatory limits both in raw water and at the outlet of the existing traditional water treatment works [190].

Table 3-1 Average, minimum and maximum water quality values detected in raw water at the inlet on water treatment plants based on 300 samples collected Scottish-wide in 2006-2009 - Source: Drinking Water Quality Regulator of Scotland [184]

Parameter	Unit	DL ¹	Average Values	Minimum Values
Colour	Pt/Co	2	44.4	< 2
Turbidity	NTU	0.25	0.73	< 0.25
pH	-	-	7.10	3.2
Aluminium	µg/L	10	217.10	< 10
Iron	µg/L	17	470.60	< 17
Manganese	µg/L	1	90.51	< 1
Total Coliforms	number/100mL	-	99.64	0
E.Coli	number/100mL	-	25.80)	0
Enterococci	number/100mL	-	2.74	0
Parameter	Unit	Maximum Values	PCV ²	WHO ³ Guidelines
Colour	Pt/Co	358	20	
Turbidity	NTU	5.78	4	0.1 ⁴
pH	-	10.2	6.5 - 9.5	6.5 - 8.5 ⁴
Aluminium	µg/L	9,640	200	200 ⁴
Iron	µg/L	44,586	200	300 ⁴
Manganese	µg/L	25,974	50	400
Total Coliforms	number/100mL	9,640	0	0
E.Coli	number/100mL	2,200	0	0
Enterococci	number/100mL	160	0	0

¹Analytical instrument Detection Limit (DL)

²Prescribed Concentration Value [183]

³World Health Organization guidelines [17]

⁴Recommendation based on aesthetic considerations such as taste and colour

3.3 Membrane plants in Scotland

The existence of small remote communities and of strict drinking water regulations, the type, nature and quality of the water sources, and the variability in the water demand due to tourism have determined the choice of membrane plants as the main water technology for remote Scottish areas.

Membrane plants were chosen by Scottish Water, the water company in Scotland, as best treatment process due to their small physical footprint, the minimisation of civil works compared to traditional plants and their modularity and availability as turn-key

plants that are particularly suitable for remote area that are difficult to access. Their lower maintenance requirements and reduced use of chemicals with respect to traditional plants were also deemed an advantage as they allow operators to visit the sites less frequently and reduce problems of supply and disposal of large quantities of chemicals at distant sites. Moreover, the single-stage process was considered able to deal with fluctuating water quality and provide consistent final water in compliance with the regulations [9].

Scottish Water installed the first membrane plant in 1994 and currently 82 membrane plants are operating across Scotland (Figure 3-3a). In the last five years Scottish membrane plants delivered more than 80,000 m³/day of drinking water, with variable output depending on demand. Individual plant capacity ranges from 3 m³/day for the smaller plants up to 50,000 m³/day for the biggest plant, with 80% of the plants having a capacity of less than 450 m³/day (Figure 3-3b).

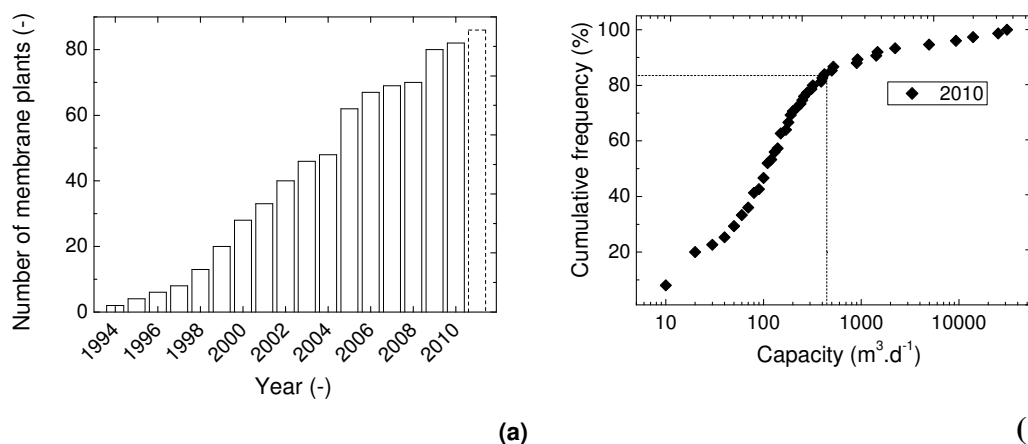


Figure 3-3 (a) Number of membrane plants installed in Scotland from 1994 to 2010
(b) Cumulative frequency (%) versus capacity (m³/day) on logarithmic axis of Scottish membrane plants Source: Scottish Water [187]

As shown in Figure 3-4, there are more than 50 membrane plants located in areas classified as “remote rural” according to the Scottish Government 6-Fold Urban Classification [178]. Some of these sites, such as those situated in the northern and western islands can be isolated from the mainland for long periods during winter. It

is interesting to note that membrane plants are not present in the eastern part of Scotland where pesticides are found, despite the successful use of NF membranes for pesticide removal [47, 191].

Apart from a minority of ceramic membranes, the majority of the NF modules in Scotland are spiral wound CA membranes supplied by Koch Membrane System [192] and tubular CA or PES membranes supplied by PCI Membrane Ltd. [193]. Tubular membranes constitute approximately 60% of the total membrane plants [194, 195].

Spiral wound modules usually need pre-treatment as they get clogged with particulate matter and require daily chemical cleaning [9, 194]. Tubular membranes are more robust than spiral wound membranes and do not require pre-treatment, but they are more complex to produce, have a lower packing density, hence require larger land areas and they are more energy intensive as they are operated at higher crossflow velocity [194, 196].

Despite the high number of membrane plants in Scotland and the availability of operational and water quality data, there is a lack of dedicated studies assessing the performance of membrane plants. Apart from a few publications [47, 197, 198], analyses of the performance of full scale NF treatment plants are limited.

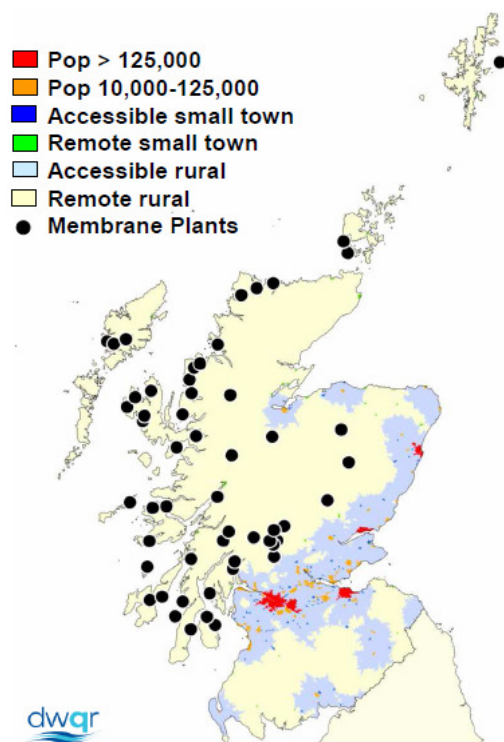


Figure 3-4 Map of Scotland indicating remote rural areas (yellow areas) as categorised according to the Scottish Government 6-Fold Urban Classification [178] with location of membrane plants marked. Source: Drinking Water Quality Regulator of Scotland [184]

3.4 Occurrence and removal of organic and inorganic contaminants

The review of the existing literature undertaken in Chapter 2 showed that although removal and transport mechanisms have been intensively studied in the past two decades, a complete and quantitative understanding of NF principles is still to be achieved. The co-influence of solute-membrane interactions and solute-solute interactions on solute removal and transport needs to be investigated to better explain NF mechanisms.

Among the contaminants of interest in drinking water production, NOM has the leading role. NOM is ubiquitous in surface water and is a precursor of disinfection by-products which are considered carcinogenic [36, 37]. As described in Section

2.3.2, the interactions between contaminants and NOM have been shown to highly influence contaminant removal by NF.

NOM is composed of a hydrophobic fraction, represented by humin, humic acids and fulvic acids, a hydrophilic fraction, constituted by polysaccharides, amino acids, proteins and a transphilic fraction of carboxylic acids and carbohydrates [130, 199]. In upland source waters, the dominant fraction of NOM is represented by the hydrophobic fraction, while the hydrophilic part might be dominant in other types of waters [200, 201]. For this reason in this work, commercial HA were chosen to represent NOM because they have been extensively characterised in the literature [202-207]. Moreover, the use of commercial substances allows the comparison of results with findings in the literature [208].

Manganese was chosen as a model inorganic because it is one of the most abundant elements in Scottish water and it is difficult to remove with conventional treatments (Section 3.2). Removal mechanisms of manganese from drinking water by NF have never been systematically investigated. Although NF is known to remove divalent ions, removal is solute specific due to solute speciation and different solute interactions with the membranes.

Manganese is known to form complexes with HA [209-212] but the impact of HA on manganese removal by NF is unknown. The study of the removal of manganese and HA complexes will increase the knowledge of the role of inorganic solutes-NOM interactions in removal mechanisms by NF, that have so far received little attention (Section 2.3.2).

Manganese can precipitate at pH above 7.5-8 [211, 213, 214] but the effects of manganese scaling on NF membrane flux and solute retention are unknown. The impact of scaling on micropollutant removal will be investigated for the first time in this work.

Pesticide ES was selected as a model micropollutant because it is extensively used worldwide, it is very persistent in the environment, it is toxic to aquatic life and it has been shown to have estrogenic properties similar to DDT [43, 215-219]. ES is a particularly suitable compound for investigating the role of micropollutant-NOM interactions and solute-membrane interactions on NF retention because it is hydrophobic, neutral over a large pH range [220] and forms complexes with NOM [221-224].

In the following sections, the physicochemical characteristics of the selected model contaminants will be described together with a brief summary of their removal achieved by traditional treatments and membrane processes.

3.4.1 Humic acids

HA are complex and heterogeneous mixtures of high to low molecular species containing both aromatic and aliphatic components with primarily carboxylic and phenolic functional groups [225, 226]. A proposed structure of HA has been reported in the literature [227, 228] and it is shown in Figure 3-5.

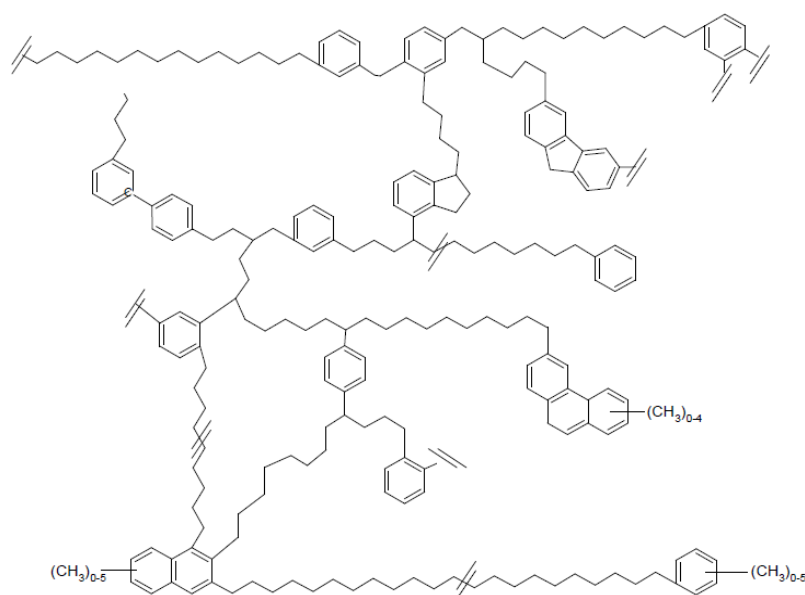


Figure 3-5 Proposed structure of HA. Adapted from [227]

Characteristics of HA such as molecular weight, radius and structure that are presented in the literature vary considerably depending on the source (soil or water)

and the method of extractions and purification. Commercial HA were shown to have different characteristics from natural HA [204]. However, properties such as charging behaviour and ion binding are believed to be less diverse as humic substances from various sources have similar functional groups from a physical point of view [229].

HA molecular weights reported in the literature vary from 3 to 100,000 g/mol [200, 203, 205] and molecular radii vary from fractions of nanometres to several hundreds of nanometres [230]. Even if HA are structurally stable, their molecular size varies in natural water, since they continuously undergo association and dissociation [231]. HA are insoluble at pH < 2 and most of their functional groups dissociates at pH > 4, so they become more negative with increasing pH [225, 229].

The structure of soil HA was found to be dependent on sample concentration, pH and ionic strength. At high concentration, low pH or high electrolyte concentration soil HA have been shown to behave like rigid spherocolloids with a small hydrodynamic radius, while at low sample concentration, high pH or low electrolyte concentration they behave as flexible linear colloids with a bigger hydrodynamic radius [232, 233]. These structural characteristics are believed to be applicable also to water HA and commercial HA [125, 153, 206, 234].

Commercial HA used in this study are peat-derived humic with molecular weights ranging from 4,000 to 20,000 g/mol [203, 229]. Further characteristics are reported in Table 3-2.

Table 3-2 Elemental composition and inorganic impurities of Aldrich Humic Acids

Composition	C	H	O	N	S	P	ash	Ref.
%	63.15	5.60	34.98	0.80	4.58	<0.05	31.21	[204]
Inorganic impurities	Al	Ca	Cr	Fe	Mg	Na	Si	Ref.
µg/g	2950	9931	15.2	12207	698	75116	3333	[205]

NOM has been traditionally removed with coagulation, granular active carbon and ion exchange resins, with rate of removals depending on the polarity and/or hydrophilicity of NOM. Conventional water treatment processes are ineffective in the removal of NOM with a molecular weight of less than 500 g/mol [200].

NF membranes can obtain good NOM removal via size exclusion and charge repulsions. HA retention between 80% and 100% is usually achieved, depending on the membrane MWCO and HA concentration in the feed [125, 153, 206, 207, 235]. At low pH, HA have a smaller size and lower charge and they are less retained by TFC NF membranes, whose charge is also lower at low pH, while at high pH HA retention increases [125, 235].

Aromatic/hydrophobic interactions between HA and the membrane also play an important role in HA retention [236]. Adsorption of HA to polymeric membranes is more favourable at low pH, since both HA and membrane are less negatively charged and HA are more hydrophobic, and minimum at high pH [125].

HA-membrane interactions affect membrane characteristics. HA in solution increased membrane negative charge in comparison with a solution containing NaCl only, due to electrostatic and hydrophobic interactions [24, 57, 125]. Membranes with different charges were shown to acquire a similar (negative) charge after HA filtration and it was inferred that the new charge reflected the zeta potential of the deposited HA layer [154, 235, 237]. Similarly, the contact angle measurements of different membranes fouled by HA showed similar values, indicating the deposit of a HA layer of intermediate hydrophobicity [65, 133, 161, 163].

Membrane MWCO has been shown to increase after HA filtration and fouling, as a result of increased membrane negative charge and consequent membrane swelling [49, 87, 133].

3.4.2 Manganese

Manganese is one of the most abundant elements on Earth, naturally occurring in water and food and introduced into the environment by anthropogenic activities such as manufacturing of iron and alloys, batteries, glass, fertilizers, fungicides and varnishes [17].

A small amount of manganese is necessary in the human diet and the World Health Organisation (WHO) estimates that the adequate manganese intake for adults is 2-3 mg per day resulting in a health-based guideline value for drinking water of 0.4 mg/L [17]. A concentration of manganese exceeding 0.1 mg/L creates problems of undesirable metallic taste and coloured water at the consumer tap and so the Scottish regulatory limit has been set to 0.05 mg/L [238]. Nevertheless, a recent paper [239] has criticised the WHO guideline value for manganese on the basis of studies linking exposure to manganese (at low concentrations of 0.1 mg/L) with intellectual impairments and neurotoxic effects in children [34, 35, 240]. Potential relationship between manganese concentrations (down to 0.3 mg/L), cancer death rates and infant mortality rates have been reported [241-243].

Speciation of manganese in natural waters is difficult to determine and various techniques, such as ion-selective electrodes, anodic-stripping voltammetry, differential pulse polarography, UF, dialysis, ion-exchange, nuclear magnetic spectrometry and electron paramagnetic resonance have been employed [213].

In natural water manganese can occur in three common oxidation states: +II, +III and +IV, but mixed oxidation states can also be present [213]. The dominant manganese species is Mn(II) which is present as soluble Mn^{2+} in acidic conditions. Mn^{2+} can precipitate as $MnCO_3$ at pH about 7.5 or as $Mn(OH)_2$ when pH > 11 and reducing conditions exist. $MnCO_3$ is more stable than $Mn(OH)_2$ under the conditions of most natural waters and it is therefore the most likely insoluble form of Mn(II) [214]. Mn(III) does not appear to be stable in natural water, unless Mn_3O_4 is produced [213]. Mn(IV) species can be obtained by oxidation of Mn(II), but the oxidation by

oxygen is very slow and it is very unlikely to occur without the addition of other strong oxidants (ozone, chlorine, potassium permanganate) [213, 214].

Field investigations have confirmed that in natural water the dominant manganese species is Mn^{2+} [244-246]. Crystal, Stokes and hydrated radii have been derived for Mn^{2+} [70] and are presented in Table 3-3.

Table 3-3 Crystal, Stokes and hydrated radii at 25 °C for Mn^{2+} [70]

Element	Crystal radius	Stokes Radius	Hydrated radius
Mn^{2+}	0.08 nm	0.368 nm	0.438 nm

Manganese is conventionally removed by filtration preceded by vigorous oxidation as part of the clarification processes. Oxidisation of manganese to its precipitated MnO_2 form is an autocatalytic process, requiring either strong oxidants (ozone, chlorine, or potassium permanganate) or dissolved oxygen and a catalyst (manganese ore or filter sand that has to be pre-treated with manganese ore). The process is difficult to start up, the filterability of MnO_2 is low and when the manganese concentration is higher than 5 mg/L too much solid is produced that shortens filtration cycles and makes the process unprofitable. Furthermore, process control is difficult for waters of variable quality, such as surface waters [247].

Conventional methods have proven to be insufficient for manganese removal, in particular in the presence of manganese concentrations higher than 5 mg/L and dissolved organic matter. The presence of NOM increases the coagulant demand and further decreases manganese removal by filtration [187, 247-250]. Natural and synthetic adsorbent have also been employed to remove manganese, but their efficiency is dependent on the sorbent material, manganese concentration, pH and temperature [251].

Removal of manganese, alone or with organic matter, by MF and UF has been investigated in several studies, as summarised in Table 3-4. Soluble manganese passes through MF and UF membranes and pre-treatments that precipitate

manganese are necessary to achieve effective removal. Strong oxidation has been shown to be the most effective pre-treatment but it increases the cost of the process, in both economical and environmental terms.

Table 3-4 Summary of manganese (Mn) removal studies with MF and UF membranes

Feed Water	Source	Process	Pretreatment	Mn Removal	Ref.
Mn	artificial	MF	aeration	not effective	[245]
			pH adjustment to 9.7	97%	
			H ₂ O ₂ + UV irradiation	not effective	
Mn	artificial	MF	H ₂ O ₂ + UV irradiation ay pH 9.3	95% after 50 h	[246]
			Mn sand	over 95%	
Mn	natural groundwater (GW)	MF	fluidised-bed with Cl ₂ oxidation	90%	[247]
			fluidised-bed with biological oxidation	87%	
			fixed-bed with biological oxidation	100%	
Mn and Fe	- artificial - natural (GW)	MF	oxidation + KMnO ₄	96%	[239]
Mn and Fe	artificial	MF/ UF	aeration	not effective	[248]
			KMnO ₄	not effective	
			ClO ₂	not effective	
			NaClO	90%	
Mn	artificial	UF	Polyacrylic acid dosed to form Mn complexes	Almost 100% at pH 9; 5% at pH 4	[160]
Mn	artificial	UF	None	14.7-17.4%	[249]
Mn and HA	Natural river water	MF	Biological oxidation	90% but bacteria not effective at water temperature < 5 °C	[250]
			Powdered Activated Carbon (PAC) + biological oxidation		
Mn and HA	artificial	UF	None	17- 38%	[249]
Mn, Fe and NOM	Dam water spiked with MnCl ₂ and FeCl ₂	UF	Chlorination (3 mg/L of Cl ₂)	31%	[251]

A limited number of studies have examined removal of manganese by NF membranes [165, 166, 252]. Lastra *et al.* [165] studied the removal of manganese, iron and organic content by NF from the effluent of a bleaching plant used in the pulp industry. NF was preceded by a chelating stage with an acetic acid based agent. Polymeric membranes gave almost complete retention of chelates of iron and manganese whereas ceramic membranes had 70-90% rejection. However, this research was specific to the effluent studied, which was characterised by TOC content 500 times higher than the average in natural waters and by a high temperature (80 °C). As a consequence, these findings can hardly be applied to drinking water treatment.

Molinari *et al.* [252] performed NF tests with tap water spiked with HA, nitrates, silica and Mn²⁺ at pH 7.2. HA retention showed an average of 40%, while average

Mn^{2+} retention was 80%. However, manganese and HA concentrations were up to 10 times higher than the average in natural waters and information on the tap water analysis and membrane characteristics was not provided, so removal mechanisms were not elucidated.

Potgieter *et al.* [166] tested NF membranes for removal of iron and manganese in the presence of dissolved organic matter in a South African river. Removal of manganese by NF membranes was around 65% and FeCl_3 and H_2O_2 were tested as pre-treatments. FeCl_3 and H_2O_2 together seemed to worsen manganese retention, while H_2O_2 alone gave better results. Nevertheless, manganese concentrations in the river water were very low (0.15-0.29 mg/L), probably approaching the instrument detection limit, thereby increasing the error in measurement of the membrane permeate composition. In addition, different samples with different solute concentrations were used, making results incomparable.

The Fyne process using NF PCI membranes has been reported to work satisfactorily for the removal of organic matter, manganese and iron in North America and Scotland [9, 196, 253]. However, the obtained removal rates were site and condition dependent and cannot be generalised.

A systematic study of the mechanisms of manganese removal by NF in the presence of HA as a function of speciation will be undertaken in Chapter 6, where the influence of solute-solute and solute-membrane interactions in manganese and HA removal will be investigated.

Manganese precipitates have been indicated as potential scalants for MF and UF membranes causing flux decline and loss of performance [247, 254-258]. Manganese was found, together with other organic and inorganics, on the fouling layer of a NF membrane, but its contribution to flux decline was not evaluated [259]. The impact of manganese on NF fouling and solute removal will be investigated in Chapter 9.

3.4.3 Endosulfan

ES, also known as Benzoepin, Endocel, Parrysulfan, Phaser, Thiodan, Thionex, is a organochloride insecticide of the cyclodiene group commonly applied to cereals, fruits, vegetables and cotton [260]. ES is transported to water bodies by surface runoff following rain.

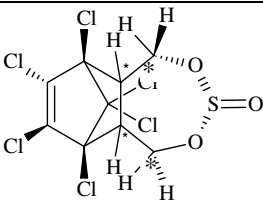
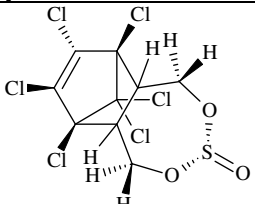
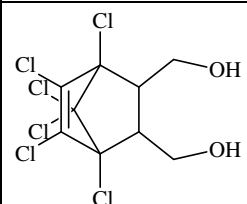
ES is extensively used worldwide and has been detected in surface water in several countries such as India, where it is one of the most common pesticides, Australia, Taiwan, Portugal, Greece, Canada, South America, China and Turkey [215, 224, 261-267]. ES has also been detected in air samples in regions far away from where it had been applied, for example in the Arctic Region, thus showing its persistence in the environment [216, 217].

ES is detected in natural water in concentrations ranging from 0.02 µg/L to 60 µg/L [262, 263, 265-267]. The regulatory limit for pesticides in Europe is 0.1 µg/L [268].

Due to ES high toxicity to terrestrial and aquatic species and the high hazard it poses to humans and the environment, since April 2011 it has been included in the list of Persistent Organic Pollutants (POP) by the Stockholm Convention, an international treaty that lists particularly dangerous pollutants whose use is to be restricted or banned. As a consequence, ES will be banned in 173 countries in 2012, joining the list of 21 other substances previously banned [269].

ES is commercially produced as a 7:3 isomeric mixture of α and β forms and it disperses in water with the same ratio [270]. ES isomers degrade by hydrolysis mainly to ES-diol and ES-sulphate. Formation of ES-diol is caused by chemical hydrolysis, favoured in alkaline conditions. ES-sulphate can only be formed in the presence of microbiological activity or strong chemical oxidants and it was not detected in synthetic water samples produced in the laboratory after eight weeks [261, 271]. For this reason the formation of ES-sulphate can be ruled out in the experimental conditions used in this research. Characteristics of α -ES, β -ES and ES-diol are presented in Table 3-5.

Table 3-5 Characteristics of Endosulfan isomers

	α-ES	β-ES	Endosulfan diol
			
Formula	C ₉ H ₆ Cl ₆ O ₃ S	C ₉ H ₆ Cl ₆ O ₃ S	C ₉ H ₈ Cl ₆ O ₂
Molecular Weight (g/mol)	406.93	406.93	360.88
Log K _{ow}	3.83 [272]	3.83 [272]	3.68 [273]
pK _a [273]	-	-	14.62–15.22
Dipole Moment [220]	1.02	3.18	Not available
Diffusion coefficient D _∞ (m ² /s) [274]	4.50 * 10 ⁻¹⁰	4.50 * 10 ⁻¹⁰	Not available
Henry's constant (Pa*m ³ /mol) [275]	0.72	0.04	1.3*10 ⁻⁴
Solubility in water (mg/L) [275]	0.45	0.51	300
Estimated Stoke radius (nm)	0.476	0.476	-

Note: Asterisk (*) on α -ES indicated the position of ¹⁴C label within the ES structure. Numbers in brackets refer to references where values used in this research were reported.

The Stokes radius r_s has been estimated from the diffusion coefficient using the Boltzmann equation:

$$r_s = \frac{k_b T}{6\pi\eta D_\infty} \quad (3.1)$$

where k_b is the Boltzmann constant, T is temperature, D_∞ diffusion coefficient of the solute in water and η is the liquid viscosity.

The hydrolysis rate K_h (hour⁻¹) of ES isomers in water can be expressed as [261]:

$$\alpha\text{-ES: } \log K_h = 0.895 \text{ pH} - 9.648 \quad (3.2)$$

$$\beta\text{-ES: } \log K_h = 0.800 \text{ pH} - 8.550 \quad (3.3)$$

The half life of α -ES and β -ES, that is the time required for 50% of the compound to disappear, can be calculated as follows [276]:

$$t_{1/2} = \frac{\ln 2}{K_h} \quad (3.4)$$

Using equations 3.2-3.4 the degradation of ES isomers to ES-diol can be determined as a function of pH (Figure 3-6). At pH > 8 α -ES and β -ES have a half life of less than 10 hours, therefore ES-diol can be considered the dominant form of ES in solution after 20 hours.

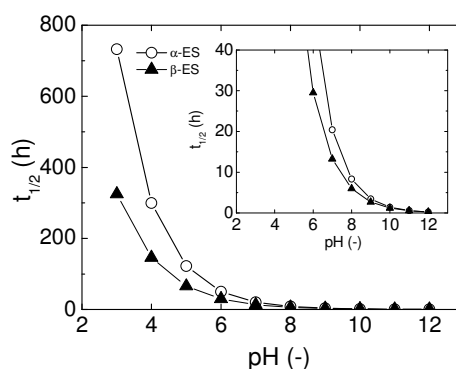


Figure 3-6 Half life of α -ES and β -ES as a function of pH – from equations developed by [261]

Pesticides are difficult to remove from water because of the low concentrations in which they are present. Conventional treatments, i.e. flocculation, coagulation and filtration, are not sufficient for pesticide removal and pre-oxidation, usually using ozone, is required to achieve desired standards [277]. Filtration by activated carbon is commonly used for pesticide removal but the presence of NOM can lower treatment efficiency. Concentration of NOM is usually much higher than the concentration of pesticides and it occupies the whole adsorption capacity of the activated carbon columns, increasing their regeneration frequency and therefore the treatment costs [191].

NF has achieved satisfactory removal of pesticides and other micropollutants [7, 13, 22, 23, 47]. To the best knowledge of the author, ES retention by NF has never been evaluated. Various authors [22, 23, 72] have developed methodologies to predict

micropollutant removal on the basis of known parameters but prediction remains only qualitative. The lack of precision has been attributed to the use of a limited set of parameters for predicting retention [22]. A better knowledge of micropollutant removal mechanisms by NF will contribute to improved removal prediction.

Micropollutant removal by NF is influenced by size exclusion, charge repulsion and hydrophobic-hydrophobic interactions. As a rule of thumb, micropollutants of larger size (MW, width or length), higher hydrophilicity and/or higher charge are well rejected by NF [71, 72]. As explained before (Section 2.2.2), hydrophobic micropollutants like ES adsorb on polymeric membranes and retention is overestimated if membrane saturation is not reached [91-93]. Removal mechanisms of hydrophobic micropollutants are not well understood after adsorption equilibrium has been reached [87] and further studies are required.

The influence of solute-solute interactions, solute-membrane interactions and pressure on ES removal in the presence of HA will be investigated in Chapters 7 and 8. In Chapter 9 the impact of Mn deposits on ES removal will be elucidated.

3.5 Conclusions

The review of NF principles and mechanisms carried out in Chapter 2 highlighted the need to study the contributions of solute-membrane interactions and solute-solute interactions to solute retention and transport through NF. In particular, the role of inorganic-NOM interactions and micropollutant-NOM interactions in NF requires thorough investigation. The review also highlighted the lack of studies on the impact of scaling on NF flux and solute retention, especially for micropollutants.

The review of water quality in Scotland carried out in Section 3.2 identified NOM and manganese as contaminants of interest. Both are ubiquitous in Scottish waters and manganese exceeded the regulatory limits in the outlet of conventional treatment plants more than other inorganics such as iron and aluminium. Herbicides were also identified as a growing concern in the eastern part of Scotland.

As a result of this review, manganese was chosen as a model inorganic contaminant and the herbicide ES was chosen as a model micropollutant for the purposes of this study. Commercial HA were selected as representative of the highest fraction of NOM, since the hydrophobic fraction of NOM is usually dominant in upland waters. The use of commercial HA overcomes the drawback of difficult comparison between the results in the literature where scarcely characterised NOM are employed. However, the other fractions of NOM, such as hydrophilic components, might influence solute-solute interactions and solute-membrane interactions, limiting the application of the results of this study to upland waters. Sometimes conventional methods have proven to be insufficient for manganese removal and studies on manganese retention mechanisms in the presence of HA by NF are lacking. Moreover, manganese precipitates at pH above 8 allowing the study of the effect of scaling on membrane performance. ES was chosen because it is hydrophobic, neutral over a large pH range and forms complexes with NOM, making it a suitable compound for the investigation of the role of solute-membrane and solute-solute interactions. Moreover, ES is extensively used worldwide, extremely toxic and its removal by NF has never been investigated.

4. Materials and Methods

4.1 Introduction

This chapter will describe the chemical solutions, analytical equipment and experimental equipment used in this project. Reference to this chapter will be made throughout the following chapters.

The work carried out in this study has employed artificial water to which known quantities of solutes were added. The analytical equipment used for the analysis of the solution, the organic and inorganic solutes and the radiolabeled ES will be presented. Equipment employed for characterizing the membranes will be depicted. The experimental equipment used during the work, stirred cells and diffusion cells, will be described together with the experimental protocol. Experimental protocols specific to particular experiments will be detailed in the respective chapters. The negligible-depletion solid phase micro-extraction (nd-SPME) methodology developed by Neale *et al.* [278] will be described. The characteristics of the membrane used in this work will be presented.

4.2 Chemicals and background solutions

All solutions were made in ultra-pure water obtained by PuraLab Ultra (Elga LabWater, UK), if not otherwise specified. All chemicals were of analytical grade.

HA were purchased from Sigma Aldrich UK and stock solutions containing 250 mgC/L were conserved in glass bottles in the fridge in the dark for one week maximum. HA concentration used in the experiments ranged from 5 to 250 mgC/L. While concentrations of 5-12.5 mgC/L represent typical NOM concentrations found in natural water [207, 226], experiments with higher HA concentration were performed to study the mechanisms of formation of ES-HA complexes [279].

Manganese was purchased as MnCl_2 from Fisher Scientific, UK. Manganese stock solutions of 10 g/L were acidified at $\text{pH} < 2$ with nitric acid (Aristar VWR

International, UK) and conserved in glass bottles in the fridge for two weeks maximum. Manganese was used at a concentration of 5 mg/L, as it is the typical concentration found in Scottish water (Section 3.2). Concentrations up to 1,500 mg/L were used to simulate fouling conditions in the laboratory (Chapter 9).

Radiolabeled [2,3-¹⁴C] ES (>95% purity; 18.5 MBq solid form) was purchased from the Institute of Isotopes Co., Ltd. (Hungary). Radiolabeled ES was employed due to ease of detection with the liquid scintillation counter at very low concentrations (up to 0.1 µg/L). Moreover, the position of the ¹⁴C label in the ES structure (Table 3-5) allowed the detection of ES irrespectively of the isomer formed (α-ES, β-ES and/or ES diol), although individual identification was not possible. Since detected concentration of ES in natural water ranges from 0.02 µg/L to 60 µg/L [262, 263, 265-267], 10 µg/L was chosen as ES feed concentration. Due to the low solubility of α-ES and β-ES in water (Table 3-5), stock solutions of 10 mg/L were prepared in ethanol (C₂H₅OH, Fisher Scientific, UK) and intermediate stock solutions of 100 µg/L were prepared in methanol (CH₃OH, Fisher Scientific, UK) and conserved in glass bottles in the fridge for 6 months maximum. Feed solutions (10 µg/L) were prepared in ultra-pure water the day before the experiments were conducted (Section 7.2).

Electrolyte background solution consisted of 1 mM NaHCO₃ and 20 mM NaCl [207], both supplied by Fisher Scientific, UK. pH was adjusted with 1M HCl and NaOH (Fisher Scientific, UK).

Calcium was purchased as CaCl₂ from Fisher Scientific, UK. A concentration of 2.5 mM (278 mg/L) of CaCl₂ was used in fouling experiments, since this concentration was shown to increase fouling of NF membranes by HA [207]. Feed solutions were prepared from acidified stock solutions containing 50 mM (5.56 g/L) of CaCl₂ and conserved in the fridge in glass bottles for one week maximum.

Inert organics for membrane MWCO and pore size determination consisted of 25 mgC/L of dioxane, dextrose PEG 400, PEG 600, PEG 100 (Fisher Scientific, UK)

and xylose (Acros Organics, UK) prepared in stock solutions of 10 gC/L and conserved in glass bottles in the fridge for one week maximum.

4.3 Analytical Equipment

4.3.1 pH and conductivity meters

pH and conductivity of the solution were measured with a pH/conductivity 340i meter (WTW, Germany). The pH probe was calibrated every day with pH buffer solutions at pH 4, 7 and 10 (Fisher Scientific, UK) and the conductivity meter was calibrated when required with 0.01 M KCl (Fisher Scientific, UK). When only NaCl was used, conductivity measurements were used for determining NaCl concentration and the following relationship between conductivity and NaCl concentration was developed:

$$\text{NaCl [M]} = 0.011 \times \text{Conductivity [mS.cm}^{-1}\text{]} \quad (r^2=0.999) \quad (4.1)$$

The detection limit for NaCl was 0.01 M.

4.3.2 Inductively-coupled plasma optical emission spectroscopy

Analysis of manganese and sodium was performed with an inductively-coupled plasma optical emission spectroscopy (ICP-OES) instrument (Perking Elmer Optima 5300 DV, UK). Samples for inorganic analysis (10 mL in volume) were acidified with nitric acidic (Aristar VWR International, UK) at pH<2 and conserved in polyethylene centrifugal vials in the fridge for a maximum of three months. ICP-OES calibration standards were made using ICP multi-element standard and manganese standard (Merck, Germany) and verified using a certified reference material, ICP multi-element standard solutions VI (CertiPUR, Germany). Calibration curves were performed before each analysis. The detection limit for Mn was 0.01 mg/L and for Na was 0.5 mg/L. Maximum concentration for the inorganics was 300 mg/L, therefore samples with higher concentrations were diluted with ultrapure water prior to analysis. No dilution was required for the experiments carried out in Appendix 1. For the fouling experiments in Chapter 9, a ten time dilution for Mn and a hundred

time dilution for Na were required since solute concentration in the samples was higher than the maximum detection limit.

4.3.3 Total organic carbon analyser

The concentration of organic solutes was measured with a TOC V_{CPH/CPN} Shimadzu analyser in a non-purgeable organic carbon mode. The high sensitivity mode was employed for the analysis of inert organics. Samples for TOC analysis (20 mL in volume) were collected in glass vials and analysed the same day of collection. Calibration standards were prepared using potassium hydrogen phthalate (Acros Organics). Calibration curves were performed each time the catalyst was substituted (about every 6 months). The detection limit for the TOC was 0.1 mgC/L, while when the high sensitivity mode was employed detection limit reduced to 0.01 mgC/L. In order to avoid sample carry over, a maximum TOC concentration of 20 mgC/L was analysed. Samples with higher concentrations were diluted ten times with ultrapure water.

The oxidation efficiency for HA was determined to be 69.7%, due to chemical properties of the humic substances (Figure 4-1). The concentrations of HA reported in this study are the concentration measured by the TOC analyser in mgC.L⁻¹.

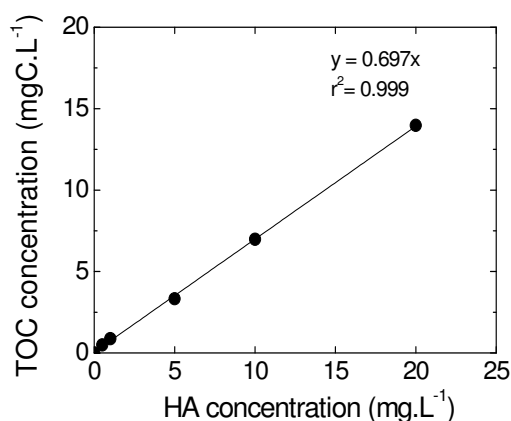


Figure 4-1 TOC efficiency for HA

4.3.4 UV-visible spectrophotometer

Ultraviolet absorbance of HA was measured at a wavelength of 254 nm with an Ultraviolet Visible (UV-Vis) Spectrophotometer Cary 100 (Varian). Samples (3 mL in

volume) were collected in glass vials and analyzed within a few hours from collection. Ultraviolet absorbance measures the aromatic part of HA [207].

When radiolabeled ES was employed in the experiments, it was not possible to determine the concentration of HA with the TOC analyser, due to the methanol present in the ES stock solution. The concentration of HA was estimated by measuring the UV absorbance and the following relationship between UV absorbance and HA concentration was established:

$$\text{HA [mgC/L]} = 23.544 \times \text{Absorbance [cm}^{-1}\text{]} \quad (r^2=1) \quad (4.2)$$

Detection limit for HA was 0.1 mgC/L and maximum HA concentration analysed was 50 mgC/L. Samples with higher concentrations were diluted ten times with ultrapure water.

4.3.5 Liquid scintillation counter

The activity of ES radiolabeled with carbon (^{14}C) was measured with a liquid scintillation counter (Beckman LS 6500, USA). 1mL of sample was analysed in glass scintillation vials containing 7 mL of scintillation liquid (Ultima Gold LLT, UK). Each sample was counted in triplicate with a counting time of 10 minutes and counting precision was set at 2% in the counter [280]. Detection limit for ES was 100 ng/L. The instrument was calibrated every time a new stock solution was prepared to establish a relationship between activity (disintegrations per minute, dpm) and concentration.

The presence of coloured HA can affect the detection of the activity as colour adsorbs the light emitted by the liquid scintillation cocktail. The relationship between activity and ES concentration was determined at different concentrations of HA, as indicated in Figure 4-2.

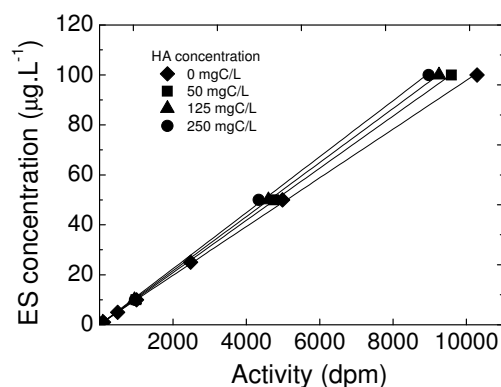


Figure 4-2 Relationship between activity and ES concentration as a function of HA concentration.

4.3.6 Contact angle measurement

The hydrophobicity of the membranes was determined by measuring membrane contact angle with the sessile drop method [63] using two instruments, Easy Drop Kruss (Germany), located at Imperial College London (UK) and CAM 100, KSV Instrument Ltd (US), located at ITM-CNR (Italy). The sessile drop method measures the contact angle of air dried membranes and it might not be fully representative of the contact angle of membranes in water, as polymers change their surface energy depending on the surrounding medium. Furthermore, results might be affected by contamination of the membrane specimen by hydrophobic components present in the air and evaporation from the water droplet. It has been shown that the sessile drop method overestimates the membrane contact angle, hence its hydrophobicity, with respect to the captive bubble method, that measures the contact angle of the membrane in water [63].

Virgin membranes were rinsed thoroughly and soaked in deionised water for 24 hours prior to measurement. The membranes were then left to dry for at least 8 hours at room temperature to ensure that the results were not affected by the degree of dryness of the membrane [63]. At least three measurements per membrane were taken.

Contact angles were also measured for compacted membranes through which solutions of ultrapure water, HA, HA + Ca, Mn, Mn + HA and Mn + Ca + HA were filtered. After the filtration experiments, the membranes were conserved in the fridge and let dry for at least 8 hours at room temperature prior to measurement. At least three measurements per membrane were performed and in the case of membranes that presented zones of different colour, measurements were repeated in triplicate for different zones.

The membranes were glued to a glass holder to obtain a perfect plane surface. A pure water drop was placed onto the membranes and it was photographed within 15 seconds and then every minute for at least 6 minutes to automatically calculate the contact angle with a goniometer. The contact angle decreased with time (Figure 4-3). This was mainly attributed to the evaporation of the water drop, as a decrease was also observed for a very hydrophobic PTFE surface.

For TFC-SR3 the decrease with time was higher than for the other membranes (results repeated six times) and it was inferred that adsorption of the water droplet to the membrane occurred.

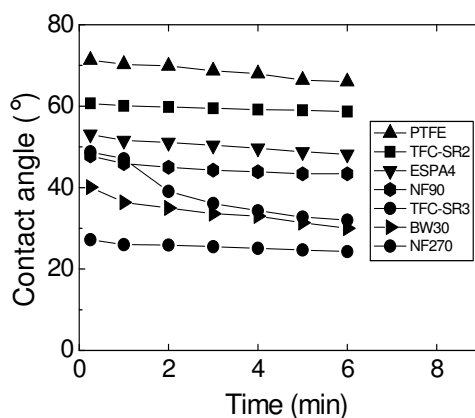


Figure 4-3 Contact angle of nanofiltration membranes versus time

4.3.7 Zeta potential measurement

The charge of the membranes was determined by measuring the membrane zeta potential (Section 2.2.1). Zeta potential can be measured with several techniques and streaming potential is widely recognised as the most suitable for membrane surfaces

[58]. The streaming potential was measured using an electrokinetic analyser EKA, Anton Paar KG (Austria) located at Imperial College London (UK). The streaming potential method only provides semi-quantitative values of membrane charge since results depend on the methodology employed for the measurements [281]. Therefore in this work the zeta potential measurements are not considered as absolute values but discussed relatively to each other.

The membrane zeta potential ζ was calculated from the streaming potential measurements using the Helmholtz- Smoluchowski equation [282]:

$$\zeta = \frac{U}{\Delta P} \frac{\eta}{p p_0} \frac{\ell}{r q} \quad (4.3)$$

where U is the streaming pressure measured by the electrodes, ΔP is the induced pressure between the membrane samples, η is the liquid viscosity, p is the liquid permittivity, p_0 is the permittivity of the vacuum, ℓ and q are the length and cross-sectional area of the channel and r is the electric resistance.

ℓ , q and r were calculated by the Fairbrother-Mastin equation [283]:

$$\frac{\ell}{r q} = \kappa \quad (4.4)$$

where κ is the specific conductivity of the electrolyte solution.

The streaming potential measurements were performed using the protocol developed by Elimelech *et al.* [57, 58]. Virgin membranes were rinsed thoroughly and soaked in deionised water for 24 hours prior to measurement before being cut in two pieces (7.5 cm x 2.5 cm) and being left in a beaker containing the electrolyte solution for 30 minutes. The same electrolyte solution as in the filtration experiments was used (was 20 mM NaCl, and 1 mM NaHCO₃) since membrane charge is dependent on the conductivity of the solution with which it comes into contact [57]. After assembling the membrane pieces in the measuring cell, the system was flushed first with ultra-pure water for 3 minutes, then with the electrolyte solution for 30 minutes, taking care of removing all the air bubbles from the cell. The pH of the electrolyte solution

was adjusted automatically from 3 to 12 by the instrument autotritator and six measurements were taken for each pH value, three in each direction.

4.3.8 Atomic force microscopy

The roughness of the membrane was estimated with an atomic force microscopy (AFM) instrument (Bruker Corporation, formally Veeco, USA). Measurements were performed in a tapping mode [284] with a silicon probe (Mikromasch CSC38/AIBS type B). The probe had a spring constant of 0.01-0.08 N/m, a resonant frequency of 7-14 kHz, nominal tip radius of 10 nm and cantilever length of 350 μm . Virgin membranes were rinsed thoroughly and soaked in deionised water for 24 hours prior to measurement. Four measurements per membrane were performed.

The roughness analysis considers that the membrane surface occupies a mean x-y plane area, which in this study had size 2.0 x 2.0 μm . The size of the scanned area is very important in determining the roughness, since the larger the area the larger the roughness [284]. The cantilever tip measures the relative height z at each x, y location.

The parameters chosen for determining membrane roughness were the average roughness, R_a , and the root-mean square roughness, R_q . R_a is the average of the measured z-values, while R_q describes the standard deviation of the z-values. R_q is considered the most accurate measure of roughness since R_a takes less into account the roughness at low frequencies [284]. Hoek *et al.* [285] showed that for NF membranes a relationship between R_a and R_q existed: R_q values increased in the same order as R_a values and they were larger than R_a values. In this study both parameters will be reported.

4.3.9 Scanning electron microscopy

Images of the membrane surface and cross-section were obtained with scanning electron microscopy (SEM), using a Quanta FENG 200 (FEI Company, US) microscope located at ITM-CNR (Italy). An accelerating voltage of 12.5 kV and

magnification of 50,000 were used for the images of the membrane surface, while a magnification of 1,000 was employed for the cross section.

Compacted membranes through which solutions of ultrapure water, HA, HA + Ca, Mn, Mn + HA and Mn + Ca + HA were filtered were conserved in the fridge and let dry for at least 48 hours at room temperature prior to measurement. Membrane samples were prepared by freeze fracturing the membrane coupons in liquid nitrogen.

Membrane thickness was measured from the cross-section images using the image processing program ImageJ developed by the US National Institute of Health (<http://rsbweb.nih.gov/ij>). At least 3 measurements per cross section were performed.

Solute deposits on the membrane were characterised with SEM in a back scattering electron (BSE) mode (Cambridge Stereoscan 360, UK) and by coupling SEM with energy dispersive X-ray spectroscopy (EDX or EDS) employing a Philips EDAX analysis system.

The BSE mode visualizes the presence of solutes of different atomic weights deposited on the membrane [286]. Solute with low atomic weight appear dark in the SEM image, while solutes with higher atomic weight (such as manganese) appear clearer.

The chemical composition of the inorganic deposits was analysed with the EDX technique. By determining the energies of X-rays emitted by the area excited with the electron beam, this technique offer a semi-qualitative chemical analysis of the inorganic solutes deposited on the membrane. EDX is performed on the membrane surface, so information on the spatial distribution of the solutes is not available [287]. For this reason, in this study the information obtained with EDX was analysed together with SEM-BSE.

4.3.10 Infrared spectroscopy

Characterisation of membranes was performed with a Fourier transformed infrared (FTIR) spectrophotometer (Spectrum One, Perkin Elmer, US) equipped with an attenuated total reflectance (ATR) device with a micrometer torque and a Diamond/ZnSe crystal as internal reflection element, located at ITM-CNR (Italy). ATR-FTIR provides semi-quantitative information on the functional groups of the membrane layers, mainly at the surface [288].

Compacted membranes through which solutions of ultrapure water, HA, HA + Ca, Mn, Mn + HA and Mn + Ca + HA were filtered were conserved in the fridge and let dry for at least 48 hours at room temperature prior to measurement. An average of 30 scans in the range of $650 - 4000 \text{ cm}^{-1}$ wavelength was performed for each membrane. The depth of penetration was up to $1.66 \mu\text{m}$, therefore both active layer and support layer were reached, and the spectra were recorded at a resolution of 4 cm^{-1} .

ATR-FTIR characterisation returns spectra of the polymeric layers of the membrane in which peaks obtained at certain wavelengths correspond to functional groups. Changes in chemicals bonds due to the presence of deposited solutes can be investigated [289].

4.4 Experimental equipment and protocol

4.4.1 Stirred cells

Filtration experiments were performed with a custom-made apparatus consisting of three “dead-end” stainless steel stirred cells operating in parallel (Figure 4-4). Stirred cells were selected because they allow performing experiments in controlled conditions for filtration, at the same time reproducing the hydrodynamic conditions of full-scale spiral wound membrane modules [290].



Figure 4-4 Stirred cell apparatus used for filtration experiments

Each cell had a volume of 990 mL and a diameter of 70 mm, resulting in a membrane area of 38.5 cm^2 (Figure 4-5). The membrane coupon was mounted at the bottom of the cell and the cell was filled with feed solution and tightly closed with clamps. The cell was pressurised with filtered air; the pressure was kept constant during the whole duration of the experiment and automatically measured with a pressure transducer (Omega Engineering, UK). Temperature inside the cell was measured with a thermocouple (Omega Engineering, UK) and the permeate was collected in beaker seating on an electronic balance (Advancer Pro, Ohaus, UK). Pressure, temperature and permeate weight were automatically measured every minute and the data collected on a PC using LabView 8.0 (National Instruments, UK).

The feed solution was constantly stirred with a plastic stirrer (Millipore, UK) guided by a digital magnetic stirrer plate (Fisher Scientific, UK) on which the cell was placed. The stirring speed, corresponding to the crossflow velocity of membrane modules, was kept at 300 rpm in all experiments to minimize concentration polarisation.

In all filtration experiments carried out in this study, the membrane coupons were cut the day before from a flat sheet batch, thoroughly rinsed with ultrapure water to wash the preservative away, and left overnight in ultrapure water to allow the polymer to swell.

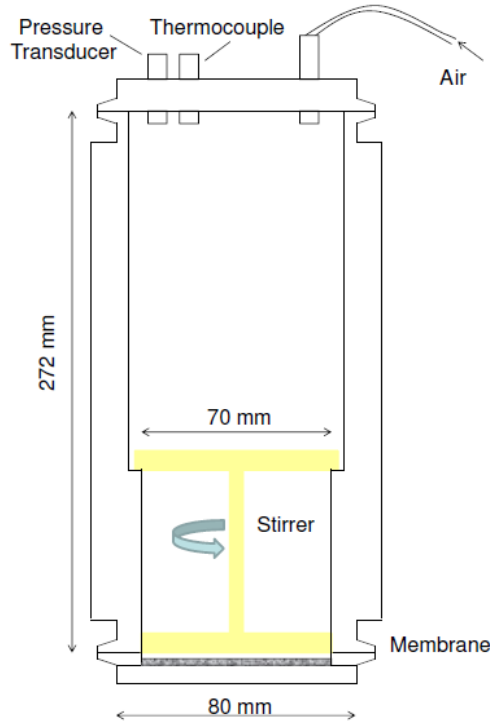


Figure 4-5 Schematic of the stainless steel stirred cell used in this work. (not to scale)

One batch flat sheet membrane was employed per set of experiments, since different batches can have slightly different characteristics. A new membrane coupon was used for each experiment.

The membranes were compacted for an hour at a pressure 3 bar higher than the pressure used during the experiments up to 15 bar, that was the maximum pressure obtainable with the apparatus (see Appendix 2). Flux of ultra pure water was measured for half an hour before and after the experiments at the same pressure employed during the experiments, to check changes in membrane permeability during solute filtration due to fouling.

Experimental protocols for the filtration of specific solutes and fouling experiments will be detailed in the respective chapters.

4.4.2 Diffusion cells

Diffusion experiments, whose results are presented in Chapter 8, were performed in custom-made diffusion cells (Figure 4-6) to determine diffusion coefficient of pesticide ES through NF membranes.

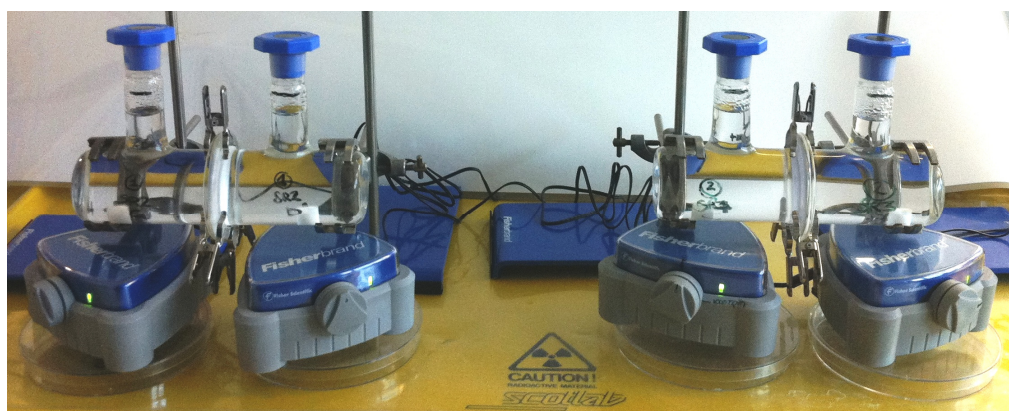


Figure 4-6 Diffusion cells for pesticide ES diffusion experiments through NF membranes

Each diffusion cell consisted of two glass chambers of 250 mL volume with the membrane separating the feed from the permeate side (Figure 4-7). The membrane area in the cell was 19.6 cm^2 . To study ES diffusion through the membrane, the feed cell was filled with a solution containing ES and background electrolyte while the permeate cell was filled with ultrapure water and background electrolyte only.

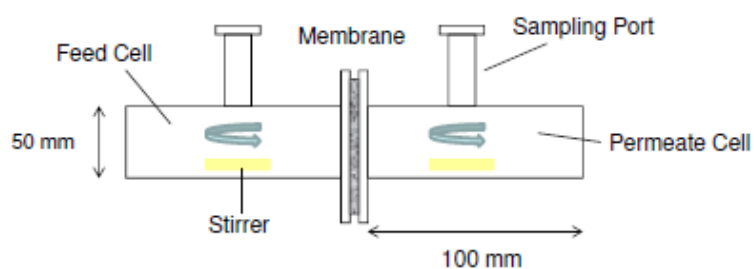


Figure 4-7 Schematic of the diffusion cell used in this work. Not to scale.

The model used for the determination of the diffusion coefficient in the membrane D_m is derived from the Fick's law [116]

$$C_F(t) - C_P(t) = [C_F(t_0) - C_P(t_0)] \exp \left[-A_m * \frac{D_m}{\Delta \delta_m} \left(\frac{1}{V_F} + \frac{1}{V_P} \right) t \right] \quad (4.5)$$

where C_F and C_P are the solute concentration in the feed and permeate cells respectively, V_F and V_P are the volumes of the feed and permeate, A_m is the membrane area and $\Delta \delta_m$ is the membrane thickness (active layer and support layer).

Equation 4.5 is based on the following assumptions [291]:

- The main force driving solute transport through the membrane is the solute concentration gradient between the two cells. Additional effects such as concentration polarisation and flow resistances are not considered.
- Membrane cells are fully mixed.
- D_m is constant with concentration in the range of concentrations used in this study.
- The amount of solute adsorbing to the membrane is negligible with respect to the amount in the cells. If the amount of solute adsorbed to the membrane is not negligible a non-stationary model that can only be integrated numerically should be adopted [291].
- The phenomenon of diffusion coupling is negligible. Since water is soluble in the membranes, a concentration gradient of solutes across the membrane causes a corresponding concentration gradient of water in the opposite direction, causing diffusion coupling between the solute and the water inside the membrane [291].

The main errors in the determination of D_m are (apart from errors in measuring the thickness of the membrane, the cell volume and solute concentration in the cells) the presence of concentration polarisation, adsorption of solute to the membrane and diffusion coupling.

In order to avoid concentration polarisation at the membrane surface, both feed and permeate solutions were stirred with a magnetic stirrer (Fisher Scientific, UK) at 1000 rpm for the whole duration of the diffusion experiments.

Before being mounted in the diffusion cells the membranes were compacted with ultrapure water and saturated with ES in the stirred cells. By compacting the membrane the swelling due to water solubility in the membrane should be limited, limiting the diffusing coupling effect. By pre-saturating the membrane the amount of solute adsorbed to the membrane during diffusion experiments should be negligible, allowing the use of the stationary diffusion model.

Six samples of 1 mL each were taken from the feed and the permeate solution at regular intervals up to 121 hours. The total sample volume withdrawn from each cell (6 mL) was small with respect to the total cell volume (250 mL), so the error due to change in solution volume was deemed negligible.

Diffusion experiments were performed simultaneously for the two NF membranes employed in this study to limit the influence of temperature on the diffusion coefficients.

The diffusion coefficient was calculated by determined the slope $\frac{D_m}{\Delta\delta_m}$ of the linear fitted line:

$$\log\left(\frac{C_F(t) - C_P(t)}{C_F(t_0) - C_P(t_0)}\right) = -\frac{D_m}{\Delta\delta_m}\left(\frac{1}{V_F} + \frac{1}{V_P}\right)A_m * t \quad (4.6)$$

where $\Delta\delta_m$ was determined by SEM measurements (Section 4.3.9)

4.5 Speciation modelling

Modelling of the speciation of manganese and the formation of manganese and HA complexes as a function of pH (Chapter 5) was performed with the programme Visual MINTEQ 2.5 [292].

The software, available free from the internet [293], models equilibria among dissolved, adsorbed, solid and gas species in dilute aqueous systems using an extensive thermodynamic database. Solute saturation indexes are taken into account, making it possible to model solid precipitation.

Modelling was carried out for the experimental conditions used in Chapter 5: manganese concentration of 5 mg/L, HA concentration of 5 mgC/L, 21 mM of background electrolyte, pH from 4 to 12.

4.5.1 Manganese speciation

During the filtration experiments, the stirred cell solution was pressurized with air, increasing the dissolved oxygen content of the feed solution and the partial pressure of CO₂ in the air above the solution. This is expected to affect the speciation of the carbonates species in solution and in particular their precipitation. As a consequence, speciation was performed both at atmospheric pressure (1.01 bar) and at the pressure of 5 bar used during the filtration experiments.

Mn(II) was assumed to be the only oxidation state at which manganese was present during the filtration experiments. Redox of MnCl₂ to Mn(IV) was not considered to occur during the experiments, despite the presence in the stirred cells of dissolved oxygen at concentrations higher than in a solution in equilibrium with the atmosphere. The oxidation reaction of Mn(II) into Mn(IV) is very slow (several hours) in absence of catalytic effects, and aeration alone has been shown to be insufficient to precipitate manganese as MnO₂, the dominant form of Mn(IV) [213, 214].

Mn²⁺ may precipitate as MnCO₃ (Rhodochrosite) and Mn(OH)₂ (Pyrochroite) [214]. The formation constant K and enthalpy constant H used in Visual MINTEQ 2.5 for the considered species are presented in Table 4-1.

Table 4-1 Formation constant and enthalpy constant used in the speciation modelling [294]

Specie	Log K	H (kJ/mol)
MnOH ⁺	-10.5970	55.8100
MnHCO ₃ ⁺	11.6290	-10.6000
OH ⁻	-13.9970	55.8100
H ₂ CO ₃ (aq)	16.6810	-23.7600

HCO ₃ ⁻	10.3290	-14.6000
Mn(OH) ₂ (s)	15.194	-97.0099
MnCO ₃ (s)	-11	-1.88

4.5.2 Manganese and humic acids complexation

Modelling the complexation of metals with HA presents several difficulties, due to the heterogeneous and complex nature of humic binding sites, the competing binding of protons, since they interact with the same sites as metals ions, and the presence of electrostatic interactions [295].

Commonly used complexation models are Model V/VI and VI-S, NICA-Donnan Model and Stockholm Humic Model [295-299].

The NICA-Donnan Model present in Visual MINTEQ 2.5 was chosen in this study since it has been extensively validated over experimental data for several elements, such as H⁺, Ca²⁺, Cd²⁺, Cu²⁺, Pb²⁺, Al²⁺ [299-302] and Fe³⁺ [303, 304].

The NICA-Donnan model is composed of two sub-models. The NICA sub-model simulates the specific binding of NOM and metals by using two binding functions corresponding to the carboxylic and phenolic groups of HA. A continuous distribution of binding site types is assumed. The Donnan sub-model simulates non-specific binding due to the electrostatic forces caused by the net negative charge of dissociated carboxylic and phenolic groups. The organic matter is considered as a gel phase with homogenous charge and homogenous potential distribution and counter-ions are assumed to accumulate in the gel volume.

The two sub-models are interrelated, as the concentration of ions accumulated electrostatically competes with the ions bound specifically, and they are employed simultaneously. Detailed description of the NICA-Donnan model can be found in the literature [295, 299].

Since specific experimental data with manganese and HA were not available in the literature, NICA-Donnan model parameters derived by Milne *et al.* [305] were used. Manganese parameters were estimated using the variation of the hydrolysis behaviour as an indication of the likely binding capacity of humic substance [305]. These parameters can be used as a starting point for general speciation modelling and they were deemed accurate enough for the scope of this study.

Also for the modelling of Mn-HA complexes, the formation of Mn(IV) species has not been considered. Moreover, natural organic matter lowers the redox intensity pE of the solution and in turn the likelihood of any oxidation of Mn (II) to Mn(IV) [212, 214].

4.6 Solid-phase micro-extraction

The formation of complexes between ES and HA was quantified with the nd-SPME methodology developed by Neale *et al.* [278].

nd-SPME is a technique that measures the freely dissolved concentration of a micropollutant in a water matrix by determining, at equilibrium, the micropollutant uptake to a fibre [306]. nd-SPME uptake depends on the affinity of the compound for the fibre coating and on the compound's hydrophobicity [307].

nd-SPME has been used to evaluate the interactions between organic micropollutants and NOM and determine the partition coefficient K_{oc} between dissolved organic carbon and water for various micropollutants [278, 308-312]. The determination of K_{oc} is based on the valid assumption that only the micropollutant freely dissolved and not the fraction bound to the organic matter is measured by the fibre [313].

Several conditions must be verified in order for nd-SPME to give reliable results: equilibrium must be reached, the micropollutant must not be depleted and the matrix in the sample must not interfere with the fibre [306, 307, 314]. In particular, if the micropollutant is depleted, accurate measurements of the freely dissolved concentration can be prevented [315].

SPME has been largely employed as a technique for extracting organic micropollutants from aqueous solution to be analysed by gas chromatography (GC) and high-performance liquid chromatography (HPLC) [316]. Both polydimethylsiloxane (PDMS) and polyacrylate (PA*) fibres have been used for ES extraction [317-321]. In this study PA* fibres were chosen to allow the comparison of results with the work by Neale *et al.* [278].

PA* fibres with a fibre coating thickness of 34.5 μm bought from Polymicro Technologies (Phoenix, US) were cut in 5 cm length to obtain a volume of the fibre V_{fb} of 0.77 μL . Further fibre characteristics can be found in Neale [168].

4.6.1 Fibre calibration and determination of K_{fw}

The SPME fibres were calibrated to establish the time necessary to reach equilibrium and calculate the fibre-water partition coefficient K_{fw} for ES as a function of pH.

Seven PA* fibres, 10, 25, 50, 100 $\mu\text{g/L}$ of radiolabeled ES and background electrolyte (1mM NaHCO_3 and 20 mM NaCl) were put in 100 mL solutions adjusted at pH from 4 to 12. The solutions were sampled before introducing the fibres to determine the freely dissolved ES concentration before the extraction m_{TOT} . The solutions were shaken at 200 rpm at 25 $^\circ\text{C}$ in a Certomat BS-1 incubator shaker (Sartorius Germany). At time intervals 0.5, 1, 2, 5, 8, 24, 33, 48, 96 and 146 hours a fibre was extracted with tweezers, cut into three pieces, added to a scintillation vial with 7 mL of scintillation cocktail, manually shaken and left to desorb overnight before being analyzed to determine the mass of ES on the fibre (m_{fb}) by liquid scintillation counter (Section 4.3.5). Control solutions without fibres were also sampled at the same time intervals to establish ES adsorption to the glass.

A kinetic approach was used to quantify K_{fw} at equilibrium

$$K_{fw} = \frac{C_{fb}}{C_w} = \frac{m_{fb}}{m_w} \times \frac{V_w}{V_{fb}} \quad (4.7)$$

where C_{fb} ($\mu\text{g/L}$) is the concentration of ES in the fibre, C_w ($\mu\text{g/L}$) is the concentration of freely dissolved ES in aqueous solution, m_w (μg) is the mass of

freely dissolved ES in aqueous solution as sampled from the solution at the end of the fibre experiments and V_W (L) is the volume of the aqueous solution.

The uptake experimental curve was used to calculate m_{fb} at the equilibrium by fitting the kinetic model

$$m_{fb} = \frac{K_1^*}{K_2} (1 - \exp^{-K_2 t}) \quad (4.8)$$

where K_1^* and K_2 are the uptake and release rate and were calculated using Microsoft Solver and t is time (h).

To ensure negligible-depletion this condition must be satisfied [322]:

$$K_{fw} \cdot x \frac{V_{fb}}{V_W} \lll 1 \quad (4.9)$$

K_{fw} can be assumed to be constant with micropollutant concentration [276].

4.6.2 Determination of K_{HA}

The HA-water partitioning coefficient for ES, K_{HA} , was estimated as a function of pH and HA concentration.

Solutions of 100 mL volume containing 10, 25, 50 and 100 $\mu\text{g/L}$ of ES, 12.5 mg/L of HA and background electrolyte were prepared and the pH adjusted from 4 to 12. Other 100 mL solutions containing 10, 25, 50 and 100 $\mu\text{g/L}$ of ES, 12.5, 50, 125, 250 mgC/L of HA and background electrolyte were prepared at pH 4 and 8.

ES-HA solutions were shaken at 200 rpm at 25 °C in in a Certomat BS-1 incubator shaker (Sartorius Germany) for 24 hours to allow the formation of ES-HA complexes and the solution was sampled to determine the initial mass of ES in solution m_{TOT} . One PA* fibre was introduced in each solution and shaken for 96 hours (chosen as equilibrium time on the basis of the fibre calibration) before being removed and analysed in the liquid scintillation counter to determine m_{fb} .

By definition:

$$K_{HA} = \frac{C_{HA}}{C_W} = \frac{m_{HA}}{m_{DOM}} \cdot x \frac{V_W}{m_W} \quad (4.10)$$

where C_{HA} ($\mu\text{g}/\text{kg}$) is the concentration of ES sorbed to HA, m_{HA} (μg) is the mass of ES sorbed to HA and m_{DOM} (kg) is the total mass of dissolved HA in solution.

The following equation was used to quantify K_{HA} :

$$\log C_{HA} = \log K_{HA} + n_i \log C_w \quad (4.11)$$

where n_i is the slope of the linear regression.

K_{HA} can be calculated from the linear regression of C_{HA} as a function of C_w if the sorption isotherm is linear, i.e. $n_i=1$ [278]. Therefore four values of C_w corresponding at four concentrations of ES (10, 25, 50 and 100 $\mu\text{g}/\text{L}$) were plotted on a logarithmic scale against the determined four values of C_{HA} to quantify the partition coefficient K_{HA} . The use of four ES concentration was necessary to determine the slope of equation 4.11 and therefore K_{HA} .

C_w in equation 4.11 was calculated as

$$C_w = \frac{m_w}{V_w} \quad (4.12)$$

where m_w was calculated with the following equation

$$m_w = \frac{m_{fb}}{K_{fw}} \times \frac{V_w}{V_{fb}} \quad (4.13)$$

where K_{fw} was previously determined at equilibrium as described in Section 4.6.1, m_{fb} was determined during the ES-HA experiments and V_w and V_{fb} are known

C_{HA} was calculated as

$$C_{HA} = \frac{m_{HA}}{m_{DOM}} \quad (4.14)$$

where m_{HA} was calculated with the full mass balance

$$m_{HA} = m_{TOT} - m_{fb} - m_w \quad (4.15)$$

The full mass balance was required since m_F was similar to m_{HA} and m_{TOT} was similar to m_w [278].

The fraction of ES bound to HA f_{HA} (%) was determined as [279]:

$$f_{HA} = \frac{1}{\frac{V_w}{m_{DOM} \cdot K_{HA}} + 1} \quad (4.16)$$

4.7 Membrane characteristics

Two commercial TFC NF membranes, TFC-SR2 and TFC-SR3 provided by Koch (http://www.kochmembrane.com/support_nf_lit.html) were selected for the work carried out in this study. The membranes were extensively characterised (Appendix 2) and were chosen because they have a high NOM retention and low salt retention, being therefore particularly suited for treating surface water. SEM images of the membrane surfaces are presented in Figure 4-8.

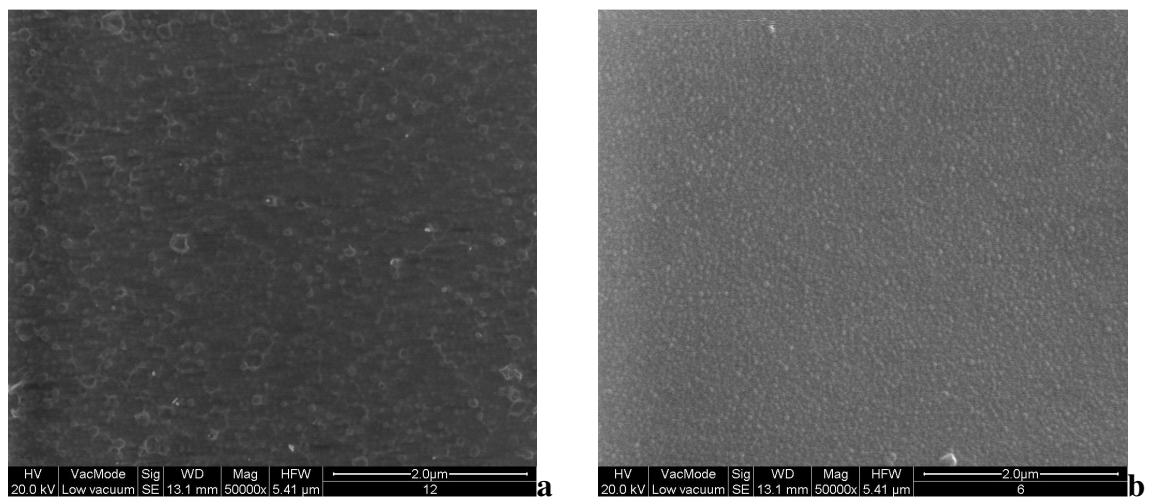


Figure 4-8 Surface SEM images of (a) TFC-SR2 and (b) TFC-SR3 by SEM

The two membranes are both made of a PA active layer on a PS support layer but they have different pore size, hydrophobicity and roughness (Table 4-2). The MWCO and pore size of TFC-SR2 is bigger than the MW and radius of manganese and ES (Table 3-3 and Table 3-5), while the MWCO and pore size of TFC-SR3 is smaller. Their size difference allowed the study of the effect of steric exclusion on solute removal and on solute-solute and solute-membrane interactions. Characteristics of the virgin membranes are summarized in Table 4-2. A detailed description of membrane characterization is present in Appendix 2.

Table 4-2 Characteristics of virgin TFC-SR2 and TFC-SR3 membranes

	Average permeability ($L \cdot h^{-1} \cdot m^{-2} \cdot bar^{-1}$)	MWCO ¹ ($g \cdot mol^{-1}$)	Estimated pore radius ¹ (nm)	NaCl retention ² (%)
TFC-SR2	16.10 ± 0.98	460 ± 20	0.52 ± 0.03	21 ± 8
TFC-SR3	6.74 ± 1.79	167 ± 10	0.38 ± 0.03	30 ± 8
	pH of point of zero charge ³ (-)	Roughness (nm)	Thickness $\Delta\delta_m$ (μm)	Contact angle (°)
TFC-SR2	4.25 ± 0.01	17.9 ± 0.6	158 ± 3	61.5 ± 2.6
TFC-SR3	3.84 ± 0.01	5.2 ± 0.6	142 ± 1	48.5 ± 1.4

¹ pressure 10 bar, neutral pH

² 20 mM NaCl and 1 mM NaHCO₃, pressure 5 bar, pH 6

³ background electrolyte 1 mM NaHCO₃ and 20 mM NaCl

4.8 Quality assurance and quality control

This section describes the procedures and practices of quality assurance and control employed in this work [323].

The laboratory in which the experiments were conducted was kept tidy and regularly cleaned. The areas in which experiments with radiolabeled ES were carried out were decontaminated at the end of each experiment using RBS[®] solution (Sigma Aldrich, UK) and checked for radioactivity every month or when a spill occurred using a portable Geiger–Müller counter. Protective personal equipment (laboratory coat, nitrile gloves, and safety goggles) was worn when in the laboratory.

All chemicals were of analytical grade, dated once opened and discarded when outdated, or when evidence of deterioration was detected. All solutions were properly labelled and stored according to the type of solute, as detailed in Section 4.2. All glassware used in the laboratory was of high quality borosilicate glass. Glassware and laboratory supplies in contact with chemical solutions were rinsed with ultrapure water, washed with cleaning solution, rinsed thoroughly with ultrapure water and dried with hot air. The cleaning solutions were chosen according to the type of solute. Solutions of 8% in volume of acetic acid, (Fisher Scientific, UK) were employed for inorganic solutes, NaOH solutions (5% in weight) were employed for

organic solutes and RBS[®] solutions (30% in volume) were used to decontaminate from radiolabeled ES. All chemical waste and radioactive waste was stored and disposed according to the university regulations.

Samples were analysed according to standard methods [323], as described in Sections 4.3.1-4.3.5. All analytical instruments were calibrated prior to the analysis to obtain a calibration curve with concentrations bracketing the range of concentrations in the samples. The calibration was verified during sample analysis by analysing a standard at specific intervals. Limits of detection were identified for each analyte. Instrument blanks, i.e. samples containing ultrapure water only, were analysed before, after and during sample analysis to determine instrument contamination. Equipment rinse blanks were analysed regularly to check the effectiveness of the decontamination procedures. All samples were analysed in triplicate and the average of the three measurements was reported. Instrumental errors were determined as the standard deviation of the three measurements (Table 4-3).

Table 4-3 Instrumental errors

	Error E (%)
Pipette	0.6
Balance	0.1
Volumetric flask	0.04
TOC	6
ICP-OES	5
Liquid scintillation counter	0.8

Loss of ES due to volatilisation and adsorption to glass and plastic (i.e. adsorption to the plastic stirrer used during stirred cells experiments) was evaluated. Volatilisation of α -ES and β -ES from aqueous solution might be expected due to their low water solubility (Table 3-5). 900 mL feed solutions containing ES were prepared in 1 L closed glass bottles and left to stir overnight before experiments were conducted (Section 7.2). The concentration of α -ES and β -ES in air was estimated from the

Henry's constant [280] and resulted to be 0.03% and 0.002% respectively. As a result, volatilisation was considered negligible.

In order to estimate adsorption to glass and plastic, ten solutions containing 10 µg/L of ES and background electrolyte (Section 4.2) and adjusted at pH 3-12 were prepared in glass bottles containing plastic stirrers. Solutions were left stirring for 96 hours and sampled at time 0, 33, 48, and 96 hours. The variation of concentration of ES after 96 hours was $\pm 1.8\%$. Adsorption of ES to glass and plastic was therefore considered negligible.

The determination of the error in calculating flux, retention and solute adsorption during filtration experiments presented several challenges. When a quantity is a function of measured quantities, the error is estimated via error propagation. The error of the measured quantities is calculated and it is propagated via mathematical expressions to determine the error of the quantity [324].

By following the rules described above, the error of flux could be determined by propagating the error linked with measurement of the permeate volume and the membrane area (equation 2.3), the error of retention could be determined by propagating the error in measuring permeate and feed concentration (equation 2.2) and the error of adsorption by propagating the errors in permeate, feed, concentrate retention and volume (equation 2.4).

However, flux, retention and adsorption not only depend on the above listed quantities but, as explained in Chapter 2, are affected by other variables like pressure and temperature that are not taken into account in the formulas used to calculate them. As a result, when the same experiment is repeated several times, the variability in flux, retention and adsorption is higher than the error calculated by propagating the errors in the measurements.

For these reasons, in the membrane field, experiments are sometimes repeated in triplicate and the standard deviation of the obtained retention and adsorption is used

to calculate the experimental error [325]. Nevertheless, statistical analysis of experiments repeated only three times is questionable.

In this study it was not possible to repeat all experiments three times or more due to the limited number of membrane coupons available. As a consequence, an analysis of the factors affecting the reproducibility of results was carried out. Pressure in the stirred cells during the experiments had a variability of $\pm 0.8\%$ while the variability in pressure of repeated experiments (conducted at the same pressure) was $\pm 0.44\%$. Variability in temperature among experiments was $\pm 5\%$. The highest variability ($\pm 15\%$) was caused by the difference in pure water flux among different membrane coupons (all the other conditions being the same). A new membrane coupon was used for each experiment and, even if the coupons belonged to the same flat sheet, differences in flux were observed.

The variability in pure water flux of different membrane coupons is the factor that most affected retention and adsorption results. By repeating in triplicate and duplicate experiments with coupons that had a pure water flux $\pm 15\%$ of the average pure water flux, the retention had a variability of $\pm 8\%$ and adsorption had variability of $\pm 10\%$. The variability in retention and adsorption cannot be rigorously defined error as it is not calculated using standard deviation. The variability values above were used for all the experiments in this work in which results from different membrane coupons were compared. For quality control, only coupons with a pure water flux $\pm 15\%$ of the average pure water flux were employed in this study.

For experiments that use the same membrane coupons, such as experiments carried out for the determination of the average membrane pore size (Appendix 2), only instrumental errors were considered and the error propagation rule was adopted. In these cases, the error was obviously lower, as the variability due to flux difference among membrane coupons was eliminated.

5. Transport models

Transport of solutes through NF membrane is described by transport to the membrane surface and transport across the membrane.

5.1 Film theory

Solute transport to the membrane surface is described by the film theory [19].

It is assumed that outside the boundary layer, i.e. at a distance δ from the membrane, complete mixing occurs, so c_f is constant, while in the boundary layer the solute concentration increases with proximity to the membrane, reaching a maximum value c_{mf} at the membrane surface (Figure 5-1). The accumulation of solute at the membrane surface results in a diffusive back flow towards the bulk feed.

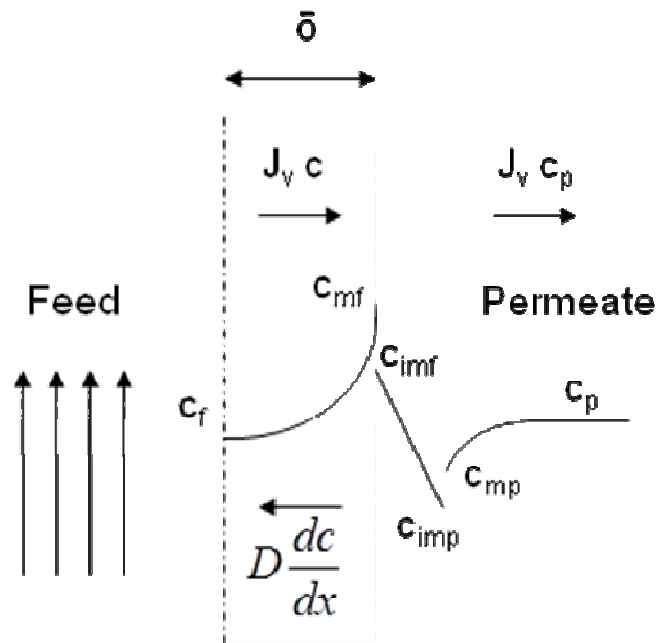


Figure 5-1 Concentration polarisation according to the film theory (adapted from [19])

From the mass balance on the boundary layer among the flux towards the membrane, the back flow towards the bulk feed and the permeate flow:

$$J_v c + D_\infty \frac{dc}{dx} = J_v c_p \quad (5.1)$$

where c is the solute concentration at axial distance x from the membrane and D_∞ is the diffusion coefficient of the solute (at infinite dilution).

Integrating using boundary conditions and introducing the real retention R_r

$$R_r = 1 - \frac{c_p}{c_{mf}} \quad (5.2)$$

$$\ln \frac{1 - R_r}{R_r} = \ln \frac{1 - R_o}{R_o} - \frac{J_v}{k_f} \quad (5.3)$$

where k_f is the mass transfer coefficient defined as:

$$k_f = \frac{D_\infty}{\delta} \quad (5.4)$$

According to equation 5.3 the observed retention is lower than the real retention ($c_{mf} > c_f$) therefore ($c_p/c_{mf} < c_p/c_f$) and ($1 - c_p/c_{mf} > 1 - c_p/c_f$) and as the concentration polarisation increases, J_v/k_f increases and the observed retention become lower.

The ratio J_v/k_f , represents the back-diffusion transport of solute in the boundary layer and it can be used as an indication of the hydrodynamic operating conditions. J_v/k_f shows the ratio of solute transport towards the membrane by convection and solute back transport by diffusion [19]. The smaller than J_v/k_f ratio the closer the solute concentration at the membrane will be to the concentration in the bulk [326]. When J_v/k_f is larger than unity convection dominates solute transport to the membrane surface, when it is less than unity, back-diffusion dominates solute transport to the membrane surface [87].

From equation 5.3 the smaller J_v/k_f the closer the real retention is to the actual retention, indicating lowest concentration polarisation. Since J_v/k_f increases with pressure (J_v increases with pressure while k_f is constant), the higher the pressure the higher the concentration polarisation at the membrane surface.

Various empirical equations have been developed to determine k_f [327]. k_f depends on the system geometry, hydrodynamic conditions (cross flow velocity), solute diffusivity and solvent viscosity.

In this study, the mass transfer coefficient for the stirred cells was determined using the following expression [113, 328]:

$$k_f = k' \omega^{0.567} \quad (5.5)$$

where ω is the stirring speed and

$$k' = 0.23 \left(\frac{r_{sc}^2}{\nu} \right)^{0.567} \left(\frac{\nu}{D_\infty} \right)^{0.33} \frac{D_\infty}{r_{sc}} \quad (5.6)$$

with r_{sc} is the radius of the cell and ν is the solution kinematic viscosity.

The empirical equations for the calculation of the mass transfer coefficient have been demonstrated to be valid for stirred cells of different geometries [290, 329].

According to equations 5.5 and 5.6, k_f depends on the type of solute, on the geometry of the membrane and on the crossflow velocity, but it is independent from the solute concentration at the membrane surface. The independence of concentration polarisation from c_{mf} was demonstrated by van den Berg *et al.* [329].

5.2 Hydrodynamic Model

As explained in Section 2.2.3, in this work the hydrodynamic model has been chosen to describe transport of solutes across the membrane [103].

According to the hydrodynamic model the flux of the solute J_s is expressed as:

$$J_s = -K_d D_\infty \frac{dc}{dx} + \frac{J_v}{\epsilon} K_c c \quad (5.7)$$

where K_d is the hindrance factor due to diffusion and K_c is the hindrance factor due to convection.

The transport of solute through the membrane is therefore composed by a diffusion term, dependent on the solute concentration, and a convection term, dependent on the permeate flux (i.e. on pressure).

K_c and K_d are dependent on λ and they have been calculated as [328]

$$K_c = (2 - \Phi)(1 + 0.054 \lambda - 0.988 \lambda^2 + 0.441 \lambda^3) \quad (5.8)$$

$$K_d = 1 - 2.3 \lambda + 1.154 \lambda^2 + 0.224 \lambda^3 \quad (5.9)$$

$$\text{with } \lambda = \frac{r_s}{r_p} \quad (5.10)$$

Since in NF membranes a distribution of pore sizes exists, empirical equations have been developed for expressing λ as a function of the pore size distribution [101]. Due to the errors linked to the empirical equations and to complexity of the characterisation of membrane pore distribution, equation 5.10 was used in this study. A small deviation between model prediction and experimental values is expected as a result [27].

Φ is the solute partitioning coefficient in the membrane polymeric matrix defined as [27]:

$$\Phi = \frac{c_{imf}}{c_{mf}} = \frac{c_{imp}}{c_{mp}} \quad (5.11)$$

where c_{imf} is the concentration inside the membrane at the feed side, c_{imp} is the concentration inside the membrane at the permeate side and c_{mp} is the concentration at the membrane surface on the permeate side, as represented in Figure 5-1.

Integrating equation 5.7 with the boundary conditions within the pores and using equation 5.2 to express retention, the hydrodynamic model can determine the real solute retention as a function of the hydrodynamic parameters:

$$R_r = 1 - \frac{\Phi K_c}{1 - \exp(-Pe)(1 - \Phi K_c)} \quad (5.12)$$

where Pe is the Peclet number

$$Pe = \frac{K_c J_v L}{K_d \varepsilon D_\infty} \quad (5.13)$$

with L the active layer thickness.

Using equations 5.12 and 5.3 the observed solute retention can be predicted by the model. The only unknown parameter is the partition coefficient Φ since c_{imf} , c_{imp} and c_{mp} in equation 5.11 cannot be measured. A purely steric model, valid only when interactions between solute and membrane can be considered negligible, is used to determine Φ as follows [103]

$$\Phi = (1 - \lambda)^2 \quad (5.14)$$

Other expressions for Φ have been developed in order to take into account different shapes and orientations of the molecules [148]. For solute whose interactions with the membrane cannot be considered negligible, such as hydrophobic organic micropollutant that adsorb to the membranes, expressions for Φ dependent both on steric exclusion and micropollutant-membrane affinity have been developed [27, 90].

Verliefde *et al.* [27] proposed the following equation for Φ :

$$\Phi = (1 - \lambda)^2 \exp\left(-\frac{\Delta G_i}{k_b T}\right) \quad (5.15)$$

where ΔG_i expresses the solute-membrane affinity as free energy of interaction between solute and membrane, k_b is the Boltzmann constant and T is temperature. Equation 5.15 was shown to predict satisfactorily transport of several organic micropollutants through NF and RO [32].

If λ is constant, a decrease in ΔG_i results in an increase in Φ , that is an increase in solute-membrane affinity and a decrease in retention (equation 5.12). Vice versa if Φ decreases repulsion between solute and membrane increases and solute retention is improved.

5.3 Limitations of the Hydrodynamic Model

The hydrodynamic model described in the previous section is based on the following assumptions [103]:

- Solutes are rigid spheres of radius r_s that behave as hydrodynamic particles
- Membrane have rigid cylindrical pores of radius r_p .
- λ expressed with equation 5.10 is a fixed property of the membrane
- If $\lambda > 1$ solute retention is total
- Electrostatic forces between solute and membrane are not taken into account
- The effects of osmotic pressure are not taken into account

The above listed assumptions constitute also the model limitations. Solutes do not behave as rigid spheres and their molecular structure (width, length) influences retention [71, 73, 76, 148]. Membrane pores are not rigid and cylindrical, pores bigger and smaller than the average r_p exist and solute transport can occur through these existing bigger and smaller pores. Moreover, the same existence of pores in NF is under discussion with some authors referring to “free volume” within the active layer [50, 51]. As a consequence, retention of solutes whose r_s is bigger than r_p ($\lambda > 1$) can be lower than the theoretical 100% retention predicted by the model.

In order to use the hydrodynamic model when $\lambda > 1$ and retention is less than 100%, the model can be fitted using the obtained retention results for the studied solute to determine a new pore radius r_p^* . r_p^* represents the average radius of an “hypothetical” membrane whose hindrance to the studied solute passage is equivalent to the hindrance experienced by the solute through the actual membrane [27, 54].

If electrostatic forces between the solute and the membrane cannot be considered negligible, the modified Nernst-Planck equation, which contains a transport term due to the electric field gradient should be employed to describe solute transport through the membranes [54, 100, 105, 330, 331].

5.4 Sieving coefficients

Solute retention can be expressed through sieving coefficients, with S_o defined as the observed sieving coefficient and S_a as the actual (real) sieving coefficient [101, 111, 113]:

$$S_o = 1 - R_o \quad (5.16)$$

$$S_a = 1 - R_r \quad (5.17)$$

Equations 5.12 and 5.13 can be expressed as:

$$S_a = \frac{\Phi K_c}{1 - \exp(-J_v K_c L / K_d D_\infty \varepsilon)(1 - \Phi K_c)} \quad (5.18)$$

When S_a is plotted against J_v a characteristic curve is obtained according to equation 5.18 (Figure 5-2): at low values of J_v (i.e. pressure) S_a is maximum (i.e. retention is minimum) and with increasing J_v S_a decreases up to an asymptotic value ($S_\infty = \Phi K_c$), which represents the maximum theoretical retention of the membrane for that particular solute.

S_o can be plotted against J_v by substituting S_o to S_a in equation 5.18 using equations 5.3, 5.16 and 5.17. The plot of S_o against J_v (Figure 5-2) shows a characteristic U-shaped curve: at low J_v the plot is similar to the curve of S_a , reaches a minimum with increasing J_v (i.e. maximum observed retention) and increases at high J_v peeling away from the S_a curve due to concentration polarisation [101, 113]. The position of the minimum of the curves with respect to the x and y axes depends on λ , K_d and K_c , k_f and L/ε and can be determined by differentiating equation 5.18 with respect to J_v . At low J_v retention increases with J_v because diffusion dominates transport, so while water passage increases with pressure, solute transport does not change as it is driven by the concentration gradient and not by pressure. As J_v goes to zero retention tends to zero (S_o and S_a tend to one) as feed and permeate equilibrate by diffusion [101].

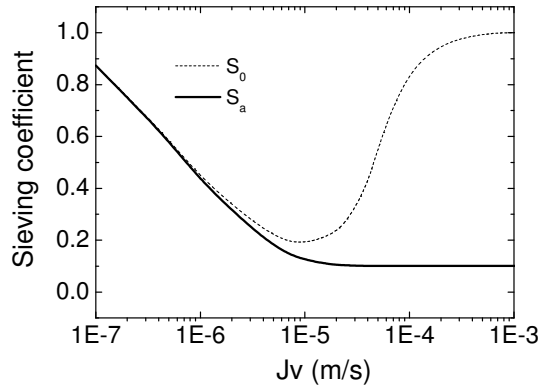


Figure 5-2 Sieving coefficients S_0 and S_a as a function of J_v according

According to equation 5.18 S_a (and therefore R_r) can be predicted as a function of J_v once the solute characteristics (r_s and D_∞), the membrane characteristics (r_p and L/ε) and Φ are known.

6. Manganese and humic acid removal mechanism

6.1 Introduction

The investigation of the co-influence of solute-membrane interactions and solute-solute interactions on solute removal and transport by NF is of paramount importance to explain NF removal mechanisms.

This chapter aims to investigate the role of solute-membrane and solute-solute interactions in mechanisms of removal of inorganic solutes and NOM. As explained in Section 3.4, manganese was chosen as model inorganic and HA were chosen as representative of NOM. Manganese is one of the most abundant inorganic solutes in surface water in Scotland and exceeds its regulatory limit more frequently than other inorganic elements at the outlet of Scottish water treatment plants (Figure 3-2). Scottish waters are rich in organic matter and NOM removal is necessary to avoid the potential formation of carcinogenic trihalomethanes [36, 37]. Commercial HA were chosen to represent NOM because they have been extensively characterised in the literature (Section 3.4.1).

Removal mechanisms of manganese from drinking water by NF will be for the first time systematically investigated. As explained in Section 3.4.2, NF has been shown to be a suitable process for manganese removal, especially considering the drawbacks of conventional treatments and the insufficient removal achieved by UF and MF if manganese precipitation is not achieved before filtration. However, manganese removal mechanisms by NF have never been evaluated before. Removal of divalent ions by NF depends on the type of solute as it is affected by speciation (solute-solute interactions) and solute-membrane interactions and results obtained for other divalent ions or metal cannot be generalised. A dedicated study is therefore required.

Relating solute removal and flux to solution pH has been shown to be mandatory for understanding removal mechanisms by NF membranes, as the variation of solution

pH affects not only membrane characteristics (as described in Section 2.3.1) but also the different forms (species) at which solutes exist [24]. Different species of the same element exhibit different size, charge and mobility [214, 332] and they are removed differently by NF. Despite this, the number of NF studies in which a detailed knowledge of solute speciation is related to the membrane removal mechanisms is limited.

Furthermore, the impact of NOM on manganese retention by NF has not been taken into account in previous studies. Manganese is known to form complexes with HA [209-212] but the influence of complexation (solute-solute interactions) on manganese removal is unknown.

The study of removal of manganese and HA complexes will increase the knowledge of the role of inorganic solutes-NOM interactions in removal mechanisms by NF, that, as outlined in Section 2.3.2, has so far received less attention in the literature. NF membranes TFC-SR2 and TFC-SR3 are particularly indicated for investigating the role of membrane characteristics in the removal of manganese (with and without HA) because their pore size (0.52 nm for TFC-SR2 and 0.38 nm for TFC-SR3) is respectively bigger and smaller than the manganese hydrated radius (0.44 nm). Hydrated radius has been shown to predict ion passages through membranes better than crystal and Stokes radius [69].

The objectives of this chapter are to investigate:

- the impact of speciation and manganese complexation with HA (solute-solute interactions) on manganese and HA removal by NF;
- the role of membrane characteristics, pore size and charge (solute-membrane interactions) on manganese and HA removal by NF;
- the mechanisms of manganese and HA removal by NF.

In this chapter, manganese speciation and complexation with HA as a function of pH will be firstly quantified using Visual MINTEQ 2.5 [292]. Finally, removal of

manganese with and without HA will be determined and underlying mechanisms explained.

6.2 Filtration protocol

Filtration experiments were carried out as described in Section 4.4. The manganese concentration used in the experiments was 5 mg/L, as this is the typical concentration found in Scottish water (Section 3.2). HA concentration was 5 mgC/L, representing typical NOM concentration found in natural water [207]. Electrolyte background solution consisted of 1 mM NaHCO₃ and 20 mM NaCl (Sections 4.2).

The feed solution (500 ml) was prepared at the desired pH (varied from 4 to 12) the day before and stirred overnight at 100 rpm at ambient temperature (21 ± 2 °C) to allow the formation of species and complexes. All experiments were carried out at pressure 5 bar. Permeate was collected in three aliquots of 40 mL each (24% recovery).

Three types of experiment were conducted:

1. Manganese only: feed solution contained 5 mg/L of manganese and background electrolyte.
2. HA only: feed solution contained 5mgC/L of HA and background electrolyte.
3. Manganese and HA: feed solutions contained 5 mg/L of manganese, 5 mgC/L of HA and background electrolyte.

6.3 Manganese and humic acids speciation

Visual MINTEQ 2.5 [292] was used in this study to model both manganese speciation and manganese and HA complexation as a function of pH as described in Section 4.5.

6.3.1 Manganese speciation

Manganese speciation was performed both at atmospheric pressure (1.01 bar) and at the pressure of 5 bar used during the filtration experiments. Figure 6-1 shows the variation of the manganese concentration, expressed as logarithmic of its activity,

with pH at the two considered pressures. The activity coefficients were calculated with the Davies equation [292, 332]:

$$- \text{Log}(\text{activity}) = 0.5z_1z_2 \left(\frac{\sqrt{I}}{1 + \sqrt{I}} - 0.15I \right) \quad (6.1)$$

where z_1 and z_2 are the charges of the ions in which manganese dissociate (Mn^{2+} and Cl^{-1}) and I is the ionic strength.

As expected, the higher partial pressure of CO_2 affects the precipitation of carbonates in solution. At atmospheric pressure, MnCO_3 precipitation starts at pH 7.5 (dashed line in Figure 6-1a) and it is completed at pH 10, while at 5 bar, it starts at pH 7.1 (dashed line in Figure 6-1b) and it is completed at pH 9.6. At higher pressure the speciation graph is “shifted” to the left and a higher content of solids in solution at lower pH occurs.

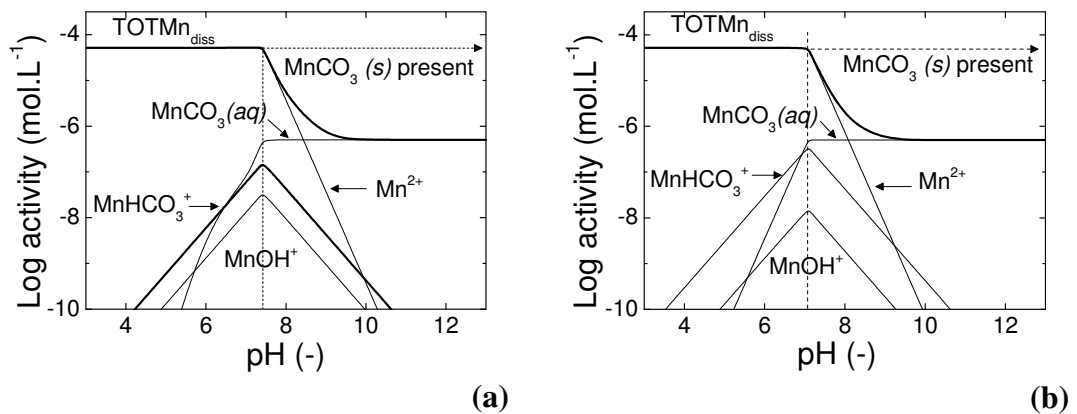


Figure 6-1 Manganese speciation in absence of HA as logarithmic of the activity. Mn concentration: Mn concentration 5 mg/L, background electrolyte 1 mM NaHCO_3 and 20 mM NaCl . Pressure: (a) 1.01 bar (b) 5 bar.

Apart from a slight shift in the pH of manganese precipitation, at both pressures the speciation graphs are quite similar. At low pH the majority of manganese is dissolved in solution ($\text{TOTMn}_{\text{diss}}$) as Mn^{2+} , MnCO_3 (aqueous), MnHCO_3^+ and MnOH^+ . Mn^{2+} constitutes the majority of the dissolved manganese present in solution. At pH greater than 7 manganese starts precipitating as MnCO_3 (solid) and

the total concentration of dissolved manganese decreases. The concentration of dissolved Mn^{2+} , MnHCO_3^+ and MnOH^+ decreases and the concentration of MnCO_3 (aqueous) stays constant.

Figure 6-1b has been redrawn showing the species of manganese as percentage of the total manganese (Figure 6-2). At lower pH all manganese is dissolved while with increasing pH manganese starts precipitating as MnCO_3 (solid). As indicated in Figure 6-1b, where the logarithmic scale of the activity allows visualising the distribution of the dissolved species, at lower pH dissolved manganese is mainly present as Mn^{2+} . At $\text{pH} > 9.6$ dissolved manganese constitutes only 1% of the total manganese and it is present as MnCO_3 (aqueous), while 99% of the manganese in solution is precipitated as MnCO_3 (solid).

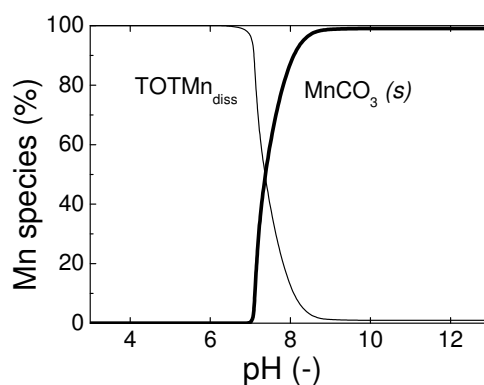


Figure 6-2 Manganese speciation in absence of HA as percentage of total manganese concentration: Mn concentration 5 mg/L, background electrolyte 1 mM NaHCO_3 and 20 mM NaCl , pressure 5 bar.

The obtained speciation graphs are in agreement with published investigations on the chemistry of manganese in natural waters. Chisweel and Mokthar [211, 213] observed that in acidic conditions and in absence of complexing ligands the stable form of manganese is Mn^{2+} . MnCO_3 (solid) is the most likely form of insoluble Mn(II), while MnO and $\text{Mn}(\text{OH})_2$ only precipitate at $\text{pH} > 11$ when the redox intensity of the solution, $p\epsilon$, is negative (reducing solutions). In the pH range of natural waters $p\epsilon$ is usually between 12 and 14 [214], confirming that manganese precipitates as MnCO_3 .

6.3.2 Manganese and humic acids complexation

Modelling of complex formation between manganese and HA was performed as described in Section 4.5.2 both at atmospheric pressure (1.01 bar) and at the pressure of 5 bar used during the filtration experiments. Figure 6-3 shows the variation of the manganese concentration, expressed as logarithmic of its activity, with pH at the two considered pressures in the presence of HA.

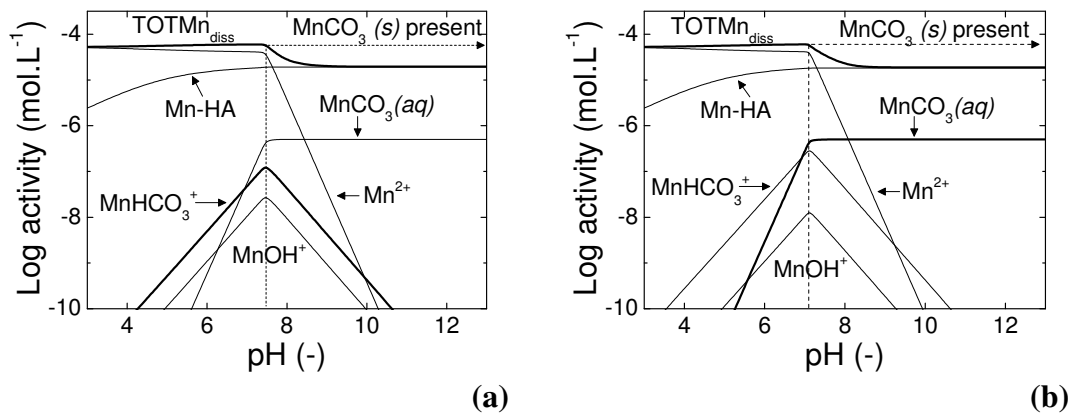


Figure 6-3 Manganese speciation in the presence of HA as logarithmic of the activity. Mn concentration: Mn concentration 5 mg/L, HA 5 mgC/L, background electrolyte 1 mM NaHCO₃ and 20 mM NaCl. Pressure: (a) 1.01 bar (b) 5 bar.

As for the case without HA, at atmospheric pressure MnCO₃ precipitation starts at pH 7.5 and it completed at pH 10, while at 5 bar it starts at pH 7.1 and it is completed at pH 9.6, indicating that HA does not influence the pH at which the precipitation occurs. Also in this case the effect of pressure on speciation is to “shift” the graph to the left.

The presence of HA does not change dramatically the speciation of dissolved manganese. At low pH the majority of manganese is dissolved in solution (TOTMn_{diss}), mainly as Mn²⁺. MnCO₃ (aqueous), MnHCO₃⁺ and MnOH⁺ are also present. Some of the dissolved manganese, mainly Mn²⁺, is complexed with HA. At pH greater than 7 manganese starts precipitating as MnCO₃ (solid) and the total concentration of dissolved manganese decreases. As for the speciation graphs

without HA, with increasing pH the concentration of dissolved Mn^{2+} , MnHCO_3^+ and MnOH^+ decreases and the concentration of MnCO_3 (aqueous) stays constant. The concentration of Mn complexed with HA increases with pH and becomes constant with the formation of MnCO_3 (solid).

The presence of Mn-HA complexes impacts the formation of precipitated MnCO_3 . As observed by comparing Figure 6-1 and Figure 6-3 much less precipitate is formed when HA are present since Mn-HA complexes are formed.

When the species are presented as percentage of the total manganese in solution (Figure 6-4), the influence of HA on manganese speciation is more obvious. At low pH all manganese is dissolved, mainly as Mn^{2+} (as depicted in Figure 6-3). At higher pH dissolved manganese decreases as it starts precipitating as MnCO_3 (solid) and it complexes with HA. While it is not possible to identify a pK_a value for HA, due to their complexity and heterogeneity, the majority of HA functional groups dissociates at $\text{pH} > 4$ [225, 229], so HA are expected to be negatively charged in the pH range considered. The formation of Mn-HA complexes is limited at low pH and is maximum at pH above 7. Due to the formation of Mn-HA complexes the quantity of precipitate when HA are present is 35% less than the precipitate formed when HA are not in solution (Figure 6-2).

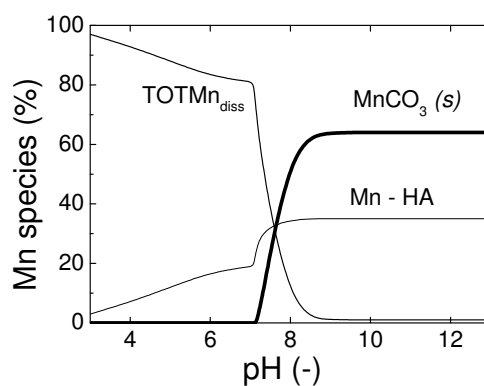


Figure 6-4 Manganese speciation in the presence of HA as percentage of total manganese concentration: Mn concentration 5 mg/L, HA 5 mgC/L, background electrolyte 1 mM NaHCO_3 and 20 mM NaCl , pressure 5 bar.

The obtained speciation graph of manganese in the presence of HA must be used with caution, given the high number of assumptions made by the complexation model and the lack of experimental data validating the results (Section 4.5.2). Despite these limitations, the results are in general agreement with findings for other inorganics.

Organic matter has been shown to influence the solubility of inorganic compounds [209] and in particular to increase metal ion solubility through binding [207, 299, 304]. In the case of manganese, the formation of Mn-HA complexes reduce the quantity of precipitated MnCO_3 by 35%. Figure 6-4 is in agreement with speciation graphs obtained for Fe^{3+} in the presence of HA [303] and iron and manganese have been shown to have very similar complexing characteristics for carbonates and sulphates [333]. The increase of inorganic-HA complex formation with pH has been observed for Fe^{3+} and Ca^{2+} and it has been attributed to the availability of carboxyl functional groups of HA at higher pH [125, 304].

6.4 Membrane flux

Flux of ultra pure water was determined with equation 2.2 by measuring the volume of permeate produced for half an hour before and after solute filtration at the same pressure employed during the experiments in order to check changes in membrane permeability during solute filtration (Section 4.4). The ratio of J , pure water flux after the experiments and J_0 pure water flux before the experiments can be used as an indicator of fouling, since if flux decline occurs the J/J_0 ratio would be lower than one.

The ratio of J and J_0 as function of pH is presented in Figure 6-5a. Water flux decline after the experiments was not observed, showing that membrane fouling did not occur. Lack of fouling can be attributed to the short duration of the experiments, the low concentrations of the solutes and the relatively low flux obtained in the stirred cells. The absence of fouling allowed relating the obtained retention results directly to the membrane characteristics (solute-membrane interactions) and solute

speciation (solute-solute interactions), without considering membrane and solute modification due to the formation of the fouling layer.

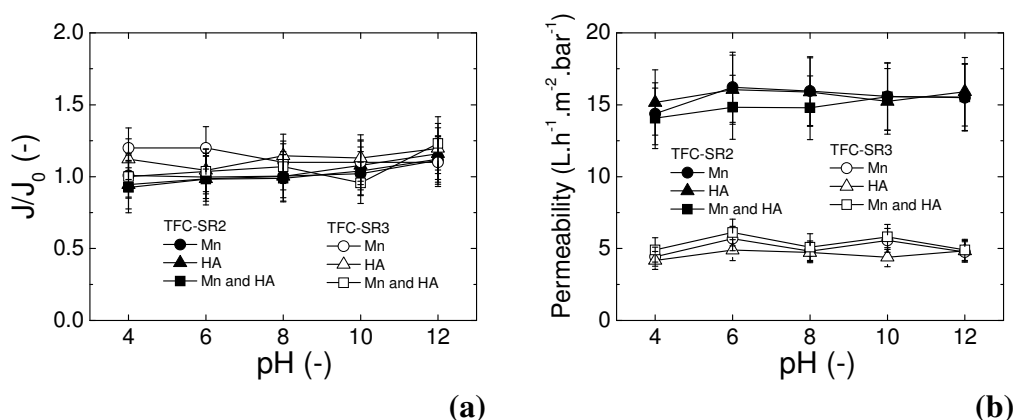


Figure 6-5 (a) Ratio of pure water flux after (J) and before (J_0) experiments as a function of pH, (b) Permeability ($J_v/\text{pressure}$) of TFC-SR2 and TFC-SR3 as a function of pH. Mn concentration: 5 mg/L, HA concentration: 5 mgC/L, pressure: 5 bar, background electrolyte 1 mM $NaHCO_3$ and 20 mM $NaCl$.

In some cases, especially for TFC-SR3, water flux after experiments was enhanced, resulting in a flux ratio greater than one. This phenomenon was observed with HA in a study by Hong and Elimelech [125] and was attributed to the hydrophilization of membrane surface by adsorbed solutes. Adsorption of negative solutes, such as HA, can increase the membrane negative charge, thus its hydrophilicity. However in this study, flux enhancement occurred for TFC-SR3 also when Mn^{2+} alone was present indicating that ions might enhance permeability also. TFC-SR2 experienced a slight flux ratio increase at higher pH, while no trend could be observed for TFC-SR3.

6.5 Manganese and humic acid retention

Manganese and HA retention was calculated using equation 2.3 for manganese only, HA only and when both manganese and HA were present (Figure 6-6).

Manganese retention was higher for the tighter TFC-SR3 than for looser TFC-SR2 (Table 4-2). Manganese retention by TFC-SR3 did not show high variation with pH and it was high (94.7%) also at lower pH when manganese is mainly present as dissolved Mn^{2+} (Figure 4-3). Hydrated radius for Mn^{2+} has been calculated to be 0.44

nm [70], while the average pore radius of TFC-SR3 is 0.38 nm (Table 4-2). When the hydrated radius is larger than the membrane pore radius, as for TFC-SR3, steric hindrance effects are predominant [67]. As a consequence, ions are hindered to enter the pores and size exclusion is the main removal mechanism.

Manganese retention by TFC-SR2 was high at pH 4 (92.2%) and at pH 10-12 (99.1%) with a minimum (37.3%) at pH 8 (Figure 6-6). At pH 10 and 12 manganese is predominantly present as visible MnCO_3 (solid) that precipitates on the membrane, so manganese removal was mainly due to size exclusion. Between pH 4 and 7 almost all manganese is present as soluble Mn^{2+} . High manganese retention at pH 4 cannot be explained by steric hindrance, as the hydrated radius of Mn^{2+} (0.44 nm) is smaller than the average pore size of TFC-SR2 (0.52 nm), nor by charge repulsion forces between the membrane surface and the solute, as TFC-SR2 has point of zero charge at pH 4.25 (Table 4-2). Minimum retention of ions is expected in correspondence of the point of zero charge of the membrane surface, when the electrostatic repulsion forces are minimum [53]. In this study, instead, minimum retention for TFC-SR2 occurred at pH 6 and at pH 8, higher than the point of zero charge of the membrane surface.

Childress and Elimelech [24] observed minimum retention of NaCl at pH higher than the pH corresponding to the point of zero charge of the membrane surface. They inferred that minimum retention occurred at the point of zero charge of the membrane pores. The streaming potential, hence the charge, of capillary pores might differ from the streaming potential measured on the membrane surface because the Debye length (i.e. thickness of the double layer) may be larger than the pore radius, resulting in double layer overlapping [334]. Moreover, zeta potential of capillary pores has been demonstrated to depend on the pore radius, on the surface conductivity of the walls, on the double layer thickness and on the fixed charge of the capillary walls [335, 336]. These parameters are not taken into account in equation 4.3 (Section 4.3.7) employed for determining the zeta potential of surfaces.

According to Childress and Elimelech [24], when pores are charged, the electrostatic repulsion between the membrane functional groups causes the pore to expand. When pores are neutral, i.e. at their point of zero charge, the pore size would not be reduced, flux would be maximum and salt retention minimum. They inferred that for “loose” porous membranes pore charge could be more important than surface charge in controlling flux and salt retention, since pore charge might become important when solutes are not hindered to enter the pores. Pontalier *et al.* [68] also inferred that when the hydrated radius is smaller than the pore radius, ions can enter the pores and electrostatic and friction forces within the pores acquire importance.

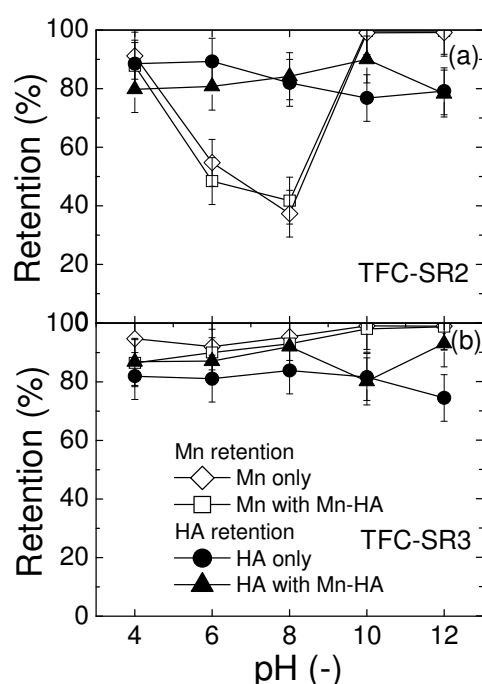


Figure 6-6 Manganese and humic acid retention for (a) TFC-SR2 and (b) TFC-SR3 as a function of pH. Manganese concentration: 5 mg/L, HA concentration: 5 mgC/L, pressure: 5 bar, background electrolyte 1 mM NaHCO₃ and 20 mM NaCl

For TFC-SR2 and TFC-SR3, minimum retention of NaCl and slight increase in permeate flux was observed at pH 6 and 8 (Appendix 2), corroborating the theory by Childress and Elimelech [24]. It is therefore inferred that for the loose TFC-SR2 lower manganese retention at pH 6 and 8 occurred at the point of zero charge of the

membrane pores. Furthermore, a slight increase in permeate flux was observed at pH 6 and 8 (Figure 6-5b). This mechanism might also explain the increase of retention at pH 4, where the pores will be positively charged and charge repulsion could occur.

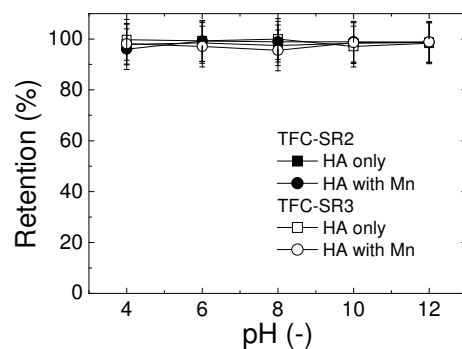


Figure 6-7 Retention of aromatic fraction of HA for TFC-SR2 and TFC-SR3 as a function of pH. Manganese concentration: 5 mg/L, HA concentration: 5 mgC/L, pressure: 5 bar, background electrolyte 1 mM NaHCO₃ and 20 mM NaCl

Retention of HA was high for both membranes (about 80%) and did not present a specific trend with pH. HA were retained by size exclusion by both membranes. When HA retention was determined by calculating HA concentration with ultraviolet absorbance (Section 4.3.4), both membranes showed high retention (83-93% for TFC-SR2 and 80-100% for TFC-SR3) and no trend with pH could be observed (Figure 6-7). Ultraviolet absorbance measures the aromatic part of HA [207], indicating that both membranes removed mainly the aromatic compounds of the HA.

The presence of manganese did not affect HA retention. Also manganese retention was not affected by the presence of HA, as evident by the same trend of the curves for Mn²⁺ only and for Mn²⁺ and HA in Figure 6-5. Several studies documented the formation of complexes between manganese and HA [209-212] and the NICA-Donnan model predicted that 37% of manganese in solution would complex to HA at pH above 7.2 (Figure 6-3). However, in this study enhancement of manganese and HA retention when both elements were present was not observed. In the case of TFC-SR3 membrane, high retention was already achieved due to size exclusion mechanisms, while for TFC-SR2 precipitation overlapped with complexation effects.

6.6 Mass deposited on the membranes

Mass deposit on the membranes was determined with equation 2.4 to substantiate the results obtained in the previous section.

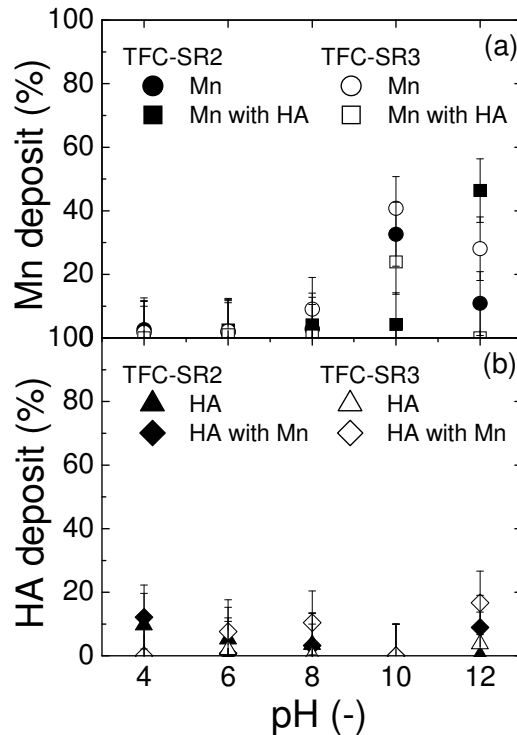


Figure 6-8 (a) Percentage of manganese deposit and (b) HA deposit on TFC-SR2 and TFC-SR3 as a function of pH. Manganese concentration: 5 mg/L, HA concentration: 5 mgC/L, pressure: 5 bar, background electrolyte 1 mM NaHCO₃ and 20 mM NaCl

As shown in Figure 6-8 the deposit of solutes was low, generally less than 10%. Nevertheless, when manganese only was present in solution, manganese deposit was higher for pH 10 and 12, as manganese deposited as precipitated MnCO₃, and the membranes showed a yellow-brownish layer. For both membranes, manganese deposit at high pH was generally less when HA were present, with the exception of TFC-SR2 at pH 12. Considering the high error associated with HA mass deposit calculation (10.0%), HA deposit with and without manganese can be considered negligible for both membranes at any pH. This result agreed with visual observations, confirming that fouling did not occur during the experiments.

Fouling conditions were not obtained during the experiments performed in this chapter, probably due to the short duration of the experiments (2-3 hours) and the low concentration of the solutes. However, in the long term the presence of HA and manganese precipitation at high pH are likely to decrease membrane flux and reduce membrane performance. The precipitation of inorganic compounds on membrane has been shown to affect solute retention [29, 74, 81, 337]. As observed in Section 2.2.4, the effects of inorganic precipitation on solute retention and permeate flux have been scarcely studied and will be investigated in Chapter 9.

6.7 Manganese and humic acid retention in real Scottish water

In order to validate the obtained results, manganese retention from real Scottish water was investigated.

The water was collected from a well in the Isle of Mull, an island located on the west of Scotland. The quality parameters of the water are presented in Table 6-1. The collected water was rich in organic matter and very low in manganese and iron (below the detection limits of ICP-OES). Arsenic was slightly above the regulatory limit.

Table 6-1 Quality parameter of well water collected in the Isle of Mull

Parameter	Concentration	PCV¹	Unit
pH	8.5	6.5 – 9.5	-
TOC	10.85	-	mgC/L
Calcium	159.61	-	mg/L
Potassium	12.23	-	mg/L
Magnesium	7.64	-	mg/L
Nitrate	34.63	50	mg/L
Aluminium	42.855	200	µg/L
Manganese	< 2	50	µg/L
Iron	< 12	200	µg/L
Arsenic	11.35	10	µg/L

¹PCV Prescribed Concentration Values according to Scottish regulations [338].

Since manganese was not naturally present in the collected real water, commercial manganese (see Section 4.2) was spiked at a concentration of 5 mg/L the day before

the experiments and the feed solution (500 mL) stirred overnight at 100 rpm at ambient temperature. Filtration experiments were carried out as described in Section 4.4 and Section 6.2.

As reported in Table 6-2, retention of TOC was high for both membranes and about 80%, confirming what was obtained for commercial HA retention in synthetic water (Figure 6-6b). Retention of manganese was higher for TFC-SR3 (80%) and lower for TFC-SR2 (55%). Considering that the pH of the water was 8.5, the obtained manganese retention is in good agreement with the results obtained for synthetic water in which both HA and manganese were added (Figure 6-6a). Arsenic retention for both membranes was quite high allowing the achievement of its regulatory limits.

Table 6-2 Retention of TFC-SR2 and TFC-SR3

Parameter	Retention (%)	
	TFC-SR2	TFC-SR3
TOC	81.89	82.42
Calcium	64.15	83.24
Potassium	10.60	25.64
Magnesium	84.94	87.86
Nitrate	39.77	57.65
Aluminium	73.21	52.11
Arsenic	98.21	72.12
Manganese	55.69	79.32

These results indicate that commercial HA selected for this study have similar organic matter retention properties with respect to TFC-SR2 and TFC-SR3 than real Scottish NOM. Moreover, retention of commercial manganese was similar in the presence of commercial HA and Scottish NOM, showing that in this case commercial HA were representative of Scottish NOM. Unfortunately, the lack of natural manganese in the collected Scottish water prevented the validation of the results obtained with the commercial manganese.

6.8 Conclusions

This chapter investigated the impact of solute-solute interactions and solute-membrane interactions on manganese and HA removal by TFC-SR2 and TFC-SR3.

Manganese retention was influenced by speciation (solute-solute interactions) and membrane pore size and charge (solute-membrane interactions). In the conditions of the experiments (pressure 5 bar and only manganese in solution), manganese was present mainly as dissolved Mn^{2+} at pH lower than 7 and started precipitating as MnCO_3 at higher pH. For the tighter TFC-SR3 manganese retention was higher than 90% and independent of pH due to size exclusion. For the looser TFC-SR2, high retention (99%) was achieved at high pH, due to size exclusion, while lower retention (about 45%) was achieved at pH 6 and 8. The hydrated radius of Mn^{2+} is lower than the average pore size of TFC-SR2, so at those pH manganese can enter the pores. It was inferred that pH 6-8 corresponds to the point of zero charge of the membrane pores; therefore the lack of electrostatic repulsion caused the lower retention. High manganese retention (90%) at pH 4 was attributed to charge repulsion between Mn^{2+} and the positively charged pores.

Complexation of manganese with HA (solute-solute interactions) occurred at pH above 7. However, enhancement of manganese and HA retention when both components were present was not observed during the experiments, as manganese retention was not affected by the presence of HA and, vice versa, HA retention was not affected by the presence of manganese. In the case of TFC-SR3 high retention was already achieved due to size exclusion mechanisms, while for TFC-SR2 precipitation overlapped with complexation effects.

The deposition of manganese on the membranes was speciation dependent and higher manganese deposits were formed at high pH when MnCO_3 precipitated. Nevertheless, flux decline due to manganese precipitation was not observed, probably due to the short duration of the experiments and the low concentration of the solutes. Scaling due to manganese deposits will be further investigated in Chapter 9. HA deposits were negligible for both membranes for any pH.

It can be concluded that at pH 7, i.e. the pH of most natural waters, the behaviour of the two membranes was drastically different for manganese retention. TFC-SR3 presented retention above 95%, while TFC-SR2 presented retention of about 45%. To achieve a drinking water quality of 0.05 mg/L with feedwater concentration of 5 mg/L of manganese, retention of 99% is required. This can only be achieved at pH 10 and 12 for both membranes. Both membranes proved to be particularly suitable for surface waters where NOM is present since they showed high retention of HA (about 80%) for any pH. The results obtained with synthetic water spiked with manganese and commercial HA were in good agreement with manganese and TOC retention achieved by spiking manganese in real Scottish water collected from a well in the Isle of Mull.

7. Endosulfan and humic acid removal mechanisms

7.1 Introduction

This chapter investigates the role of solute-membrane and solute-solute interactions on removal of micropollutants and NOM. In previous studies [31, 75, 87, 142, 172-175] the impact of NOM on micropollutant removal by NF showed conflicting results since the presence of NOM could increase, decrease or have negligible effect on micropollutant removal by NF.

The increase of micropollutant retention in the presence of NOM was attributed to the formation of micropollutant-NOM complexes (solute-solute interactions) of bigger size and higher charge [30, 31, 172-174, 339]. Jin *et al.* [31] attempted to estimate estrone removal by NF in the presence of HA using the percentage of estrone bound to HA from the literature. Poor estimation was attributed to difference in estrone concentration between the experiments and the literature and to the hypothesis that most of the estrone-HA interactions took place on the membrane rather than in solution.

Neale and Schäfer [279] were able to quantify the contribution of hormone-HA interactions on increased hormone removal by UF in the presence of HA by determining organic matter-water partition coefficients. Increasing HA concentration led to more hormone-HA partitioning and in turn to greater hormone removal by UF, demonstrating the role of micropollutant-NOM interactions on micropollutant removal by UF.

Increase of micropollutant removal by NF in the presence of NOM was also attributed to the modification of the membrane surface caused by adsorption of NOM (solute-membrane interactions). NOM deposition can cause pore clogging and change membrane surface charge, resulting in improved retention by steric and electrostatic mechanisms [31, 87].

Retention of micropollutants did not change when NOM was present and this was attributed to an inferred lack of binding between NOM and the studied micropollutants [30, 31].

When the presence of NOM decreased micropollutant retention, several explanations, sometimes contrasting, were offered in the literature. Nghiem *et al.* [142] speculated that reduced micropollutant retention was due to a bigger membrane pore size than the micropollutant-NOM complex size (solute-membrane interactions). Reduced micropollutant retention in the presence of NOM was attributed to increased membrane MWCO caused by the presence of organic matter (solute-membrane interactions) [87, 133]. Organic matter has been shown to enhance the negative charge of NF membranes, increasing electrostatic repulsion within the membrane pores and in turn MWCO [57, 153]. In another study [339], organic matter was also inferred to increase membrane hydrophilization (solute-membrane interactions), since pure water flux after organic matter filtration was enhanced, and in turn to reduce estrone removal by NF membranes.

In previous studies [87, 133, 142, 339] decreased micropollutant retention in the presence of NOM was observed in “loose” NF membranes (MWCO bigger than micropollutant MW), indicating a possible correlation between micropollutant removal mechanisms in the presence of NOM and the ratio of micropollutant MW and membrane MWCO.

Lower micropollutant retention in the presence of NOM has also been linked to the competition of micropollutant-NOM adsorption on the membrane (solute-membrane interactions). However, different authors offered contradictory explanations of the potential mechanisms. Yoon *et al.* [340] observed that in the presence of NOM micropollutant adsorption to the membrane decreased. They also observed that after membrane saturation occurred, retention increased for micropollutants that adsorbed more. Therefore, they inferred that lower retention was due to decreased micropollutant adsorption. Boussahel *et al.* [30] observed higher micropollutant adsorption to the membrane in the presence of NOM. They linked the increased

adsorption to a decrease in retention since micropollutants might experience higher diffusion to the permeate side.

In summary, previous studies have inferred the following main mechanisms responsible for increase/decrease of micropollutant retention by NF in the presence of NOM:

- solute-solute interactions: formation of micropollutant-NOM complexes;
- solute-membrane interactions: pore blocking by NOM, increased membrane MWCO and hydrophilization due to the presence of NOM and competition of micropollutant-NOM adsorption on the membrane.

A correlation seemed to exist between the ratio of micropollutant MW, membrane MWCO and the decrease in micropollutant retention in the presence of NOM.

Interpretation of results and proposed mechanisms in the literature is complicated by the lack of indication, in some studies [30, 75, 173, 174], that membrane saturation was reached. As explained in Section 2.2.2, for hydrophobic compounds that adsorb to the membranes, retention decreases with time until membrane saturation is reached; therefore retention could be overestimated if adsorption on the membrane is not taken into account [91, 92].

The conflicting results obtained in the literature for micropollutant retention in the presence of NOM have been attributed to the different types of micropollutants and organic matter used and to the complexity of the retention mechanisms [23, 30, 31]. However, the contradictory explanations of findings presented in the literature are due to the lack of systematic investigation of the inferred mechanisms. Apart from the study of Neale and Schäfer [279], in which the contribution of estrone-NOM complexation to estrone removal by UF was effectively quantified, only hypotheses were offered in the other studies. A systematic investigation of the factors affecting increase/decrease of micropollutant retention by NF in the presence of NOM will be accomplished for the first time in this chapter.

As explained in Section 3.4, ES was selected as a model micropollutant because it is hydrophobic, neutral over a large pH range [220] and forms complexes with organic matter [221-224]. To the best knowledge of the author, ES retention by NF has never been evaluated. As in the previous chapter, HA were selected as representative of NOM.

TFC-SR2 and TFC-SR3 membranes are particularly indicated for investigating the role of membrane characteristics in the removal of ES (with and without HA) because their MWCO (460 g/mol for TFC-SR2 and 167 g/mol for TFC-SR3) is respectively bigger and smaller than ES MW (407 g/mol). Their different ratio of micropollutant MW and membrane MWCO allows investigating if a correlation exists between pore size and micropollutant removal mechanisms in the presence of HA. Furthermore, TFC-SR2 is a more hydrophobic membrane than TFC-SR3 (Table 4-2). Their different hydrophilicity allows studying the role of micropollutant adsorption to the membrane in micropollutant removal mechanisms in the presence of HA.

The objectives of this chapter are to investigate:

- the influence of ES-HA complexation (solute-solute interactions) on ES removal by NF;
- the role of membrane characteristics, MWCO and hydrophobicity (solute-membrane interactions) on ES retention with and without HA;
- the mechanisms of ES retention by NF in the presence of HA.

The retention of ES with and without HA will be investigated as a function of pH and HA concentration. The role of pH in understanding the contribution of different interactions in ES removal is important since pH not only influences ES chemistry (Section 3.4.3) and potentially complexation with HA, but also membrane characteristics (Section 2.3.1). Likewise, studying ES removal as a function of HA concentration allows the investigation of the role of ES-HA complexes in ES removal. In order to quantify the role of ES-HA complexes in ES removal, the

formation of ES-HA complexes as a function of pH and HA concentration will be determined using the methodology described in Section 4.6.

7.2 Filtration protocol

Filtration experiments were carried out as described in Section 4.4. ES concentration used in the experiments was 10 $\mu\text{g/L}$ since ES concentration in natural water typically ranges from 0.02 $\mu\text{g/L}$ to 60 $\mu\text{g/L}$ [262, 263, 265-267]. Experiments with HA ranging from 5 to 250 mgC/L were performed to study the effects of HA concentration on ES-HA complex formation. A concentration of 12.5 mgC/L of HA was then selected because it represents typical NOM concentration found in natural water and it was found to increase the percentage of ES complexed with HA more than a concentration of 5 mgC/L . Electrolyte background solution consisted of 1 mM NaHCO_3 and 20 mM NaCl (Sections 4.2).

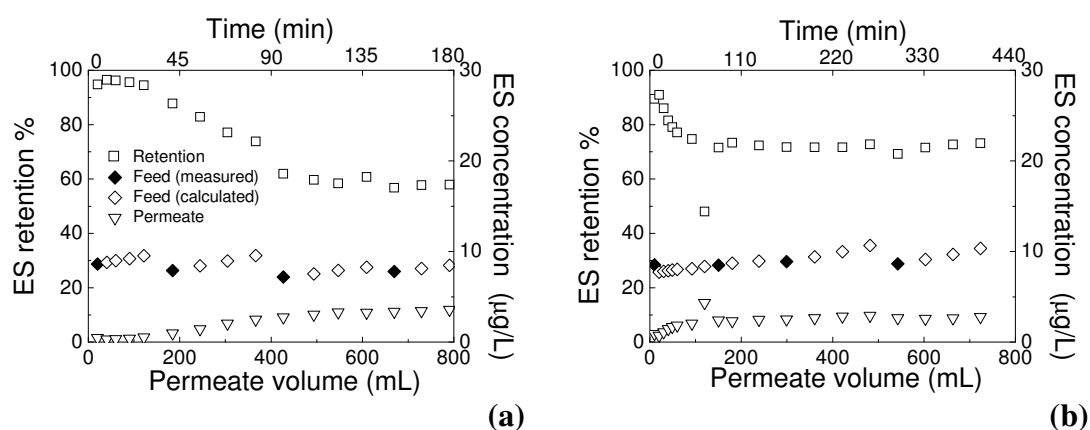


Figure 7-1 ES retention, feed and permeate concentration during ES filtration through (a) TFC-SR2 and (b) TFC-SR3, ES 10 $\mu\text{g/L}$, pressure: 5 bar, background electrolyte 1 mM NaHCO_3 and 20 mM NaCl , pH 6. Values of the feed concentration that were not directly measured by sampling were calculated with a mass balance.

The feed solution (900 ml) was prepared at the desired pH (varied from 4 to 12) the day before and stirred at 100 rpm at ambient temperature for 24 hours to allow the formation of ES-HA complexes. In order to ensure membrane saturation by ES, 480 mL of permeate were filtered and 6 samples were collected. For both membranes, filtration of 480 mL was sufficient to reach ES saturation, as indicated by the plateau

reached by the permeate concentration in Figure 7-1. After saturation was reached the permeate was recirculated back into the cell and four permeates of 60 mL each were collected (recovery of 26%). Retention was constant for the last four permeates since equilibrium was reached.

7.3 Formation of ES-HA complexes

The formation of complexes between ES and HA was quantified with the nd-SPME methodology developed by Neale *et al.* [278] and described in Section 4.6.

Previous studies [221-224] investigated sorption/desorption of ES to soil. ES was observed to sorb more and faster in soils rich with organic matter and it was concluded that ES molecules strongly attached to soil organic matter [224]. Values of K_{oc} for ES isomers were determined for various soils (Table 7-1). Interactions between NOM and ES in water have never been studied and, to the best knowledge of the author, there are no published data on aquatic HA-water partition coefficients for ES.

Table 7-1 K_{oc} values for ES isomers determined for soils rich in organic matter.

Isomer	K_{oc}	Ref.
α -ES	7800-21300	[221]
β -ES	8600-13900	
ES-Sulphate	5700-11500	
ES-Diol	700-1200	
α -ES	7969-21347	[222]
β -ES	8612-13906	
ES-Sulphate	5667-1145	
α -ES	7969-21347	[223]
β -ES	8612-13906	

The quantification of aquatic HA-water partition coefficients for ES is important because K_{oc} determined with soil might differ from K_{HA} . Aquatic HA-water partition coefficient for pesticide atrazine was found to be three orders of magnitude greater than soil organic carbon-water partition coefficient, possibly indicating that atrazine associated with dissolved organic matter was higher than atrazine associated with solutions of suspended soils [341].

Moreover, it is fundamental to quantify K_{fw} and K_{HA} (as defined in Section 4.6) at the same conditions (concentration, pH, ionic strength) used during the experiments with membranes as environmental conditions have shown to influence the obtained coefficients [307].

7.3.1 Fibre calibration and determination of K_{fw}

The SPME fibres were calibrated to establish the time necessary to reach equilibrium and calculate the fibre-water partition coefficient K_{fw} for ES as a function of pH, as described in Section 4.6.1.

SPME has been largely employed as a technique for extracting organic micropollutants before analysis by GC and HPLC [316]. Therefore, values of K_{fw} for α -ES and β -ES are available in the literature [318-320], as reported in Table 7-2. To the best knowledge of the author, there are no published data on the variation of K_{fw} for ES with pH. Moreover, the free-standing fibre method used in this work differs from the traditionally employed techniques using fibre holders. Fibre calibration was therefore required to establish equilibrium time and determine K_{fw} . The difference in values obtained in the literature for the same type of fibre can be considerable (Table 7-2) even though a difference of ± 0.5 log units is usually considered acceptable for K_{fw} values obtained using SPME fibres [315]. Differences in partitioning values could be attributed to the fact that the criterion of negligible depletion was not always respected and temperature and ionic strength might vary in different experiments [307].

As indicated in Figure 7-2a, PA* fibres reached equilibrium after 48 hours. Therefore 96 hours were chosen for the determination of the partitioning coefficients. In order to check ES adsorption to the glass, ES concentration with time was determined in control samples which did not contain fibres. No adsorption of ES to the glass was measured (Figure 7-2b).

Table 7-2 K_{fw} values for ES isomers (numbers in italics are calculated and numbers in normal font are published)

Isomer	Type of fibre	K_{fw}	$\log K_{fw}$	Ref
α -ES	PA*	8491±23	3.93	[318]
β -ES	PA*	6582±18	3.82	
α -ES	PDMS	27820 ±18	4.44	
β -ES	PDMS	6253±123	3.80	
α -ES	PDMS	25000	4.40	[319]
β -ES	PDMS	10000	4.00	
α -ES	PDMS	2138	3.33	[320]
β -ES	PDMS	1995	3.30	

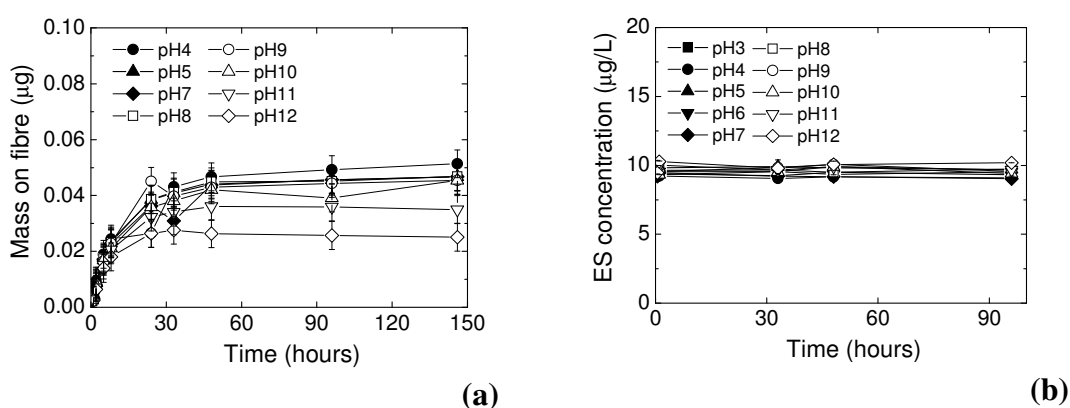


Figure 7-2 (a) Uptake of ES to PA* coated fibres as a function of time for pH 4 to 12 **(b)** ES concentration as function of time for pH 4 to 12 in the control samples, ES 10 µg/L, background electrolyte 1 mM NaHCO₃ and 20 mM NaCl.

K_{fw} for ES as a function of pH was determined by firstly establishing the mass on the fibre, m_{fb} , at the equilibrium with the kinetic model (equation 4.8, Section 4.6.1). As shown in Figure 7-3, PA* fibre uptake was constant with pH up to pH 8 and then decreased rapidly. Since ES does not dissociate, this was attributed to the hydrolysis of α -ES and β -ES to ES-diol, which has lower $\log K_{ow}$ and therefore less affinity to the fibres [307].

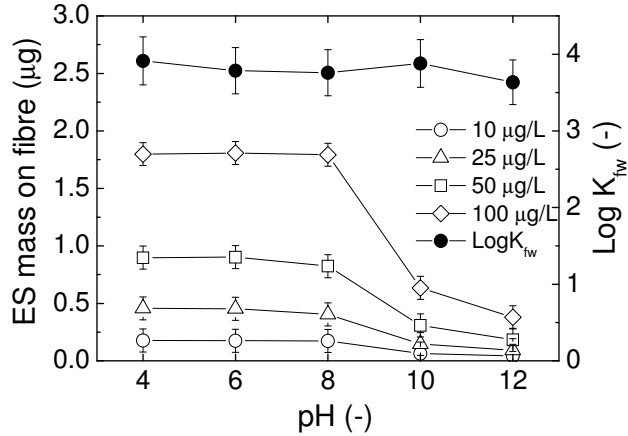


Figure 7-3 Mass of ES on the fibre for different ES concentrations and log K_{fw} values for ES as function of pH, background electrolyte 1 mM NaHCO_3 and 20 mM NaCl.

Once m_{fb} at the equilibrium was determined, K_{fw} for ES as a function of pH was calculated with equation 4.7 in Section 4.6.1. In order to obtain a more precise value for K_{fw} , four concentrations of ES were employed. K_{fw} for ES was constant with pH up to pH 8 and then decreased. However, the decrease at pH 10 and 12 can be considered negligible once the logarithmic is calculated (the difference was less of 0.3 log units) and log K_{fw} for ES can be considered constant with pH (Figure 7-3). The obtained values of log K_{fw} were in agreement (maximum difference 0.3 log units) with the values obtained by Valor *et al.* [318] for PA* coated fibres (Table 7-2)

For all studied pH the negligible-depletion condition (equation 4.9) was fulfilled (Table 7-3).

Table 7-3 Negligible depletion condition for PA* fibres at different pH values

	pH 4	pH 6	pH 8	pH 10	pH 12
$K_{fw} \cdot x \frac{V_F}{V_W}$	0.0630	0.0470	0.0442	0.0584	0.0332

7.3.2 Determination of K_{HA} and percentage of ES bound to HA

The HA-water partition coefficient for ES, K_{HA} , was estimated as a function of pH and HA concentration, as described in Section 4.6.2. It can be assumed that no interactions between HA and the fibres occurred since no HA fouling on the same PA* fibres was detected in a previous study [168] and no colour on the fibres was visually observed during this work.

The mass on the fibre m_{fb} was determined in order to estimate the mass and concentration of freely dissolved ES in aqueous solution, m_w and C_w (equations 4.12 and 4.13 in Section 4.6.2), the mass and concentration of ES sorbed to HA, m_{HA} and C_{HA} (equations 4.14 and 4.15) and in turn calculated K_{HA} with equation 4.11. Different concentrations of ES were employed to determine K_{HA} with more precision.

Figure 7-4a shows m_{fb} as a function of pH for different ES concentrations with and without HA (HA concentration 12.5 mgC/L). The results indicated greater extraction of ES when HA was not present, since ES was bound with HA and there was less freely dissolved ES available in solution to be removed by the fibre. These results are confirmed by the values of m_{fb} as a function of HA concentration (Figure 7-4c), as lower extraction is achieved with increasing HA concentration due to the increase of percentage of ES bound to HA.

Figure 7-4b and Figure 7-4d show the sorption isotherms (equation 4.11) obtained as a function of pH and HA concentration, respectively. The slopes of all the obtained isotherms were close to unity, so n_i was set equal to 1 for the determination of K_{HA} [278]. All isotherms had a correlation coefficient r^2 above 0.98

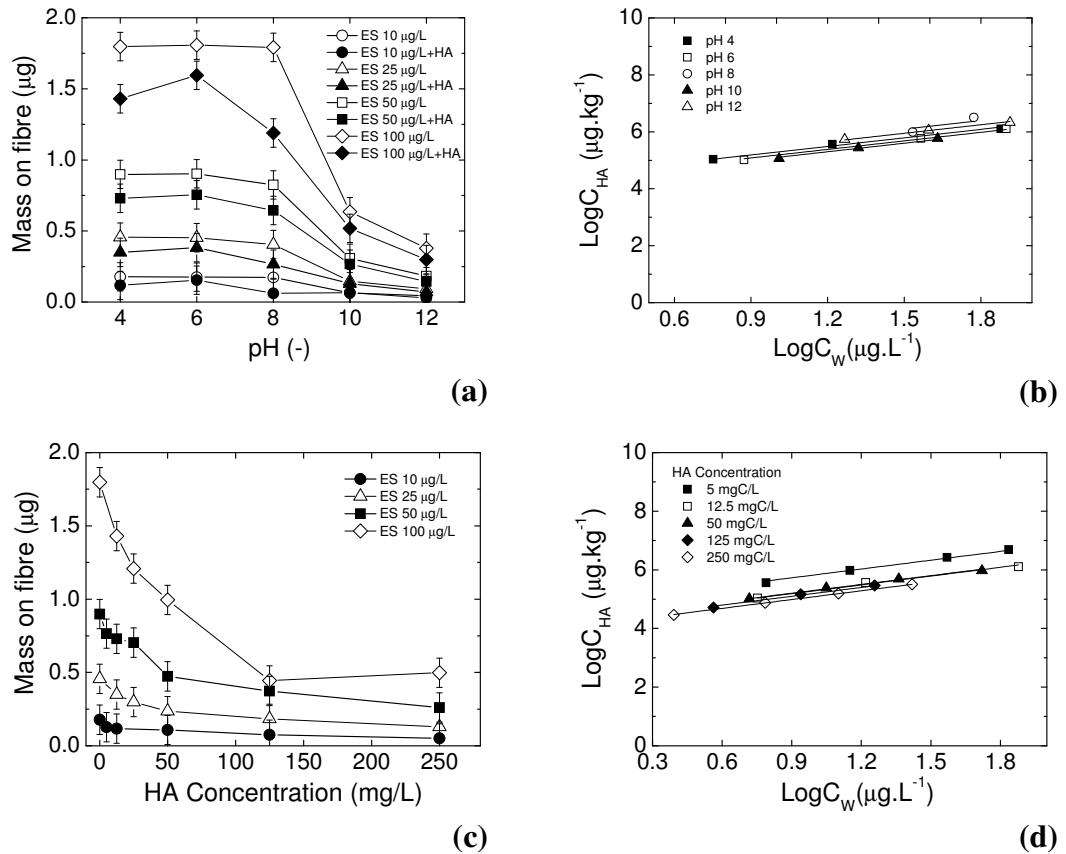


Figure 7-4 (a) Uptake of ES by PA* fibre as a function of pH, HA 12.5 mgC/L (b) Humic Acid-water sorption isotherms for ES as a function of pH (c) uptake of ES by PA* fibre as a function of HA concentration (d) Humic Acid-water sorption isotherms for ES as a function of HA concentration, background electrolyte 1 mM NaHCO_3 and 20 mM NaCl .

The logarithmic values of K_{HA} obtained from the slope of the sorption isotherms are represented in Figure 7-5, together with the fraction of ES bound to HA, f_{HA} , determined with equation 4.16.

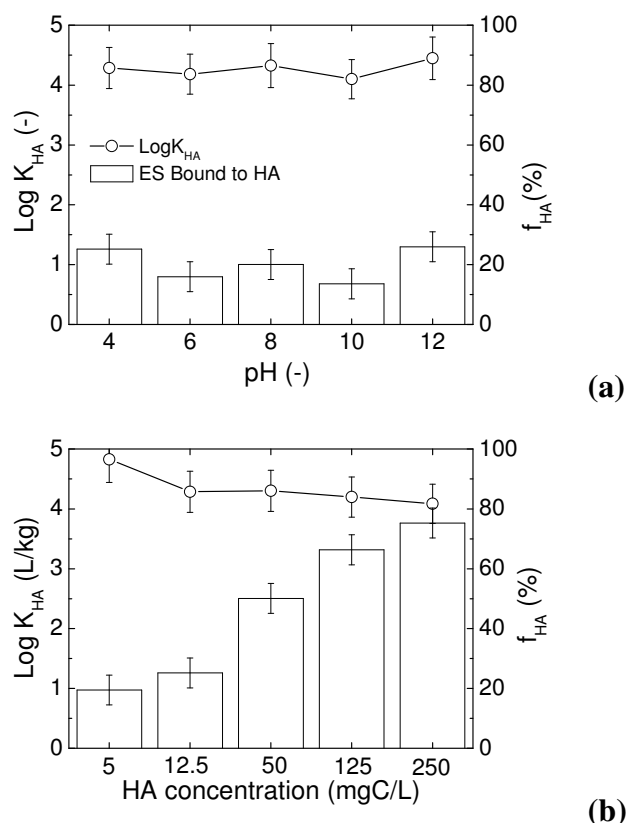


Figure 7-5 (a) HA-water partition coefficient and fraction of ES bound to HA as a function of pH, HA 12.5 mgC/L and **(b)** as a function of HA concentration, ES 10 $\mu\text{g/L}$, background electrolyte 1 mM NaHCO_3 and 20 mM NaCl .

$\text{Log } K_{\text{HA}}$ and the fraction of ES bound to HA can be considered constant with pH, in agreement with what was found for other organochloride pesticides [309]. $\text{Log } K_{\text{HA}}$ decreased with increasing HA concentration indicating that complexation is limited by the ES mass available [168]. The percentage of ES bound to HA increased with HA concentration.

7.4 Influence of pH on ES retention

The correlation between micropollutant MW/membrane MWCO ratio and ES removal in the presence of HA was investigated by determining ES retention with and without HA for TFC-SR2 and TFC-SR3 as a function of pH. While pH did not influence the formation of ES-HA complexes and the percentage of ES bound to HA (Figure 7-5a), it is known to influence membrane pore size [153].

Ratio of permeate flux J_v and initial pure water flux J_0 , that is an indicator of membrane fouling, together with ES adsorption to the membrane were determined as they might affect ES retention [30, 132, 339, 340].

Figure 7-6 shows that for both membranes, J/J_0 (dark symbols) was above unity and fouling did not occur. For similar membranes and the chosen HA concentration (12.5 mgC/L) fouling has been shown to occur only in the presence of calcium [130]. When ES only was filtered J_v/J_0 (open symbols) was constant with pH and close to unity for both membranes. When ES and HA were filtered J_v/J_0 (open symbols) was close to unity for the tighter TFC-SR3 but increased with pH for the looser TFC-SR2. Increased permeate flux in the presence of NOM at pH greater than 4 has been previously observed for “loose” NF membranes [153, 339].

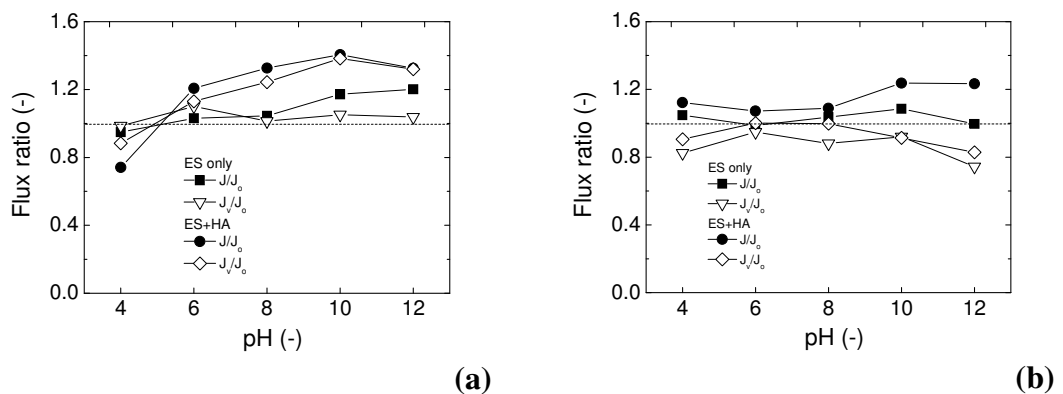


Figure 7-6 Ratio of pure water flux after the experiments J and initial pure water flux J_0 (dark symbols) and ratio of permeate flux J_v and initial pure water flux J_0 (open symbols) for filtration of ES only and ES and HA as a function of pH for (a) TFC-SR2 (b) TFC-SR3. ES 10 $\mu\text{g/L}$, HA 12.5 mgC/L, pressure: 5 bar, background electrolyte 1 mM NaHCO_3 and 20 mM NaCl (error bars not shown for clarity)

ES adsorption to the membranes was calculated with a mass balance using equation 2.4 (Section 2.2.2). ES adsorption onto the membranes was independent of pH (Figure 7-7). For TFC-SR3, ES adsorption was low and not influenced by HA, while for the more hydrophobic TFC-SR2 ES adsorption was higher and increased slightly with HA.

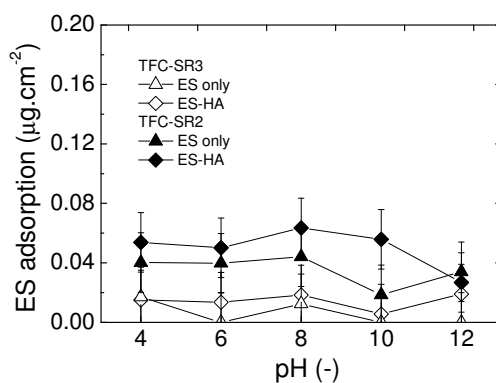


Figure 7-7 ES adsorption to the membranes with and without HA as a function of pH. ES 10 µg/L, HA 12.5 mgC/L, pressure: 5 bar, background electrolyte 1 mM NaHCO₃ and 20 mM NaCl.

ES retention was determined as a function of pH with and without HA. For both membranes, in the absence of HA, ES retention varied with pH (Figure 7-8) and this was attributed to the variation of membrane characteristics (MWCO) with pH combined with hydrolyzation of ES isomers to ES-diol, which has a lower molecular weight and higher polarity (Table 3-5) and it is therefore expected to have lower retention [76].

For TFC-SR3 (micropollutant MW/membrane MWCO ratio > 1) HA increased ES retention at any pH. For TFC-SR2 (micropollutant MW/membrane MWCO ratio < 1) ES retention in presence of HA decreased at pH 6, 8 and 10 and was similar at pH 4 and 12. Decrease in ES retention in presence of HA was observed for the “loose” membrane, confirming the inferred correlation between micropollutant MW/membrane MWCO ratio and micropollutant removal in presence of NOM. Decreased ES retention in the presence of HA for TFC-SR2 corresponded to an increase in flux ratio and ES adsorption, as observed in previous studies [30, 339]. The mechanisms behind the lower ES retention in the presence of HA for TFC-SR2 will be elucidated in Section 7.7.

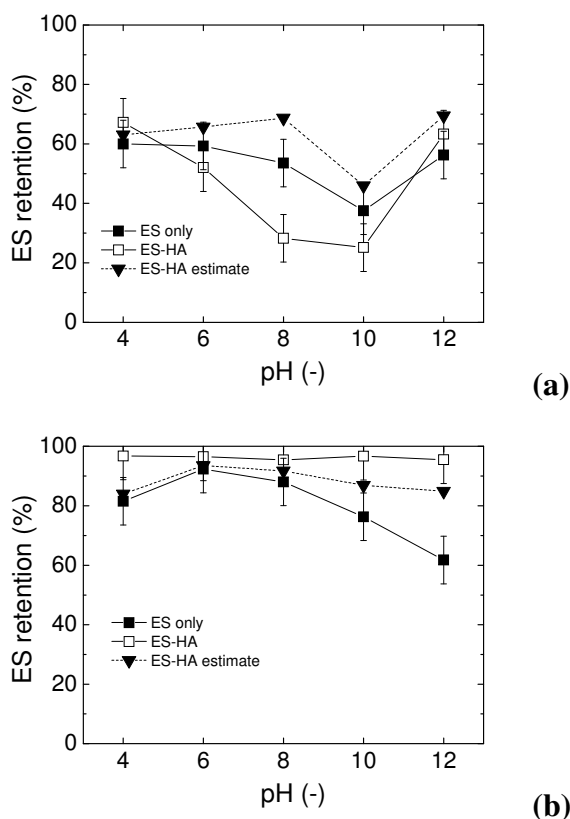


Figure 7-8 ES retention with and without HA as a function of pH for **(a)** TFC-SR2 **(b)** TFC-SR3. ES 10 $\mu\text{g/L}$, HA 12.5 mgC/L, pressure: 5 bar, background electrolyte 1 mM NaHCO_3 and 20 mM NaCl. Dotted lines indicate ES retention in the presence of HA estimated using the calculated partition coefficient K_{HA} .

7.5 Influence of HA on ES retention

In order to investigate the role of ES-HA complexes on ES removal, retention of ES as a function of HA concentration was studied. Since HA concentration influenced ES-HA complex formation and percentage of ES bound to HA (Figure 7-5b), ES retention in presence of HA was expected to be affected by HA concentration.

For both membranes ES retention was studied at pH 4 in order to minimize charge exclusion effects between the membrane surface and HA. At pH 4 both membranes are neutral (Table 4-2) and most of HA functional groups dissociates at pH > 4 [225, 229], while ES does not dissociate at any of the studied pH (Section 3.4.3). For TFC-SR2 ES retention as a function HA concentration was investigated also at pH 8, where the presence of HA decreased ES retention (Figure 7-8a). For TFC-SR3 ES

retention as a function of HA concentration at pH 8 was not studied since ES retention in presence of HA was independent of pH (Figure 7-8b).

For both membranes, flux ratio as a function of HA concentration (Figure 7-9) confirmed what was observed in Figure 7-6. For TFC-SR2 fouling occurred at pH 4 for HA concentration above 125 mgC/L, while at pH 8 J/J_0 was above the unity for HA concentration greater than 12.5 mgC/L. The presence of HA increased J_v and J with respect to J_0 for the looser TFC-SR2 at pH 8. Fouling did not occur also for TFC-SR3 (J/J_0 close to unity), even though during filtration J_v/J_0 was slightly below unity. It is inferred that for the tighter TFC-SR3 concentration polarisation occurred during filtration, lowering permeate flux. Nevertheless, concentration polarisation did not result in membrane fouling.

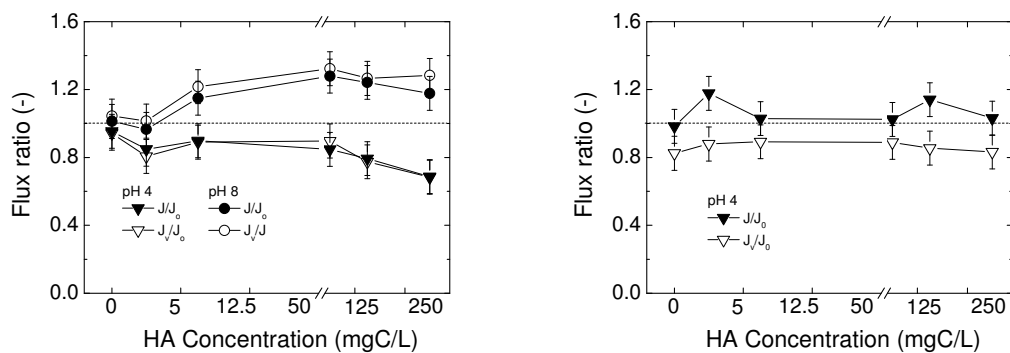


Figure 7-9 Ratio of pure water flux after the experiments J and initial pure water flux J_0 (dark symbols) and ratio of permeate flux J_v and initial pure water flux J_0 (open symbols) for filtration of ES as a function of HA concentration for **(a)** TFC-SR2 at pH 4 and pH 8 and **(b)** TFC-SR3. ES 10 $\mu\text{g/L}$, HA 5 - 250 mgC/L, pressure: 5 bar, background electrolyte 1 mM NaHCO_3 and 20 mM NaCl.

As shown in Figure 7-10, for TFC-SR3 (open symbols) ES adsorption was independent from HA concentration, while for TFC-SR2 (dark symbols) ES adsorption increased slightly with HA concentration up to HA 50 mgC/L. The decrease in ES adsorption for HA greater than 50 mgC/L might be caused by the

high HA concentration preventing ES to adsorb to the membrane. As observed in Figure 7-7, ES adsorbed more to TFC-SR2 and adsorption was pH independent.

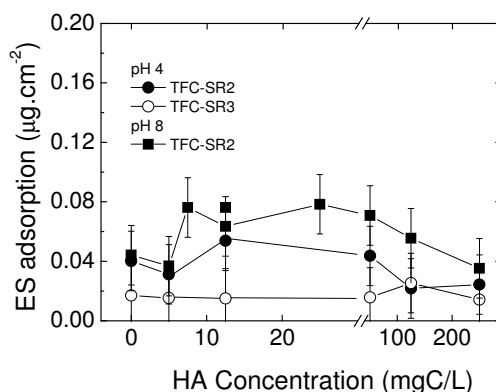


Figure 7-10 ES adsorption to the membranes with and without HA as a function of pH. ES 10 µg/L, HA 5-250 mgC/L, pressure: 5 bar, background electrolyte 1 mM NaHCO₃ and 20 mM NaCl.

ES retention was determined for both membranes (Figure 7-11). For the tighter TFC-SR3 ES retention was independent from HA concentration. For the looser TFC-SR2 ES retention increased with HA concentration at pH 4, while decreased with HA concentration at pH 8 up to HA 50 mgC/L, confirming what observed for HA 12.5 mgC/L in Figure 7-8.

In summary, the presence of HA (at concentration lower than 125 mgC/L) did not foul TFC-SR2 or TFC-SR3 and, on the contrary for TFC-SR2 it increased the permeate flux and the pure water flux after filtration at pH above 4. A correlation between micropollutant removal mechanisms in the presence of NOM and the ratio of micropollutant MW and membrane MWCO was previously inferred, since decreased micropollutant retention in the presence of NOM was observed in “loose” NF membranes (Section 7.1). The presence of HA increased ES retention for the tighter TFC-SR3 and decreased ES retention for TFC-SR2, confirming this hypothesis. However, decrease of ES retention in the presence of HA for TFC-SR2 was pH dependent, indicating that other mechanisms occurred.

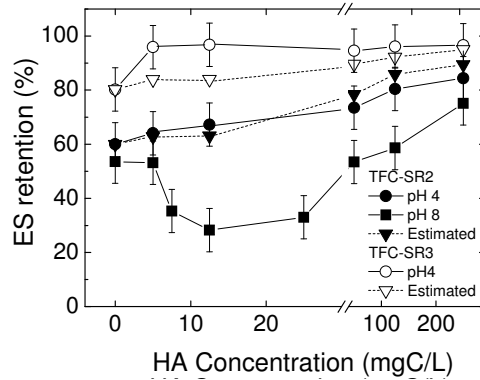


Figure 7-11 ES retention as a function of HA concentration for TFC-SR2 at pH 4 and pH 8 and for TFC-SR3 at pH 4. ES 10 $\mu\text{g/L}$, HA 5- 250 mgC/L, pressure: 5 bar, background electrolyte 1 mM NaHCO_3 and 20 mM NaCl. Dotted lines indicate ES retention in the presence of HA estimated using the calculated partition coefficient K_{HA} .

While a relationship between increase/decrease of micropollutant retention in the presence of NOM and competition of micropollutant-NOM adsorption on the membrane has been inferred [340, 342], in this study ES adsorption to the membranes was not believed to influence ES retention in the presence of HA. For TFC-SR2 ES adsorption was similar at pH 4 and pH 8 (Figure 7-10) while ES retention in the presence of HA increased at pH 4 and decreased at pH 8 (Figure 7-11).

7.6 Estimation of ES removal in the presence of HA

In order to understand the mechanisms of ES removal in the presence of HA, the role of solute-solute interactions (formation of ES-HA complexes) and solute-membrane interactions on ES retention was quantified.

The influence of the formation of ES-HA complexes on ES retention was estimated from the calculated partition coefficient, K_{HA} , and the fraction of ES bound to HA, f_{HA} , using the approach developed by Neale and Schäfer for UF [279] and adapted in this study for NF.

From equation 2.3:

$$R_o = 1 - \frac{c_p}{c_f} = 1 - \frac{m_p}{m_f} \frac{V_f}{V_p} \quad (7.1)$$

Therefore, in order to determine ES retention in the presence of HA, the mass of ES in the feed and in the permeate was estimated.

Some assumptions were made to determine the mass of ES bound to HA and freely dissolved in solution in the feed and in the permeate:

- (1) The total mass of ES in solution ($m_{ES\text{tot}}$) is either freely dissolved (m_{fES}) or complexed to HA (m_{ES-HA}):

$$m_{ES\text{tot}} = m_{ES-HA} + m_{fES} \quad (7.2)$$

therefore in the feed solution

$$m_{ES\text{totfeed}} = m_{ES-HA\text{feed}} + m_{fES\text{feed}} = f_{HA} \cdot m_{ES\text{totfeed}} + (1 - f_{HA}) \cdot m_{ES\text{totfeed}} \quad (7.3)$$

- (2) ES complexed with HA is retained together with the HA to which it is complexed to;
- (3) ES freely dissolved in solution has the same retention of ES during experiments without HA carried out at the same conditions (pH, pressure and background electrolyte).

The first two assumptions can be considered generally valid, since ES does not sorb to the glass and HA have a much bigger MW than ES. However, the last assumption will not be true if the presence of HA influences the retention of freely dissolved ES via solute-membrane interactions. Even in absence of fouling HA-membrane interactions can influence the retention of freely dissolved ES and result in different overall ES retention than the estimated retention. As discussed before, HA can adsorb on the membrane surface resulting in pore blocking [87] and increasing membrane charge [87, 125, 154], membrane MWCO [133] and membrane hydrophilicity [125, 339].

From assumption (1) the total retention of ES in the presence of HA, $R_{ES\text{tot}}$, is the “sum” of the retention of the freely dissolved ES, R_{fES} , and the retention of the ES complexed with HA, R_{ES-HA} [343]. From assumption (2) retention of ES complexed

to HA, R_{ES-HA} , can be considered similar to R_{HA} and from assumption (3) retention of freely dissolved ES, R_{ESf} , can be considered similar to the retention of ES during experiments without HA, R_{ES} .

The total mass of ES in the permeate can be therefore calculated as:

$$m_{ES\text{totperm}} = m_{ES-HA\text{perm}} + m_{fES\text{perm}} = (1-R_{HA}) m_{ES-HA\text{feed}} + (1-R_{ES}) m_{fES\text{feed}} \quad (7.4)$$

$R_{ES\text{tot}}$ can then be determined from $m_{ES\text{totfeed}}$ and $m_{ES\text{totperm}}$ as indicated by equation 7.1.

The mass of ES adsorbed to the membrane during filtration in the different cases was not explicitly considered in this methodology since retention of ES was determined after saturation was reached. Moreover, the difference of ES adsorbed to the membranes with and without HA was negligible with respect to the full mass balance.

$R_{ES\text{tot}}$ determined with the method described above is similar to the retention of ES measured during experiments with ES and HA if all the assumptions are valid. Therefore, if $R_{ES\text{tot}}$ differs from the experimental retention it can be concluded that assumption (3) is not verified and solute-membrane interactions play a role. $R_{ES\text{tot}}$ is the total retention of ES due to the formation of ES-HA complexes. If $R_{ES\text{tot}}$ is similar to the experimental retention it can be concluded that solute-solute interactions (the formation of ES-HA complexes) are the dominant retention mechanism. However, if $R_{ES\text{tot}}$ and the experimental retention differ, solute-membrane interactions can be considered more important.

7.7 Mechanisms of ES removal in the presence of HA

$R_{ES\text{tot}}$ estimated from the calculated partition coefficient K_{HA} (i.e. from f_{HA}) with the methodology described in Section 7.6 is indicated with a dotted line in Figure 7-8 for different pH and Figure 7-11 for different HA concentrations, where it was compared with the experimental retention obtained for ES in the presence of HA.

For both membranes at pH 4 estimated and experimental retention as a function of HA concentration were similar (Figure 7-11), confirming that at this pH ES-HA interactions were the dominant removal mechanism. ES-HA interactions increased with HA concentration (Figure 7-5b) and ES retention in the presence of HA increased with HA retention since ES-HA complexes were retained by size exclusion. For TFC-SR3 increase in ES retention at high HA concentration was less pronounced than for TFC-SR2 due to the high retention already achieved.

For TFC-SR3 estimated and experimental retention were similar for all the studied pH (Figure 7-8b), indicating that solute-solute interactions and size exclusion were the dominant retention mechanisms for this membrane. The formation of ES-HA complexes did not change with pH (Figure 7-5a) and ES retention in the presence of HA was constant with pH for TFC-SR3 (Figure 7-8).

For TFC-SR2 estimated and experimental retention differed at pH 6, 8 and 10, when ES retention in the presence of HA was lower than retention of ES only (Figure 7-8b). It is evident that the formation of ES-HA complexes, which was constant with pH, was not the dominant removal mechanism and solute-membrane interactions played a role.

The difference between estimated retention (dotted line) and experimentally obtained retention for TFC-SR2 is evident in Figure 7-11, where ES retention at pH 8 is depicted as a function of HA concentration. At low concentrations of HA, solute-membrane interactions were dominant, ES retention decreased with increasing HA concentration and the difference between estimated and experimental retention increased. At high HA concentrations, the percentage of ES bound to HA increased (Figure 7-5b), the importance of solute-solute interactions with respect to solute-membrane interactions increased, ES retention in the presence of HA increased and the difference between estimated and experimental retention decreased.

The U-shape of the retention curve in Figure 7-11 indicated that solute-membrane interactions were dominant for intermediate HA concentrations while ES-HA

interactions became more important at high HA concentrations. Nevertheless, even at high HA concentrations ES retention was lower than the estimated retention since solute-membrane interactions could not be considered negligible.

In order to investigate further the contribution that solute-membrane interactions had on ES retention in the presence of HA, the characteristics of both membranes at neutral pH were evaluated with and without HA. Retention of inert organics and Na was calculated for clean membrane and membranes pre-filtered with 12.5 mgC/L of HA and background electrolyte. Membrane MWCO, Na retention and contact angle were determined as described in Appendix 2 to evaluate changes in membrane pore size and hydrophilicity due to the presence of HA.

As depicted in Table 7-4, membrane MWCO increased after HA filtration and Na retention decreased for both membranes, confirming similar results found in previous studies [87, 133]. Since the presence of charged HA was shown to increase membrane charge [57] and the membrane pore size is believed to increase at higher membrane charge [153], it can be concluded that the filtration of HA was responsible for the increase in MWCO and the decrease in Na retention.

Table 7-4 MWCO, contact angles and sodium retention for a clean TFC-SR2 and TFC-SR3 and membranes through which 12.5 mgC/L of HA and background electrolyte were filtered

	TFC-SR2		TFC-SR3	
	Clean	HA	Clean	HA
MWCO	460	496	165	179
Contact angle	57 ± 2	49 ± 1	44 ± 1	59 ± 2
Na retention (%)	21	15	61	27

The increase in MWCO for TFC-SR3 did not influence ES retention as the increased MWCO was still smaller than ES molecular weight (407 g/mol). In the case of TFC-SR2, for which micropollutant MW/membrane MWCO ratio < 1 and ES was

partially retained, the increased MWCO decreased the ratio further, decreasing in turn ES retention.

After HA were filtered the observed contact angle decreased for TFC-SR2 and increased for TFC-SR3. For membranes fouled by NOM contact angle measurements have been shown to be representative of the fouling layer. In the case of fouling by HA, contact angles indicated the adhesion of a layer of intermediate hydrophobicity [65, 133, 161, 163].

After HA filtration TFC-SR3 had a visible brownish layer, indicating HA deposits, and the increased contact angle is thought to represent the hydrophobicity of the deposits. Not only the hydrophobic HA could be responsible for higher contact angle, but their roughness are likely to increase the observed contact angle [344]. Since a coloured layer was not visible on TFC-SR2 after filtration of HA, the decreased contact angle for this membrane is thought to reflect the membrane hydrophilization due to filtration of charged HA [125]. Although HA did not foul TFC-SR2, the penetration of small HA fractions through the membrane pores (HA retention by TFC-SR2 was about 80%, as shown in Figure 6-6) is believed to influence membrane characteristics. Increase in hydrophilization can also explain the observed increase in permeate flux at high pH (Figure 7-6a).

A schematic of the proposed mechanisms is presented in Figure 7-12. At pH 4 when charge repulsion between solute and membrane is minimum, since the membrane is neutral and HA are not completely dissociated, size exclusion and solute-solute interactions (i.e. formation of ES-HA complexes) dominated ES retention. At neutral pH, negatively charged HA are filtered through the membrane pores, increasing their negative charge and in turn membrane MWCO. The increased intra-membrane electrostatic repulsion due to interactions with HA is believed to expand the membrane matrix, increasing the pore size [153]. For the looser TFC-SR2, whose micropollutant MW/membrane MWCO ratio < 1 , interactions between charged HA and the membrane resulted in decreased ES retention. For the tighter TFC-SR3, whose micropollutant MW/membrane MWCO ratio > 1 , the increase in MWCO was

not sufficient to allow the increase in ES passage and ES-HA interactions were the dominant mechanism of retention by size exclusion.

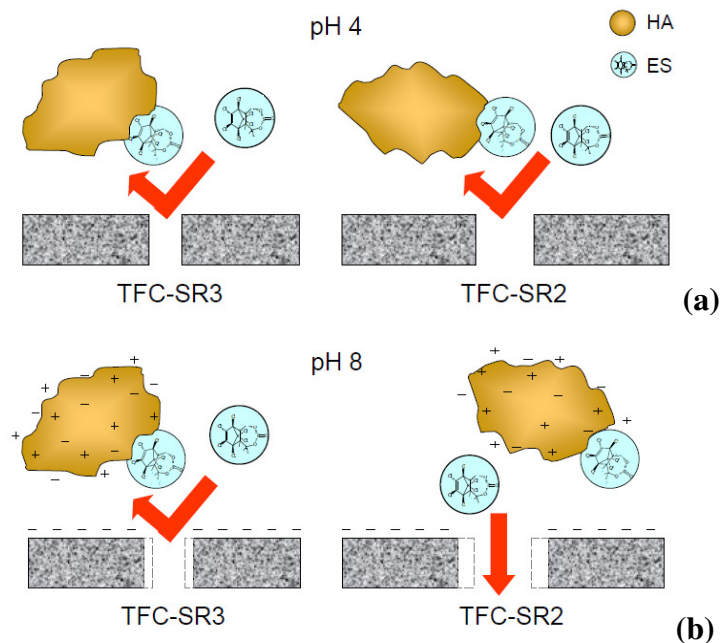


Figure 7-12 Conceptual sketch of main retention mechanisms for freely dissolved ES and ES-HA complexes by TFC-SR2 and TFC-SR3 at (a) pH 4 and (b) pH 8.

7.8 Conclusions

This chapter investigated and quantified the role of solute-solute interactions and solute-membrane interactions on ES removal in the presence of HA. For the first time the formation of complexes between ES and aquatic HA was quantified and the contribution of the ES-HA complexes to ES retention by NF was estimated.

The percentage of ES complexed with HA increased with HA concentration and it was not affected by pH. For the tighter TFC-SR3, for which ES MW/membrane MWCO ratio was higher than 1, ES retention increased in the presence of HA independently from pH and HA concentration. For the looser TFC-SR2, for which ES MW/membrane MWCO ratio was lower than 1, ES retention in the presence of HA increased with HA concentration at pH 4 but decreased with increasing concentration at pH 8 (up to HA concentration of 50 mgC/L).

For TFC-SR3 ES retention in the presence of HA was due to solute-solute interactions (formation of ES-HA complexes) and size exclusion. For TFC-SR2 solute-solute interactions and size exclusion were dominant at pH 4, when charge interactions between HA and the membrane were minimum. With increasing pH charged HA increased the MWCO of TFC-SR2, decreasing ES retention: solute-membrane interactions were more important than solute-solute interactions for ES removal in the presence of HA.

The estimation of the specific contributions of ES-HA complex formation (solute-solute interactions) and HA-membrane interactions (solute-membrane interactions) to ES removal was necessary to explain retention mechanisms of ES in the presence of HA.

8. Effects of pressure on solute retention

8.1 Introduction

This chapter investigates the role of pressure on solute retention by taking into account solute-solute interactions and solute-membrane interactions. As explained in Chapter 1 understanding the influence of operating parameters on solute retention is crucial for operating membrane plants in a more economical and environmentally friendly manner. Nevertheless, the effects of operational parameters on the retention of some solutes are still not well understood [7].

In Section 2.2.5 and Chapter 5 it was shown that pressure, which is the driving force in the transport of water and solutes through NF membranes, affects permeate flux J_v , solute flux J_s and solute retention. Retention of metals, ions and salts by NF has been shown to increase with operating pressure [54, 66, 114, 138, 330, 331]. Transport of inorganic solutes and salts through NF and RO membranes is believed to be dominated by diffusion and it can be well described by the solution-diffusion model, neglecting the convection term in the transport equation [102, 110, 114]. If diffusion is dominant, the driving force for the transport of solutes becomes the concentration gradient between the feed and the permeate (equation 4.5 in Section 4.4.2). With increasing pressure the permeate flux increases while diffusion remains constant, since it depends on the concentration gradient not on pressure. Therefore, if diffusion is the main mechanism of solute transport, retention increases with pressure as water flux increases but solute flux does not.

Retention of organic micropollutants by NF and RO was shown to increase with pressure and the solution-diffusion model was successfully applied to predict their retention [71, 106, 107], indicating that also the transport of micropollutants through NF might be dominated by diffusion. However, several studies [75, 91, 116, 139-142] showed that micropollutant retention could be constant or could decrease with pressure.

Retention of NOM, disinfection by products and halogenated solvents by NF was observed to decrease with increasing pressure and this was attributed to convective dominated transport through the membranes [116, 345]. If convection is the dominant transport mechanism, higher pressure is expected to increase both water flux and solute flux, resulting in decreasing or constant retention. It is widely accepted that transport of organic solutes by convection cannot be neglected in NF membranes [7, 23, 108] and both diffusion and convection terms are present in the hydrodynamic model (Section 5.2).

From the literature it can be inferred that the relative importance of diffusion and convection on organic solute transport might be responsible for increase/decrease of solute retention with pressure. However, this hypothesis has never been systematically investigated for micropollutants. Studies on the importance of diffusion and convection on transport of organic solutes through NF membranes have focused on evaluating the contribution of each term to solute transport, without correlating it with increase/decrease of retention with pressure [108, 116, 117].

Diffusion was shown to contribute more than convection to transport of organic solutes for NF membranes that had the smallest pores [108, 116] and for organic solutes that had the smallest MW [117], indicating the importance of the ratio of solute size to pore size λ on the relative role of diffusion and convection. In another study on micropollutant retention, convection was found to be dominant for hydrophobic polar compounds, hydrophilic compounds and charged organic compounds, while diffusion was dominant for hydrophobic non-polar compounds [116]. However, micropollutant adsorption to the membranes was not taken into account, limiting the correctness of the obtained results. As expected from the hydrodynamic model equation, convection became dominant at high pressure (i.e. high J_v) [108, 116].

From the results obtained in the literature, it can be inferred that the ratio of solute size to pore size λ (equation 5.10 in Chapter 5) might be responsible for the predominance of diffusion or convection in micropollutant transport through NF

[346]. If $\lambda < 1$ convection should be the dominant transport mechanism, while if $\lambda > 1$ solute cannot penetrate inside the pores and diffusion should be prevailing. As a consequence, it could be expected that for $\lambda < 1$ retention should decrease with pressure, while for $\lambda > 1$ retention should increase with pressure.

Nghiem *et al.* [142] inferred that micropollutant adsorption to the membrane could be responsible for decrease of retention with increasing pressure. They inferred that when pressure increases, permeate flux and the drag forces within the membrane pores increase, desorption of micropollutants might be enhanced or adsorption time reduced, contributing to lower the retention.

In summary, it can be hypothesized that increase or decrease of micropollutant retention with pressure might depend on:

- solute size/pore size ratio λ (solute-membrane interactions), in turn affecting the importance of diffusion and convection contributions to solute transport through NF membranes;
- solute adsorption to the membranes (solute-membrane interactions).

A systematic study to investigate these hypotheses will be carried out in this chapter.

The influence of NOM on micropollutant retention with pressure has been scarcely studied. Xu *et al.* [87] observed both increase and decrease of retention with pressure for charged hydrophobic organics through several NF membranes. In the presence of NOM, retention of the charged hydrophobic organics was constant with pressure for all the studied membranes. The mechanisms behind this phenomenon were not examined. As shown in the previous chapter, HA can influence the size of the solutes by forming complexes with them (solute-solute interactions) and can influence the pore size of the membranes by solute-membrane interaction, in turn modifying λ . HA might also influence micropollutant adsorption to the membranes [340, 342]. Therefore HA are expected to influence solute retention with pressure and their effects on ES retention with pressure will be studied in this chapter.

In the first part of this chapter, retention of manganese, the chosen model inorganic, by TFC-SR2 and TFC-SR3 will be investigated as a function of pressure in order to verify findings in the literature for retention of inorganics with pressure. The influence of HA on manganese retention with pressure will not be investigated since results obtained in Chapter 6 showed that manganese-HA complexation did not affect manganese retention.

In the second part of this chapter, retention of pesticide ES, the chosen model micropollutant, by TFC-SR2 and TFC-SR3 will be investigated as a function of pressure. The contrasting results obtained in the literature for micropollutant retention with pressure invites a systematic investigation of the underlying mechanisms. The pore size of TFC-SR2 ($r_p = 0.52$ nm) and TFC-SR3 ($r_p = 0.38$ nm) is respectively bigger and smaller than the size of ES (Stoke radius $r_s = 0.48$ nm), allowing the study of the influence of λ on retention trends with pressure. Retention of ES in the presence of HA, chosen as representative of NOM, will also be investigated as a function of pressure.

The objectives of this chapter are to:

- confirm findings in the literature for retention of inorganic solutes as a function of pressure;
- investigate the role of λ , convection, diffusion and adsorption (solute-membrane interactions) on ES retention as a function of pressure;
- investigate the role of HA on ES retention as a function of pressure (solute-solute interactions);
- elucidate the transport mechanisms responsible for increase/decrease of ES retention with pressure.

ES diffusion was quantified with experiments in diffusion cells (Section 4.4.2) in order to establish the contribution of convection and diffusion to ES transport. Consequently, a similar approach to the one adopted by Opong and Zydney [113] and Yuan and Kilduff [101] was employed to elucidate solute transport mechanisms with pressure. The mentioned authors combined the hydrodynamic model with the

film model (Chapter 5) and utilised them in a phenomenological and non predictive manner to provide insight into how operating variables affected protein and NOM transport mechanisms through UF membranes. In this work, the models were applied in a phenomenological way to evaluate the transport mechanisms of ES through NF. While the hydrodynamic model has been already applied to predict the transport of several micropollutants through NF [27, 92, 347], its use in a phenomenological and non-predictive fashion for studying the influence of pressure on micropollutant retention is novel.

8.2 Filtration protocol

Filtration experiments for manganese and ES were carried out as described in Section 4.4.1 and Section 6.2. Manganese concentration of 5 mg/L, 1 mM NaHCO₃ and 20 mM NaCl of electrolyte background solution were employed in the experiments with manganese (Section 4.2). Pressure was varied between 5 and 15 bar and experiments were carried out at pH 7.

ES concentration of 10 µg/L, HA concentration of 12.5 mgC/L, 1 mM NaHCO₃ and 20 mM NaCl of electrolyte background solution were employed in the experiments with ES (Section 4.2). Membrane saturation by ES was reached in all experiments. The amount of ES required to reach membrane saturation was constant with pressure and depended on the volume of the filtered solution (i.e. on the mass of ES filtered). All experiments were carried out at pH 4 to minimise electrostatic interactions between HA and the membranes (Section 7.5), in turn minimizing the influence of HA on membrane pore size (Section 7.7) and allowing the use of the hydrodynamic model without the electrostatic term (Section 5.3).

8.3 Influence of transmembrane pressure on Mn removal

Figure 8-1 shows J/J_0 (the ratio of pure water flux before and after the manganese filtration experiments) and J_0 (pure water flux) and J_v (permeate flux) as a function of pressure. For TFC-SR3 flux ratio was slightly above the unity for any pressure and fouling did not occur, while for TFC-SR2 fouling occurred at high pressure (Figure 8-1a).

From Figure 8-1b it is possible to calculate the membrane permeability from the slope of the best linear fit. For both membranes the permeability did not change considerably between the filtration of pure water flux and the filtration of manganese. For TFC-SR3 the permeability decreased from 7.6 L/m².h.bar during the filtration of pure water flux to 6.7 L/m².h.bar during the filtration of manganese, while for TFC-SR2 the permeability decreased from 15.4 L/m².h.bar during the filtration of pure water flux to 13.5 L/m².h.bar¹ during the filtration of manganese. Decrease of permeability was attributed to concentration polarisation. Concentration polarisation was more pronounced for TFC-SR2 and increased with increasing pressure.

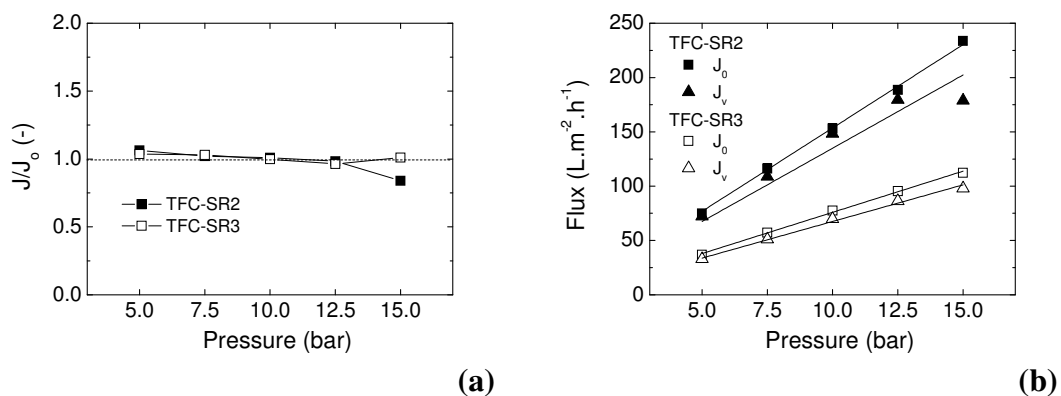
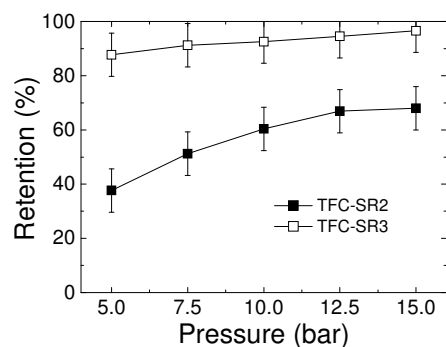
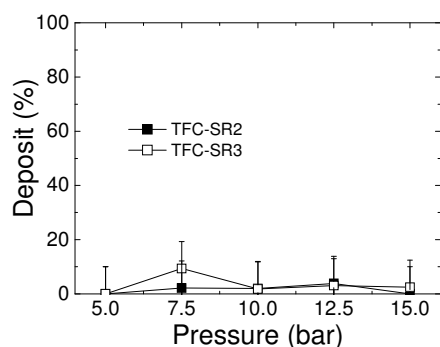


Figure 8-1 (a) Ratio of pure water flux after the experiments J and initial pure water flux J_0 and J and (b) J_0 and J_v as a function of pressure for TFC-SR2 and TFC-SR3. Manganese 5 mg/L, background electrolyte 1 mM NaHCO₃ and 20 mM NaCl, pH 7 (error bars not shown for clarity)

Manganese retention with pressure was higher for TFC-SR3 than for TFC-SR2 confirming the results obtained in Chapter 6 at pH 7. Manganese retention increased with pressure confirming findings in the literature for other salts and metals [54, 66, 114, 138, 331]. Manganese deposits on both membranes were negligible for any pressure, confirming results obtained in Chapter 6 for pH below 10.



(a)



(b)

Figure 8-2 (a) Manganese retention and **(b)** manganese deposits as a function of pressure for TFC-SR2 and TFC-SR3. Manganese 5 mg/L, background electrolyte 1 mM NaHCO₃ and 20 mM NaCl, pH 7

A study of the impact of NOM on retention of inorganics as a function of pressure would be valuable in order to investigate the influence of solute-solute interactions on transport mechanisms of inorganic solutes. In the case of manganese, complexation with HA occurred at pH above 8.5 (Figure 6-4) when manganese retention was high (99%) due to precipitation of MnCO₃ (Figure 6-6) and manganese transported across both membranes was negligible. For this reason, it was not possible to study the influence of HA on manganese transport as a function of pressure.

8.4 Influence of transmembrane pressure on ES removal

The retention of ES with and without HA as a function of pressure was determined for TFC-SR2 and TFC-SR3. As shown in Figure 8-3, for both membranes fouling

did not occur during ES filtration, since J/J_0 (ratio of pure water flux after filtration and initial pure water flux) and J_v/J_0 (ratio of permeate flux and initial pure water flux) were close to unity and constant with pressure. In the presence of HA, fouling occurred for TFC-SR2 with increasing pressure. The increase of flux reduction with increasing pressure in the presence of HA was attributed to cake layer formation and concentration polarisation [126]. For TFC-SR3 in the presence of HA J_v/J_0 was lower than unity and decreased with pressure, while J/J_0 was close to unity. For this membrane HA filtration decreased the flux, but the flux was easily restored once pure water was filtered.

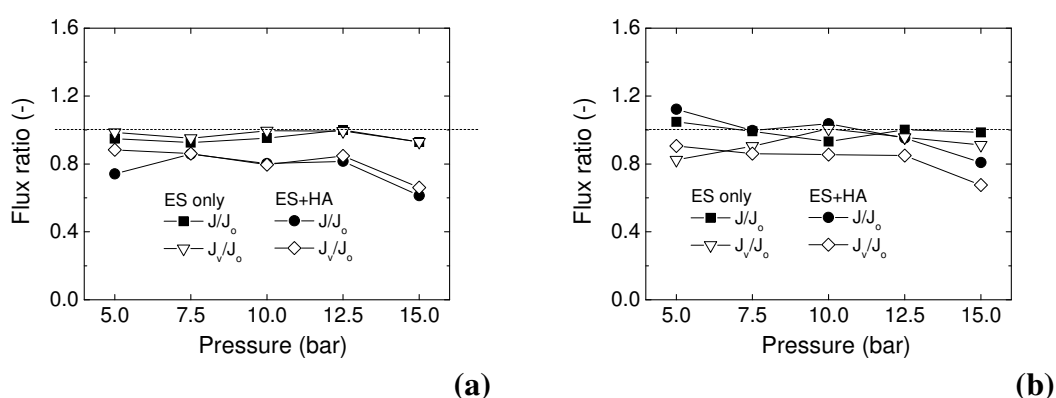


Figure 8-3 Ratio of pure water flux after the experiments J and initial pure water flux J_0 (dark symbols) and ratio of permeate flux J_v and initial pure water flux J_0 (open symbols) for filtration of ES only and ES and HA as a function of pressure for (a) TFC-SR2 (b) TFC-SR3. ES 10 $\mu\text{g/L}$, HA 12.5 mgC/L , pH 4, background electrolyte 1 mM NaHCO_3 and 20 mM NaCl (error bars not shown for clarity)

Figure 8-4 shows that pressure did not influence the mass of ES adsorbed to the membranes ($\pm 0.02 \mu\text{g/cm}^2$ variability). ES adsorption to the more hydrophobic TFC-SR2 was higher than to TFC-SR3. The presence of HA slightly decreased ES adsorption on TFC-SR2, while it had negligible influence on ES adsorbed to TFC-SR3, confirming what was observed in the previous chapter.

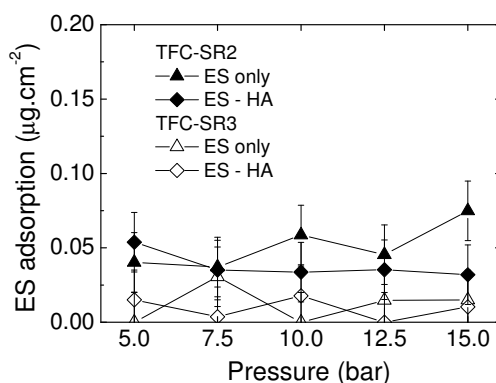


Figure 8-4 ES adsorption to the membranes with and without HA as a function of pressure. ES 10 µg/L, HA 12.5 mgC/L, pH 4, background electrolyte 1 mM NaHCO₃ and 20 mM NaCl.

Results of ES retention with pressure showed that for the tighter TFC-SR3 ($\lambda > 1$) ES retention increased with pressure, while for the looser TFC-SR2 ($\lambda < 1$) ES retention decreased with pressure (Figure 8-5a). In the presence of HA, ES retention slightly decreased for TFC-SR2 and was constant with pressure for TFC-SR3.

The flux of ES, determined as the passage of ES mass to the permeate side with time, confirmed the retention results (Figure 8-5b). For TFC-SR3 ES flux was constant with pressure and since J_v increased with pressure, it resulted in increasing ES retention. For TFC-SR2 both ES flux and J_v increased with pressure, decreasing ES retention. For both membranes ES flux in the presence of HA was lower than the flux of ES alone, resulting in higher ES retention.

These results confirmed the findings in the literature and seemed to endorse the hypotheses that λ and HA have a role in increase/decrease of retention with pressure. Decrease in retention was observed for TFC-SR2, which has higher ES sorption, in agreement with the hypothesis by Nghiem *et al.* [142] that micropollutant adsorption to the membrane could be responsible for decrease of retention with increasing pressure.

In the previous chapter it was concluded that when HA interacted with the membranes an increase of MWCO occurred. HA-membrane interactions were influenced by pH and their effects on ES retention depended on the ratio of ES MW and membrane MWCO (i.e. λ). The presence of HA increased the membrane MWCO at neutral pH, but HA-membrane interactions were negligible at pH 4. For the looser TFC-SR2 the increase in MWCO decreased the retention of ES in the presence of HA with respect to the retention of ES alone. In the case of the tighter TFC-SR3 the increase of MWCO was not sufficient to decrease ES retention in the presence of HA. In Figure 8-5a ES retention increased in the presence of HA for both membranes, confirming that HA did not increase membrane MWCO at pH 4 and therefore ES-HA interactions were the dominant mechanisms of ES retention.

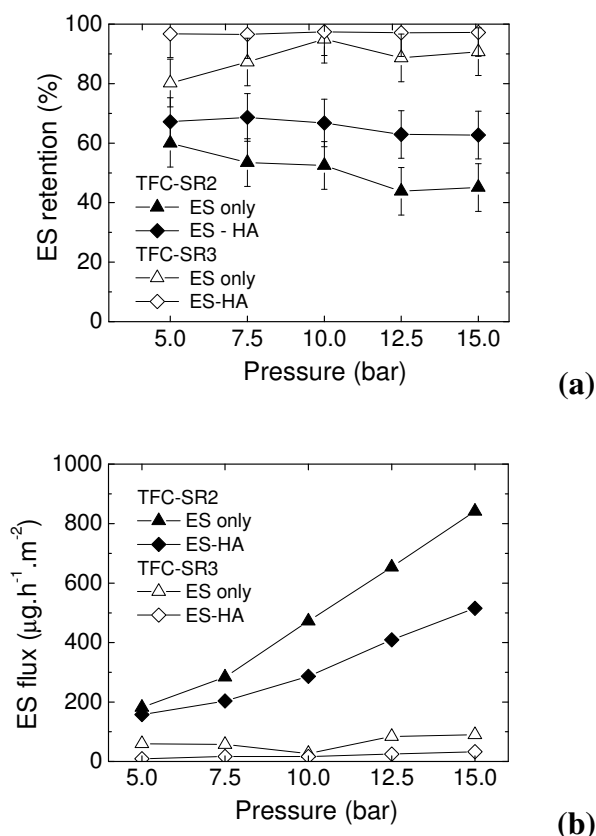


Figure 8-5 (a) ES retention with and without HA as a function of pressure for TFC-SR2 and TFC-SR3 (b) ES flux with and without HA as a function of pressure for TFC-SR2 and TFC-SR3. ES 10 µg/L, HA 12.5 mgC/L, pH, 4, background electrolyte 1 mM NaHCO₃ and 20 mM NaCl.

8.5 ES diffusion through NF membranes

In order to establish the contribution of convection and diffusion to ES transport, ES diffusion through TFC-SR2 and TFC-SR3 was quantified in diffusion cells, as described in Section 4.4.2. The aim was to verify the hypothesis that increase of micropollutant retention with pressure (TFC-SR3 case) was due to diffusion and decrease of retention with pressure (TFC-SR2 case) was due to convection.

Figure 8-6 shows the variation of the concentration of ES in the feed cell and in the permeate cell (C_f and C_p in equation 4.5) with time. Four concentrations of ES were employed in order to determine the diffusion coefficient D_m as the slope of the fitted equation 4.6. Even if both membranes were pre-saturated with ES in the stirred cell filtration apparatus, equilibrium during diffusion was not reached after 121 hours for any ES concentration.

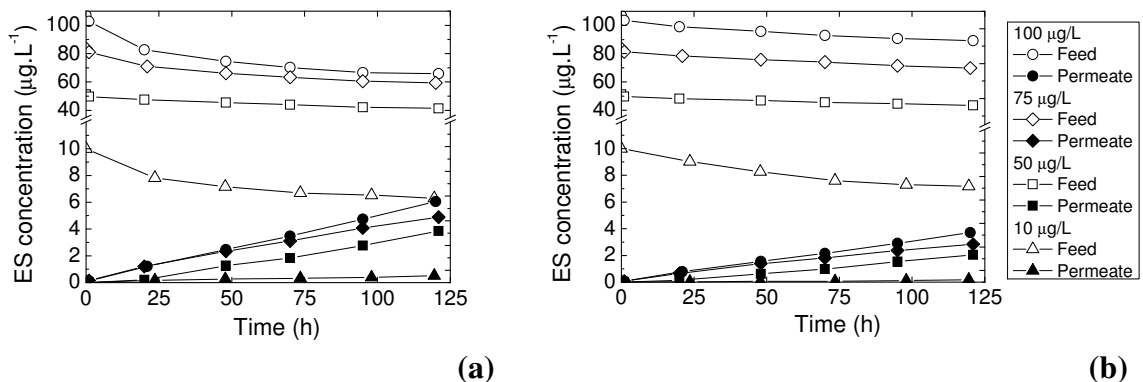


Figure 8-6 ES concentration in feed and permeate diffusion cells with time (a) TFC-SR2 and (b) TFC-SR3. ES 10-100 µg/L, pH 4.

Values of D_m for TFC-SR2 and TFC-SR3 are shown in Table 8-1. D_m was higher for the looser TFC-SR2 than for the tighter TFC-SR3, confirming that diffusion is more hindered in smaller pores and denser membranes [117].

The goodness of fitting (represented by r^2) for TFC-SR2 was worse than for TFC-SR3 (Table 8-1). One of the hypotheses of the Fick's law used for calculating D_m is that mass adsorbed to the membrane during diffusion is negligible with respect to the

mass in the diffusion cells (Section 4.4.2). The mass of ES adsorbed to TFC-SR3 during the whole diffusion experiments was negligible (Figure 8-7b). In the case of TFC-SR2 a small percentage of ES (0.2% of the mass of ES in the feed cell after 25 hours) adsorbed to the membrane at the beginning of the diffusion experiments (Figure 8-7a). Although both membranes were pre-saturated with ES during filtration experiments to reduce the amount of ES adsorbed during the diffusion experiments, a small quantity of ES still adsorbed to TFC-SR2 till its saturation. While the mass of ES adsorbed to TFC-SR2 was too small to invalidate the use of Fick's law, it is believed to be responsible for the lower goodness of fitting.

Diffusion coupling, i.e. the passage of water from the permeate cell to the feed cell, was between 2-3 mL for TFC-SR3 and 3-9 mL for TFC-SR2 out of the 250 mL of solution in each cell and it was considered negligible.

Table 8-1 Diffusion coefficients for ES through TFC-SR2 and TFC-SR3 membranes determined by fitting Fick's equation with experimental data obtained with diffusion cells. The coefficient of determination r^2 indicates the goodness of fitting. The membrane thickness $\Delta\delta_m$ was determined by SEM measurements.

Membrane	$\frac{D_m}{\Delta\delta_m}$ (cm/s)	r^2	$\Delta\delta_m$ (μm)	D_m (cm^2/s)
TFC-SR2	2.12E-06	0.933	157.85 \pm 2.60	3.34E-08
TFC-SR3	1.19E-06	0.993	142.07 \pm 3.72	1.69E-08

In order to estimate the contribution of diffusion to the total passage of ES through the membranes during the filtration experiments, the flux of ES through the membranes during diffusion experiments was compared with the flux of ES during the filtration experiments. According to the hydrodynamic model the flux during filtration is composed by a diffusion term and a convection term (in absence of electrostatic interactions). It was assumed that the diffusion term could be quantified during the diffusion experiments [116, 117].

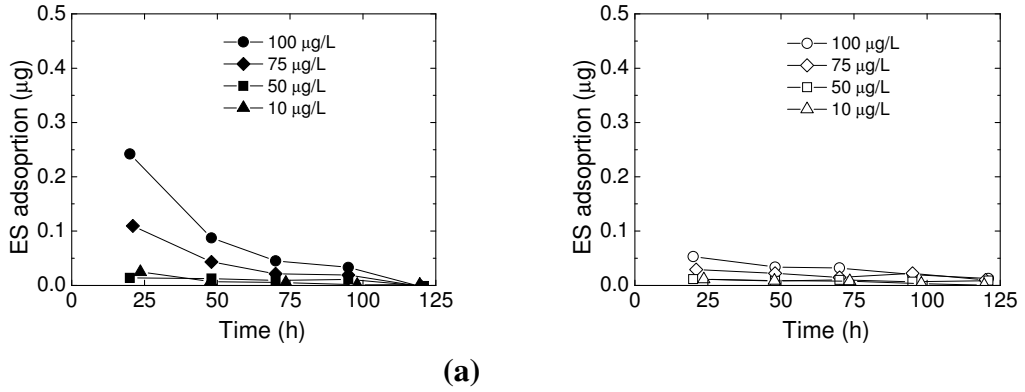


Figure 8-7 Adsorption of ES to **(a)** TFC-SR2 and **(b)** TFC-SR3 during diffusion experiments. ES 10-100 µg/L, pH 4.

While D_m has been inferred to be constant with solute concentration in the range of concentrations used in this study (Section 4.4.2), the flux of solute through the membrane is affected by the solute initial concentration, as observed for ES flux through TFC-SR2 and TFC-SR3 (Figure 8-6). ES fluxes during diffusion and filtration experiments were therefore compared by expressing the flux as a function of the estimated concentration of ES in the membrane boundary layer, c_{mf} (Figure 8-8).

In the case of diffusion experiments, c_{mf} was considered equal to C_F since concentration polarisation was assumed to be negligible (high stirring speed was employed). For the filtration experiments with the stirred cells, c_{mf} was calculated with the following equation derived from the film theory (see Section 5.1):

$$\frac{c_{mf} - c_p}{c_f - c_p} = \exp\left(\frac{J_v}{k_f}\right) \quad (8.1)$$

where the mass transfer coefficient k_f for ES was determined with equations 5.5 and 5.6 in Chapter 5 and corresponded to 2.10E-05 m/s.

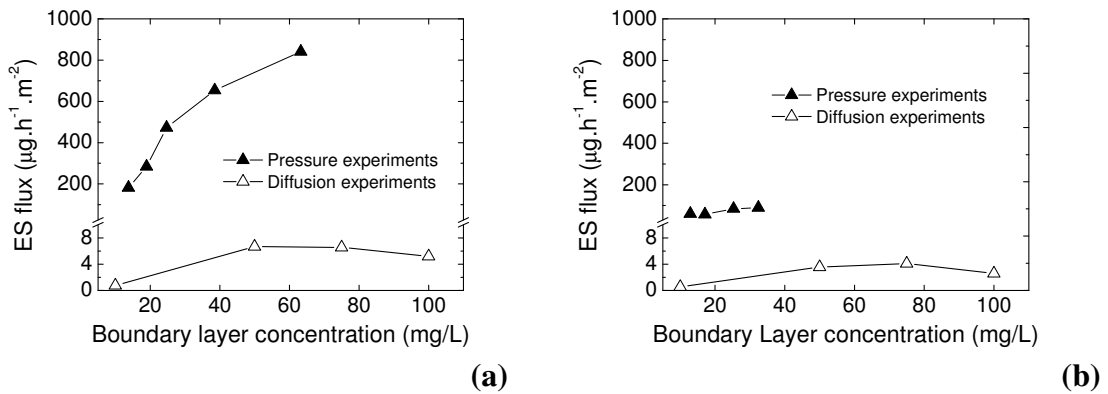


Figure 8-8 ES flux through (a) TFC-SR2 and (b) TFC-SR3 during diffusion experiments (open symbols) and filtration experiments (dark symbols) as a function of the estimated concentration in the membrane boundary layer.

It can be noted from Figure 8-8 that during filtration experiments c_{mf} increased with pressure more for TFC-SR2 than for TFC-SR3 (feed concentration c_f was 10 $\mu\text{g/L}$ for all the filtration experiments). The higher increase of c_{mf} for TFC-SR2 was due to higher J_v values for a certain pressure, since k_f in equation 8.1 was the same for both membranes. It can be concluded that for the same pressure higher concentration polarisation occurred for the looser TFC-SR2.

ES flux determined in diffusion experiments was higher for the looser TFC-SR2, confirming that the diffusion rate is higher through bigger pores. The percentage of ES flux due to diffusion with respect to the total flux obtained during filtration was lower for TFC-SR2 (0.9%) than for TFC-SR3 (2.9%). The obtained results confirmed that convection contribution to transport is higher for the looser membrane [116].

Findings from the diffusion experiments indicated that convection was the main transport mechanisms of ES through TFC-SR2 and TFC-SR3. The convection dominated transport of ES through both membranes invalidated the hypothesis for which when $\lambda > 1$ diffusion should be prevailing.

It must be highlighted that diffusive flux obtained with diffusion experiments is only an approximation of the diffusive flux considered in the hydrodynamic model [110, 117]. In filtration, solute retention and transport are controlled by the active layer; therefore solute transport through the membrane depends only on diffusion and convection through the active layer. The two transport terms of the hydrodynamic model (equation 5.7 in Chapter 5) refer to solute transport through the active layer only, without considering transport through the support layer and the non-woven fabric as these layers do not contribute to solute retention. In diffusion experiments, the diffusive flux of the entire membrane is measured. The support layer and the non-woven fabric hinders solute diffusion even if their pores are much bigger than the pores of the active layer because their thickness is two-three orders of magnitude bigger than the thickness of the active layer. The resistance of the support layer and of the non-woven fabric to diffusion cannot be neglected [113, 348]. As a result, the diffusive flux obtained with diffusion experiments is lower than the diffusive flux term in the hydrodynamic model.

8.6 Transport of ES through NF membranes

From diffusion experiments it appeared that convection was the dominant transport mechanism for ES through TFC-SR2 and TFC-SR3. As a result, the contribution of convection and diffusion could not explain ES retention trends with pressure. In order to understand how pressure influenced ES retention and examine transport mechanisms of ES, the hydrodynamic model combined with the film model was employed in a phenomenological, non-predictive way.

Opong and Zydney [113] and Yuan and Kilduff [101] compared experimental data for sieving of bovine serum albumin and NOM with the predictions of the hydrodynamic model to determine the convective and diffusive contributions to solute transport through UF membranes. According to the hydrodynamic model equation, the plots of the observed and actual sieving coefficients, S_o and S_a , versus J_v show characteristic curves (Section 5.4). At low values of J_v the sieving coefficients tend to one and diffusion is dominant. At high values of J_v , S_o tends to one, S_a decreases to an asymptotic value and convection dominates transport [101].

In the vicinity of the minimum of S_0 both convection and diffusion contribute to solute transport [113]. In previous studies, the hydrodynamic model was used to estimate the contribution of diffusion and convection to solute transport by determining the position of the sieving coefficients obtained experimentally with respect to the minimum of the curve.

Furthermore, in the same study Yuan and Kilduff [101] fitted the hydrodynamic model with experimental results to estimate the effective size of NOM. The authors treated the effective radius of NOM as the unknown parameter in the model. Other authors fitted the hydrodynamic model with experimental results obtained by organic solutes to evaluate unknown parameters, such as the membrane pore radius and/or Φ , the solute partitioning coefficient in the membrane [27, 99, 148, 347]. In these studies, the hydrodynamic model was used in phenomenological, non-predictive fashion to acquire information on unknown parameters and in turn on transport mechanisms.

In this work, the approach described above was adopted to investigate the transport of ES through TFC-SR2 and TFC-SR3. The validity of the hydrodynamic model for predicting micropollutant retention by NF has been demonstrated for several organic micropollutants [27, 92, 99, 347]. The hydrodynamic model can describe well the transport of micropollutants through NF provided r_p , L/ε and Φ in equation 5.18 (Chapter 5) are known.

For TFC-SR2 and TFC-SR3 r_p and L/ε were determined, as shown in Section A.2.3 in Appendix 2, by calibrating the purely steric hydrodynamic model with inert organics. Φ was estimated in two ways: firstly using the purely steric model (equation 5.14 in Chapter 5) and secondly by fitting the experimental results obtained with ES, following the approach used by Verliefde *et al.* [99]. The authors showed that the purely steric hydrodynamic model overestimated solute retention for micropollutants. Discrepancies between the purely steric model and experimental results were attributed to the existence of non negligible solute-membrane interactions, represented by Φ .

For TFC-SR3, r_p estimated with inert organics cannot be used to evaluate ES transport since the size of ES, r_s , is bigger than the estimated r_p . According to the hydrodynamic model when $\lambda > 1$ retention is 100%, while for TFC-SR3 total retention did not occur (Figure 7-8a). As observed in Section 5.3, when $\lambda > 1$ and retention is less than 100%, the model can be fitted using the obtained retention results for the studied solute to determine a new pore radius r_p^* . r_p^* represents the average radius of an “hypothetical” membrane whose hindrance to the solute passage is equivalent to the hindrance experienced by the solute through the actual membrane [54]. As a consequence, for TFC-SR3 both r_p and Φ were estimated simultaneously in the hydrodynamic model by fitting the experimental results obtained with ES.

The objectives of fitting the experimental results for ES to the hydrodynamic model were dual:

- establish the position of the sieving coefficients obtained experimentally with respect to the minimum of the hydrodynamic model curve and obtain information on the prevalence of convection and diffusion in ES transport through the membranes (to compare with the results obtained with the diffusion cells);
- acquire information about the unknown parameters and in turn explain transport mechanisms of ES through the membranes.

Figure 8-9 shows the experimental sieving coefficients obtained for TFC-SR2 and TFC-SR3 as a function of J_v (i.e. pressure). J_v was determined by dividing the permeate flow measured during the experiments by the membrane area as indicated in equation 2.2 in Section 2. S_o was calculated from the observed retention (Figure 7-8) with equation 5.16 (Chapter 5). S_a was calculated from the real retention (equation 5.17 in Chapter 5) using equations 5.3, 5.5 and 5.6 in Chapter 5.

Figure 8-9 also shows the curves of S_a and S_o , continuous lines for TFC-SR2 and dotted lines for TFC-SR3. The curve of S_a was determined with equation 5.18 (Chapter 5) and the curve of S_o was calculated by substituting S_o to S_a in equation 5.18 using equations 5.3, 5.16 and 5.17. As stated before, r_p and L/ε were determined

by fitting the purely steric hydrodynamic model with retention results obtained for inert organics (Chapter 5).

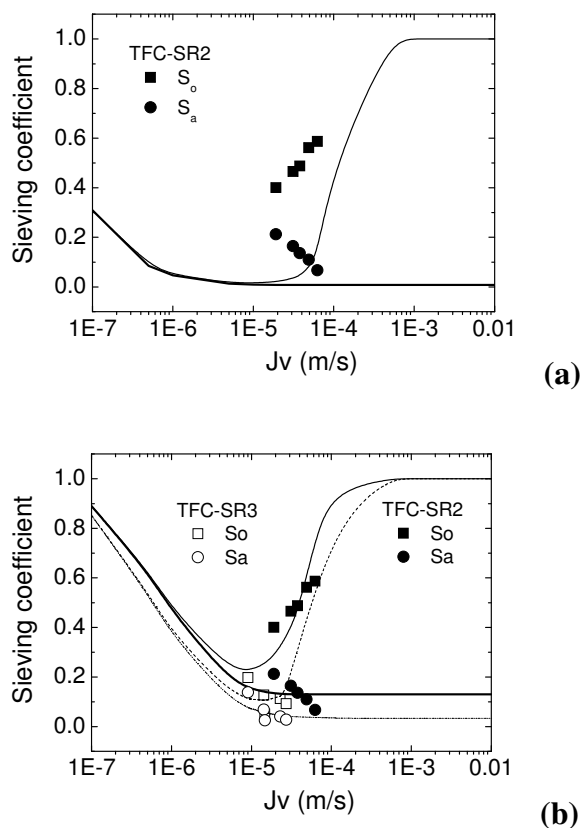


Figure 8-9 Observed sieving coefficients S_o and actual sieving coefficients S_a as a function of permeate flux J_v for TFC-SR2 and TFC-SR3. The continuous lines indicate (a) the purely steric hydrodynamic model (b) the hydrodynamic model with Φ fitted for TFC-SR2. The dotted lines indicate the hydrodynamic model with Φ and r_p fitted for TFC-SR3.

Figure 8-9a shows the curves of S_a and S_o for TFC-SR2 with Φ estimated with equation 5.14 in Chapter 5 (purely steric model). For TFC-SR2 the purely steric hydrodynamic model underestimated the experimental values, confirming that ES-membrane interactions were not negligible for this membrane [27, 92]. As a result, the hydrodynamic model was fitted with S_o values obtained experimentally to determine Φ (Figure 8-9b). The parameters obtained in the two cases and the correlation coefficients between experimental and modelled values are presented in Table 8-2. Both S_a and S_o showed a better correlation with the experimental results

and Φ increased with respect to the steric model. Since λ was considered constant with pressure, the increase of Φ reflected the affinity between ES and TFC-SR2 [27], as expected from the results of ES adsorption to TFC-SR2 in Figure 8-4.

Table 8-2 Hydrodynamic model parameters and correlation coefficients between experimental and modelled values

TFC-SR2					
Steric model			Φ unknown		
r_p (nm)	Φ	r^2 (S_o/S_a)	r_p (nm)	Φ	r^2 (S_o/S_a)
0.52	0.01	0.91/0.81	0.52	0.12	0.99/0.82
TFC-SR3					
Steric model			Φ and r_p^* unknown		
r_p (nm)	Φ	r^2 (S_o/S_a)	r_p (nm)	Φ	r^2 (S_o/S_a)
0.38	-	-	0.49	0.03	0.90/0.89

For TFC-SR3 the purely steric hydrodynamic model could not be used and r_p and Φ were estimated by fitting the hydrodynamic model with experimental results for ES. Values of r_p and Φ obtained with the purely steric hydrodynamic model were used as starting points. The two parameters are not independent as Φ is a function of λ , in turn function of r_p (Equation 5.15 in Chapter 5), therefore they were fitted simultaneously. The pair of values that achieved the best correlation coefficient was chosen. The new average membrane radius was bigger than the average membrane radius calculated with the inert organics (Table 8-2), in agreement with the findings by Verliefde *et al.* [27]. It is inferred that inert organics underestimated the radius of TFC-SR3 because the interactions of inert organics and the membrane were not negligible [27]. The obtained Φ for TFC-SR3 was lower than Φ for TFC-SR2 confirming the lowest affinity (adsorption) of ES for TFC-SR3 (Figure 8-4).

A fitting simulation was also carried out for TFC-SR3 to determine simultaneously r_p , L/ε and Φ . The value of L/ε did not change with respect to the value determined with the inert organics (Table A-2.2, Appendix 2). Similarly, Φ and r_p were determined simultaneously for TFC-SR2. The value of r_p was identical to the value determined with the purely steric model (0.52 nm). It can be concluded that the pore

radius determined by inert organics described well the hindrance behaviour towards ES for TFC-SR2.

From the position of the experimental sieving coefficients with respect to the modelled S_o and S_a curves, it is possible to see graphically the influence of convection and diffusion on ES transport. The percentage of transport by diffusion with respect to the total solute transport in filtration can also be estimated by comparing the total flux of ES during filtration (Section 8.5) with the diffusive flux of ES, determined with the transport equation of the hydrodynamic model (equation 5.7 in Chapter 5) fitted with the experimental results. In the hydrodynamic model, the diffusion coefficient through the active layer is determined by the term $K_d \times D_\infty$ [349], where K_d is the hindrance factor due to diffusion (function of λ) and D_∞ is the diffusion coefficient of the solute in water ($4.50E-06$ cm²/s for ES [274]). The estimated diffusion coefficients of ES through the active layer and the percentage of ES diffusive flux with respect to the total ES flux during filtration are shown in Table 8-3.

Table 8-3 Diffusion coefficients and percentage of ES diffusive flux, estimated with diffusion experiments and the hydrodynamic model, with respect to the total ES flux during filtration.

	Diffusion experiments		Hydrodynamic model	
	D_m (cm ² /s)	% ES diffusive flux to total ES flux	$K_d * D_\infty$ (cm ² /s)	% ES diffusive flux to total ES flux
TFC-SR2	3.34E-08	0.9	1.5E-07	2.0
TFC-SR3	1.69E-08	2.9	1.26E-07	10.8

Figure 8-9b shows that ES retention by TFC-SR2 was dominated by convection, since the experimental sieving coefficients are on the right of the minimum of the S_o curve and diffusion is estimated to be 2% of the total ES flux during filtration (Table 8-3). The experimental sieving coefficients for TFC-SR3 are located on the bottom of the curve and diffusion is estimated to be 10.8% of the total ES flux during filtration (Table 8-3).

Table 8-3 compares the diffusion coefficients of ES through the membranes and the percentage of flux by diffusion (with respect to the total ES flux during filtration) estimated by the diffusion cells and the hydrodynamic model. As expected, values obtained with diffusion cells underestimated ES diffusion determined with the hydrodynamic model, since the resistances of the support layer and the non-woven fabric were taken into account in the diffusion experiments. The highest difference was obtained for the tighter TFC-SR3.

Despite the discrepancies, the hydrodynamic model confirmed the findings obtained with the diffusion cells, showing that convection was the dominant transport mechanisms of ES through both membranes. The increase of retention with pressure for TFC-SR3 was due to the lower J_v obtained with the tighter membrane at the studied pressures, which located the experimental sieving results at the bottom of the hydrodynamic model curve. The decrease of retention with pressure for TFC-SR2 was due to the high J_v obtained at the chosen pressures and to concentration polarisation.

Fitting the hydrodynamic model with the experimental results obtained for ES allowed establishing quantitatively that convection was the dominant mechanism of ES transport through both membranes and ES-membrane interactions played a role in ES transport. However, the goodness of fitting for hydrodynamic model was not ideal (i.e. $r^2 > 0.999$).

Pressure has been shown to influence membrane pore radius r_p (i.e. λ) even if there is not agreement in the literature if r_p increases or decreases as a consequence [108, 147, 148]. If λ varies with pressure, Φ also varies with pressure (see equation 5.15 in Chapter 5). However, the hydrodynamic model considers r_p and Φ constant with J_v . It is inferred that this simplification of the hydrodynamic model might be the cause of the relatively low goodness of fitting obtained in this work.

8.7 Transport of ES through NF membranes in the presence of HA

Figure 7-8a showed that in the presence of HA, ES retention slightly decreased for TFC-SR2 and was constant with pressure for TFC-SR3. The obtained results seemed to confirm the findings by Xu *et al.* [87], for which in the presence of NOM micropollutant retention was constant with pressure. In order to explore transport mechanisms of ES in the presence of HA, the same approach described in Section 8.6 was adopted and the hydrodynamic model combined with the film model was employed in a phenomenological, non-predictive way. Experiments with diffusion cells were not carried out because the determination of the diffusion of a solute through membranes in the presence of a second solute cannot be correctly estimated if the complexation between the solutes is not 100% [350]. In the case of ES, 100% complexation with HA was never reached (Figure 7-5).

In the previous chapter it was found that at pH 4 and with HA concentration of 12.5 mgC/L, 25% of ES in solution was complexed with HA. The presence of ES-HA complexes increased ES retention as a function of pressure with respect to the retention of ES only (Figure 8-5a), indicating that ES-HA complexes influenced ES transport through TFC-SR2 and TFC-SR3. Nevertheless, the existing transport models do not take into account solute-solute interactions in their formulation. The hydrodynamic model describes the transport of a solute of radius r_s , without taking into account the potential formation of higher size complexes.

In order to overcome this drawback, the hydrodynamic model was fitted with the experimental results to determine λ and Φ simultaneously. It was assumed that the newly fitted r_s^* represented the average radius of all solutes passing through the membranes, i.e. the average radius of ES molecules and ES-HA complexes, and the newly fitted r_p^* represented the hindering behaviour of the membranes for the passage of ES and ES-HA complexes. The mass transfer coefficient k_f was assumed to have the same value as in the case of transport of ES only.

While this approach might seem far-fetched, it must be remembered that not only r_p is a non-physical parameter representing an average pore size, but also r_s represents the size of solutes considered rigid and perfectly spherical (see Section 5.3). The above assumptions were considered acceptable for this study since the objective was to estimate the contribution of diffusion and convection to ES transport and acquire information on ES transport mechanisms. However, the higher number of unknown variables with respect to the ES only case did not allow gaining information on r_s and r_p .

Figure 8-10 shows the S_o and S_a coefficients for TFC-SR2 and TFC-SR3 with the fitted hydrodynamic models and Table 8-4 reports the obtained parameters and the correlation coefficients. λ increased for both membranes with respect to the ES only, probably due to the increase of r_s caused by the formation of ES-HA complexes, while Φ decreased with respect to the ES only case. Decrease of Φ is due to the increase in λ causing a decrease of the term $(1 - \lambda)^2$ in equation 5.15 of Chapter 5. Unfortunately, the higher number of unknown parameters with respect to the ES only case did not allow gaining information on the physical meaning of λ and Φ .

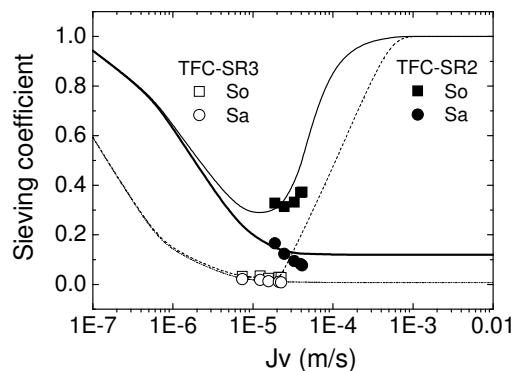


Figure 8-10 Observed sieving coefficients S_o and actual sieving coefficients S_a as a function of permeate flux J_v for TFC-SR2 and TFC-SR3. The continuous lines indicate the hydrodynamic model with Φ and λ fitted TFC-SR2 and the dotted lines indicate the hydrodynamic model with Φ and λ fitted for TFC-SR3.

Table 8-4 Hydrodynamic model parameters and correlation coefficients between experimental and modelled values

TFC-SR2			TFC-SR3		
λ	Φ	$r^2 (S_o/S_a)$	λ	Φ	$r^2 (S_o/S_a)$
0.97	0.09	0.90/0.99	0.99	0.007	0.80/0.94

These results suggested that, since the experimental sieving coefficients of TFC-SR2 and TFC-SR3 were located after or close to the bottom of the S_o curve, convection was the dominant mechanism also for the transport of ES with HA. As observed in Figure 8-3, the permeate flux J_v was lower in the presence of HA than in the case of ES only. Therefore the experimental sieving coefficients were located closer to the flat bottom of the S_o curve than the experimental coefficients obtained for ES only. As a consequence, retention did not show the marked increasing/decreasing trend observed for ES only but was more constant with pressure.

8.8 Conclusions

This chapter investigated solute transport mechanisms through TFC-SR2 and TFC-SR3 membranes in order to explain the role of pressure on solute retention. The role of solute-solute interactions on solute transport was also studied by investigating the influence of HA on solute retention as a function of pressure.

Manganese retention increased with pressure confirming findings in the literature for inorganic solutes. The influence of HA on manganese retention with pressure was not investigated since manganese-HA complexes are formed at pH above 10, when manganese precipitated and retention was almost total. Further work is required to study the influence of HA-inorganic interactions in the retention of inorganic solutes with pressure. Inorganic solutes which are not totally retained when complexed with NOM should be selected to investigate the influence of pressure on their transport through NF membranes.

Results of ES retention with pressure showed that for the tighter TFC-SR3 ($\lambda > 1$) ES retention increased with pressure, while for the looser TFC-SR2 ($\lambda < 1$) ES retention decreased with pressure. From the hypotheses in the literature it was inferred that

convection and diffusion might be responsible for increase/decrease of ES retention with pressure. Since previous studies stated that convection was dominant when $\lambda < 1$ and diffusion was dominant when $\lambda > 1$, it was inferred that λ could be responsible for increase/decrease of ES retention with pressure.

By contrast, results obtained with diffusion cells and the hydrodynamic model showed that convection dominated ES transport through both membranes. The increase of retention with pressure for TFC-SR3 was due to the lower J_v obtained with the tighter membrane at the studied pressures, while the decrease of retention with pressure for TFC-SR2 was due to the high J_v obtained at the chosen pressures and to concentration polarisation.

It can be concluded that λ did not directly influence convection and diffusion mechanisms, as inferred in previous studies, but influenced J_v and concentration polarisation. The hydrodynamic model indicated that the increase/decrease of retention with pressure depended on the parameters J_v and k_f .

Experiments with diffusion cells underestimated ES diffusion through the membranes due to the non-negligible resistance of the support layer and the non-woven fabric. While diffusion experiments can only give an approximation of the diffusive flux in filtration, they can offer an independent indication of the predominance of diffusion or convection in micropollutant transport.

In the presence of HA, ES retention slightly decreased for TFC-SR2 and was constant with pressure for TFC-SR3. The presence of HA lowered J_v and changed λ affecting in turn the increase/decrease of ES retention with pressure.

The hydrodynamic model was shown to be a valuable instrument in quantifying the contribution of diffusion and convection on solute transport and in evaluating the parameters that influence ES retention. Further studies are required to understand the influence of pressure on the membrane characteristics, especially membrane pore size, and incorporate findings into the hydrodynamic model. Furthermore, the

hydrodynamic model describes the transport of a single solute through the membrane, without taking into account the potential formation of higher size complexes. Incorporation of a bimodal distribution of solutes into the model might overcome this drawback.

9. Effect of manganese scaling on NF performance

9.1 Introduction

This chapter will investigate the impact of manganese scaling on the flux and solute retention of TFC-SR2 and TFC-SR3 membranes, highlighting the role of solute-membrane interactions and solute-solute interactions. The review carried out in Chapter 2 concluded that fouling of NF membranes is a complex phenomenon, which, despite several studies, is not totally understood. Less attention has been given so far to the study of the effects of scaling of non-colloidal inorganic components on membrane flux and solute retention. While the impact of NOM and colloidal fouling on micropollutant retention has been investigated in several studies [112, 132-134, 137, 351], there is a lack of investigations on the impact of non-colloidal scaling on the retention of micropollutants [33].

The mechanisms of non-colloidal scaling have been investigated for iron hydroxide and calcium sulphate [28, 84, 85]. It was proposed that the formation of the scaling layer followed two mechanisms: (1) surface blockage by surface crystallization and (2) cake layer formation by bulk crystallization. The phases of nucleation and growth characterise the surface blockage mechanism. During the nucleation phase small nuclei are deposited on the membrane, while during the growth phase polymerization reactions occur to build up the fouling layer. Surface crystallization was inferred to depend on pressure and crossflow velocity, the former responsible to bring more particles to the membrane and the latter controlling the shear force to erode the thickness of the fouling layer. Membrane fouling was more severe for more permeable membranes due to pore blockage.

The mechanism of cake layer formation by bulk crystallization was inferred to be characterised by crystal particle formation in the bulk phase that would precipitate and form a layer on the membrane. Cake layer formation was more dominant than surface blockage at higher crossflow velocities and low pressures. At low pressures the concentration polarisation is low, so surface crystallization was reduced and cake

layer formation was dominant. At higher pressures the rate of growth of the cake was increased, probably due to increase deposition of particles on the membrane. For calcium sulphate the two mechanisms could be observed by SEM images: crystals were visible when surface crystallization occurred, while a cake layer could be observed for bulk crystallization [28].

Scaling was shown to reduce salt retention. Decrease in salt retention by a RO membrane fouled by iron hydroxide was attribute to cake enhanced concentration polarisation, where the cake layer hindered the back diffusion of solutes to the feed, increasing concentration polarisation [135]. Reduction of magnesium sulphate retention by NF membranes fouled by calcium sulphate was attributed to the reduced charge of the membrane due to the presence of the scaling layer and/or to the reduced thickness of the active layer that caused more ion transport [29]. However, the number of studies elucidating the impact of scaling on solute retention is scarce and results are solute specific.

In Chapter 6, manganese was shown to precipitate at pH grater than 7 as $MnCO_3$, with 99% precipitated at pH 10, resulting in 99% retention for both TFC-SR3 and TFC-SR2. Manganese is ubiquitous in surface water, but the effects of its precipitation on membrane performance have never been studied. During filtration of 5 mg/L of manganese fouling did not occur, probably due to short duration of the experiments and low solute concentration. Nevertheless, it was inferred that in the long term manganese precipitation would reduce membrane flux, hence its performance.

The objectives of this chapter are to:

- Determine the effect of manganese precipitates on membrane fouling (solute-membrane interactions).
- Quantify the retention of pesticide ES as a result of membrane scaling by manganese (solute-solute interactions)
- Propose the mechanisms responsible for the effects of manganese scaling on ES retention by the membranes.

9.2 Filtration protocol

Filtration experiments were carried out as described in Section 4.4. All experiments had a background electrolyte of 1 mM NaHCO₃ and 20 mM NaCl (Sections 4.2). Feed solution (900 ml) containing manganese (150-1500 mg/L) was prepared the day before and stirred overnight at 100 rpm at ambient temperature. pH was not adjusted and was around 7 (± 0.3) in all experiments. Since the scope was to determine the effects of manganese precipitates on the fouling of TFC-SR2 and TFC-SR3, the experiments were carried out at 80% recovery. High recovery increases solute concentration in the feed, increasing concentration polarisation and hence scaling [129, 143, 144].

After the experiments with manganese, the membranes were rinsed with ultrapure water without being dismantled from the stirred cells to remove any manganese loosely deposited on the membrane. The pure water flux after filtration J was consequently measured.

Three different sets of experiments were carried out. The first set of experiments had the scope to determine the effects of manganese precipitates on the fouling of TFC-SR2 and TFC-SR3 and was carried out according to the following procedure:

1. Experiments with manganese (Mn) concentration varied from 150 mg/L to 1,500 mg/L (and background electrolyte) at pressure 10 bar and stirring speed of 300 rpm.
2. Experiments with Mn concentration of 500 mg/L (and background electrolyte), pressure varied from 5 to 15 bar and stirring speed of 300 rpm.

Four permeates were collected and analysed for manganese with ICP-OES as described in Section 4.3.2.

Manganese concentrations employed in this study were unrealistic and much higher than the average concentrations found in natural water (Section 3.2), but they were chosen to accelerate fouling in the stirred cells. The scope was to simulate long-term operation of membranes with short term experiments in the laboratory. Experiments as a function of pressure had the scope to evaluate pressure influence on manganese

scaling. High pressure was shown to increase the rate of fouling by increasing the deposition of organic and inorganic solutes on the membrane [84, 125].

The second set of experiments had the scope to compare the effects of manganese precipitates on membrane performance with the effects of other solutes whose mechanisms have been thoroughly investigated in the literature. The experiments were carried out at pressure 15 bar, pH 7 and stirring speed 300 rpm as follows:

- (a) filtration of background electrolyte (1 mM NaHCO₃ and 20 mM NaCl)
- (b) filtration of HA (12.5 mgC/L) and background electrolyte
- (c) filtration of HA (12.5 mgC/L) + Ca (2.5 mM) and background electrolyte
- (d) filtration of Mn (500 mg/L) and background electrolyte
- (e) filtration of HA (12.5 mgC/L) + Mn (500 mg/L) and background electrolyte
- (f) filtration of HA (12.5 mgC/L) + Mn (500 mg/L) + Ca (2.5 mM) and background electrolyte.

Nine permeates of 80 mL were collected and analysed for Na and HA with ICP-OES and TOC analyser respectively as described in Section 4.3.2 and Section 4.3.3. The higher number of permeates with respect to the first set of experiments allowed studying in more detail solute retention mechanisms in the presence of manganese scaling. Analysis of Na by ICP-OES was necessary to determine its retention in solutions containing HA and other inorganics, as conductivity cannot represent Na retention correctly when several solutes are present. Analysis of Mn was not carried out since 99% of manganese retention was observed in the first experiments (Section 9.3).

The effects of scaling by manganese precipitates was compared with fouling potential by HA alone and HA + Ca, since the fouling mechanisms of these compounds have been extensively investigated [125, 128, 129, 132, 162]. Schäfer *et al.* [130] obtained maximum flux decline when 12.5 mgC/L of HA and 2.5 mM of Ca were filtered through Koch TFC membranes similar to TFC-SR2 and TFC-SR3. For this reason the same concentrations were employed in this work. Experiments with HA + Mn were aimed at establishing if Mn²⁺ could behave as Ca²⁺ in increasing

membrane fouling. Experiments with HA + Mn + Ca has the scope to determine if Mn could prevent/enhance fouling by HA and Ca.

During the third set of experiments, pesticide ES (10 µg/L) was filtered through the membranes used in the experiments (b) to (f) and results were compared with ES filtration through “clean” (virgin) membranes. The filtration protocol used in Section 7.2 was employed. The membranes were not removed from the stirred cells and ES filtration was carried out the day after the second set of experiments. The scope was to investigate the impact of manganese scaling on ES retention and compare it with ES retention obtained after fouling by HA and calcium. Mechanisms of micropollutant retention by membranes fouled by NOM have been investigated in previous studies [112, 134], while the effects of non-colloidal inorganic scaling on micropollutant retention are unknown.

9.3 Effect of manganese on membrane fouling

The effect of manganese on membrane flux decline was determined by measuring the pure water flux before and after the filtration experiments (J_0 and J) and the permeate flux during solute filtration (J_v).

9.3.1 Effect of manganese concentration and pressure

The first set of experiments investigated the influence of manganese concentration and pressure on membrane fouling. Due to the high manganese concentration employed in the experiments manganese deposits were visible on both membranes (Figure 9-1).

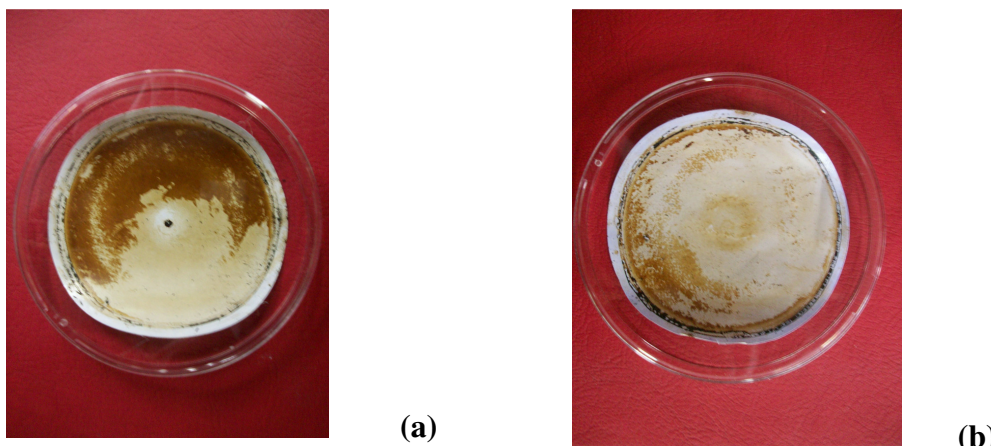


Figure 9-1 (a) TFC-SR2 and (b) TFC-SR3 after manganese filtration at neutral pH. Manganese concentration: 500 mg/L, pressure: 10 bar, background electrolyte 1 mM NaHCO₃ and 20 mM NaCl

As shown in Figure 9-2, for the looser TFC-SR2 the filtration of Mn increased J_v and J compared to J_0 . The trend $J > J_v > J_0$ was independent from the concentration of manganese in the feed and from pressure. For the tighter TFC-SR3 J_v decreased compared to J_0 while J increased. Also for this membrane the trend $J > J_0 > J_v$ was independent from the concentration of manganese in the feed and from pressure.

Flux decline was observed only during manganese filtration through the tighter TFC-SR3 and was independent from pressure. These results are in contrast with findings obtained during filtration of Fe(OH)₃ and HA, where higher flux decrease was observed at higher pressures and looser membranes had higher flux decline than tighter ones [85, 126]. Since fouling by Fe(OH)₃ and HA was attributed to pore blocking, this mechanism did not seem to occur in the case of manganese precipitates.

Since J constantly increased with respect to J_0 it can be concluded that manganese precipitates did not foul the membranes and on the contrary they enhanced membrane flux.

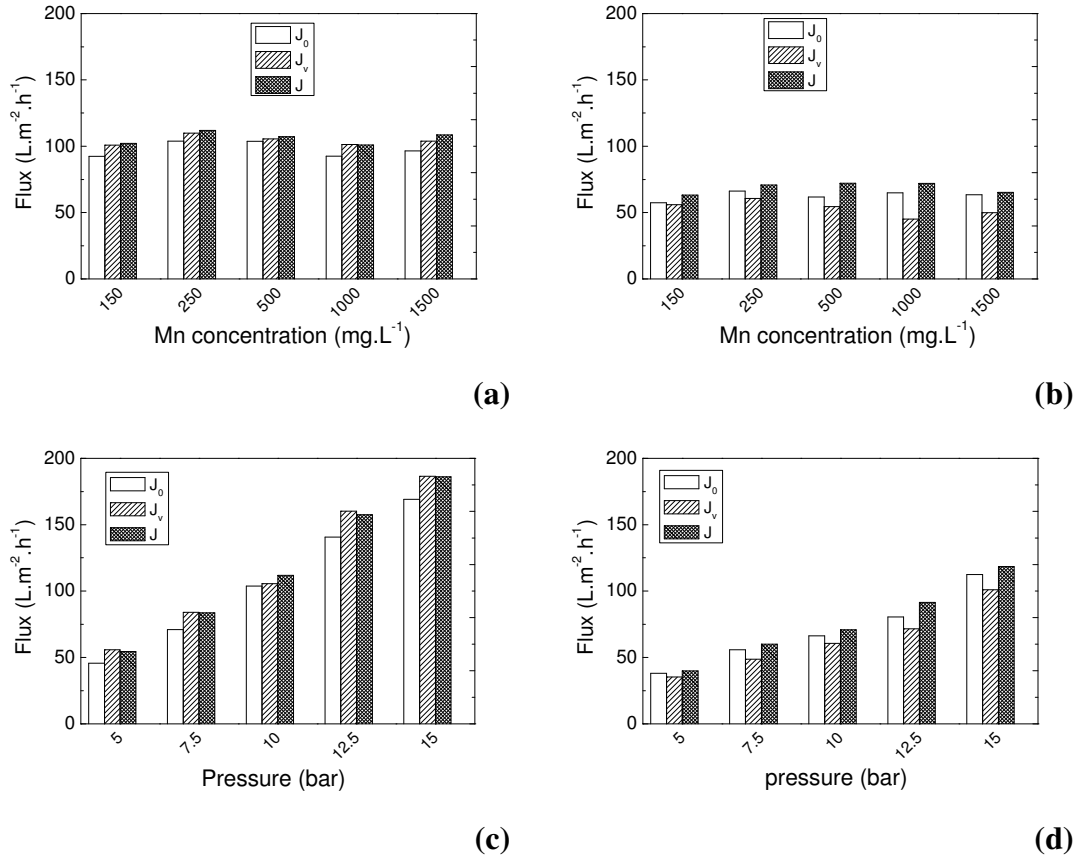


Figure 9-2 (a,b) Pure water flux before experiments J_0 , permeate flux J_v and pure water flux after experiments J as a function of manganese concentration, pressure 10 bar, pH 7, background electrolyte 1 mM NaHCO_3 and 20 mM NaCl for TFC-SR2 and TFC-SR3 membranes **(c,d)** J_0 , J_v and J as a function of pressure, manganese 500 mg/L, pH 7, background electrolyte 1 mM NaHCO_3 and 20 mM NaCl for TFC-SR2 and TFC-SR3 membranes.

9.3.2 Comparison with fouling by other solutes

The second set of experiments compared the effects of manganese filtration on membrane flux with the effects of other solutes filtered alone or with manganese. Since the effects of manganese precipitates on J_v and J were independent from the feed concentration and pressure, a concentration of 500 mg/L of manganese was selected and all the experiments were carried out at 15 bar (Section 6.2).

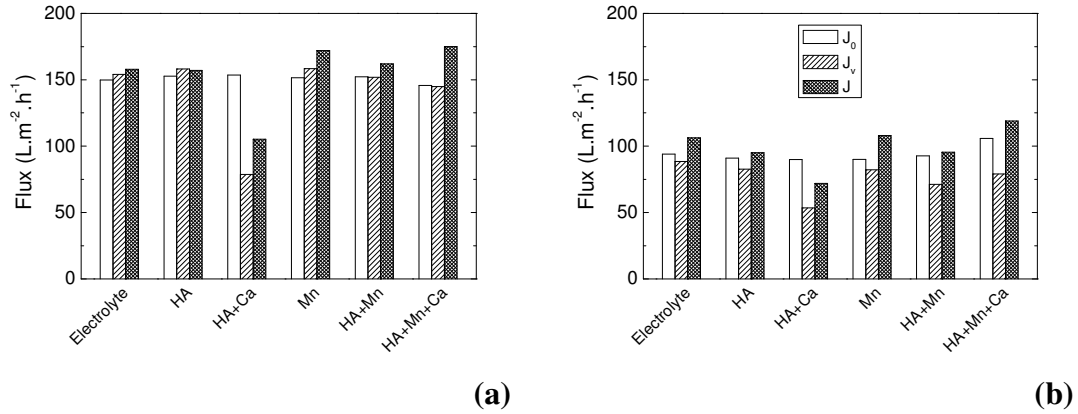


Figure 9-3 Pure water flux before experiments J_0 , pure water flux after experiments J and permeate flux J_v during filtration of background electrolyte only, humic acids (HA), humic acids and calcium (HA+Ca), manganese (Mn), humic acids and manganese (HA+Mn), humic acid, manganese and calcium (HA+Mn+Ca) by (a) TFC-SR2 and (b) TFC-SR3; HA 12.5 mgC/L, CaCl_2 2.5 mM (278 mg/L of Ca), MnCl_2 500 mg/L as Mn, background electrolyte 1 mM NaHCO_3 and 20 mM NaCl, pH 7, pressure 15 bar.

Filtration of HA and calcium (HA+Ca) (experiment *c*) caused decline of J_v and J with respect to J_0 for both membranes. Flux decline was worst for the looser TFC-SR2. These findings confirmed the results obtained by previous studies on NOM fouling in the presence of calcium, where looser membrane were more prone to fouling [125, 128, 129, 132, 162]. Filtration of HA alone (experiment *b*) did not foul the membranes, in agreement with previous results obtained for TFC membranes similar to the ones employed in this study [125, 130].

J , J_v and J_0 during filtration of background electrolyte only (experiment *a*) and HA only (experiment *b*) followed the same trends as for manganese: for TFC-SR2 $J > J_v > J_0$ and for TFC-SR3 $J > J_0 > J_v$. Flux enhancement was more pronounced after filtration of manganese. Flux enhancement was also observed during the filtration of HA and manganese (experiment *e*). Despite manganese forming complexes with HA at pH > 7 (Chapter 6), manganese did not behave like calcium in increasing membrane fouling. Manganese addition prevented irreversible fouling caused by HA and Ca, as already observed in previous studies where coagulants dosed to increase

NOM removal prevented fouling [82, 83, 286]. These results confirmed the ability of manganese to enhance pure water flux after filtration and prevent fouling by HA and calcium.

Flux enhancement after solute filtration was observed in previous chapters during the filtration of 5 mg/L of manganese, especially for TFC-SR3 (Section 6.4) and during the filtration of HA (12.5 mgC/L) and ES for TFC-SR2 at pH > 6 and for TFC-SR3 at pH > 10 (Section 7.4 and Section 7.5). Flux enhancement after solute filtration was first observed with vanillin and NaCl by Nyström *et al.* [52] and with HA by Hong and Elimelech [125]. Following studies confirmed that filtration of NaCl and NOM could increase the membrane pure water flux [87, 133, 339, 352, 353].

Recently, calcium sulphate deposits on NF membranes were shown to increase membrane flux [29]. Other non-colloidal inorganics, such as ferric chloride [83] alum sulphate, ferrous sulphate [82] and polysilicato-iron hydroxide [286], dosed as coagulants in the feed to improve solute removal by membranes, were shown to improve flux decline caused by NOM, reducing fouling.

In order to explain the mechanisms of flux enhancement and fouling prevention, the following hypotheses were inferred in the literature:

- NOM filtration increases membrane charge, increasing repulsion between the membrane pores and in turn MWCO [87, 133];
- NOM filtration increases membrane hydrophilization [125, 339];
- Calcium sulphate deposits decrease the thickness of the active layer [29];
- NaCl filtration increases the membrane free volume due to internal electrostatic repulsion within the membrane pores [52];
- the interactions between NaCl and the membrane cause swelling of the active layer [353];
- polysilicato-iron deposits prevent foulants to sorb onto the membranes [286].
- Coagulants cause the precipitation of foulants, increasing their retention and in turn decreasing fouling.

The applicability of these above hypotheses for manganese will be discussed in Section 9.7.

Flux enhancement and decrease of solute retention have also been linked to membrane degradation caused by free chlorine (HClO) and chloramines solutions [354-356]. Cl⁺ is thought to attack the aromatic ring of the polyamide layer chemically modifying the membrane.

9.4 Solute retention during manganese filtration

In order to understand the impact of manganese precipitates on membrane performance, retention of manganese, sodium and HA was investigated. The examination of solute retention and passage through the membranes had the objective to offer an insight into the mechanisms responsible for the flux change.

The calculation of manganese retention and manganese deposits on the membranes during the first set of experiments were related with the flux results presented in Section 9.3.1. The calculation of sodium and HA retention obtained during the second set of experiments were related with the flux results presented in Section 9.3.2. In the case of sodium and HA, which were not completely retained by the membranes, solute flux, determined as the mass of solute that is filtered through the membrane in a determined time, was calculated. The variation of solute flux with volume of permeate collected (i.e. recovery) was correlated with the permeate flux to investigate mechanisms of flux enhancement/decline.

9.4.1 Retention of manganese

Manganese retention and precipitation on the membranes as a function of manganese concentration and pressure obtained during the first set of experiments are presented in Table 9-1 and Table 9-2.

Table 9-1 Manganese retention, mass of manganese deposits and percentage of manganese deposits as a function of manganese concentration in the feed solution as a function of concentration of manganese in the feed. Pressure 10 bar, pH 7, background electrolyte 1 mM NaHCO₃ and 20 mM NaCl.

Mn Feed Concentration (mg/L)	TFC-SR2			TFC-SR3		
	Mn retention (%)	Mn deposit (mg)	Mn Deposit (%)	Mn retention (%)	Mn deposit (mg)	Mn Deposit (%)
150	98.43	12.06	14.58	98.90	0	0
250	99.38	33.32	24.65	95.85	36.30	28.89
500	89.45	40.75	12.75	97.78	95.81	30.25
1000	96.48	397.01	72.80	95.90	136.26	26.05
1500	97.84	353.94	41.81	99.23	273.56	27.87

Table 9-2 Manganese retention, mass of manganese deposits and percentage of manganese deposits as a function of manganese concentration in the feed solution as a function of pressure. Manganese 500 mg/L, pH 7, background electrolyte 1 mM NaHCO₃ and 20 mM NaCl.

pressure (bar)	TFC-SR2			TFC-SR3		
	Mn retention (%)	Mn deposit (mg)	Mn Deposit (%)	Mn retention (%)	Mn deposit (mg)	Mn Deposit (%)
5	97.16	151.22	36.70	99.35	101.96	27.32
7.5	97.21	139.45	33.87	98.34	53.66	16.16
10	92.56	211.61	48.30	97.78	95.81	30.25
12.5	97.02	225.37	51.75	99.32	98.82	26.05
15	98.69	210.43	47.81	99.70	60.73	18.06

Manganese retention was high (more than 89%) for both membranes for any concentration and pressure studied, confirming that precipitates are well retained. The mass of manganese deposited on the membrane was higher for TFC-SR2, which has bigger pore size and higher roughness (Table 4-2). Manganese deposits increased with manganese concentration in the feed (slightly decrease observed when the feed was 1500 mg/L is attributed to the error due to sample dilution for analysis) but no trend could be indicated with pressure.

These results are in contrast with the findings obtained during membrane fouling by $\text{Fe}(\text{OH})_3$ and HA, where increasing pressure was shown to increase solute deposition on the membranes [84, 125]. The obtained results confirmed that the behaviour of manganese precipitates was different from the behaviour of $\text{Fe}(\text{OH})_3$ and HA deposits, which were shown to foul the membranes by pore blocking.

9.4.2 Retention of sodium

Retention of sodium obtained during the second set of experiments was calculated in order to explain the flux trends obtained in Section 9.3.2. Sodium retention was higher for TFC-SR3 due to size exclusion (Figure 9-4a).

The results obtained for manganese and sodium retention gave an indication on the reason for the trend $J > J_0 > J_v$ for TFC-SR3 in contrast with the trend $J > J_v > J_0$ for TFC-SR2 allowing to explain why permeate flux J_v was lower than J for the tighter TFC-SR3 only.

When fouling does not occur ($J \geq J_0$), lower permeate flux during solute filtration has been attributed to four causes: concentration polarisation, increase of membrane resistance due to the presence of deposits, pore blocking and/or increase of osmotic pressure [52, 84, 125, 126, 357].

In the case of the membranes used in this study, concentration polarisation was higher for the looser TFC-SR2, which had higher J_v than TFC-SR3 for the same pressure. Concentration polarisation depends on the ratio J_v/k_f and the mass transfer coefficient k_f is independent from the type of membrane and the solute concentration at the membrane surface (Chapter 5), so concentration polarisation depended only on J_v . As a consequence, if concentration polarisation was the cause of the decline of J_v with respect to J_0 , TFC-SR2 should show permeate flux decline instead of permeate flux enhancement.

Increase of membrane resistance due to manganese deposits could also be ruled out. The mass of manganese deposited on the membranes was higher for TFC-SR2 than

for TFC-SR3 (Tables 9-1 and 9-2), therefore if the increase in membrane resistance caused by manganese deposits was the cause of flux decline, higher J_v decline would have occurred for TFC-SR2.

If pore blocking was the cause of permeate flux decline for TFC-SR3, flux decline and manganese deposits should have increased with pressure, as observed for $\text{Fe}(\text{OH})_3$ and HA [84, 125]. Instead, as shown in Figure 9-2 and Table 9-2, both flux decline and manganese deposits were independent from pressure.

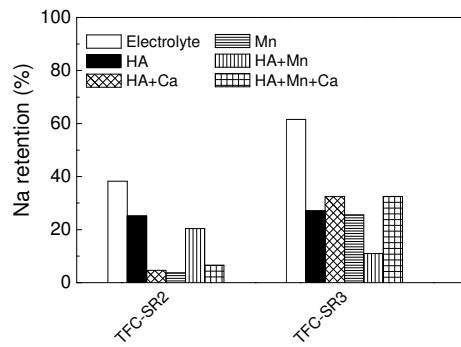
Osmotic pressure is the most likely cause of flux decline during manganese filtration through TFC-SR3. Osmotic pressure depends on the difference between the solute concentration at the membrane surface c_{mf} and the solute concentration in the permeate c_p according to this relationship [177]:

$$\Delta\pi = \alpha (c_{mf} - c_p) \quad (9.1)$$

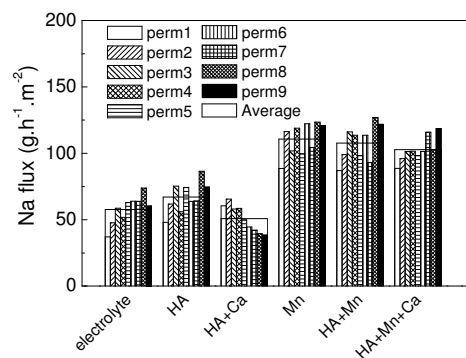
where α is an osmotic pressure coefficient depending on the solute and on the temperature.

In the case of TFC-SR3 the difference ($c_{mf} - c_p$) was higher than for TFC-SR2 as sodium and manganese retention were higher, so the osmotic pressure was higher for TFC-SR3. Other authors [52, 177, 357] also attributed the decrease of permeate flux during NaCl filtration to the increased osmotic pressure.

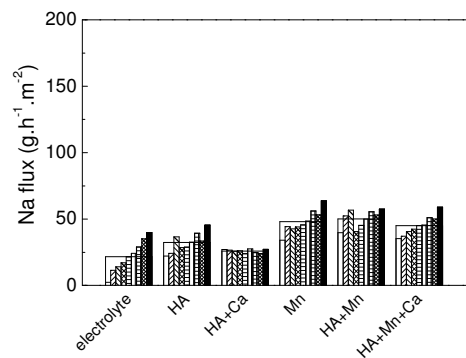
The calculation of the flux of Na as a function of the volume of permeate collected is showed in Figure 9-4b and Figure 9-4c. For both membranes, during filtration of all solutions, sodium flux increased with increasing permeate volume. The more the solutes were filtered, the faster they seemed to pass through the membranes. However, the opposite trend happened when both HA and calcium were filtered. The more the solutes were filtered, the more difficult their passage through the membranes seemed to be. It might be inferred that a relationship might exist between increase of solute passage with permeate volume and increase in pure water flux J and vice versa, decrease in solute passage and membrane fouling.



(a)



(b)



(c)

Figure 9-4 (a) Retention of sodium and (b, c) sodium flux during filtration of background electrolyte only, humic acids (HA), humic acids and calcium (HA+Ca), manganese (Mn), humic acids and manganese (HA+Mn), humic acid, manganese and calcium (HA+Mn+Ca) by TFC-SR2 and TFC-SR3 respectively. HA 12.5 mgC/L, CaCl₂ 2.5 mM (278 mg/L of Ca), MnCl₂ 500 mg/L as Mn, background electrolyte 1 mM NaHCO₃ and 20 mM NaCl, pH 7, pressure 15 bar.

It is also possible to note a considerable increase in sodium flux in the experiments in which manganese was filtered, alone or together with other solutes. This increase was more pronounced for TFC-SR2 than for TFC-SR3. The presence of manganese seemed to enhance the transport of sodium across the membranes.

9.4.3 Retention of humic acids

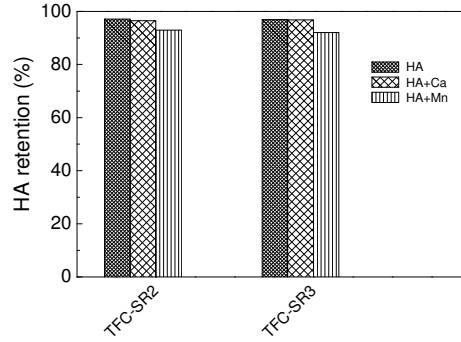
The retention and flux of HA was determined for the experiments (b), (c) and (e) detailed in Section 9.2 in order to examine the flux results obtained in Section 9.3.2. HA retention was high for both membranes confirming results obtained in previous chapters (Figure 9-5a).

The results of HA flux (Figure 9-5b and Figure 9-5c) confirmed what was obtained for sodium flux. HA flux decreased with the volume of permeate in the case in which both HA and Ca were filtered, i.e. when fouling occurred. When flux enhancement after solute filtration occurred, HA flux increased with recovery. For both membranes, HA flux was highly enhanced in the presence of manganese.

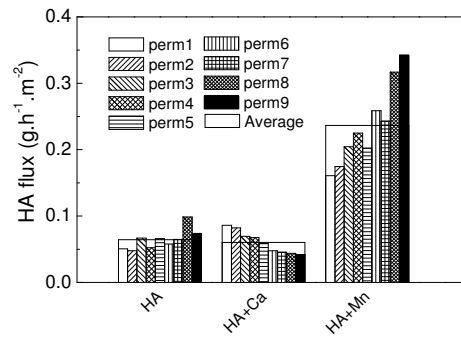
9.5 Retention of pesticide Endosulfan

In the third set of experiments, pesticide ES was filtered through the membranes used in the second set of experiments. The scope was to estimate the influence of solute filtration on ES retention and in particular the influence of manganese scaling with respect to fouling by HA and calcium.

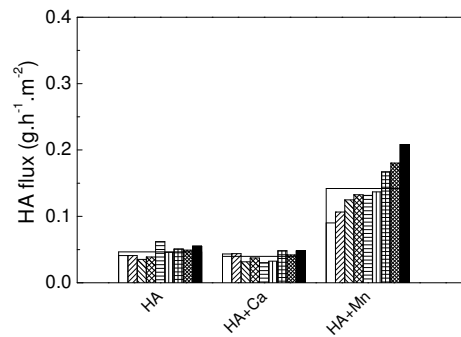
As shown in Figure 9-6a, ES retention was higher for the tighter TFC-SR3 due to size exclusion, confirming results obtained in Chapter 7. ES retention by membrane previously filtered with HA and HA + Ca did not change with respect to the retention by virgin membranes. Fouling by HA and calcium did not have any impact on ES retention, in agreement with previous findings of retention of pharmaceuticals through membranes fouled by NOM [112].



(a)



(b)



(c)

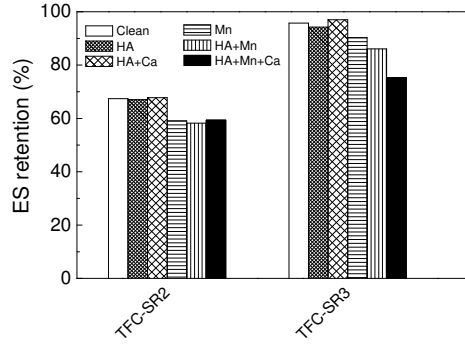
Figure 9-5 (a) Retention of humic acids and (b, c) humic acids flux during filtration of humic acids (HA), humic acids and calcium (HA+Ca), humic acids and manganese (HA+Mn), humic acids, manganese and calcium (HA+Mn+Ca) by TFC-SR2 and TFC-SR3 respectively. HA 12.5 mgC/L, CaCl₂ 2.5 mM (278 mg/L of Ca), MnCl₂ 500 mg/L as Mn, background electrolyte 1 mM NaHCO₃ and 20 mM NaCl, pH 7, pressure 15 bar.

ES retention by membranes previously filtered with manganese decreased with respect to retention through virgin membranes. These findings were confirmed by the results obtained when ES flux was calculated (Figure 9-6b and Figure 9-6c). Higher ES flux was observed when ES was filtered through membrane pre-filtered with manganese, while the lowest ES flux was obtained through the fouled membranes, due to the lower water flux that the fouled membrane experienced. Filtration of manganese seemed to increase both water flux and solute flux through the membranes.

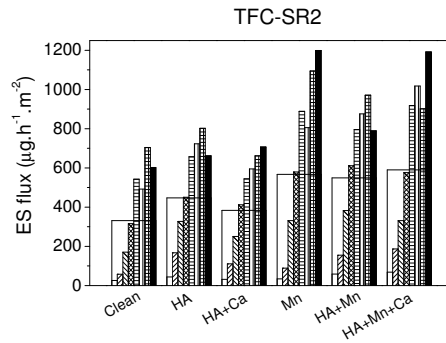
ES flux increased with recovery for both membranes in all cases. During ES experiments permeate flux was constant, as ES neither fouled the membranes nor enhanced flux (Table 9-3). The decrease with recovery observed for the flux of sodium and HA was therefore linked to fouling.

Table 9-3 J_v/J_0 (ratio of permeate flux and pure water flux before experiments) and J/J_0 (ratio of pure water flux after experiments and pure water flux before experiments) for TFC-SR3 during experiments with pesticide Endosulfan. ES 10 $\mu\text{g/L}$, background electrolyte 1 mM NaHCO_3 and 20 mM NaCl at 15 bar pH 7.

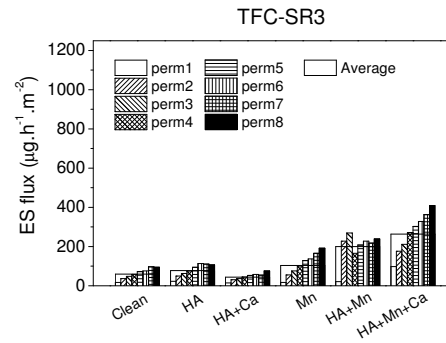
	TFC-SR2		TFC-SR3	
	J_v/J_0	J/J_0	J_v/J_0	J/J_0
clean	1.00	1.09	0.92	1.16
HA	0.96	1.06	0.86	1.02
HA+Ca	0.97	1.12	0.87	1.09
Mn	1.02	1.02	0.87	1.03
HA+Mn	1.01	1.08	0.87	1.03
HA+Mn+Ca	1.00	1.05	0.91	1.05



(a)



(b)



(c)

Figure 9-6 (a) Retention of pesticide Endosulfan and (b, c) Endosulfan flux for TFC-SR2 and TFC-SR3. ES 10 µg/L, background electrolyte 1 mM NaHCO₃ and 20 mM NaCl at 15 bar pH 7. Membrane previously filtered with humic acids (HA), humic acids and calcium (HA+Ca), humic acids and manganese (HA+Mn), humic acid, manganese and calcium (HA+Mn+Ca). HA 12.5 mgC/L, CaCl₂ 2.5 mM (278 mg/L of Ca), MnCl₂ 500 mg/L as Mn, background electrolyte 1 mM NaHCO₃ and 20 mM NaCl, pH 7, pressure 15 bar.

9.6 Effect of manganese deposits on membrane characteristics

Membranes used in the second set of experiments were thoroughly characterised to identify the changes in chemical and physical properties caused by solute filtration. Membrane characterisation is an effective tool for investigating foulant-membrane interactions and for explaining retention and flux results obtained during the experiments [133].

The objectives were to investigate the changes in membrane properties due to manganese scaling in order to explain:

- increase of membrane flux due to manganese filtration;
- decrease of solute retention after manganese filtration.

The mechanisms inferred in the literature and summarised in Section 9.3.2 were systematically investigated. Membrane charge, hydrophilicity and MWCO were determined. SEM images were performed to visualize the deposits and infer the mechanisms of manganese scaling. ATR-FTIR was performed to investigate potential changes in functional groups due to solute filtration. The methods used for membrane characterisation are described in Chapter 4.

9.6.1 Visualization of deposits

SEM images of membrane surface and cross section are reported in Appendix 3. Images of the virgin membranes confirmed that TFC-SR2 has higher roughness than TFC-SR3, as indicated by AFM results (Appendix 2, Section A.2.6).

HA deposits looked different on the two membranes. HA deposits looked like inhomogeneous crystals on the looser TFC-SR2 while appeared as a more compact layer on TFC-SR3. EDX graphs showed presence of sodium, aluminium, silicon and iron on both membranes, in agreement with the inorganic impurities found in commercial Aldrich Humic Acids (Table 3-2). The presence of calcium made the HA layer more compact and homogenous for both membranes, even though the presence of crystals was more visible for TFC-SR2.

Manganese deposits looked as a cake layer on both membranes and appeared more homogenous on the tighter and less rough TFC-SR3. Since crystals were not visible, the mechanisms of manganese scaling might be described as cake layer formation by bulk crystallization (Section 9.1). The presence of HA did not alter the aspect of the manganese deposits. However, the co-presence of HA and calcium resulted in a less homogenous cake on both membranes. It is interesting to note from the EDX spectra that for both membranes calcium was barely detected when filtered together with manganese and HA, while it showed a clear peak when filtered with HA only. It is possible that the presence of manganese masked the calcium signal but reasons for this are unclear.

The images of the membrane cross-section confirmed the existence of the layer of manganese deposits on the membranes. Manganese could be easily visualised in the BSE mode, since it appeared clearer than the membrane due its higher atomic weight. For TFC-SR2 manganese could not be visualised when manganese was filtered together with HA and HA+Ca. On the contrary, for TFC-SR3 manganese was visible in all the membranes. For both membranes, manganese seemed present along the whole cross-section and not limited to the membrane surface. These images need to be interpreted with caution, as manganese might have been removed and/or displaced during membrane cutting.

Membrane thickness was measured on the cross-section images (Section 4.3.9). The scope was to determine if manganese deposits decreased the thickness of the active layer, as observed by Nanda *et al.* [29] in the case of calcium sulphate deposits (Section 9.3.1). Variation in the active layer thickness among membranes used in different experiments was less than 10% and no conclusion could be drawn. The magnification reached with the instrument used in this work might have been too low to visualise any change in the active layer thickness resulted from solute filtration or deposition.

9.6.2 Membrane chemical composition

Membrane function groups were analysed using ATR-FTIR as described in Section 4.3.10 in order to identify any change in chemical bonds resulting from solute filtration. The ATR-FTIR results of the virgin membranes (membrane only compacted with ultrapure water) shown in Appendix 2 (Figure A-2.9) revealed that TFC-SR2 and TFC-SR3 had the same spectra in terms of both signal positions and shape. Both membranes displayed the same chemical composition and structure.

ATR-FTIR spectra of the membranes used in the second set of experiments were graphically compared with the spectra of the virgin membranes in Appendix 3. When HA was filtered through TFC-SR2 and TFC-SR3, the membrane spectra showed major differences. The spectra of TFC-SR2 with HA deposits decreased at 3,200-3,600 cm^{-1} with respect to the spectra of the virgin membrane, but other dissimilarities were not observed. The spectra of TFC-SR3 with HA deposits was different from the spectra of the virgin membrane probably due to the adsorption of HA on the membrane. The increase of the height of the signal might indicate the increased amount of OH groups of HA in the sample or the presence of water molecules. The increase of the C-H stretch signals (2,918 and 2,850 cm^{-1}) might reflect the enhanced amount of carbonaceous material on the sample due to HA adsorption. The increased intensity of the band at 1,714 cm^{-1} (carbonyl of carboxylic functionalities) strengthened this interpretation. The ATR-FTIR spectra seemed to show a preferential adsorption of HA to TFC-SR3, confirming the more compact HA layer observed in SEM images for TFC-SR3 compared with the less homogenous HA layer on TFC-SR2 (Section 9.6.1).

When HA and calcium were filtered the spectra of TFC-SR2 and TFC-SR3 returned to be similar. Both spectra showed an increase of the height and the broadening of the band 3200-3600 cm^{-1} with respect to the virgin membranes. In the presence of calcium, HA seemed more effective in covering TFC-SR2 surface with respect to the case of HA alone, as confirmed by SEM images (Section 9.6.1).

The spectra of TFC-SR2 and TFC-SR3 with manganese deposits did not show major differences with respect to the spectra of the virgin membranes. Peak intensity was consistently reduced due to the presence of the scaling layer that attenuated the infrared signal. TFC-SR3 showed a more intense spectrum than TFC-SR2 indicating less manganese deposition. This interpretation was confirmed by the results obtained during manganese filtration, where the mass of manganese deposited on the membrane was higher for TFC-SR2 (Section 9.4.1). From the spectra it was not possible to perceive any change in chemical bonds resulting from manganese deposits.

The filtration of other solutes (HA alone and HA+Ca) together with manganese, completely attenuated the infrared signal for TFC-SR2. The membrane was completely covered by a non-infrared adsorbing layer. The spectra of TFC-SR3 were more similar to the spectrum of the virgin membrane, with a shift and an increase of the band at 3,200-3,600 cm^{-1} , which might be due to the presence of HA. These results seem to confirm the preferential deposition of manganese to TFC-SR2.

9.6.3 Molecular weight cut-off

The MWCO of the membranes used in the second set of experiments was determined with the methodology described in Appendix 2, Section A.2.2. Pure water fluxes were measured for 30 minutes after filtration of each inert organic. The pure water fluxes changed less than 7% for TFC-SR2 and less than 5% for TFC-SR3 in agreement with flux variability (Section 4.8), showing that the inert organics did not disturb the deposits on the membranes.

As shown in Figure 9-7, inert organic retention did not change considerably for the membranes filtered with HA only and HA+Ca. By contrast, the filtration of Mn decreased inert organic retention considerably, especially in the presence of HA and calcium. The decrease in retention was so substantial that MWCO could not be defined for the membranes filtered with manganese, HA and calcium, since the retention of PEG1000 and PEG 800 was much lower than 90%. The presence of manganese seemed to increase the MWCO, confirming the hypothesis inferred in

previous studies [87, 133] that flux increase and reduction of solute retention was due to increased MWCO.

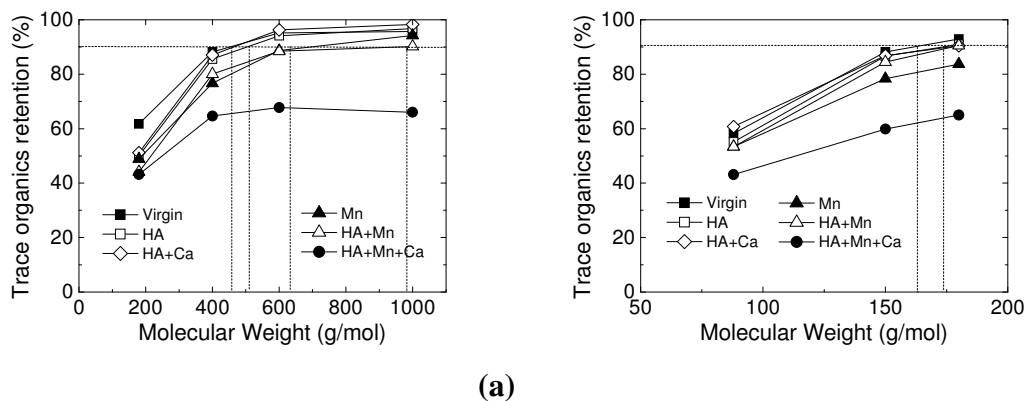


Figure 9-7 Retention as function of molecular weight for (a) TFC-SR2 and (b) TFC-SR3, molecular weight at 90% retention shows membrane MWCO; concentration organic solutes 25mgC/L, pressure 15 bar, pH 6.5 ± 0.5 (no pH adjustment); membranes previously filtered with HA 12.5 mgC/L, CaCl_2 2.5 mM (278 mg/L), Mn 500 mg/L, background electrolyte 1 mM NaHCO_3 and 20 mM NaCl.

9.6.4 Contact angle

Contact angle of the membranes used in the second set of experiments was measured as described in Section 4.3.6 and compared with the contact angle of virgin membranes (membrane only compacted with ultrapure water). As mentioned in Section 7.7, contact angle values for membrane through which solutes have been filtered represent the hydrophilicity of the deposit layer.

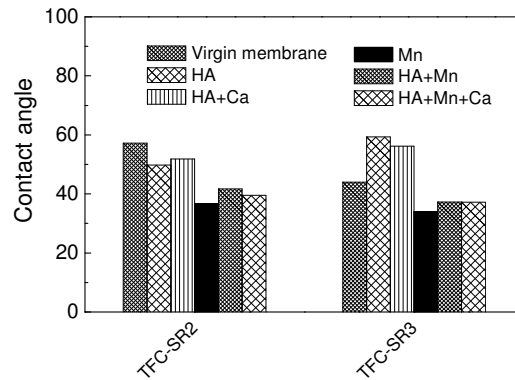


Figure 9-8 Contact angle of TFC-SR2 and TFC-SR3. Membranes previously filtered with HA 12.5 mgC/L, CaCl₂ 2.5 mM (278 mg/L), Mn 500 mg/L, background electrolyte 1 mM NaHCO₃ and 20 mM NaCl.

As shown in Figure 9-8, the presence of HA decreased the contact angle for TFC-SR2 and increased it for TFC-SR3, as already commented in Section 7.7. The presence of calcium did not change the contact angle with respect to the case of HA only. The presence of manganese decreased the contact angle of both membranes, increasing their hydrophilicity. This seemed to confirm the hypothesis that flux increase and reduction of solute retention was due to increased membrane hydrophilization [125, 339].

9.6.5 Surface charge

The membrane surface charge in the presence of manganese deposits was measured according to the method described in Section 4.3.7 and compared with the charge of virgin membranes (Figure 9-9).

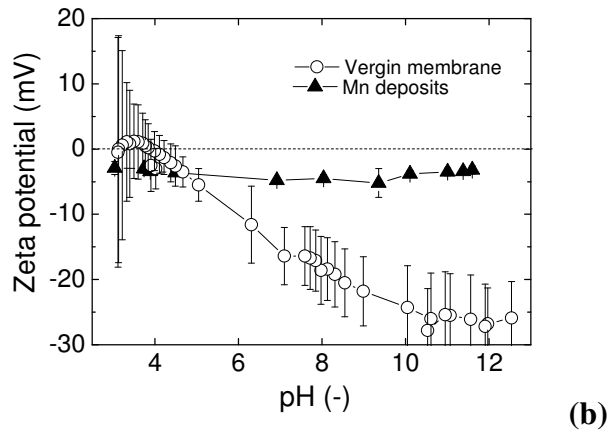
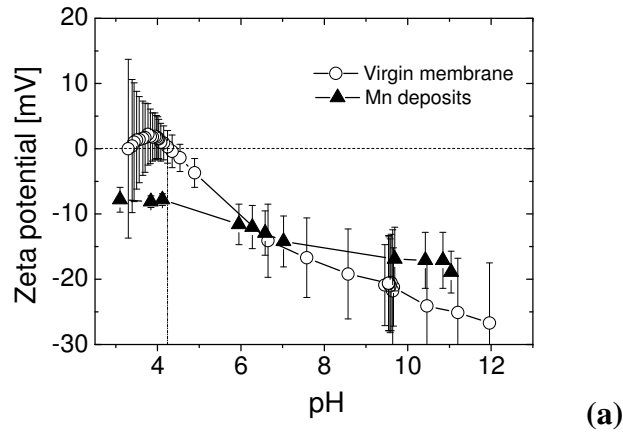


Figure 9-9 Zeta potential of (a) TFC-SR2 and (b) TFC-SR3. Virgin membranes and membranes previously filtered with Mn 500 mg/L and background electrolyte 1 mM NaHCO_3 and 20 mM NaCl .

Manganese increased the negative charge of TFC-SR2 at pH lower than 7 and slightly decreased it at higher pH, while it decreased the negative charge of TFC-SR3 at pH above 5. For both membranes, manganese seemed to form a surface layer whose charge did not vary with pH. The reduced negative charge of both membranes at pH 7 (the pH of the experiments) could have contributed to the decrease in sodium and HA retention, but it would not explain the decrease in ES retention, as ES is not charged. These results allowed discarding the hypothesis that the increase in MWCO could be attributed to an increase in membrane negative charge (Section 9.3.1).

9.7 Suggested mechanisms

Manganese filtration caused enhancement of pure water flux and reduction of solute retention by both TFC-SR2 and TFC-SR3. The cake-enhanced concentration polarisation model usually used to explain decrease of solute retention caused by colloidal fouling (Section 2.2.4) could not be applied for manganese since flux decline did not occur.

The hypotheses inferred in the literature to explain the increase of flux after solute filtration and the reduction of solute retention, as listed in Section 9.3.2, were systematically investigated. Modification of membrane chemical composition as a result of manganese filtration could not be observed so chemical degradation was excluded. At the pH employed in the experiments, the presence of manganese increased membrane MWCO and hydrophilicity without increasing the membrane negative charge. The hypothesis that increase in membrane MWCO was due to increasing repulsion between the membrane pores caused by higher negative charge could not be applied in the case of manganese filtration.

It is proposed that manganese-membrane interactions could increase membrane swelling. The presence of manganese along the cross-section of both membranes (Table A-3.3 and Table A-3.4 in Appendix 3) seems to substantiate that manganese entered the membrane pores, even if SEM images need to be interpreted with caution, as manganese might have been removed and/or displaced during membrane cutting. Increase in swelling of the active layer would increase the membrane free volume, which plays an important role in the transport of small solute through membranes [50, 358]. Membrane swelling due to the contact with water solution has been shown to be connected with membrane permeability and solute retention [51]. Increase in membrane swelling due to membrane exposure to 20% sulphuric acid was shown to cause increase in water flux and decrease in glucose retention [359].

It is inferred that prolonged exposure to manganese would modify physically (but not chemically) the membranes and the resulting increase in free volume would be responsible for pure water flux enhancement and decrease in solute retention. These

hypotheses would need to be verified by measuring quantitatively the increase in active layer thickness after membrane contact with manganese deposits. Freger *et al.* [51, 359] developed a methodology to measure swelling and morphological changes in the active layer of NF membranes using AFM. The methodology is semi-quantitative, relies heavily on the skills and precision of the technicians performing the measurements and needs to be tailored to the different solutions in contact with the active layer. The development of an easy to implement and standardised methodology to measure membrane swelling would be extremely valuable.

9.8 Conclusions

The impact of manganese scaling on the performance of TFC-SR2 and TFC-SR3 has been investigated. Manganese deposits were shown to enhance the pure water flux of both membranes and prevent fouling by HA and calcium. Reduced permeate flux during manganese filtration for the tighter TFC-SR3 was attributed to concentration polarization.

The impact of manganese scaling on the retention of the pesticide ES was investigated. Filtration of manganese through the membranes resulted in reduced ES retention with respect to retention by virgin membranes or membranes filtered with HA alone and HA + Ca. Manganese is one of the most abundant elements in surface water and these findings indicate that manganese deposits can lower solute retention without causing fouling (i.e. flux decline). Since membrane plant operators usually clean the membranes when fouling occurs, the frequency of the cleaning cycle might need to be increased when feed water is rich in manganese.

TFC-SR2 and TFC-SR3 were thoroughly characterized in order to elucidate the mechanisms of manganese scaling. Cake layer formation by bulk crystallization was proposed as the scaling mechanisms for manganese deposits. Manganese filtration increased membrane MWCO and hydrophilicity, without increasing membrane negative charge. It was inferred that prolonged exposure to manganese could modify physically the membranes by increasing the membrane free volume. In turn, membrane swelling would cause flux enhancement and lower solute retention.

10. Conclusions and future work

10.1 Conclusions

This research investigated the contribution of solute-solute interactions and solute-membrane interactions on solute retention and transport by NF. NF membranes are increasingly selected for the removal of organic and inorganic pollutants from drinking water, but a comprehensive understanding of NF mechanisms has yet to be achieved, limiting the application and performance of NF plants. The general aim of this work was to contribute to the knowledge and understanding of the mechanisms of solute retention and transport by NF.

The objectives of this thesis were to:

- Elucidate the role of solute-NOM interactions and NOM-membrane interactions in solute retention by NF.
- Evaluate the role of solute-solute interactions and solute-membrane interactions in the influence of pressure on solute removal.
- Examine the effects of manganese precipitate on the performance of NF membranes (solute-membrane interactions) and the effects of scaling on micropollutant retention (solute-solute interactions).

In order to achieve the thesis objectives within this research, this investigation was limited to specific solutes chosen as model contaminants: commercial HA were selected as representative of NOM, manganese was chosen as model inorganic and pesticide ES was selected as model micropollutant. Two commercial NF membranes, TFC-SR2 and TFC-SR3, particularly suited for treating surface water, were employed for this study.

The role of solute-solute and solute-membrane interactions in manganese removal in the presence of HA was elucidated. The removal mechanisms of manganese by NF were for the first time thoroughly investigated. Manganese retention was influenced by speciation (solute-solute interactions) and membrane pore size and charge (solute-

membrane interactions). Manganese retention depended on size exclusion, but for the looser TFC-SR2, whose pore diameter was larger than the hydrated radius of manganese, pore charge played a role too. Complexation of manganese and HA (solute-solute interactions) did not enhance manganese retention because precipitation overlapped with complexation effects.

The influence of solute-solute and solute-membrane interactions on ES removal in the presence of HA was evaluated. ES is hydrophobic and uncharged and once the membranes were saturated it was removed by size exclusion (solute-membrane interactions) only. For the first time the formation of ES-HA complexes was quantified as a function of pH and HA concentration and the contribution of ES-HA complexes to ES removal was estimated. ES-HA complexes (solute-solute interactions) contributed to increase ES retention with respect to the retention of ES alone. The strength of ES-HA interactions depended on the concentration of HA but was independent from pH. HA-membrane interactions were shown to be responsible for increased membrane MWCO and become important at alkaline pH. For the looser TFC-SR2, HA-membrane interactions decreased ES retention in the presence of HA with respect to the retention of ES alone. For the tighter TFC-SR3, the increase of MWCO due to HA-membrane interactions was not sufficient to allow higher ES passage. These results explained the contrasting results obtained in the literature regarding the influence of NOM on micropollutant retention.

The role of pressure on solute retention was examined. In the case of manganese, retention increased with pressure, confirming results obtained in the literature for inorganic solutes. The influence of HA on manganese retention as a function of pressure was not investigated as manganese-HA complexation occurs at alkaline conditions, when precipitation take places and retention is almost complete. In the case of ES, the retention as a function of pressure was found to be dependent on permeate flux and concentration polarization. The hydrodynamic model was employed in a phenomenological way to study the prevalence of diffusion and convection in ES transport through NF membranes and explain transport mechanisms. Results showed that ES transport was dominated by convection. Lower

permeate flux obtained for the tighter membrane was responsible for increase of ES retention with increasing pressure, while higher permeate flux obtained for the looser membrane caused concentration polarization and decrease of ES retention with pressure. The presence of HA lowered permeate flux for both membranes, resulting in less pronounced variation of ES retention with pressure. These findings elucidated the impact of pressure on ES retention, which was not well understood before the start of this work.

Finally, the effects of manganese precipitation on membrane flux (solute-membrane interactions) and on solute retention (solute-solute interactions) were investigated. The mechanisms of manganese scaling on NF membranes were studied for the first time. It was proposed that manganese formed a cake layer on the membranes by bulk crystallization. Results showed that manganese precipitates did not foul the membranes but on the contrary enhanced pure water flux after filtration and decreased solute retention. Retention of ES decreased after filtration of manganese with respect to ES retention by virgin membranes, while pre-filtration of HA alone and HA+calcium (which fouled the membranes) did not affect ES removal. Manganese precipitates did not modify the chemical composition of the membranes but increased membrane MWCO and hydrophilicity, decreasing membrane negative charge. It was proposed that manganese filtration impacted membrane free volume, increasing membrane swelling, which in turn might be responsible for enhancement of flux and solute passage.

The findings of this research highlighted the importance of considering both solute-membrane interactions and solute-solute interactions when investigating the removal and transport mechanisms through NF membranes. The quantification of the influence of ES-HA interactions and HA-membrane interactions on ES retention was shown to be critical for explaining ES retention mechanisms. ES-HA interactions affected ES retention with pressure, confirming their importance in transport mechanisms. Solute-membrane interactions were also found to be essential for understanding retention mechanisms. HA-membrane interactions were responsible for the decrease of ES retention in the presence of HA, a phenomenon that had

already been observed in other studies but was unexplained. Manganese-membrane interactions, for the first time investigated in this thesis, were shown to impact membrane flux and solute retention.

This work contributed to the knowledge of mechanisms of solute removal and transport through NF membranes. The findings in this research not only have practical applications in the operation of membrane plants, but can be valuable to develop new membranes and extend their applications. Novel membranes and novel materials, with better removal properties and reduced fouling and energy consumption, could be developed as a consequence of better understanding of removal and transport mechanisms. Novel applications of membrane technology could be conceived following the increased knowledge in membrane processes, contributing in turn to the challenge of providing clean fresh drinking water to the world.

10.2 Future work

This research was limited to a selected number of compounds chosen as model contaminants. Further work in evaluating the impact of the interactions between a broader range of solutes on membrane performance would be valuable. Firstly, it would be important to quantify the interactions of solutes with the different fractions of NOM and with NOM extracted from real water. Secondly, it would be relevant to consider several inorganic solutes commonly found in water (i.e. iron, aluminium, arsenic) and micropollutants with diverse characteristics. The interactions between HA and manganese happened at alkaline pH when manganese precipitated and was fully retained, so it was not possible to study the influence of HA on manganese retention and transport. The choice of inorganic compounds, like arsenic, that do not precipitate would allow investigating the contribution of solute-solute interactions on transport of inorganic solutes through NF. Pesticide ES employed in this study is hydrophobic and uncharged, so micropollutants with different size, hydrophilicity and charge could be chosen. A comprehensive assessment of the influence of different types of solute-solute interactions carried out for a number of micropollutant could reveal trends and mechanisms, in turn contributing to

qualitative prediction of micropollutant retention in the presence of NOM. Research focused on including solute-solute interactions in transport models would be extremely important, since it would allow quantitative prediction of solute retention.

Likewise, the introduction of solute-membrane interactions, such as influence of solutes on membrane characteristics or fouling, in transport models would increase considerably their prediction capability. Further work is required to quantify the interactions between different solutes and different type of membranes and in a second time, evaluate the impacts of these interactions on solute removal and transport. It would be interesting to measure the influence of different fractions of NOM on different membrane materials, in terms of impact on pore size, charge and hydrophilicity. Findings would also be useful to increase the understanding of fouling by NOM. Impact of scaling on membrane performance and membrane characteristics also warrants further work, especially the impact of different types of scalants on micropollutant removal.

Methods of membrane characterization have an essential role in enabling the examination of solute-membrane interactions. Future work on improving the current characterization methods and in finding new methods is therefore paramount. The quantification of membrane free volume and its role on solute transport and retention is an exciting new topic which promises to shed light on many NF mechanisms. Research has been limited to hydrogels and copolymers [358, 360, 361], so its application to composite NF membranes has huge potential in increasing the understanding of membrane processes.

References

- [1] UNICEF, World Health Organization. Progress on Drinking Water and Sanitation: 2012 Update. 2012.
- [2] World Health Organization. <http://www.who.int/features/factfiles/water> (accessed March 2012).
- [3] Elimelech M, Phillip WA. The Future of Seawater Desalination: Energy, Technology, and the Environment. *Science* 2011; **333**: 712-717.
- [4] Shannon MA, Bohn PW, Elimelech M, Georgiadis JG, Marinas BJ, Mayes AM. Science and technology for water purification in the coming decades. *Nature* 2008; **452**: 301-310.
- [5] Schwarzenbach RP, Escher BI, Fenner K, Hofstetter TB, Johnson CA, von Gunten U, Wehrli B. The challenge of micropollutants in aquatic systems. *Science* 2006; **313**: 1072-1077.
- [6] Boxall A, Monteiro S, Fussell R, Williams R, Bruemer J, Greenwood R, Bersuder P. Targeted monitoring for human pharmaceuticals in vulnerable source and final waters - Drinking Water Inspectorate Project No. WD0805 (Ref DWI 70/2/231). 2011.
- [7] Semião AJC, Schäfer AI. *Xenobiotics removal by membrane technology: an overview in "Xenobiotics in the urban water cycle; Mass flows, environmental process, mitigation and treatment strategies"*, D. Fatta-Kassinos, K. Bester and K. Kümmeler Editors, *Environmental Pollution, Vol. 16, Springer Science*, 2010.
- [8] Drioli E, Macedonio F. *Membrane operation in water treatment and reuse in "Water in mineral processing"*, J. Drelich Editor: Society for Mining Metallurgy and Exploration, 2012.
- [9] Grose ABF, Smith AJ, Donn A, O'Donnell J, Welch D. Supplying high quality drinking water to remote communities in Scotland. *Desalination* 1998; **117**: 107-117.
- [10] Peter-Varbanets M, Zurbrugg C, Swartz C, Pronk W. Decentralized systems for potable water and the potential of membrane technology. *Water Research* 2009; **43**: 245-265.

-
- [11] Schäfer AI, Broeckmann A, Richards BS. Membranes and renewable energy - a new era of sustainable development for developing countries. *Membrane Technology* 2005; **2005**: 6-10.
- [12] Schäfer AI, Fane AG, Waite TD. *Nanofiltration principles and applications*. UK: Elsevier: Oxford, 2004.
- [13] Plakas KV, Karabelas AJ. Removal of pesticides from water by NF and RO membranes - A review. *Desalination* 2011.
- [14] Mnif A, Ben Sik Ali M, Hamrouni B. Effect of some physical and chemical parameters on fluoride removal by nanofiltration *Ionics* 2010; **16**: 245-253.
- [15] Yangali-Quintanilla V, Sadmani A, McConville M, Kennedy M, Amy G. Rejection of pharmaceutically active compounds and endocrine disrupting compounds by clean and fouled nanofiltration membranes. *Water Research* 2009; **43**: 2349-2362.
- [16] Figoli A, Cassano A, Criscuoli A, Mozumder MSI, Uddin MT, Islam MA, Drioli E. Influence of operating parameters on the arsenic removal by nanofiltration. *Water Research* 2012; **44**: 97-104.
- [17] World Health Organization. *Guidelines for drinking-water quality*. Geneva, 2008.
- [18] Service RF. Desalination Freshens Up. *Science* 2006; **313**: 1088-1090.
- [19] Mulder M. *Basic principles of membrane technology*. Dordrecht: Kluwer Academic Publishers, 2000.
- [20] AWWA. *Water Treatment Membrane Processes* McGraw-Hill, 1996.
- [21] Van der Bruggen B, Mänttari M, Nyström M. Drawbacks of applying nanofiltration and how to avoid them: A review. *Separation and Purification Technology* 2008; **63**: 251-263.
- [22] Van der Bruggen B, Verliefde A, Braeken L, Cornelissen E, Moons K, Verberk J, Van Dijk H, Amy GL. Assessment of a semi-quantitative method for estimation of the rejection of organic compounds in aqueous solution in nanofiltration. *Journal of Chemical Technology and Biotechnology* 2006; **81**: 1166-1176.

-
- [23] Bellona C, Drewes JE, Xu P, Amy G. Factors affecting the rejection of organic solutes during NF/RO treatment - a literature review. *Water Research* 2004; **38**: 2795-2809.
- [24] Childress AE, Elimelech M. Relating nanofiltration membrane performance to membrane charge (electrokinetic) characteristics. *Environmental Science & Technology* 2000; **34**: 3710-3716.
- [25] Mulder M, Van Voorthuizen EM, Peeters JMM. *Membrane characterization in "Nanofiltration Principles and Applications"*, A. I. Schäfer, A. G. Fane, T. D. Waite Editors, Elsevier: Oxford, 2004.
- [26] Semião AJC, Schäfer AI. Estrogenic micropollutant adsorption dynamics onto nanofiltration membranes. *Journal of Membrane Science* 2011; **381**: 132-141.
- [27] Verliefde ARD, Cornelissen ER, Heijman SGJ, Hoek EMV, Amy GL, Bruggen BVd, van Dijk JC. Influence of solute-membrane affinity on rejection of uncharged organic solutes by nanofiltration membranes. *Environmental Science & Technology* 2009; **43**: 2400-2406.
- [28] Lee S, Lee C-H. Effect of operating conditions on CaSO₄ scale formation mechanism in nanofiltration for water softening. *Water Research* 2000; **34**: 3854-3866.
- [29] Nanda D, Tung K-L, Li Y-L, Lin N-J, Chuang C-J. Effect of pH on membrane morphology, fouling potential, and filtration performance of nanofiltration membrane for water softening. *Journal of Membrane Science* 2010; **349**: 411-420.
- [30] Boussahel R, Montiel A, Baudu M. Effects of organic and inorganic matter on pesticide rejection by nanofiltration. *Desalination* 2002; **145**: 109-114.
- [31] Jin X, Hu J, Ong SL. Influence of dissolved organic matter on estrone removal by NF membranes and the role of their structures. *Water Research* 2007; **41**: 3077-3088.
- [32] Verliefde A. Rejection of organic micropollutant by high pressure membranes (NF/RO), PhD Thesis, Katholieke Universiteit Leuven. 2008.
- [33] Vogel D, Simon A, Alturki AA, Bilitewski B, Price WE, Nghiem LD. Effects of fouling and scaling on the retention of trace organic contaminants by a

nanofiltration membrane: The role of cake-enhanced concentration polarisation. *Separation and Purification Technology* 2010; **73**: 256-263.

[34] Bouchard MF, Sauvé S, Barbeau B, Legrand M, Brodeur M, Bouffard T, Limoges E, Bellinger D, Mergler D. Intellectual impairment in school-age children exposed to manganese from drinking water. *Environmental Health Perspectives* 2011; **119(1)**: 138–143.

[35] Wasserman GA, Liu X, Parvez F, Ahsan H, Levy D, Factor-Litvak P, Kline J, van Geen A, Slavkovich V, LoIacono NJ, Cheng Z, Zheng Y, Graziano JH. Water manganese exposure and children's intellectual function in Araihaazar, Bangladesh. *Environmental Health Perspectives* 2006; **114**: 124–129.

[36] Jacangelo JG, DeMarco J, Owen DM, Randtke SJ. Selected processes for removing NOM: an overview. *Journal AWWA* 1995; **Jan 95**: 64-77.

[37] Gallard H, von Gunten U. Chlorination of natural organic matter: kinetics of chlorination and of THM formation. *Water Research* 2002; **36**: 65-74.

[38] Peters CJ, Young RJ, Perry R. Factors influencing the formation of haloforms in the chlorination of humic materials. *Environmental Science & Technology* 1980; **14**: 1391-1395.

[39] van Leeuwen FXR. Safe drinking water: the toxicologist's approach. *Food and Chemical Toxicology* 2000; **38**: S51-S58.

[40] Iwata H, Tanabe S, Sakai N, Nishimura A, Tatsukawa R. Geographical distribution of persistent organochlorines in air, water and sediments from Asia and Oceania, and their implications for global redistribution from lower latitudes. *Environmental Pollution* 1994; **85**: 15-33.

[41] Gilliom RJ. Pesticides in U.S. streams and groundwater. *Environmental Science & Technology* 2007; **41**: 3408-3414.

[42] Benotti MJ, Trenholm RA, Vanderford BJ, Holady JC, Stanford BD, Snyder SA. Pharmaceuticals and endocrine disrupting compounds in U.S. drinking water. *Environmental Science & Technology* 2008; **43**: 597-603.

[43] Soto A, Chung K, Sonnenschein C. The pesticide endosulfan, toxaphene and dieldrin have estrogenic effects on human estrogen-sensitive cells. *Environmental Health Perspectives* 1994; **4**: 380-383.

-
- [44] Ansar Ahmed S. The immune system as a potential target for environmental estrogens (endocrine disruptors): a new emerging field. *Toxicology* 2000; **150**: 191-206.
- [45] Ochoa-Acuna H, Frankenberger J, Hahn L, Carbajo C. Drinking-water herbicide exposure in Indiana and prevalence of small-for-gestational-age and preterm delivery. *Environmental Health Perspectives* 2009; **117**.
- [46] Van der Bruggen B, Vandecasteele C. Removal of pollutants from surface water and groundwater by nanofiltration: overview of possible applications in the drinking water industry. *Environmental Pollution* 2003; **122**: 435-445.
- [47] Cyna B, Chagneau G, Bablon G, Tanghe N. Two years of nanofiltration at the Méry-sur-Oise plant, France. *Desalination* 2002; **147**: 69-75.
- [48] Bowen WR, Welfoot JS. Modelling of membrane nanofiltration - pore size distribution effects. *Chemical Engineering Science* 2002; **57**: 1393-1407.
- [49] Lee S, Park G, Amy G, Hong S-K, Moon S-H, Lee D-H, Cho J. Determination of membrane pore size distribution using the fractional rejection of nonionic and charged macromolecules. *Journal of Membrane Science* 2002; **201**: 191-201.
- [50] Yasuda H, Lamaze CE, Ikenberry LD. Permeability of solutes through hydrated polymer membranes. Part I. Diffusion of sodium chloride. *Die Makromolekulare Chemie* 1968; **118**: 19-35.
- [51] Freger V. Swelling and morphology of the skin layer of polyamide composite membranes: an atomic force microscopy study. *Environmental Science & Technology* 2004; **38**: 3168-3175.
- [52] Nyström M, Kaipia L, Luque S. Fouling and retention of nanofiltration membranes. *Journal of Membrane Science* 1995; **98**: 249-262.
- [53] Mänttari M, Pihlajamäki A, Nyström M. Effect of pH on hydrophilicity and charge and their effect on the filtration efficiency of NF membranes at different pH. *Journal of Membrane Science* 2006; **280**: 311-320.
- [54] Bowen WR, Mukhtar H. Characterisation and prediction of separation performance of nanofiltration membranes. *Journal of Membrane Science* 1996; **112**: 263-274.

-
- [55] Petersen RJ. Composite reverse osmosis and nanofiltration membranes. *Journal of Membrane Science* 1993; **83**: 81-150.
- [56] Boussu K, Zhang Y, Cocquyt J, Van der Meeren P, Volodin A, Van Haesendonck C, Martens JA, Van der Bruggen B. Characterization of polymeric nanofiltration membranes for systematic analysis of membrane performance. *Journal of Membrane Science* 2006; **278**: 418-427.
- [57] Childress AE, Elimelech M. Effect of solution chemistry on the surface charge of polymeric reverse osmosis and nanofiltration membranes. *Journal of Membrane Science* 1996; **119**: 253-268.
- [58] Elimelech M, Chen WH, Waypa JJ. Measuring the zeta (electrokinetic) potential of reverse osmosis membranes by a streaming potential analyzer. *Desalination* 1994; **95**: 269-286.
- [59] Deshmukh S, Childress AE. Zeta potential of commercial RO membranes: Influence of source water type and chemistry. *Desalination* 2001; **140**: 87-95.
- [60] Mo H, Tay KG, Ng HY. Fouling of reverse osmosis membrane by protein (BSA): Effects of pH, calcium, magnesium, ionic strength and temperature. *Journal of Membrane Science* 2008; **315**: 28-35.
- [61] Bolt G. Analysis of the validity of the Gouy-Chapman theory of the electric double layer. *Journal of Colloid Science* 1955; **10**: 206-218.
- [62] Delgado A, González-Caballero F, Hunter R, Koopal LK, Lyklema J. Measurement and interpretation of electrokinetic phenomena (IUPAC Technical Report). *Pure and Applied Chemistry* 2005; **77**: 1753-1805.
- [63] Zhang W, Wahlgren M, Sivik B. Membrane Characterization by the Contact Angle Technique : II. Characterization of UF-Membranes and Comparison between the Captive Bubble and Sessile Drop as Methods to obtain Water Contact Angles. *Desalination* 1989; **72**: 263-273.
- [64] Bouchard CR, Jolicoeur J, Kouadio P, Britten M. Study of humic acid adsorption on nanofiltration membranes by contact angle measurements. *The Canadian Journal of Chemical Engineering* 1997; **75**: 339-345.
- [65] Palacio L, Calvo JI, Prádanos P, Hernández A, Väisänen P, Nyström M. Contact angles and external protein adsorption onto UF membranes. *Journal of Membrane Science* 1999; **152**: 189-201.

-
- [66] Seidel A, Waypa JJ, Elimelech M. Role of charge (Donnan) exclusion in removal of arsenic from water by a negatively charged porous nanofiltration membrane. *Environmental Engineering Science* 2001; **18**: 105-113.
- [67] Schaep J, Van der Bruggen B, Vandecasteele C, Wilms D. Influence of ion size and charge in nanofiltration. *Separation and Purification Technology* 1998; **14**: 155-162.
- [68] Pontalier P-Y, Ismail A, Ghouil M. Mechanisms for the selective rejection of solutes in nanofiltration membranes. *Separation and Purification Technology* 1997; **12**: 175-181.
- [69] Tansel B, Sager J, Rector T, Garland J, Strayer RF, Levine L, Roberts M, Hummerick M, Bauer J. Significance of hydrated radius and hydration shells on ionic permeability during nanofiltration in dead end and cross flow modes. *Separation and Purification Technology* 2006; **51**: 40-47.
- [70] Nightingale ER. Phenomenological theory of ion solvation. Effective radii of hydrated ions. *The Journal of Physical Chemistry* 1959; **63**: 1381-1387.
- [71] Agenson KO, Oh J-I, Urase T. Retention of a wide variety of organic pollutants by different nanofiltration/reverse osmosis membranes: controlling parameters of process. *Journal of Membrane Science* 2003; **225**: 91-103.
- [72] Verliefde A, Cornelissen E, Amy G, Van der Bruggen B, van Dijk H. Priority organic micropollutants in water sources in Flanders and the Netherlands and assessment of removal possibilities with nanofiltration. *Environmental Pollution* 2007; **146**: 281-289.
- [73] Braeken L, Ramaekers R, Zhang Y, Maes G, Bruggen BVd, Vandecasteele C. Influence of hydrophobicity on retention in nanofiltration of aqueous solutions containing organic compounds. *Journal of Membrane Science* 2005; **252**: 195-203.
- [74] Waite TD. *Chemical speciation effects in nanofiltration separation, in "Nanofiltration Principles and Applications", A. I. Schäfer, A. G. Fane, T. D. Waite Editors, Elsevier: Oxford, 2004.*
- [75] Berg P, Hagemeyer G, Gimbel R. Removal of pesticides and other micropollutants by nanofiltration. *Desalination* 1997; **113**: 205-208.

-
- [76] Van der Bruggen B, Schaep J, Wilms D, Vandecasteele C. Influence of molecular size, polarity and charge on the retention of organic molecules by nanofiltration. *Journal of Membrane Science* 1999; **156**: 29-41.
- [77] Bellona C, Drewes JE. The role of membrane surface charge and solute physico-chemical properties in the rejection of organic acids by NF membranes. *Journal of Membrane Science* 2005; **249**: 227-234.
- [78] Schäfer AI, Nghiem LD, Waite TD. Removal of the natural hormone estrone from aqueous solutions using nanofiltration and reverse osmosis. *Environmental Science & Technology* 2003; **37**: 182-188.
- [79] Simpson AE, Kerr CA, Buckley CA. The effect of pH on the nanofiltration of the carbonate system in solution. *Desalination* 1987; **64**: 305-319.
- [80] Richards LA, Richards BS, Rossiter HMA, Schäfer AI. Impact of speciation on fluoride, arsenic and magnesium retention by nanofiltration/reverse osmosis in remote Australian communities. *Desalination* 2009; **248**: 177-183.
- [81] van Oers CW, Vorstman MAG, Kerkhof PJAM. Solute rejection in the presence of a deposited layer during ultrafiltration. *Journal of Membrane Science* 1995; **107**: 173-192.
- [82] Listiarini K, Tor JT, Sun DD, Leckie JO. Hybrid coagulation-nanofiltration membrane for removal of bromate and humic acid in water. *Journal of Membrane Science* 2010; **365**: 154-159.
- [83] Schäfer AI, Fane AG, T. W. Direct coagulation pretreatment in nanofiltration of waters rich in organic matter and calcium *Water Science and Technology: Water Supply* 2001; **1**: 25-33.
- [84] Jackson JM, Landolt D. About the mechanism of formation of iron hydroxide fouling layers on reverse osmosis membranes. *Desalination* 1973; **12**: 361-378.
- [85] Staude E, Assenmacher W. A contribution to fouling in hyperfiltration induced by chemical reaction. *Desalination* 1984; **49**: 215-228.
- [86] Semião AJC, Rossiter HMA, Schäfer AI. Impact of organic matter and speciation on the behaviour of uranium in submerged ultrafiltration. *Journal of Membrane Science* 2010; **348**: 174-180.

-
- [87] Xu P, Drewes JE, Bellona C, Amy GL, Kim TU, Adam M, Heberer T. Rejection of emerging organic micropollutants in nanofiltration–reverse osmosis membrane applications. *Water Environment Research* 2005; **77**: 40-48.
- [88] Jones KL, O'Melia CR. Protein and humic acid adsorption onto hydrophilic membrane surfaces: effects of pH and ionic strength. *Journal of Membrane Science* 2000; **165**: 31-46.
- [89] Ben-David A, Bason S, Jopp J, Oren Y, Freger V. Partitioning of organic solutes between water and polyamide layer of RO and NF membranes: Correlation to rejection. *Journal of Membrane Science* 2006; **281**: 480-490.
- [90] Ben-David A, Oren Y, Freger V. Thermodynamic factors in partitioning and rejection of organic compounds by polyamide composite membranes. *Environmental Science & Technology* 2006; **40**: 7023-7028.
- [91] Kimura K, Amy G, Drewes J, Watanabe Y. Adsorption of hydrophobic compounds onto NF/RO membranes: An artifact leading to overestimation of rejection. *Journal of Membrane Science* 2003; **221**: 89-101.
- [92] Nghiem LD, Schäfer AI, Elimelech M. Removal of natural hormones by nanofiltration membranes: Measurement, modeling, and mechanisms. *Environmental Science & Technology* 2004; **38**: 1888-1896.
- [93] McCallum EA, Hyung H, Do TA, Huang C-H, Kim J-H. Adsorption, desorption, and steady-state removal of 17[beta]-estradiol by nanofiltration membranes. *Journal of Membrane Science* 2008; **319**: 38-43.
- [94] Schäfer AI, Akanyeti I, Semião AJC. Micropollutant sorption to membrane polymers: A review of mechanisms for estrogens. *Advances in Colloid and Interface Science* 2011; **164**: 100-117.
- [95] Schäfer AI, Pihlajamäki A, Fane AG, Waite TD, Nyström M. Natural organic matter removal by nanofiltration: effects of solution chemistry on retention of low molar mass acids versus bulk organic matter. *Journal of Membrane Science* 2004; **242**: 73-85.
- [96] Kiso Y, Sugiura Y, Kitao T, Nishimura K. Effects of hydrophobicity and molecular size on rejection of aromatic pesticides with nanofiltration membranes. *Journal of Membrane Science* 2001; **192**: 1-10.

-
- [97] Nghiem LD, Schäfer AI, Elimelech M. Pharmaceutical Retention Mechanisms by Nanofiltration Membranes. *Environmental Science & Technology* 2005; **39**: 7698-7705.
- [98] Teixeira MR, Rosa MJ, Nyström M. The role of membrane charge on nanofiltration performance. *Journal of Membrane Science* 2005; **265**: 160-166.
- [99] Verliefde ARD, Cornelissen ER, Heijman SGJ, Verberk JQJC, Amy GL, Van der Bruggen B, van Dijk JC. Construction and validation of a full-scale model for rejection of organic micropollutants by NF membranes. *Journal of Membrane Science* 2009; **339**: 10-20.
- [100] Lee S, Lueptow RM. Membrane rejection of nitrogen compounds. *Environmental Science & Technology* 2001; **35**: 3008-3018.
- [101] Yuan Y, Kilduff JE. Hydrodynamic modeling of NOM transport in UF: effects of charge density and ionic strength on effective size and sieving. *Environmental Science & Technology* 2009; **43**: 5449-5454.
- [102] Wijmans JG, Baker RW. The solution-diffusion model: a review. *Journal of Membrane Science* 1995; **107**: 1-21.
- [103] Deen WM. Hindered transport of large molecules in liquid-filled pores. *AIChE Journal* 1987; **33**: 1409-1425.
- [104] Spiegler KS, Kedem O. Thermodynamics of hyperfiltration (reverse osmosis): criteria for efficient membranes. *Desalination* 1966; **1**: 311-326.
- [105] Bowen RW, Welfoot JS. *Modelling the performance of nanofiltration membranes in "Nanofiltration Principles and Applications"*, A. I. Schäfer, A. G. Fane, T. D. Waite Editors, Elsevier: Oxford 2004.
- [106] Chellam S, Taylor JS. Simplified analysis of contaminant rejection during ground- and surface water nanofiltration under the information collection rule. *Water Research* 2001; **35**: 2460-2474.
- [107] Williams ME, Hestekin JA, Smothers CN, Bhattacharyya D. Separation of organic pollutants by reverse osmosis and nanofiltration membranes: Mathematical models and experimental verification. *Industrial & Engineering Chemistry Research* 1999; **38**: 3683-3695.
- [108] Van der Bruggen B, Vandecasteele C. Modelling of the retention of uncharged molecules with nanofiltration. *Water Research* 2002; **36**: 1360-1368.

-
- [109] Tandon A, Gupta SK, Agarwal GP. Modelling of protein transmission through ultrafiltration membranes. *Journal of Membrane Science* 1994; **97**: 83-90.
- [110] Bason S, Oren Y, Freger V. Ion transport in the polyamide layer of RO membranes: Composite membranes and free-standing films. *Journal of Membrane Science* 2011; **367**: 119-126.
- [111] Sharma RR, Chellam S. Temperature effects on the morphology of porous thin film composite nanofiltration membranes. *Environmental Science & Technology* 2005; **39**: 5022-5030.
- [112] Verliefde ARD, Cornelissen ER, Heijman SGJ, Petrinic I, Luxbacher T, Amy GL, Van der Bruggen B, van Dijk JC. Influence of membrane fouling by (pretreated) surface water on rejection of pharmaceutically active compounds (PhACs) by nanofiltration membranes. *Journal of Membrane Science* 2009; **330**: 90-103.
- [113] Opong WS, Zydney AL. Diffusive and convective protein transport through asymmetric membranes. *AIChE Journal* 1991; **37**: 1497-1510.
- [114] Bason S, Freger V. Phenomenological analysis of transport of mono- and divalent ions in nanofiltration. *Journal of Membrane Science* 2010; **360**: 389-396.
- [115] Gekas V, Trägårdh G, Aimar P, Sanchez V. Diffusive flows in ultrafiltration and their effect on membrane retention properties. *Journal of Membrane Science* 1993; **80**: 73-83.
- [116] Kim T-U, Drewes JE, Scott Summers R, Amy GL. Solute transport model for trace organic neutral and charged compounds through nanofiltration and reverse osmosis membranes. *Water Research* 2007; **41**: 3977-3988.
- [117] Braeken L, Bettens B, Boussu K, Van der Meeren P, Cocquyt J, Vermant J, Van der Bruggen B. Transport mechanisms of dissolved organic compounds in aqueous solution during nanofiltration. *Journal of Membrane Science* 2006; **279**: 311-319.
- [118] Al-Amoudi AS. Factors affecting natural organic matter (NOM) and scaling fouling in NF membranes: A review. *Desalination* 2010; **259**: 1-10.
- [119] Shirazi S, Lin C-J, Chen D. Inorganic fouling of pressure-driven membrane processes - A critical review. *Desalination* 2010; **250**: 236-248.
- [120] Schippers JC, Verdouw J. The modified fouling index, a method of determining the fouling characteristics of water. *Desalination* 1980; **32**: 137-148.

-
- [121] Schäfer AI, Andritsis N, Karabelas AJ, Hoek EMV, Schneider R, Nystrom M. *Fouling in nanofiltration in "Nanofiltration Principles and Applications"*, A. I. Schäfer, A. G. Fane, T. D. Waite Editors, Elsevier: Oxford, 2004.
- [122] Bacchin P, Aimar P, Field RW. Critical and sustainable fluxes: Theory, experiments and applications. *Journal of Membrane Science* 2006; **281**: 42-69.
- [123] Mänttari M, Nyström M. Critical flux in NF of high molar mass polysaccharides and effluents from the paper industry. *Journal of Membrane Science* 2000; **170**: 257-273.
- [124] Listiarini K, Chun W, Sun DD, Leckie JO. Fouling mechanism and resistance analyses of systems containing sodium alginate, calcium, alum and their combination in dead-end fouling of nanofiltration membranes. *Journal of Membrane Science* 2009; **344**: 244-251.
- [125] Hong S, Elimelech M. Chemical and physical aspects of natural organic matter (NOM) fouling of nanofiltration membranes. *Journal of Membrane Science* 1997; **132**: 159-181.
- [126] Tang CY, Kwon Y-N, Leckie JO. Fouling of reverse osmosis and nanofiltration membranes by humic acid - Effects of solution composition and hydrodynamic conditions. *Journal of Membrane Science* 2007; **290**: 86-94.
- [127] Zhu X, Elimelech M. Colloidal fouling of reverse osmosis membranes: measurements and fouling mechanisms. *Environmental Science & Technology* 1997; **31**: 3654-3662.
- [128] Hoek EMV, Elimelech M. Cake-enhanced concentration polarization: a new fouling mechanism for salt-rejecting membranes. *Environmental Science & Technology* 2003; **37**: 5581-5588.
- [129] Lee S, Cho J, Elimelech M. Combined influence of natural organic matter (NOM) and colloidal particles on nanofiltration membrane fouling. *Journal of Membrane Science* 2005; **262**: 27-41.
- [130] Schäfer AI, Fane AG, Waite TD. Nanofiltration of natural organic matter: Removal, fouling and the influence of multivalent ions. *Desalination* 1998; **118**: 109-122.

-
- [131] Ahn W-Y, Kalinichev AG, Clark MM. Effects of background cations on the fouling of polyethersulfone membranes by natural organic matter: Experimental and molecular modeling study. *Journal of Membrane Science* 2008; **309**: 128-140.
- [132] Ng HY, Elimelech M. Influence of colloidal fouling on rejection of trace organic contaminants by reverse osmosis. *Journal of Membrane Science* 2004; **244**: 215-226.
- [133] Xu P, Drewes JE, Kim T-U, Bellona C, Amy G. Effect of membrane fouling on transport of organic contaminants in NF/RO membrane applications. *Journal of Membrane Science* 2006; **279**: 165-175.
- [134] Nghiem LD, Hawkes S. Effects of membrane fouling on the nanofiltration of pharmaceutically active compounds (PhACs): Mechanisms and role of membrane pore size. *Separation and Purification Technology* 2007; **57**: 176-184.
- [135] Lipp P, Gimbel R, Frimmel FH. Parameters influencing the rejection properties of FT30 membranes. *Journal of Membrane Science* 1994; **95**: 185-197.
- [136] Schäfer AI, Fane AG, Waite TD. Cost factors and chemical pretreatment effects in the membrane filtration of waters containing natural organic matter. *Water Research* 2001; **35**: 1509-1517.
- [137] Nghiem LD, Vogel D, Khan S. Characterising humic acid fouling of nanofiltration membranes using bisphenol A as a molecular indicator. *Water Research* 2008; **42**: 4049-4058.
- [138] Lhassani A, Rumeau M, Benjelloun D, Pontie M. Selective demineralization of water by nanofiltration Application to the defluorination of brackish water. *Water Research* 2001; **35**: 3260-3264.
- [139] Ducom G, Cabassud C. Interests and limitations of nanofiltration for the removal of volatile organic compounds in drinking water production. *Desalination* 1999; **124**: 115-123.
- [140] Weber S, Gallenkemper M, Melin T, Dott W, Hollender J. Efficiency of nanofiltration for the elimination of steroids from water. *Water Science and Technology* 2004; **50**: 9-14.
- [141] Gallenkemper M, Wintgens T, Melin T. Nanofiltration of endocrine disrupting compounds. *Water Science and Technology: Water Supply* 2003; **3**: 321-327.

-
- [142] Nghiem LD, Manis A, Soldenhoff K, Schäfer AI. Estrogenic hormone removal from wastewater using NF/RO membranes. *Journal of Membrane Science* 2004; **242**: 37-45.
- [143] Thorsen T, Fløgstad H. *Nanofiltration in drinking water treatment. Techneau Report, available at <http://www.techneau.org/fileadmin/files/Publications/Deliverables/D5.4.4b.pdf> (accessed March 2012)*, 2006.
- [144] Nghiem LD, Schäfer AI. *Trace contaminant removal with nanofiltration, Nanofiltration principles and applications* N.Y.: A. I. Schäfer, A. G. Fane, T. D. Waite (Eds) Elsevier: New York, 2004.
- [145] Hofman J, Gijsbertsen A, Cornelissen ER. Nanofiltration retention models for organic contaminants, AwwaRF and Kiwa Water Research. 2007.
- [146] Chen S-S, Taylor JS, Mulford LA, Norris CD. Influences of molecular weight, molecular size, flux, and recovery for aromatic pesticide removal by nanofiltration membranes. *Desalination* 2004; **160**: 103-111.
- [147] Kosutic K, Kastelan-Kunst L, Kunst B. Porosity of some commercial reverse osmosis and nanofiltration polyamide thin-film composite membranes. *Journal of Membrane Science* 2000; **168**: 101-108.
- [148] Kiso Y, Muroshige K, Oguchi T, Hirose M, Ohara T, Shintani T. Pore radius estimation based on organic solute molecular shape and effects of pressure on pore radius for a reverse osmosis membrane. *Journal of Membrane Science* 2011; **369**: 290-298.
- [149] Seidel A, Elimelech M. Coupling between chemical and physical interactions in natural organic matter (NOM) fouling of nanofiltration membranes: implications for fouling control. *Journal of Membrane Science* 2002; **203**: 245-255.
- [150] Nghiem LD. Removal of emerging trace organic contaminants by nanofiltration and reverse osmosis, PhD Thesis, The University of Wollongong. 2005.
- [151] Dalwani M, Benes NE, Bargeman G, Stamatialis D, Wessling M. A method for characterizing membranes during nanofiltration at extreme pH. *Journal of Membrane Science* 2011; **363**: 188-194.

-
- [152] Dalwani M, Benes NE, Bargeman G, Stamatialis D, Wessling M. Effect of pH on the performance of polyamide/polyacrylonitrile based thin film composite membranes. *Journal of Membrane Science* 2011; **372**: 228-238.
- [153] Braghetta A, Di Giano FA, Ball WB. Nanofiltration of natural organic matter: pH and ionic strength effects. *Journal of Environmental Engineering* 1997; **123**: 628-641.
- [154] Shim Y, Lee H-J, Lee S, Moon S-H, Cho J. Effects of natural organic matter and ionic species on membrane surface charge. *Environmental Science & Technology* 2002; **36**: 3864-3871.
- [155] Bargeman G, Vollenbroek JM, Straatsma J, Schroen CGPH, Boom RM. Nanofiltration of multi-component feeds. Interactions between neutral and charged components and their effect on retention. *Journal of Membrane Science* 2005; **247**: 11-20.
- [156] Roudman AR, DiGiano FA. Surface energy of experimental and commercial nanofiltration membranes: effects of wetting and natural organic matter fouling. *Journal of Membrane Science* 2000; **175**: 61-73.
- [157] Schäfer AI, Akanyeti I, Semião AJC. Micropollutant sorption to membrane polymers: A review of mechanisms for estrogens. *Advances in Colloid and Interface Science* 2010: In Press doi:10.1016/j.cis.2010.1009.1006.
- [158] Bowen WR, Doneva TA, Yin HB. Atomic force microscopy studies of membrane--solute interactions (fouling). *Desalination* 2002; **146**: 97-102.
- [159] Winfield BA. A study of the factors affecting the rate of fouling of reverse osmosis membranes treating secondary sewage effluents. *Water Research* 1979; **13**: 565-569.
- [160] Vrijenhoek EM, Hong S, Elimelech M. Influence of membrane surface properties on initial rate of colloidal fouling of reverse osmosis and nanofiltration membranes. *Journal of Membrane Science* 2001; **188**: 115-128.
- [161] Jucker C, Clark MM. Adsorption of aquatic humic substances on hydrophobic ultrafiltration membranes. *Journal of Membrane Science* 1994; **97**: 37-52.
- [162] Tang CY, Kwon DJ, Leckie JO. Characterization of humic acid fouled reverse osmosis and nanofiltration membranes by transmission electron microscopy

and streaming potential measurements. *Environmental Science & Technology* 2007; **41**: 942-949.

[163] Lee N, Amy G, Croué J-P, Buisson H. Identification and understanding of fouling in low-pressure membrane (MF/UF) filtration by natural organic matter (NOM). *Water Research* 2004; **38**: 4511-4523.

[164] Han S-C, Choo K-H, Choi S-J, Benjamin MM. Modeling manganese removal in chelating polymer-assisted membrane separation systems for water treatment. *Journal of Membrane Science* 2007; **290**: 55-61.

[165] Lastra A, Gómez D, Romero J, Francisco JL, Luque S, Álvarez JR. Removal of metal complexes by nanofiltration in a TCF pulp mill: technical and economic feasibility. *Journal of Membrane Science* 2004; **242**: 97-105.

[166] Potgieter JH, Potgieter-Vermaak SS, Modise J, Basson N. Removal of iron and manganese from water with a high organic carbon loading. Part II: The effect of adsorbent and nanofiltration membranes. *Water, Air, and Soil Pollution* 2005; **162**: 61-70.

[167] Zhang M, Li C, Benjamin M, Chang Y. Fouling and natural organic matter removal in adsorbent/membrane systems for drinking water treatment. *Environ. Sci. Technol* 2003; **37**: 1663-1669.

[168] Neale P. The Influence of solutes-solutes interactions in membrane filtration, PhD Thesis, The University of Edinburgh. 2009.

[169] Fatin-Rouge N, Dupont A, Vidonne A, Dejeu J, Fievet P, Foissy A. Removal of some divalent cations from water by membrane-filtration assisted with alginate. *Water Research* 2006; **40**: 1303-1309.

[170] Sanli O, Asman G. Removal of Fe(III) ions from dilute aqueous solutions by alginic acid-enhanced ultrafiltration. *Journal of Applied Polymer Science* 2000; **77**: 1096-1101.

[171] Visvanathan C, Marsono BD, Basu B. Removal of THMP by nanofiltration: Effects of interference parameters. *Water Research* 1998; **32**: 3527-3538.

[172] Agbekodo KM, Legube B, Dard S. Atrazine and simazine removal mechanisms by nanofiltration: Influence of natural organic matter concentration. *Water Research* 1996; **30**: 2535-2542.

-
- [173] Devitt EC, Ducellier F, Côté P, Wiesner M. Effects of natural organic matter and the raw water matrix on the rejection of atrazine by pressure-driven membranes. *Water Research* 1999; **32**: 2563-2568.
- [174] Plakas KV, Karabelas AJ, Wintgens T, Melin T. A study of selected herbicides retention by nanofiltration membranes - The role of organic fouling. *Journal of Membrane Science* 2006; **284**: 291-300.
- [175] Jin X, Hu J, Ong SL. Removal of natural hormone estrone from secondary effluents using nanofiltration and reverse osmosis. *Water Research* 2010; **44**: 638-648.
- [176] Hankins N, Price R, Debacherc N. Process intensification during treatment of NOM-laden raw upland waters: Control and impact of the pre-coagulation regime during ultra-filtration. *Desalination and Water Treatment* 2009; **8**: 1-15.
- [177] Kilduff JE, Mattaraj S, Belfort G. Flux decline during nanofiltration of naturally-occurring dissolved organic matter: effects of osmotic pressure, membrane permeability, and cake formation. *Journal of Membrane Science* 2004; **239**: 39-53.
- [178] Scottish Executive. Urban Rural Classification <http://www.scotland.gov.uk/Resource/Doc/233802/0063988.pdf> (accessed March 2012), 2007-2008.
- [179] Langan SJ, Soulsby C. The environmental context for water quality variation in Scotland. *The Science of The Total Environment* 2001; **265**: 7-14.
- [180] MacDonald AM, Robins NS, Ball DF, Ó Dochartaigh BÉ. An overview of groundwater in Scotland *Scottish Journal of Geology*, 2005; **41**: 3-11.
- [181] Johnson RC, Thompson DB. Hydrology and the natural heritage of the Scottish mountains. *The Science of The Total Environment* 2002; **294**: 161-168.
- [182] Soulsby C, Gibbins C, Wade AJ, Smart R, Helliwell R. Water quality in the Scottish uplands: a hydrological perspective on catchment hydrochemistry. *The Science of The Total Environment* 2002; **294**: 73-94.
- [183] The Water Supply Regulations. <http://www.scotland-legislation.hmso.gov.uk/legislation/scotland/ssi2001/20010207.htm>. 2001.
- [184] DWQR. Analytical data supplied courtesy of Drinking Water Quality Regulator for Scotland 2010.

-
- [185] Homoncik SC, MacDonald AM, Heal KV, Ó Dochartaigh BÉ, Ngwenya BT. Manganese concentrations in Scottish groundwater. *Science of The Total Environment* 2010; **408**: 2467-2473.
- [186] <http://www.metoffice.gov.uk/weather/uk/>, (accessed August 2012).
- [187] Scottish Water. Analytical data supplied courtesy of Scottish Water, 2010.
- [188] D'Arcy B, Frost A. The role of best management practices in alleviating water quality problems associated with diffuse pollution. *The Science of The Total Environment* 2001; **265**: 359-367.
- [189] Ferrier RC, Edwards AC. Sustainability of Scottish water quality in the early 21st Century. *The Science of The Total Environment* 2002; **294**: 57-71.
- [190] Littlejohn J. *An investigation into the influence of the voluntary initiative on pesticide concentration in the river Ugie catchment and at Forehill water treatment works*: Scottish Government, 2008.
- [191] Van der Bruggen B, Schaep J, Maes W, Wilms D, Vandecasteele C. Nanofiltration as a treatment method for the removal of pesticides from ground waters. *Desalination* 1998; **117**: 139-147.
- [192] Koch Membrane System. <http://www.kochmembrane.com> (accessed March 2012).
- [193] PCI Membranes. <http://www.pcimem.com> (accessed March 2012).
- [194] Personal Communication with Catrina Attwood (Mott MacDonald, formerly Scottish Water) 28 October 2008.
- [195] Analytical data supplied courtesy of Catrina Attwood (Mott MacDonald formerly Scottish Water) in January 2009.
- [196] Wittmann E, Thorsen T. *Water treatment, Nanofiltration principles and applications*. UK: A. I. Schäfer, A. G. Fane, T. D. Waite (Eds) Elsevier: Oxford, 2004.
- [197] Ødegaard H, Thorsen T, Melin E. Practical experiences from membrane filtration plants for humic substance removal *Water Science and Technology* 2000; **41**: 33-41.
- [198] Ødegaard H, Eikebrokk B, Storhaug R. Processes for the removal of humic substances from water - An overview based on Norwegian experiences. *Water Science and Technology* 1999; **40**: 37-46.

-
- [199] Zularisam AW, Ismail AF, Salim MR, Sakinah M, Ozaki H. The effects of natural organic matter (NOM) fractions on fouling characteristics and flux recovery of ultrafiltration membranes. *Desalination* 2007; **212**: 191-208.
- [200] Collins MR, Amy GL, Steelink C. Molecular weight distribution, carboxylic acidity and humic substances content of aquatic organic matter: implications of removal during water treatment. *Environmental Science & Technology* 1986; **20**: 1028-1032.
- [201] Sharp EL, Parsons SA, Jefferson B. Seasonal variations in natural organic matter and its impact on coagulation in water treatment. *Science of The Total Environment* 2006; **363**: 183-194.
- [202] Shin H-S, Monsallier JM, Choppin GR. Spectroscopic and chemical characterizations of molecular size fractionated humic acid. *Talanta* 1999; **50**: 641-647.
- [203] Chin Y, Aiken G, O'Loughlin E. Molecular weight, polydispersity, and spectroscopic properties of aquatic humic substances. *Environmental Science & Technology* 1994; **28**: 1853-1858.
- [204] Malcom RL, MacCarthy P. Limitation in the use of commercial humic acids in water and soil research. *Environmental Science & Technology* 1986; **20**: 904-911.
- [205] Kim JI, Buckau G, Dushner H, Psarros N. Characterization of humic and fulvic acids from Gorleben groundwater. *Fresenius' Journal of Analytical Chemistry* 1990; **338**: 245-252.
- [206] Nyström M, Ruohomäki K, Kaipia L. Humic acid as a fouling agent in filtration. *Desalination* 1996; **106**: 79-87.
- [207] Schäfer AI. *Natural organics removal using membranes: principles, performance and cost*. Boca Raton: CRC Press 2001.
- [208] Plakas KV, Karabelas AJ. Triazine retention by nanofiltration in the presence of organic matter: The role of humic substance characteristics. *Journal of Membrane Science* 2009; **336**: 86-100.
- [209] Lee J. Complexation analysis of fresh waters by equilibrium diafiltration. *Water Research* 1983; **17**: 501-510.
- [210] Nifant'eva TI, Shkinev VM, Spivakov BY, Burba P. Membrane filtration studies of aquatic humic substances and their metal species: a concise overview. Part

2. Evaluation of conditional stability constants by using ultrafiltration. *Talanta* 1999; **48**: 257-267.

[211] Chiswell B, Mokhtar MB. Speciation of manganese in fresh water - I : Use of EPR studies. *Talanta* 1987; **34**: 307-311.

[212] Guy RD, Chakrabarti CL. Studies of metal–organic interactions in model systems pertaining to natural waters. *Canadian Journal Chemistry* 1976; **54**: 2600-2611.

[213] Chiswell B, Mokhtar MB. The speciation of manganese in freshwaters. *Talanta* 1986; **33**: 669-677.

[214] Stumm W, Morgan J. *Aquatic Chemistry*. New York: Wiley-Interscience, 1970.

[215] German Federal Environment Agency. Draft dossier prepared in support of a proposal of endosulfan to be considered as a candidate for inclusion in the annexes of the Stockholm Convention. 2007.

[216] Pozo K, Harner T, Wania F, Muir DCG, Jones K, Barrie LA. Toward a global network for persistent organic pollutants in air: results from the GAPS study. *Environmental Science & Technology* 2006; **40**: 4867-4873.

[217] Halsall CJ, Bailey R, Stern GA, Barrie LA, Fellin P, Muir DCG, Rosenberg B, Rovinsky FY, Kononov EY, Pastukhov B. Multi-year observations of organohalogen pesticides in the Arctic atmosphere. *Environmental Pollution* 1998; **102**: 51-62.

[218] Berrill M, Coulson D, McGillivray L, Pauli B. Toxicity of Endosulfan to aquatic stages of anuran amphibians. *Environmental Toxicology and Chemistry* 1998; **17**: 1738-1744.

[219] Wikteliu S, Chiverton PA, Meguenni H, Bennaceur M, Ghezal F, Umeh EDN, Egwuatu RI, Minja E, Makusi R, Tukahirwa E, Tinzaara W, Deedat Y. Effects of insecticides on non-target organisms in African agroecosystems: a case for establishing regional testing programmes. *Agriculture, Ecosystems & Environment* 1999; **75**: 121-131.

[220] Forman S, Durbetaki A, Choen M, Olofson RA. Conformational equilibria in cyclic sulfites and sulfates. The configurations and conformations of the two isomeric thiodans. *Journal of Organic Chemistry* 1965; **30**: 169-175.

-
- [221] Organization for Economic Co-operation and Development. Environment Monograph No. 108: Final report on the OECD project to compare pesticides data reviews. 1995.
- [222] Hillenbrand T, Marscheider-Weidemann F, Strauch M, Heitmann K. *Prioritäre Stoffe der Wasserrahmenrichtlinie Datenblatt Nr. 14: Endosulfan (in German)*, 2006.
- [223] Ministerio de Agricultura Pesca Y Alimentacion. *Endosulfan - Vol 1 - Monograph prepared in the context of the inclusion of the following active substance in Annex I of the Council Directive 91/414/EEC*, 1999.
- [224] Kumar M, Philip L. Adsorption and desorption characteristics of hydrophobic pesticide endosulfan in four Indian soils. *Chemosphere* 2006; **62**: 1064-1077.
- [225] Hayes MHB, MacCarthy P, Malcom RL, Swift RS. *The search for structure: setting the scene in Humic Substance II* New York: John Wiley & Sons, 1989.
- [226] Jones MN, Bryan ND. Colloidal properties of humic substances. *Advances in Colloid and Interface Science* 1998; **78**: 1-48.
- [227] Schulten HR, Plage B, Schnitzer M. A chemical structure for humic substances. *Naturwissenschaften* 1991; **78**: 311-312.
- [228] Schulten HR, Schnitzer M. A state of the art structural concept for humic substances. *Naturwissenschaften* 1993; **80**: 29-30.
- [229] Avena MJ, Koopal LK, van Riemsdijk WH. Proton binding to humic acids: electrostatic and intrinsic interactions. *Journal of Colloid and Interface Science* 1999; **217**: 37-48.
- [230] Balnois E, Wilkinson KJ, Lead JR, Buffle J. Atomic force microscopy of humic substances: effects of pH and ionic strength. *Environmental Science & Technology* 1999; **33**: 3911-3917.
- [231] Burba P, Aster B, Nifant'eva T, Shkinev V, Spivakov BY. Membrane filtration studies of aquatic humic substances and their metal species: a concise overview: Part 1. Analytical fractionation by means of sequential-stage ultrafiltration. *Talanta* 1998; **45**: 977-988.
- [232] Ghosh K, Schnitzer M. Macromolecular structures of humic substances. *Soil Science* 1980; **129**: 266-276.

-
- [233] Stumm W. *Chemistry of the Solid-Water Interface*: Wiley Interscience, New York 1992.
- [234] Teixeira MR, Rosa MJ. The impact of the water background inorganic matrix on the natural organic matter removal by nanofiltration. *Journal of Membrane Science* 2006; **279**: 513-520.
- [235] Tang CY, Kwon YN, J.O. L. Characterization of Humic Acid Fouled Reverse Osmosis and Nanofiltration Membranes by Transmission Electron Microscopy and Streaming Potential Measurements. *Environ. Sci. Technol* 2007; **41**: 942-949.
- [236] Cho J, Amy G, Pellegrino J. Membrane filtration of natural organic matter: initial comparison of rejection and flux decline characteristics with ultrafiltration and nanofiltration membranes. *Water Research* 1999; **33**: 2517-2526.
- [237] Thanuttamavong M, Yamamoto K, Ik Oh J, Ho Choo K, June Choi S. Rejection characteristics of organic and inorganic pollutants by ultra low-pressure nanofiltration of surface water for drinking water treatment. *Desalination* 2002; **145**: 257-264.
- [238] The Water Supply (Water Quality) (Scotland) Regulations - Scottish Statutory Instrument No. 207. 2001.
- [239] Ljung K, Vahter M. Time to re-evaluate the guideline value for manganese in drinking water? *Environmental Health Perspectives* 2007; **115**: 1533–1538.
- [240] Wasserman GA, Liu X, Parvez F, Factor-Litvak P, Ahsan H, Levy D, Kline J, van Geen A, Mey J, Slavkovich V, Siddique AB, Islam T, Graziano JH. Arsenic and manganese exposure and children's intellectual function. *NeuroToxicology* 2011; **32**: 450-457.
- [241] Spangler A, Spangler J. Groundwater manganese and infant mortality rate by county in North Carolina: an ecological analysis. *EcoHealth* 2009; **6**: 596-600.
- [242] Spangler J, Reid J. Environmental manganese and cancer mortality rates by county in North Carolina: an ecological study. *Biological Trace Element Research* 2010; **133**: 128-135.
- [243] Hafeman D, Factor-Litvak P, Cheng Z, van Geen A, Ahsan H. Association between manganese exposure through drinking water and infant mortality in Bangladesh. *Environmental Health Perspectives* 2007; **115**: 1107-1112.

-
- [244] Tanizaki Y, Shimokawa T, Nakamura M. Physicochemical speciation of trace elements in river waters by size fractionation. *Environmental Science & Technology* 1992; **26**: 1433-1444.
- [245] Ouddane B, Martin E, Boughriet A, Fischer JC, Wartel M. Speciation of dissolved and particulate manganese in the Seine river estuary. *Marine Chemistry* 1997; **58**: 189-201.
- [246] Zaw M, Chiswell B. Iron and manganese dynamics in lake water. *Water Research* 1999; **33**: 1900-1910.
- [247] Ellis D, Bouchard C, Lantagne G. Removal of iron and manganese from groundwater by oxidation and microfiltration. *Desalination* 2000; **130**: 255-264.
- [248] Mijatovic I, Matosic M, Hajduk Cerneha B, Bratulic D. Removal of natural organic matter by ultrafiltration and nanofiltration for drinking water production. *Desalination* 2004; **169**: 223-230.
- [249] Potgieter JH, Mccrindle RI, Sihlali Z, Schwarzer R, Basson N. Removal of Iron and Manganese from Water with a High Organic Carbon Loading. Part I: The Effect of Various Coagulants *Water, Air, and Soil Pollution* 2005; **162**: 29-59.
- [250] Buamah R, Petrusevski B, de Ridder D, van de Wetering TSCM, Shippers JC. Manganese removal in groundwater treatment: practice, problems and probable solutions. *Water Science and Technology: Water Supply* 2009; **9.1**: 89-98.
- [251] Al-Rashdi B, Somerfield C, Hilal N. Heavy metals removal using adsorption and nanofiltration techniques. *Separation & Purification Reviews* 2011; **40**: 209-259.
- [252] Molinari R, Argurio P, Romeo L. Studies on interactions between membranes (RO and NF) and pollutants (SiO_2 , NO_3^- , Mn^{++} and humic acid) in water. *Desalination* 2001; **138**: 271-281.
- [253] Pearson D. Surface-water systems use membranes to remove disinfection by-product precursors. *Membrane Technology* 2001; **2001**: 4-7.
- [254] Jimbo Y, Goto K. Iron and manganese removal by a membrane filtration system. *Water Science and Technology: Water Supply* 2001; **1**: 357-364.
- [255] Kabsch-Korbutowicz M, Winnicki T. Application of modified polysulfone membranes to the treatment of water solutions containing humic substances and metal ions. *Desalination* 1996; **105**: 41-49.

-
- [256] Choo K-H, Lee H, Choi S-J. Iron and manganese removal and membrane fouling during UF in conjunction with prechlorination for drinking water treatment. *Journal of Membrane Science* 2005; **267**: 18-26.
- [257] Kimura K, Hane Y, Watanabe Y, Amy G, Ohkuma N. Irreversible membrane fouling during ultrafiltration of surface water. *Water Research* 2004; **38**: 3431-3441.
- [258] Kaiya Y, Itoh Y, Fujita K, Takizawa S. Study on fouling materials in the membrane treatment process for potable water. *Desalination* 1996; **106**: 71-77.
- [259] Speth TF, Summers RS, Gusses AM. Nanofiltration foulants from a treated surface water. *Environmental Science & Technology* 1998; **32**: 3612-3617.
- [260] Schmidt W, Bilboulia S, Rice C, Fettinger J, McConnel L, Hapeman C. Thermodynamic, Spectroscopic, and Computational Evidence for the Irreversible Conversion of β - to α -Endosulfan. *Journal of Agricultural and Food Chemistry* 2001; **49**: 5372-5376.
- [261] Peterson SM, Batley GE. The fate of endosulfan in aquatic ecosystems. *Environmental Pollution* 1993; **82**: 143-152.
- [262] Cerejeira MJ, Viana P, Batista S, Pereira T, Silva E, Valério MJ, Silva A, Ferreira M, Silva-Fernandes AM. Pesticides in Portuguese surface and ground waters. *Water Research* 2003; **37**: 1055-1063.
- [263] Golfopoulos SK, Nikolaou AD, Kostopoulou MN, Xilourgidis NK, Vagi MC, Lekkas DT. Organochlorine pesticides in the surface waters of Northern Greece. *Chemosphere* 2003; **50**: 507-516.
- [264] Aslan S, Türkman A. Combined biological removal of nitrate and pesticides using wheat straw as substrates. *Process Biochemistry* 2005; **40**: 935-943.
- [265] Turgut C. The contamination with organochlorine pesticides and heavy metals in surface water in Küçük Menderes River in Turkey, 2000-2002. *Environment International* 2003; **29**: 29-32.
- [266] Zulin Z, Huasheng H, Xinhong W, Jianqing L, Weiqi C, Li X. Determination and load of organophosphorus and organochlorine pesticides at water from Jiulong River Estuary, China. *Marine Pollution Bulletin* 2002; **45**: 397-402.
- [267] Kammerbauer J, Moncada J. Pesticide residue assessment in three selected agricultural production systems in the Choluteca River Basin of Honduras. *Environmental Pollution* 1998; **103**: 171-181.

-
- [268] European Council. Council Directive 98/83/EC of 3 November 1998 on the quality of water intended for human consumption as amended by Regulation 1882/2003/EC
- [269] UNEP Stockholm Convention on Persistent Organic Pollutants. Report of the Conference of the Parties to the Stockholm Convention on Persistent Organic Pollutants on the work of its fifth meeting - UNEP/POPS/COP.5/36. 2011.
- [270] Rice C, Chernyak S, Hapeman C, Bilbouljian S. Air-water distribution of the Endosulfan isomers. *Journal of Environmental Quality* 1997; **26**: 1101- 1106.
- [271] Guerin TF. The relative significance of biodegradation and physico-chemical dissipation of endosulfan from water and soil. University of Sydney, 1993.
- [272] Hansch C, Leo A, Hoekman D. *Exploring QSAR: hydrophobic, electronic and steric constants*. Washington DC, USA: American Chemical Society, 1995.
- [273] Banasiak LJ, Van der Bruggen B, Schäfer AI. Sorption of pesticide endosulfan by electro dialysis membranes. *Chemical Engineering Journal* 2011; **166**: 233-239.
- [274] Montgomery J. *Groundwater Chemicals Desk Reference, Fourth Edition* New Jersey: CRC Press 2007.
- [275] Guerin TF. A biological loss of endosulfan and related chlorinated organic compounds from aqueous systems in the presence and absence of oxygen. *Environmental Pollution* 2001; **115**: 219-230.
- [276] Schwarzenbach RP, Gschwend PW, Imboden DM. *Environmental Organic Chemistry*. Hoboken: John Wiley and Sons, 2003.
- [277] Ormad MP, Miguel N, Claver A, Matesanz JM, Ovelleiro JL. Pesticides removal in the process of drinking water production. *Chemosphere* 2008; **71**: 97-106.
- [278] Neale PA, Escher BI, Schäfer AI. Quantification of solute-solute interactions using negligible-depletion solid-phase microextraction: measuring the affinity of estradiol to bulk organic matter. *Environmental Science & Technology* 2008; **42**: 2886-2892.
- [279] Neale PA, Schäfer AI. Quantification of solute-solute interactions in steroidal hormone removal by ultrafiltration membranes. *Separation and Purification Technology* 2012; **90**: 31-38.

-
- [280] Banasiak LJ. Removal of inorganic and trace organic contaminants by electro-dialysis. PhD Thesis, The University of Edinburgh. 2009.
- [281] Tiraferri A, Elimelech M. Direct quantification of negatively charged functional groups on membrane surfaces. *Journal of Membrane Science* 2012; **389**: 499-508.
- [282] Jacobasch HJ, Baubock G, Schurz J. Problems and results of zeta-potential measurements on fibers. *Colloid & Polymer Science* 1985; **263**.
- [283] Fairbrother F, Mastin H. Studies in Electro-endosmosis. Part I. *Journal of the Chemical Society, Transactions* 1924; **125**: 2319 - 2330.
- [284] Boussu K, Van der Bruggen B, Volodin A, Snauwaert J, Van Haesendonck C, Vandecasteele C. Roughness and hydrophobicity studies of nanofiltration membranes using different modes of AFM. *Journal of Colloid and Interface Science* 2005; **286**: 632-638.
- [285] Hoek EMV, Bhattacharjee S, Elimelech M. Effect of membrane surface roughness on colloidal-membrane DLVO interactions. *Langmuir* 2003; **19**: 4836-4847.
- [286] Tran T, Gray S, Naughton R, Bolto B. Polysilicato-iron for improved NOM removal and membrane performance. *Journal of Membrane Science* 2006; **280**: 560-571.
- [287] Meng F, Liao B, Liang S, Yang F, Zhang H, Song L. Morphological visualization, componential characterization and microbiological identification of membrane fouling in membrane bioreactors (MBRs). *Journal of Membrane Science* 2010; **361**: 1-14.
- [288] Tang CY, Kwon Y-N, Leckie JO. Probing the nano- and micro-scales of reverse osmosis membranes--A comprehensive characterization of physiochemical properties of uncoated and coated membranes by XPS, TEM, ATR-FTIR, and streaming potential measurements. *Journal of Membrane Science* 2007; **287**: 146-156.
- [289] Rice G, Barber A, O'Connor A, Stevens G, Kentish S. Fouling of NF membranes by dairy ultrafiltration permeates. *Journal of Membrane Science* 2009; **330**: 117-126.

-
- [290] Koutsou CP, Karabelas AJ. Shear stresses and mass transfer at the base of a stirred filtration cell and corresponding conditions in narrow channels with spacers. *Journal of Membrane Science* 2012; **399-400**: 60-72.
- [291] Groß A, Heintz A. Diffusion coefficients of aromatics in nonporous PEBA membranes. *Journal of Membrane Science* 2000; **168**: 233-242.
- [292] U.S. Environmental Protection Agency. "MINTEQA2/PRODEFA2, A Geochemical Assessment Model for Environmental Systems: Version 3.0 User Manual". USEPA, Athens, GA, 1991.
- [293] <http://epa.gov/ceampubl/mmedia/minteq/index.htm>, (accessed March 2012).
- [294] U.S. Environmental Protection Agency, "MINTEQA2/PRODEFA2, A Geochemical Assessment Model for Environmental Systems: User Manual Supplement for Version 4.0". USEPA, Athens, GA, 1999.
- [295] Merdy P, Huclier S, Koopal LK. Modeling metal–particle interactions with an emphasis on natural organic matter. *Environmental Science & Technology* 2006; **40**: 7459–7466.
- [296] Gustafsson JP. Modeling the acid-base properties and metal complexation of humic substances with the Stockholm Humic Model. *Journal of Colloid and Interface Science* 2001; **244**: 102-112.
- [297] Gustafsson JP, Van Schaik JWJ. Cation binding in a mor layer: batch experiments and modelling. *European Journal of Soil Science* 2003; **54**: 295-310.
- [298] Gustafsson JP, Kleja DB. Modeling salt-dependent proton binding by organic soils with the NICA-Donnan and Stockholm Humic Models. *Environmental Science & Technology* 2003; **39**: 5372-5377.
- [299] Kinniburgh DG, van Riemsdijk WH, Koopal LK, Borkovec M, Benedetti MF, Avena MJ. Ion binding to natural organic matter: competition, heterogeneity, stoichiometry and thermodynamic consistency. *Colloids and Surfaces A: Physicochemical and Engineering Aspects* 1999; **151**: 147-166.
- [300] Benedetti MF, Milne CJ, Kinniburgh DG, Van Riemsdijk WH, Koopal LK. Metal ion binding to humic substances: application of the non-ideal competitive adsorption model. *Environmental Science & Technology* 1995; **29** 446-457.

-
- [301] Christl I, Milne CJ, Kinniburgh DG, Kretzschmar R. Relating ion binding by Fulvic and Humic Acids to chemical composition and molecular size. 2. metal binding. *Environmental Science & Technology* 1995; **29**: 2512–2517.
- [302] Pinheiro JP, Mota AM, Benedetti MF. Effect of aluminum competition on lead and cadmium binding to humic acids at variable ionic strength. *Environmental Science & Technology* 2000; **34**: 5137–5143.
- [303] Weber T, Allard T, Benedetti MF. Iron speciation in interaction with organic matter: Modelling and experimental approach. *Journal of Geochemical Exploration* 2006; **88**: 166-171.
- [304] Weber T, Allard T, Tipping E, Benedetti MF. Modeling iron binding to organic matter. *Environmental Science & Technology* 2006; **40**: 7488-7493.
- [305] Milne CJ, Kinniburgh DG, Van Riemsdijk WH, Tipping E. Generic NICA–Donnan model parameters for metal-ion binding by humic substances. *Environmental Science & Technology* 2003; **37**: 958-971.
- [306] Oomen AG, Mayer P, Tolls J. Nonequilibrium Solid-Phase Microextraction for Determination of the Freely Dissolved Concentration of Hydrophobic Organic Compounds: Matrix Effects and Limitations. *Analytical Chemistry* 2000; **72**: 2802-2808.
- [307] DiFilippo EL, Eganhouse RP. Assessment of PDMS-water partition coefficients: Implications for passive environmental sampling of hydrophobic organic compounds. *Environmental Science & Technology* 2010; **44**: 6917-6925.
- [308] Prosen H, Fingler S, Zupancic-Kralj L, Drevenkar V. Partitioning of selected environmental pollutants into organic matter as determined by solid-phase microextraction. *Chemosphere* 2007; **66**: 1580-1589.
- [309] Prosen H, Troha A, Zupančič - Kralj L. Studies of interaction between some organochlorine insecticides and humic acid using solid-phase microextraction and gas chromatography. *Acta Chimica Slovenica* 2002; **49**: 561-573.
- [310] Neale PA, Escher BI, Schäfer AI. pH dependence of steroid hormone-organic matter interactions at environmental concentrations. *Science of The Total Environment* 2009; **407**: 1164-1173.

-
- [311] Poerschmann J, Kopinke F-D, Pawliszyn J. Solid phase microextraction to study the sorption of organotin compounds onto particulate and dissolved humic organic matter *Environmental Science & Technology* 1997; **31**: 3629-3636.
- [312] Urrestarazu Ramos Ea, Meijer SN, Vaes WHJ, Verhaar HJM, Hermens JLM. Using Solid-Phase Microextraction To Determine Partition Coefficients to Humic Acids and Bioavailable Concentrations of Hydrophobic Chemicals. *Environmental Science & Technology* 1998; **32**: 3430-3435.
- [313] Poerschmann J, Kopinke F-D. Sorption of very hydrophobic organic compounds (VHOCs) on dissolved humic organic matter (DOM). 2. Measurement of sorption and application of a Flory-Huggins concept to interpret the data. *Environmental Science & Technology* 2001; **35**: 1142-1148.
- [314] Heringa MB, Pastor D, Algra J, Vaes WHJ, Hermens JLM. Negligible depletion solid-phase microextraction with radiolabeled analytes to study free concentrations and protein binding: an example with [³H]Estradiol. *Analytical Chemistry* 2002; **74**: 5993-5997.
- [315] Endo S, Droge STJ, Goss K-U. Polyparameter linear free energy models for polyacrylate fiber-water partition coefficients to evaluate the efficiency of solid-phase microextraction. *Analytical Chemistry* 2011; **83**: 1394-1400.
- [316] Lord H, Pawliszyn J. Evolution of solid-phase microextraction technology. *Journal of Chromatography A* 2000; **885**: 153-193.
- [317] Aguilar C, Peñalver A, Pocurull E, Ferré J, Borrull F, Marcé RM. Optimization of solid-phase microextraction conditions using a response surface methodology to determine organochlorine pesticides in water by gas chromatography and electron-capture detection. *Journal of Chromatography A* 1999; **844**: 425-432.
- [318] Valor I, Perez M, Cortada C, Apraiz D, Molto JC, Font G. SPME of 52 pesticides and polychlorinated biphenyls: Extraction efficiencies of the SPME coatings poly(dimethylsiloxane), polyacrylate, poly(dimethylsiloxane)-divinylbenzene, carboxenpoly(dimethylsiloxane) and carbowaxdivinylbenzene. *Journal of Separation Science* 2001; **24**: 39-48.
- [319] Magdic S, Pawliszyn JB. Analysis of organochlorine pesticides using solid-phase microextraction. *Journal of Chromatography A* 1996; **723**: 111-122.

-
- [320] Deger AB, Gremm TJ, Frimmel FH, Mendez L. Optimization and application of SPME for the gas chromatographic determination of endosulfan and its major metabolites in the ng L⁻¹ range in aqueous solutions. *Analytical and Bioanalytical Chemistry* 2003; **376**: 61-68.
- [321] Scheyer A, Morville S, Mirabel P, Millet M. Analysis of trace levels of pesticides in rainwater using SPME and GC-tandem mass spectrometry. *Analytical and Bioanalytical Chemistry* 2006; **384**: 475-487.
- [322] Vaes WHJ, Ramos EU, Hamwijk C, van Holsteijn I, Blaauboer BJ, Seinen W, Verhaar HJM, Hermens JLM. Solid phase microextraction as a tool to determine membrane/water partition coefficients and bioavailable concentrations in vitro systems. *Chemical Research in Toxicology* 1997; **10**: 1067-1072.
- [323] Clesceri LS, Greenberg AE, Eaton AD. *Standard methods for the examination of water and wastewater* - 20th Edition, 1998.
- [324] Miller JN, Miller JC. *Statistics and chemometrics for analytical chemistry*. Harlow: Pearson Education Limited, 2000.
- [325] Hajibabania S, Verliefde A, McDonald JA, Khan SJ, Le-Clech P. Fate of trace organic compounds during treatment by nanofiltration. *Journal of Membrane Science* 2011; **373**: 130-139.
- [326] Cho J, Amy G, Pellegrino J. Membrane filtration of natural organic matter: comparison of flux decline, NOM rejection, and foulants during filtration with three UF membranes. *Desalination* 2000; **127**: 283-298.
- [327] Gekas V, Hallström B. Mass transfer in the membrane concentration polarization layer under turbulent cross flow: I. Critical literature review and adaptation of existing Sherwood correlations to membrane operations. *Journal of Membrane Science* 1987; **30**: 153-170.
- [328] Bowen WR, Mohammad AW, Hilal N. Characterisation of nanofiltration membranes for predictive purposes - use of salts, uncharged solutes and atomic force microscopy. *Journal of Membrane Science* 1997; **126**: 91-105.
- [329] van den Berg GB, Racz IG, Smolders CA. Mass transfer coefficients in cross-flow ultrafiltration. *Journal of Membrane Science* 1989; **47**: 25-51.
- [330] Bouranene S, Fievet P, Szymczyk A, El-Hadi Samar M, Vidonne A. Influence of operating conditions on the rejection of cobalt and lead ions in aqueous

solutions by a nanofiltration polyamide membrane. *Journal of Membrane Science* 2008; **325**: 150-157.

[331] Kotrappanavar NS, Hussain AA, Abashar MEE, Al-Mutaz IS, Aminabhavi TM, Nadagouda MN. Prediction of physical properties of nanofiltration membranes for neutral and charged solutes. *Desalination* 2011; **280**: 174-182.

[332] Benjamin M. *Water Chemistry*. N.Y.: McGraw Hill, New York, 2002.

[333] Handa BK. Chemistry of manganese in natural waters. *Chemical Geology* 1970; **5**: 161-165.

[334] Nystrom M, Lindstrom M, Matthiasson E. Streaming potential as a tool in the characterization of ultrafiltration membranes. *Colloids and Surfaces* 1989; **36**: 297-312.

[335] Oldham IB, Young FJ, Osterle JF. Streaming potential in small capillaries. *Journal of Colloid Science* 1963; **18**: 328-336.

[336] Rice CL, Whitehead R. Electrokinetic flow in a narrow cylindrical capillary. *The Journal of Physical Chemistry* 1965; **69**: 4017-4024.

[337] Choo K-H, Kwon DJ, Lee KW, Choi SJ. Selective Removal of Cobalt Species Using Nanofiltration Membranes. *Environmental Science & Technology* 2002; **36**: 1330-1336.

[338] The Water Supply (Water Quality) (Scotland) Regulations. - Scottish Statutory Instrument No. 207 available at <http://www.scotland-legislation.hmso.gov.uk/legislation/scotland/ssi2001/20010207.htm> (last accessed June 2010), 2001.

[339] Schäfer AI, Nghiem LD, Meier A, Neale PA. Impact of organic matrix compounds on the retention of steroid hormone estrone by a "loose" nanofiltration membrane. *Separation and Purification Technology* 2010; **73**: 179-187.

[340] Yoon Y, Westerhoff P, Snyder SA, Wert EC. Nanofiltration and ultrafiltration of endocrine disrupting compounds, pharmaceuticals and personal care products. *Journal of Membrane Science* 2006; **270**: 88-100.

[341] Devitt EC, Wiesner MR. Dialysis investigations of atrazine-organic matter interactions and the role of a divalent metal. *Environmental Science & Technology* 1998; **32**: 232-237.

-
- [342] Boussahel R, Bouland S, Moussaoui KM, Montiel A. Removal of pesticide residues in water using the nanofiltration process. *Desalination* 2000; **132**: 205-209.
- [343] Jermann D, Pronk W, Boller M, Schäfer AI. The role of NOM fouling for the retention of estradiol and ibuprofen during ultrafiltration. *Journal of Membrane Science* 2009; **329**: 75-84.
- [344] de Gennes PG. Wetting: statics and dynamics. *Reviews of Modern Physics* 1985; **57**: 827.
- [345] Braghetta A. The influence of solution chemistry and operating conditions on nanofiltration of charged and uncharged organic macromolecules. PhD Thesis University of North Carolina, Chapel Hill, 1995.
- [346] Nghiem LD, Schäfer AI. Adsorption and transport of trace contaminant estrone in NF/RO membranes. *Environmental Engineering Science* 2002; **19**: 441-451.
- [347] Semião AJC. Estrogenic micropollutant removal by nanofiltration, PhD Thesis, The University of Edinburgh. 2011.
- [348] Yaroshchuk AE, Ribitsch V. The uses of non-steady-state membrane characterisation techniques for the study of transport properties of active layers of nanofiltration membranes: theory with experimental examples. *Chemical Engineering Journal* 2000; **80**: 203-214.
- [349] Robertson BC, Zydney AL. Hindered protein diffusion in asymmetric ultrafiltration membranes with highly constricted pores. *Journal of Membrane Science* 1990; **49**: 287-303.
- [350] Scally S, Davison W, Zhang H. Diffusion coefficients of metals and metal complexes in hydrogels used in diffusive gradients in thin films. *Analytica Chimica Acta* 2006; **558**: 222-229.
- [351] Heijman SGJ, Verliefde A, Cornelissen ER, Amy G, van Dijk JC. Influence of natural organic matter (NOM) fouling on the removal of pharmaceuticals by nanofiltration and activated carbon filtration. *Water Science and Technology: Water Supply* 2007; **7**: 17-23.
- [352] Nilsson M, Tragardh G, Ostergren K. The influence of pH, salt and temperature on nanofiltration performance. *Journal of Membrane Science* 2008; **312**: 97-106.

-
- [353] Nilsson M, Tragardh G, Ostergren K. The influence of sodium chloride on mass transfer in a polyamide nanofiltration membrane at elevated temperatures. *Journal of Membrane Science* 2006; **280**: 928-936.
- [354] Tessaro IC, da Silva JBA, Wada K. Investigation of some aspects related to the degradation of polyamide membranes: aqueous chlorine oxidation catalyzed by aluminum and sodium laurel sulfate oxidation during cleaning. *Desalination* 2005; **181**: 275-282.
- [355] Gabelich CJ, Frankin JC, Gerringe FW, Ishida KP, Suffet IH. Enhanced oxidation of polyamide membranes using monochloramine and ferrous iron. *Journal of Membrane Science* 2005; **258**: 64-70.
- [356] da Silva MK, Tessaro IC, Wada K. Investigation of oxidative degradation of polyamide reverse osmosis membranes by monochloramine solutions. *Journal of Membrane Science* 2006; **282**: 375-382.
- [357] Freger V, Arnot TC, Howell JA. Separation of concentrated organic/inorganic salt mixtures by nanofiltration. *Journal of Membrane Science* 2000; **178**: 185-193.
- [358] Xie W, Ju H, Geise GM, Freeman BD, Mardel JI, Hill AJ, McGrath JE. Effect of free volume on water and salt transport properties in directly copolymerized disulfonated poly(arylene ether sulfone) random copolymers. *Macromolecules* 2012; **44**: 4428-4438.
- [359] Freger V, Bottino A, Capannelli G, Perry M, Gitis V, Belfer S. Characterization of novel acid-stable NF membranes before and after exposure to acid using ATR-FTIR, TEM and AFM. *Journal of Membrane Science* 2005; **256**: 134-142.
- [360] Ju H, Sagle AC, Freeman BD, Mardel JI, Hill AJ. Characterization of sodium chloride and water transport in crosslinked poly(ethylene oxide) hydrogels. *Journal of Membrane Science* 2010; **358**: 131-141.
- [361] Geise GM, Freeman BD, Paul DR. Characterization of a sulfonated pentablock copolymer for desalination applications. *Polymer* 2010; **51**: 5815-5822.

Appendix 1 – Membrane plants in remote Scottish communities

A.1.1 Introduction

Sections 3.2 and 3.3 offered an overview of the water quality and of the type of treatment selected in Scotland to provide safe drinking water. Despite the high number of membrane plants in Scotland and the availability of operational and water quality data, dedicated studies assessing the performance of membrane plants are lacking.

The majority of the NF modules in Scotland are tubular membranes, while spiral wound membranes constitute only 40% of the total membrane plants [1]. Tubular membranes are the preferred choice, as they do not require pre-treatment and daily chemical cleaning. Tubular membranes are produced by PCI [2] in modules containing 72 tubes (12.7 mm inner diameter) arranged in parallel. CA membranes of 2kDa nominal MWCO or PES membranes of 4kDa nominal MWCO are employed. PES membranes were initially installed in the majority of the plants but experienced irreversible fouling in many small plants and were retrospectively substituted with CA membranes [1].

Bowen *et al.* [3] characterised PCI CA and PES membranes extensively. CA membranes are tighter and have smaller pores (estimated pore radius 0.96 nm with respect to 1.56 nm for PES membranes), but they have a higher charge (-11 mol/m^3 as effective charge density from salt retention data with respect to -9 mol/m^3 for PES membranes). Laboratory tests on synthetic water simulating Scottish surface water showed that CA membranes have lower flux ($12.7 \text{ L/m}^2\text{h}$) than PES membranes ($37.6 \text{ L/m}^2\text{h}$) but they have similar HA and NaCl retention (HA retention was 96% for CA membranes and 89% for PES membranes, while NaCl retention was 20% for both). CA membranes have also lower fouling tendency (relative flux loss after 4 hours of HA filtration was 0.98 for CA membranes and 0.88 for PES membranes).

A mechanical method for cleaning tubular membranes called the “Fyne process” was developed by PCI in Scotland [4, 5]. A foam ball with a slightly smaller diameter than the membrane is automatically passed every 4-6 hours inside the membrane tubes at a pressure of 2-3 bar in order to remove deposits on the membrane surface by hydraulic shear force. In addition to the mechanical cleaning, PCI recommends performing chemical cleaning every 3-4 months and at the same time renew the foam balls [2].

This chapter will evaluate the performance of selected Scottish NF plants in terms of operational parameters, water quality, energy consumption and costs. The aim is to identify the challenges faced by Scottish membrane plants and highlight how the research on solute removal mechanisms can contribute to improved plant efficiency.

Two small membrane plants, Plant A located in a northern island and Plant B located on an island in the west of Scotland will be compared and their performance evaluated. These plants were chosen as they both use the same type of membranes but they are of different sizes and are operated differently. Operational parameters (flux and pressure), raw and final water quality, costs and energy consumption will be presented for both plants.

Data on water quality in the raw water (i.e. at the plant inlet) and in the final water (i.e. at the plant outlet) for parameters whose analysis are mandatory [6] were kindly received from the Drinking Water Quality Regulator for Scotland [7] and from Scottish Water [1]. Water quality data from January 2007 till December 2009 were available for both plants. Operational data and information about the plants were collected from the plant operators during one site visit to each plant. Operational data for Plant A and Plant B were available for the periods July 2009 -March 2010 and January 2007 - January 2010 respectively. Although operational data spanned a shorter period than water quality data, this was considered sufficient to understand the operating philosophy of the plants.

A.1.2 Case study A: small size plant on a Northern island

A.1.2.1 Plant Description

Plant A has a capacity of 360 m³/day, operated 23 hours/day during summer and 20 hours/day during winter and serves a population of 420 people. The plant contains 78 modules, 3.66 m long, working in parallel, with a total membrane area of 819 m² (Figure A-1.1). The plant was installed in 2005 with PES membranes, but new CA membranes were installed at the beginning of 2009 due to irreversible fouling that resulted in very low flux when the plant was operated at the maximum pressure (12 bar) recommended by the manufacturer.



Figure A-1.1 Pictures of Plant A installed in a remote north island

Raw water is pumped from a lake near-by and after being screened at the intake, is passed through a 200 μm sand filter and it is pumped through the membrane modules (Figure A-1.2). The plant operates at a recovery ranging between 65-70% and a recirculation flow rate 1.5 times higher than the raw water flow in order to maintain sufficient crossflow across the membrane (1.2-1.6 m/s) and reduce particle deposition. Any concentrate that is not recirculated can be returned to the local watercourse as it is chemical-free [4]. After the membrane treatment, a disinfection step with sodium hypochlorite (NaOCl) is performed, and a fraction of the permeate is passed through the limestone contact tank to increase the pH and blended downstream with the rest of the permeate to achieve the target pH. A clear water tank

with a volume of 0.5 million gallons (4545 m³) is used as storage tank to compensate for fluctuations in demand due to tourism and agriculture and ensure supply during plant downtime.

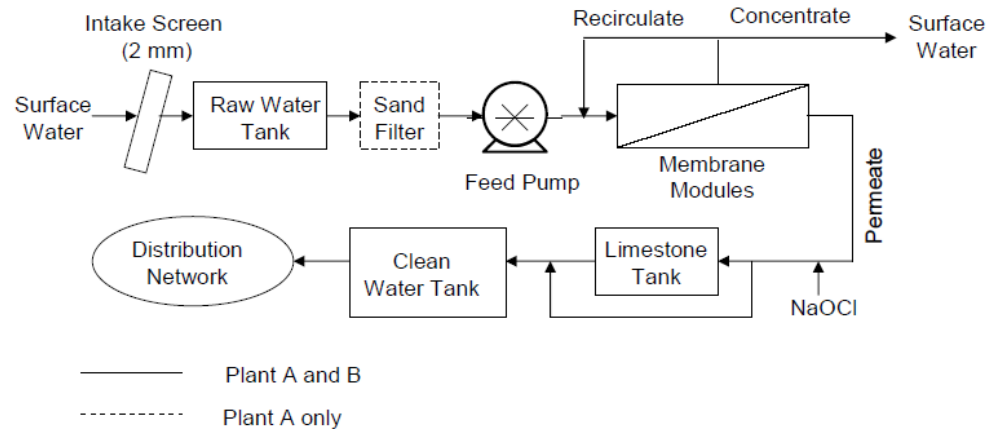


Figure A-1.2 Typical schematic of the tubular membrane plants in Scotland

A.1.2.2 Operational parameters

An operator is employed full time at the plant. Since the plant aims to deliver constant flow, the operator manually adjusts the pressure when required (even daily) to keep the flow constant. As shown in Figure A-1.3, the flux obtained since the CA membranes were installed in 2009 was very stable and only a slight pressure increase was noticeable with time (operational data before 2009 not available).

The operator performs a full chemical cleaning and foam ball replacement on-site every 6 weeks, independently of pressure build up in the plant. This high frequency was deemed necessary for PES membranes, due to rapid pressure increase caused by fouling and was retained by the operator once CA membranes were installed. To perform the chemical cleaning the operator chooses among detergent (2 g/L), citric acid (2 g/L), NaOH (0.10 g/L) or NaOCl (0.44mL/L), according to what he deems necessary. This cleaning frequency seems to prevent the pressure from increasing rapidly. However, long term data are required to establish if this type of operation will reduce irreversible fouling and increase the life span of the membranes.

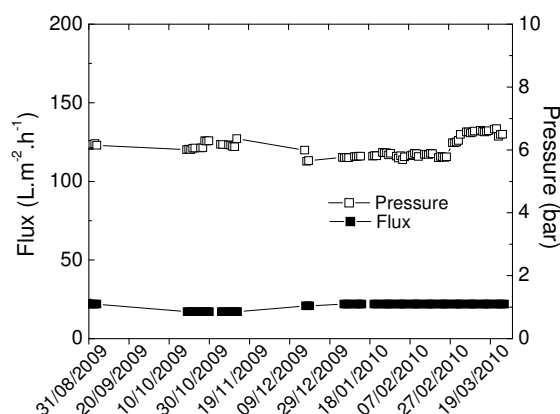


Figure A-1.3 Flux and pressure of Plant A from July 2009 to April 2010 (since installation of CA membranes)

A.1.2.3 Water quality

For Plant A, the final water quality was consistently below the PCV despite the high variability of the raw water quality (Figure A-1.4). pH values were within the target range of pH 8-9 established by Scottish Water (Figure A-1.4d). On average, a decrease of $96\pm 2\%$ in colour, $90\pm 7\%$ in aluminium, $90\pm 10\%$ in iron, and $92\pm 3\%$ in manganese concentrations was obtained in the final water compared to the raw water. Colour, i.e. organic matter, removal is particularly important to prevent THM formations.

Results depicted in Figure A-1.4 show water quality data also for PES membranes installed before 2009. No difference between the final water quality before and after the installation of the CA membranes can be noticed. In 2007 the performance of the plant for manganese was poorer than in the following years, as manganese concentration in the final water increased and one detection above PCV was registered. A deterioration of the membrane modules can be ruled out, as retention of turbidity and colour was satisfactory. It is believed that the decreased manganese retention can be attributed to higher concentration in the feed, exceeding the retention capacity of the membrane.

It can be concluded that both types of membranes, despite different characteristics, can produce very good water quality. Moreover, fouling of PES membranes did not compromise water quality but only the quantity of water produced.

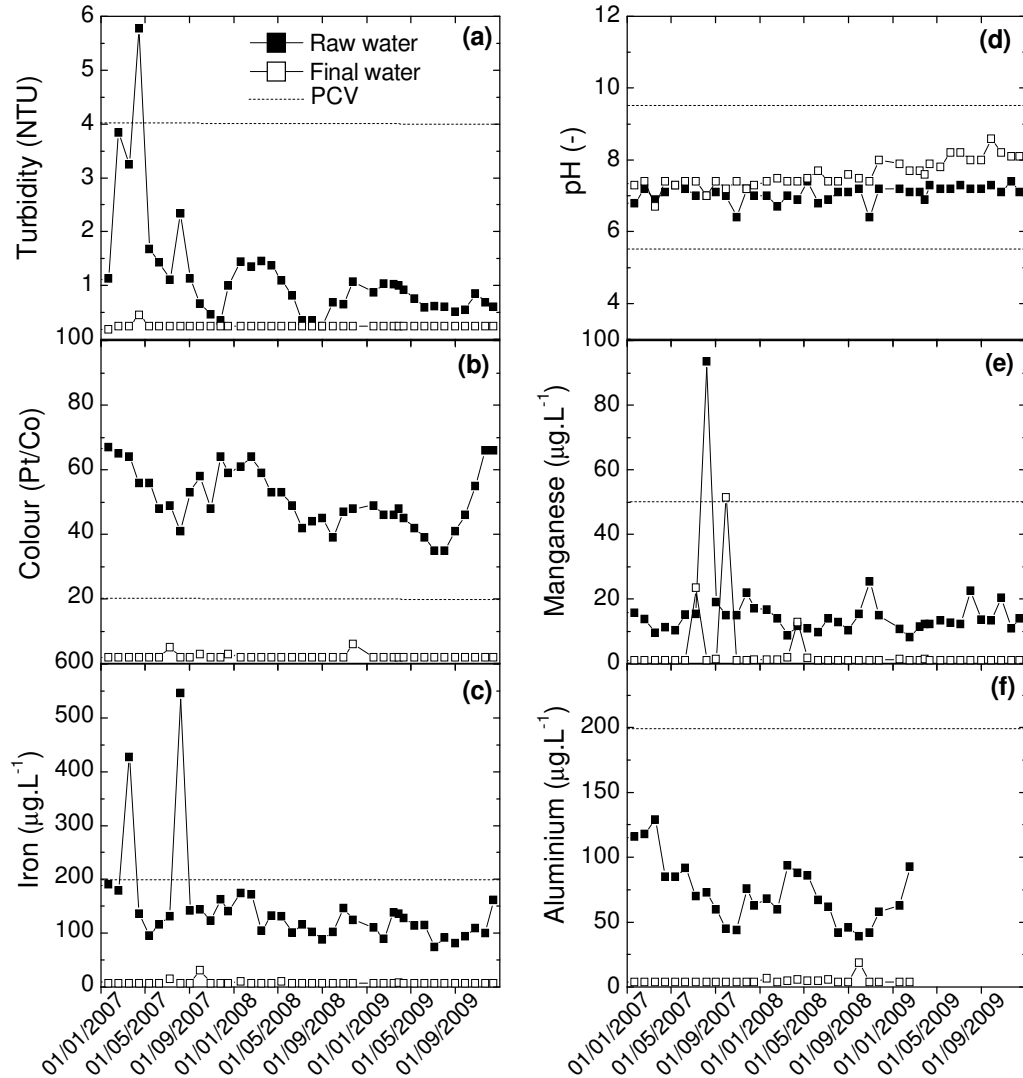


Figure A-1.4 Water quality in raw and final water for Plant A; (a) turbidity , (b) colour, (c) iron, (d) pH, (e) manganese (f) aluminium [1]. Dotted lines indicated the Prescribed Concentration Value (PCV) of each parameter.

A.1.3 Case study B: micro-plant on a Western island

A.1.3.1 Plant Description

Plant B is a small membrane unit with a design capacity of 5 m³/day, producing around 3 m³/day (for 23 hours/day operation) and serving a population of about 20 people. It contains 3 membrane modules, 0.92 m long, working in parallel, for a total membrane area of 7.9 m². The plant is the smallest unit in Scotland (together with another two identical ones) and all its components are incorporated into a single 1m x 2m skid (Figure A-1.5). These micro-plants were installed in 2006 mainly to remove *Cryptosporidium* from drinking water. Plant B was originally equipped with PES membranes, but these were exchanged with CA modules in 2007, following fouling in other plants located on the same island.



Figure A-1.5 Pictures of Plant B located on the remote western island

Raw water is supplied by gravity from a lake nearby and no pre-treatment is carried out apart from a coarse screen at the intake. A single pump is required to pressurise the feed through the membrane and recirculate part of the concentrate. The treatment schematic is identical to Plant A (Figure A-1.2), with the only difference that a sand filter is not installed before the membranes modules in Plant B. After chlorination and pH adjustment, the final water is stored in an 8 m³ clear water tank.

The plant operates with a recovery of 50% and a recirculation flow rate 5 times higher than the raw water flow. As in the case of Plant A, high recirculation flow rate is maintained to achieve the desired crossflow velocity in the membranes.

A.1.3.2 Operational parameters

An operator visits the plant once a week for a couple of hours so the plant is left to operate automatically for the rest of the time. As for Plant A, the operation philosophy aims to deliver constant flow (i.e. constant water production) by varying the pressure if necessary.

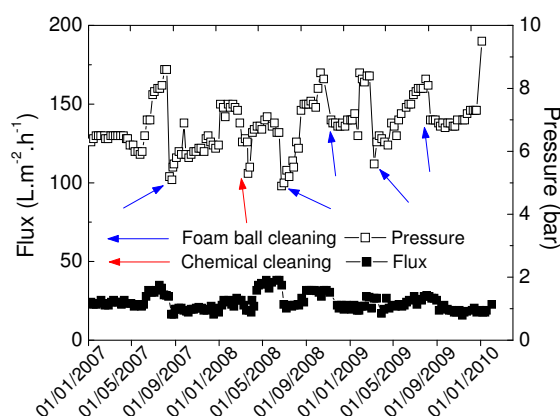


Figure A-1.6 Flux and pressure of Plant B from January 2007 to January 2010 (since installation of CA membranes)

Nevertheless, in contrast with Plant A, the flux of Plant B experienced some variations within the 4 year period since 2007 when the CA membranes were installed (Figure A-1.6). Higher flux occurred during summers when water temperatures were higher (average 16°C compared to average 11°C in winter) and from April to July 2007, when the output was increased on purpose to 5 m³/d from the 3 m³/day usually provided. The lack of an operator constantly on site did not allow obtaining the same constant flux as for Plant A.

Pressure also varied considerably with respect to Plant A. From Figure A-1.6 it is possible to note an increase in pressure caused by fouling followed by a rapid decrease corresponding to foam ball changing and/or chemical cleaning. While PCI

recommends performing the two operations simultaneously, at Plant B foam balls were changed every 4-6 months, when the pressure reached about 8 bar, without chemically cleaning the membranes. The chemical cleaning frequency was as low as 22 months since the membranes need to be transported to a different plant located on the same island that is equipped with a cleaning facility. Foam ball replacement alone lowered the feed pressure up to 2 bar, comparable with the pressure drop obtained for chemical cleaning. It can be concluded that mechanical cleaning, although it cannot replace the use of chemicals, can substantially lower their frequency and hence plays an important role in reducing fouling.

A.1.3.3 Water quality

Despite the high variability of raw water (Figure A-1.7), the quality of the final water was consistently high, with an average $90\pm 4\%$ decrease in colour, $81\pm 10\%$ decrease in aluminium, $78\pm 14\%$ decrease in iron and $54\pm 25\%$ decrease in manganese concentration compared to the raw water values. These removal values, especially for manganese, are lower than for Plant A because the concentration of contaminants in the raw water was lower while their concentration in the final water was often below the instrument detection limits for both plants.

A.1.4 Energy requirements and costs

The specific energy consumption (SEC, energy used per m^3 of permeate produced) for the two plants was determined considering the energy consumed by the pump. SEC of Plant A was 1.2 kWh/m^3 while SEC of Plant B was 10.4 kWh/m^3 . When the total energy consumed by the plant as indicated by the plant electricity bills in 2009 was taken into account, the SEC increased to 1.5 kWh/m^3 for Plant A and 21.9 kWh/m^3 for Plant B.

It is difficult to compare these values with others presented in the literature, as SEC is highly dependent on system components and their efficiency and the quantity and quality of the produced water. SEC has been shown to increase with decreasing plant size and increasing concentration of salt [8]. As a comparison, a plant using RO tubular membranes for brackish water and producing $5 \text{ m}^3/\text{day}$, obtained a SEC of

1.2 kWh/m³ [9]. Tubular membranes in Scotland are therefore highly energy intensive, due to the high pressure employed (average 6 bar compared to 3-5 of tubular membranes in Norway) and due to the high recirculation flow used for creating the high crossflow required for fouling prevention.

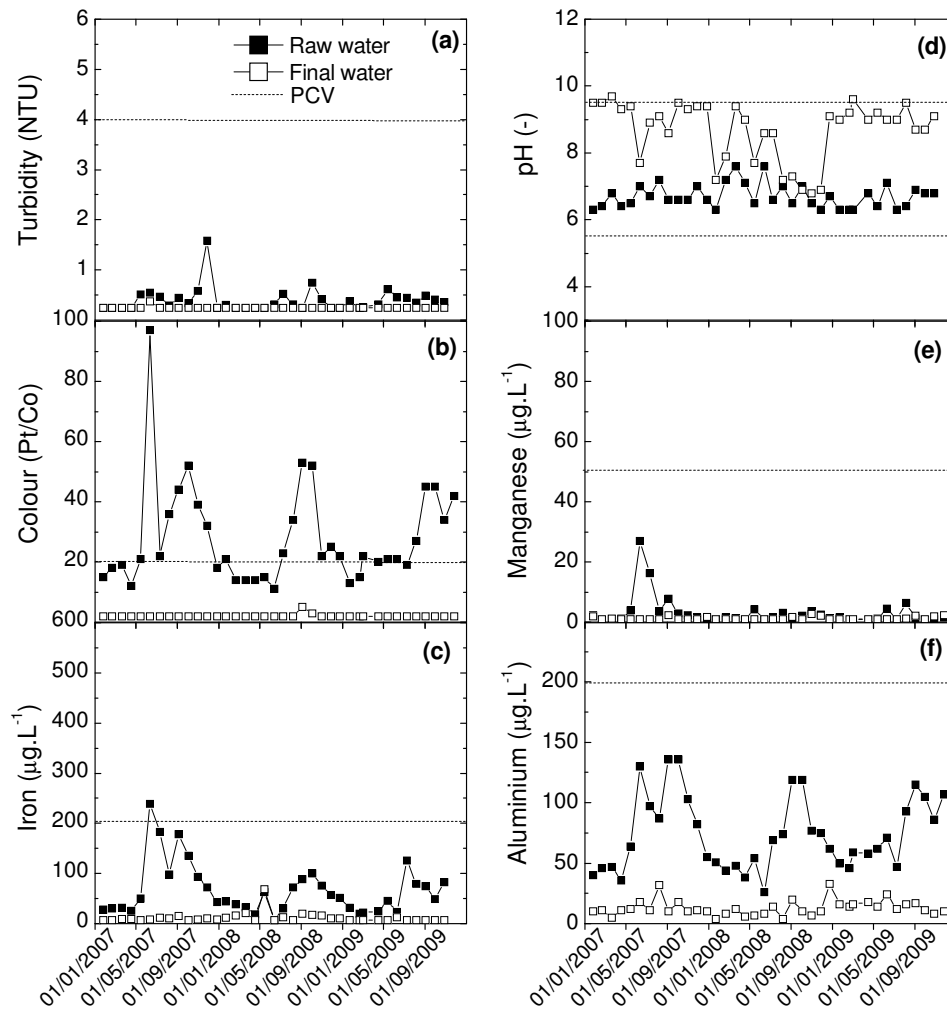


Figure A-1.7 Water quality in raw and final water for Plant B; (a) turbidity , (b) colour, (c) iron, (d) pH, (e) manganese (f) aluminium [1]. Dotted lines indicated the Prescribed Concentration Value (PCV) of each parameter.

The ratio of recirculation flow to raw water flow in Plant B is much higher than for Plant A (5 times with respect to 1.5) and this caused higher energy consumption in Plant B. The pump employed in Plant B has a theoretical efficiency of 30% with respect to 80% efficiency of the pumps in Plant A [10], increasing the energy costs.

Furthermore, the electricity consumption of the ancillary equipments (on-line meters, programmable logic controller, telemetry) constitutes a higher proportion of the whole energy for the smaller plant (50% of the total SEC with respect to 20% for Plant A). In particular, a 0.5 kW heater is left in constant operation during the winter months to prevent freezing of small pipes and thermal comfort of the operator during his duties, greatly contributing to the electricity utilization (17% of the total SEC).

Membrane plants in Scotland have not been specifically optimized for energy efficiency and lower energy consumption could be achieved. The plants could be operated at lower pressure and lower flux. Lower flux would also result in lower membrane fouling, lowering in turn the need of high recirculation flow. Moreover, a more efficient pump, an automated heating system and better building insulation would considerably reduce the energy consumption of Plant B.

Operational costs for the two plants were estimated based on the hours spent by the operators on site, the costs of electricity, chemicals (considering transport to the islands) and replacement of membranes and spare parts [11].

Table A.1-1 Estimated operational and maintenance costs for small scale membrane plants

	Plant A	Plant B
Operator	£41,200	£4,200
Electricity	£11,000	£1,300
Membrane replacement	£15,600	£300
Ancillary Equipment Maintenance	£700	£250
Chemicals	£10,000	£150
<i>Total (per annum)</i>	<i>£78,500</i>	<i>£6,200</i>
<i>Total/m³ water produced</i>	<i>£0.8/m³</i>	<i>£7.50/m³</i>

A life time of 5 years for the membrane was considered, although CA tubular membranes in Scotland are reported to last up to 8-9 years [12]. Operating costs of Plant A were estimated to be £0.8/m³, while for Plant B they were £7.5/ m³ (Table A.1-1), Especially for the small Plant B, labour and energy costs resulted to be greater than the membrane cost itself. The calculated values are comparable with

other estimation for similar PCI plants in Scotland, but higher than £0.2/m³ estimated for a conventional plant producing 3,200 m³/day and the average water rate of £0.46/m³ for the West of Scotland in 2000 [11]. On the other hand, operational costs of cartridge filter and chlorine dosing pump previously installed instead of Plant A were estimated to be about £14/m³ [13], as the operator was required daily on site for maintenance and water analysis, making the operational cost of the small membrane unit very competitive for this remote location.

A.1.5 Conclusions

The two plants presented in this study achieved final water quality in compliance with Scottish regulations, despite high variability in raw water quality with high content of organic matter, iron and manganese. Long term plant operation resulted in improvement of the original plant design. PES membranes were replaced with CA membranes due to fouling. Fouling resulted in flux decrease even at high pressure, but it did not compromise the final water quality.

The two plants operated in completely different ways. Plant A operated at constant flux and pressure is adjusted accordingly by the operator. Every 6 weeks the operator performed a chemical clean and changed the foam balls. This procedure prevented rapid pressure increase in the system, even if long term data are required to establish if it will reduce irreversible fouling. Plant B operated at variable flux and variable pressure caused by fouling. Foam balls were changed every 4-6 months without chemical cleaning and the procedure was able to reduce pressure up to 2 bar and decrease chemical cleaning frequency. The frequency of chemical cleaning and the choice of the cleaning product were left to the operator's judgment.

Research on the causes of membrane fouling would allow the establishment of a link between raw water quality and foulants in order to make an informative choice on operational and cleaning procedures. Furthermore, more information on the membrane critical flux would allow setting up optimal operation procedures for the plants to decrease fouling.

Operational costs of membrane plants decreased with increasing size but were still higher than for traditional processes. However, costs were competitive with respect to small traditional processes located in remote areas, due to operator time required for maintenance and water analysis.

Tubular membrane plants, such as those installed in Scotland are highly energy intensive, due to the high pressure and high recirculation flow used for creating high crossflow in the modules, while considerably lower energy consumption could be achieved. Energy consumption could be easily decreased by employing higher efficiency pumps and reducing electricity consumed by ancillary equipment.

Research on mechanisms of solute removal would improve plant efficiency, not only regarding to fouling prevention but also for reducing energy consumption. A comprehensive understanding of solute removal mechanisms would allow the operation of the membranes at the lowest pressure and flux which still provide water in compliance with regulations. Lower flux would also reduce membrane fouling, lowering in turn the need of high recirculation flow and hence reducing further energy consumption.

A.1.6 References

- [1] Scottish Water. Analytical data supplied courtesy of Scottish Water, 2010.
- [2] PCI Membranes. <http://www.pcimem.com> (accessed March 2012).
- [3] Bowen WR, Doneva TA, Yin H-B. Separation of humic acid from a model surface water with PSU/SPEEK blend UF/NF membranes. *Journal of Membrane Science* 2002; **206**: 417-429.
- [4] Grose ABF, Smith AJ, Donn A, O'Donnell J, Welch D. Supplying high quality drinking water to remote communities in Scotland. *Desalination* 1998; **117**: 107-117.
- [5] Wittmann E, Thorsen T. *Water treatment, Nanofiltration principles and applications*. UK: A. I. Schäfer, A. G. Fane, T. D. Waite (Eds) Elsevier: Oxford, 2004.

-
- [6] The Water Supply (Water Quality) (Scotland) Regulations. - Scottish Statutory Instrument No. 207 available at <http://www.scotland-legislation.hmso.gov.uk/legislation/scotland/ssi2001/20010207.htm> (last accessed June 2010), 2001.
- [7] DWQR. Analytical data supplied courtesy of Drinking Water Quality Regulator for Scotland 2010.
- [8] Schäfer AI, Broeckmann A, Richards BS. Renewable energy powered membrane technology. 1 Development and characterization of a photovoltaic hybrid membrane system. *Environmental Science & Technology* 2007; **41**: 998-1003.
- [9] Al Suleimani Z, Nair VR. Desalination by solar-powered reverse osmosis in a remote area of the Sultanate of Oman. *Applied Energy* 2000; **65**: 367-380.
- [10] ITT Technical Manual. <http://www.lowara.co.uk/lowdata/doc/EN/sv-td-en.pdf> (accessed March 2012).
- [11] Irvine E, Welch D, Smith A, Rachwal T. Nanofiltration for colour removal - 8 years' operational experience in Scotland. *Water Science and Technology: Water Supply* 2001; **1**: 55-63.
- [12] Scottish Water. Personal Communication with Catrina Attwood (Mott McDonald, formerly Scottish Water) on 28 October 2008. 2008.
- [13] Welch D. Personal Communication with David Welch (Mott McDonald) on 16 November 2010. 2010.

Appendix 2 – Membrane characterisation

A detailed characterisation of the membranes used in this work, TFC-SR2 and TFC-SR3 supplied by Koch, was carried out. Membrane characterisation allows identifying the chemical and physical properties of the membranes and it is a fundamental tool for understanding membrane performance and solute-membrane interactions [1].

A.2.1 Flux and Permeability

Before determining the pure water flux the membranes were compacted for an hour at a pressure 3 bar higher than the pressure used during the experiments. Membrane compaction has the scope to stabilize membrane flux as the flux is expected to reduce as a consequence of compaction. However, for both membranes pure water flux did not decrease during compaction and, once the regime in the stirred cells stabilised, it was stable both at 8 bar and 15 bar (Figure A-2.1).

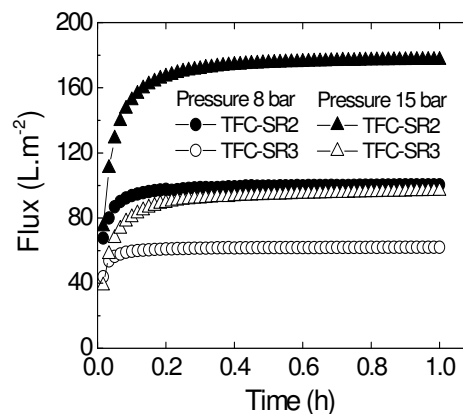


Figure A-2.1 Pure water flux during compaction at 8 bar and 15 bar for TFC-SR2 and TFC-SR3

The pure water flux as a function of pressure for TFC-SR2 and TFC-SR3 was determined using equation 2.2 (Figure A-2.2). Flux increased linearly with pressure indicating that the membrane was compacted [2].

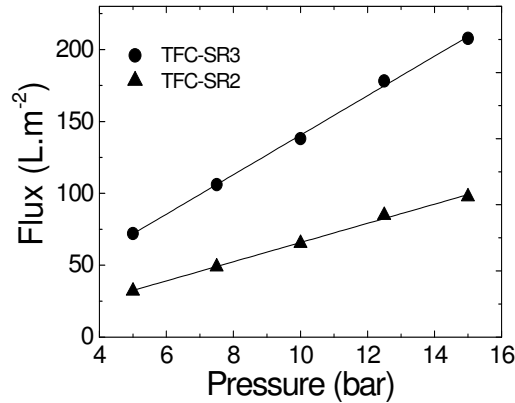


Figure A-2.2 Pure water flux as a function of pressure for TFC-SR2 and TFC-SR3

Membrane permeability was determined by dividing the pure water flux by the pressure. TFC-SR2 had an average permeability of $16.10 \text{ L} \cdot \text{h}^{-1} \cdot \text{m}^{-2} \cdot \text{bar}^{-1}$, while the average permeability of TFC-SR3 was $6.74 \text{ L} \cdot \text{h}^{-1} \cdot \text{m}^{-2} \cdot \text{bar}^{-1}$. TFC-SR2 has higher flux and permeability than TFC-SR3

Membrane flux and permeability varied with each experiment since a new membrane coupon was used for each experiment. For quality control, only coupons with a pure water flux $\pm 15\%$ of the average pure water flux were employed in this study.

A.2.2 Molecular weight cut off

Membrane MWCO was determined with the stirred cells following the method by Teixeira *et al.* [3].

The membranes were compacted and pure water flux was measured as described in Section 4.4. A 900 mL feed solution containing 25 mgC/L of a single inert inorganic (PEG 200, 400, 600 or 100, Section 4.2) was filtered at 10 bar and permeate was collected in three aliquots of 40 mL each. Retention R_o of the inert organics was determined using equation 2.3. Pure water flux was measured after the filtration of each organic to confirm that the inert organics had not effect on the membrane characteristics.

The curve fitting of $\log(R_o/(1-R_o))$ versus inert organic MW was intersected by the 91% retention line, corresponding to a value of $\log(R_o/(1-R_o))=1$, to determine the membrane MWCO [3].

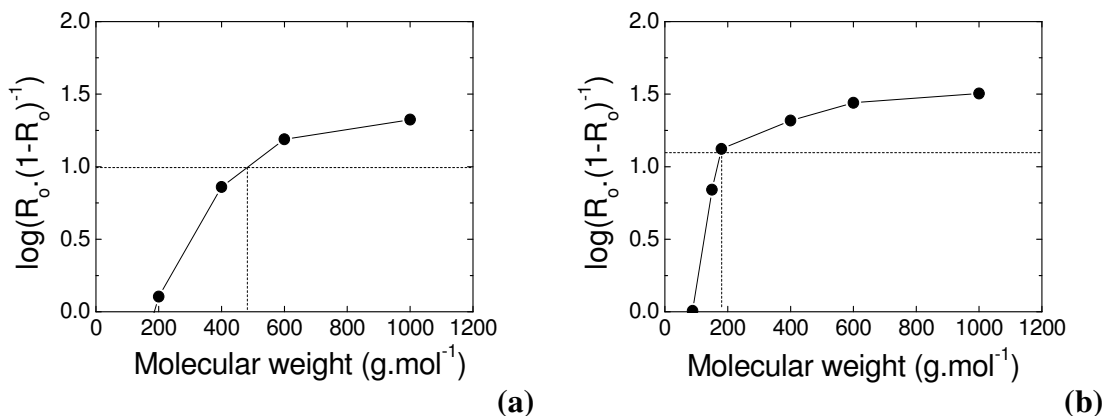


Figure A-2.3 Determination of molecular weight cut-off (MWCO) for (a) TFC-SR2 and (b) TFC-SR3

TFC-SR2 has a higher MWCO (460 g/mol) than TFC-SR3 (167 g/mol) in agreement with the higher flux and permeability (Figure A-2.3).

A.2.3 Pore size

Membrane pore size was determined with the stirred cells using the methodology described by Nghiem *et al.* [4]. Bowen *et al.* [5] observed that the determination of a pore size for NF membranes does not imply that well-defined pores with an average radius r_p exist. More appropriately, it indicates that the hindrance to solute passage through the polymer is equivalent to the hindrance to passage through pores of radius r_p .

The membranes were compacted and pure water flux was measured as described in Section 4.4. A 900 mL feed solution containing 25 mgC/L of a single inert organic (dioxane, xylose or dextrose, Section 4.2) was filtered through the membranes as pressure varied from 5 to 15 bar. The same membrane coupon was used for all experiments. To ensure the membranes were stabilized when retention was calculated, 240mL of solution was filtered at the chosen pressure before being

recirculated in the cell. After recirculation permeate was collected in three aliquots of 40 mL each and observed retention R_o of the inert organics was determined using equation 2.3. The same protocol was repeated for each pressure and for each inert organic. Pure water flux was measured after the filtration of each organic to confirm that the inert organics had not effect on the membrane characteristics.

The hydrodynamic model (Chapter 5) was employed to determine membrane characteristics, pore radius r_p and L/ϵ , by fitting the actual sieving coefficient S_a (obtained from R_o using equations 5.3, 5.5, 5.6, 5.17 in Chapter 5) in equation 5.18 in Chapter 5.

Figure A.2-4 shows the observed and calculated retention for dioxane, xylose and dextrose as a function of pressure for TFC-SR2 and TFC-SR3.

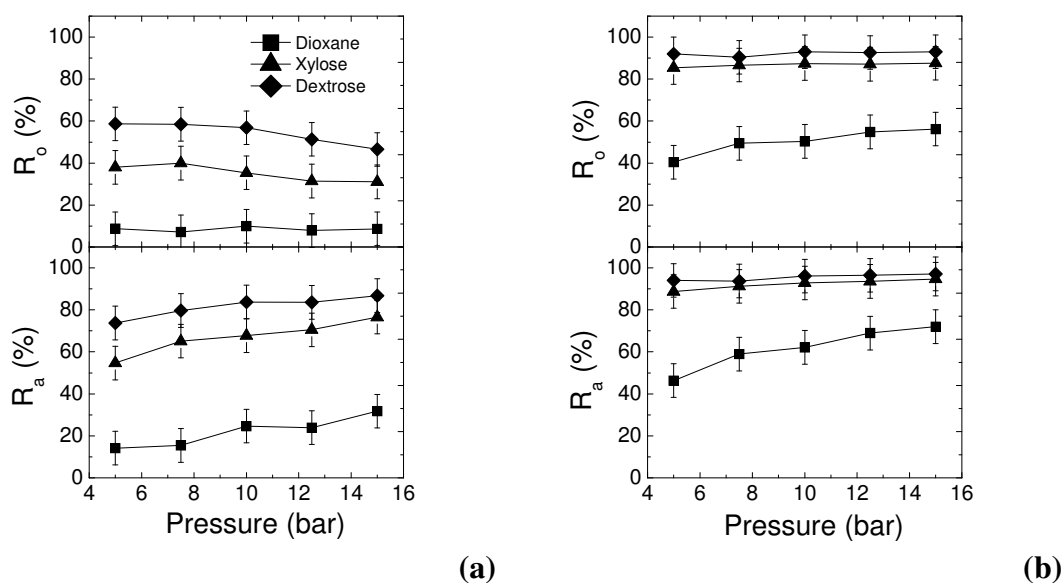


Figure A-2.4 Observed retention R_o and actual retention R_a of inert organics as a function of pressure for (a) TFC-SR2 and (b) TFC-SR3

Inert organics characteristics and hydrodynamic conditions for each organic are listed in Table A-2.1. k_f was determined with equations 5.5 and 5.6 in Chapter 5 and depended only on the solute diffusion coefficient D_∞ since the stirred cell radius and the stirring speed did not change.

Table A.2-1 Solute characteristics and hydrodynamic conditions

	Solute Stoke radius r_s (nm)	Diffusion Coefficient D_∞ (m^2/s)	k_f (m/s)
Dioxane	0.234	9.82E-09	3.50E-05
Xylose	0.290	7.40E-09	2.89E-05
Dextrose	0.324	6.72E-09	2.71E-05

Given the solute characteristics r_s and D_∞ , the hydrodynamic condition k_f , J_v (depending on pressure) and R_o measured during the experiments, the only unknowns in equation A.18 were r_p and L/ε . Φ was determined with the purely steric model (equation 5.14 in Chapter 5) since inert organics do not interact with the membranes.

Figure A-2.5 shows the curves of the hydrodynamic model calibrated with r_p and L/ε . Since the hydrodynamic model was fitted for the actual sieving coefficients S_a , the good correspondence between the model and the observed sieving coefficients S_o indicated the validity of equations 5.5 and 5.6 in Chapter 5 to determine k_f for the stirred cells.

Membrane characteristics were calculated as an average of the values obtained for the three inert organics (Table A-2.2). The low variation of r_p and L/ε obtained with the three inert organics confirms that, despite its limitations, the purely steric hydrodynamic model can be used to define average membrane characteristics when calibrated with inert organics

The obtained average pore size for TFC-SR2 and TFC-SR3 is in agreement with permeability and MWCO results, confirming that TFC-SR2 is a looser membrane while TFC-SR3 is a tighter membrane.

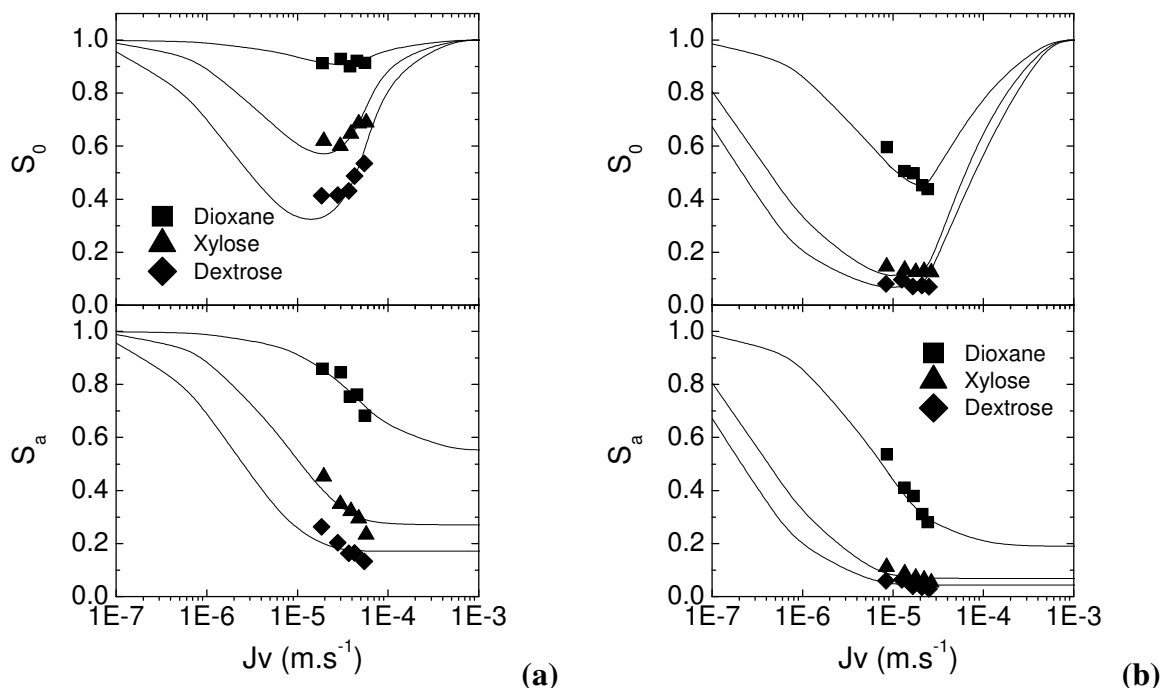


Figure A-2.5 Observed sieving coefficient S_0 and actual sieving coefficient S_a as a function of J_v for the inert organics and fitted hydrodynamic model curves for (a) TFC-SR2 and (b) TFC-SR3

Table A.2-2 Membrane characteristics determined by fitting the hydrodynamic model with sieving coefficient S_a obtained for the inert organics

TFC-SR2			TFC-SR3		
	r_p (nm)	L/ε (m)		r_p (nm)	L/ε (m)
dioxane	0.55	2.41E-06	dioxane	0.37	1.55E-06
xylose	0.51	2.42E-06	xylose	0.38	1.61E-06
dextrose	0.49	2.52E-06	dextrose	0.39	1.62E-06
<i>average</i>	<i>0.52</i>	<i>2.45E-06</i>	<i>average</i>	<i>0.38</i>	<i>1.59E-06</i>

A.2.4 Zeta potential

Membrane charge, expressed by zeta potential was measured as described in Section 4.3.7. As observed in Figure A-2.6 both membranes are amphoteric since their surface zeta potential is positive at pH lower than the point of zero charge, due to the

protonation of the amine groups ($\equiv\text{NH}_2 \rightarrow \equiv\text{NH}_3^+$), and negative at higher pH, due to the deprotonation of carboxylic groups ($\equiv\text{COOH} \rightarrow \equiv\text{COO}^-$) [6].

The two membranes showed similar surface charge characteristics, with similar point of zero charge (at pH 4.25 for TFC-SR2 and pH 3.84 for TFC-SR3) and similar zeta potential at pH 12 (-26.7 ± 9.2 for TFC-SR2 and -26.8 ± 5.5 for TFC-SR3), while TFC-SR2 was slightly more positively charged at pH 3.5 (2.2 ± 4.7 for TFC-SR2 and 1.2 ± 5.7 for TFC-SR3).

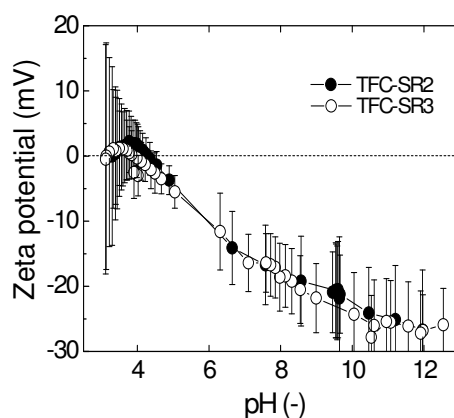


Figure A-2.6 Zeta potential as a function of pH for TFC-SR2 and TFC-SR3 (background electrolyte 1 mM NaHCO_3 and 20 mM NaCl). Error bars represent the standard deviation of five repeated measurements, while the symbols represent the average of the five measurements.

A.2.5 Contact angle

Membrane hydrophobicity was estimated by contact angle measurements carried out as described in Section 4.3.6. Contact angles of virgin membranes performed at Imperial College London, UK (Figure A-2.7) and contact angle of membranes compacted with pure water, carried out at ITM-CNR (Italy) are reported in Table A-2.3. While contact angles of compacted membranes are scarcely reported in the literature, they might better represent membrane hydrophobicity [7].

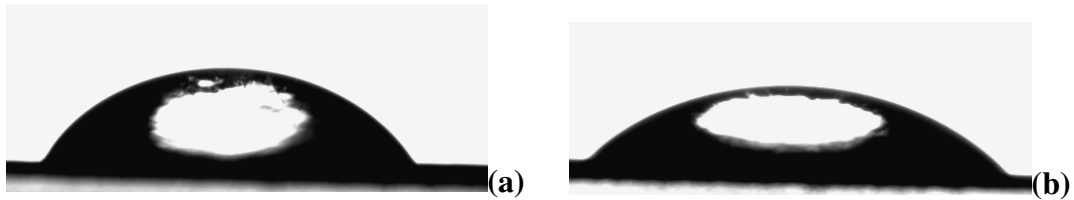


Figure A-2.7 Photographs of water drops on (a) TFC-SR2 and (b) TFC-SR3 employed to measure contact angle

Table A.2-3 Contact angle of TFC-SR2 and TFC-SR3

	TFC-SR2	TFC-SR3
Virgin membranes	$61.5^\circ \pm 2.6^\circ$	$48.5^\circ \pm 1.4^\circ$
Compacted membranes	$57.2^\circ \pm 2.1^\circ$	$44.0^\circ \pm 1.2^\circ$

TFC-SR2 has a higher contact angle and it is therefore more hydrophobic than TFC-SR3. The contact angle for the compacted membranes did not change dramatically with respect to the contact angle of the virgin membranes and the difference can be attributed to the different membrane coupons employed. Verliefde *et al.* [7] observed an increase in contact angle after compaction for two commercial NF membranes and they attributed the higher hydrophobicity to the flux decrease during compaction. For TFC-SR2 and TFC-SR3 flux remained constant during compaction (Figure A-2.1) in agreement with no change in contact angle.

A.2.6 Roughness

Membrane roughness was estimated with AFM as described in Section 4.3.8. Images of the membrane surface and cross section constructed on the basis of AFM data are presented in Figure A-2.8. Table A-2.4 presents R_q and R_a values obtained for the membranes. As reported in the literature [8] R_q values are larger than R_a values. TFC-SR2 has higher roughness than TFC-SR3.

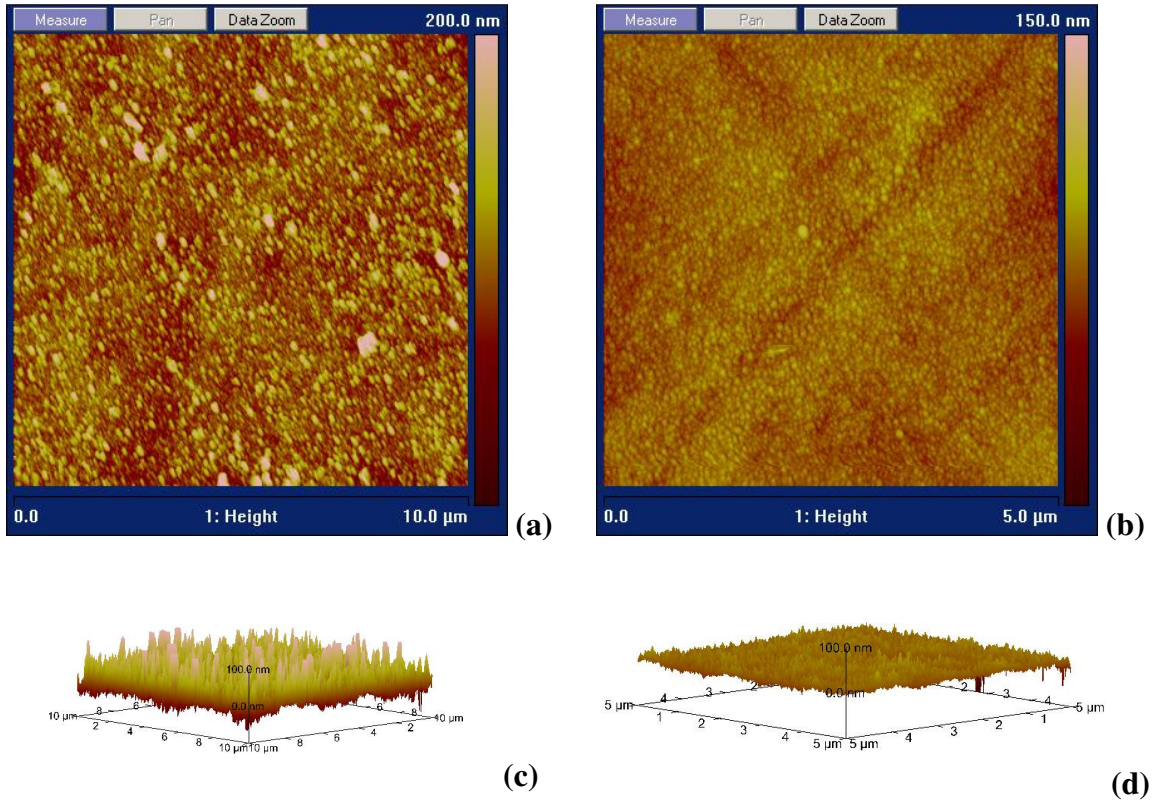


Figure A-2.8 Images of surface for (a) TFC-SR2 and (b) TFC-SR3 and three dimensional cross section for (c) TFC-SR2 and (d) TFC-SR3 obtained with AFM.

Table A.2-4 Average roughness R_a and root-mean square roughness R_q for TFC-SR2 and TFC-SR3

	TFC-SR2	TFC-SR3
R_a (nm)	5.2 ± 0.6	17.9 ± 0.6
R_q (nm)	6.8 ± 0.7	23.0 ± 1.3

A.2.7 Thickness

Total membrane thickness (active layer, support layer and non-woven fabric) was measured on SEM images of membrane cross-section as described in Section 4.3.9 (Figure A-2.9). Average of three measurements resulted in thickness of $158 \mu\text{m}$ for TFC-SR2 and $142 \mu\text{m}$ for TFC-SR3 (Table 4-2).

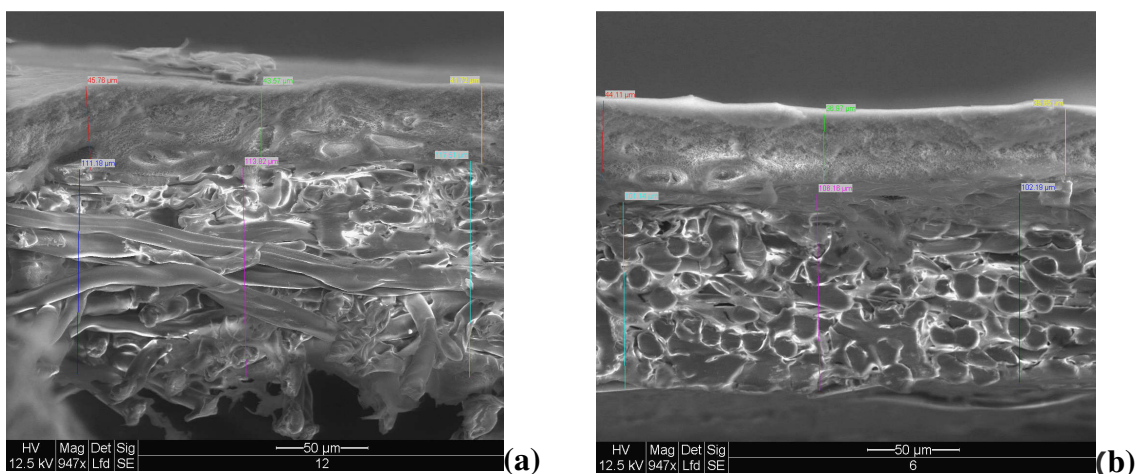


Figure A-2.9 Cross-section images of (a) TFC-SR2 and (b) TFC-SR3 by SEM with thickness measurements

A.2.8 Functional groups

The functional groups of the membranes were analysed with ATR-FTIR as described in Section 4.3.10. Both membranes had very similar spectra in terms of both signal positions and shape (Figure A-2.10).

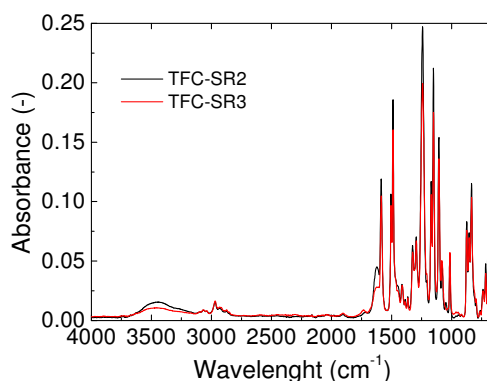


Figure A-2.10 ATR-FTIR spectra of TFC-SR2 and TFC-SR3.

Since the depth of penetration of the infrared scan was up to 1.66 μm both the support layer and the active layer were present in the spectra. All peaks at wavelengths lower than 1500 cm^{-1} can be attributed to the PS support layer.

The PA layer is visible in the amide I band at 1622 cm^{-1} (carbonyl stretching of the group $-\text{CO}-\text{NR}_2$). The absence of the amide II band at $\sim 1540\text{ cm}^{-1}$ (N-H in-plane

bending and N–C stretching of a –CO–NH– group) indicates that the polymer used for the active layer is a secondary (or fully substituted) amide. Peaks found at 1718/1734 cm^{-1} (C=O stretching of carbonyl functions: aldehydes, ketones, carboxylic groups and esters) could be attributed to additives.

At wave number greater than 2500 cm^{-1} the depth of penetration is shallower and information on the PA layer can be obtained [1]. Both membranes present peaks in the region of 2900-3000 cm^{-1} and 3000-3100 cm^{-1} . These peaks correspond respectively to the stretching of the aliphatic C-H bond and to the stretching of the aromatic =C-H bond. The absence of any predominant peak in this region might indicate that the membranes might not have any coating layer [1]. The broad peak at around 3300 cm^{-1} is due to presence of N-H and carboxylic groups of the PA layer. The relatively low intensity of this peak corroborates the hypothesis of the absence of a coating layer [1].

A.2.9 Salt retention

The retention of NaCl by TFC-SR2 and TFC-SR3 was determined as a function of pH and pressure with stirred cell experiments. The membranes were compacted and pure water flux was measured as described in Section 4.4.

A 500 mL feed solution containing 20 mM NaCl and 1 mM NaHCO_3 with pH varying from 4 to 12 was filtered at pressure 5 bar and permeate was collected in three aliquots of 40 mL each. NaCl concentration was measured by conductivity (Section 4.3.1) and NaCl retention was determined using equation 2.3. Figure A-2.11 shows membrane permeability determined during filtration experiments and NaCl retention as a function of pH. NaCl retention is pH dependent with lowest retention at pH 6. These results are discussed in Chapter 6.

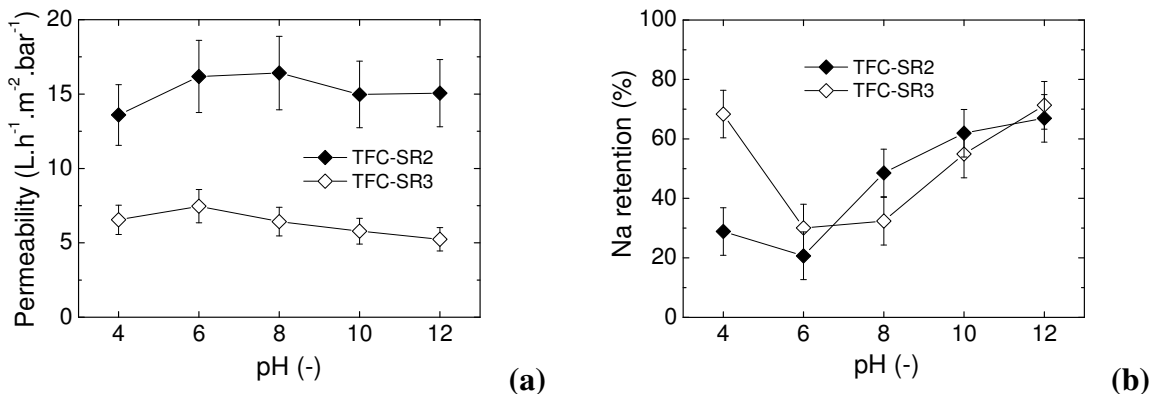


Figure A-2.11 Membrane permeability ($J_v/\text{pressure}$) (a) and NaCl retention (b) as a function of pH for TFC-SR2 and TFC-SR3 Feed solution 20 mM NaCl and 1 mM NaHCO_3 , pressure 5 bar.

A 500 mL feed solution containing 0.1 mM NaCl (pH not adjusted and around 7) was filtered and permeate was collected in three aliquots of 40 mL each. NaCl concentration was measured by conductivity (Section 4.3.1) and NaCl retention was determined using equation 2.3. At low pressure (5 bar) NaCl retention for the two membranes was similar (Figure A-2.11), confirming what was observed at pH 6-7 in Figure A-2.9. With increasing pressure NaCl retention for the tighter TFC-SR3 increased, while for the looser TFC-SR2 NaCl retention was constant with pressure (Figure A-2.10).

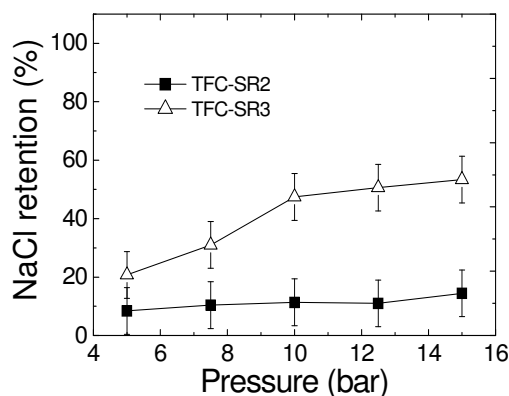


Figure A-2.12 NaCl retention as a function of pressure (pH not adjusted) for TFC-SR2 and TFC-SR3. Feed solution 0.1 mM NaCl.

A.2.10 References

- [1] Tang CY, Kwon Y-N, Leckie JO. Probing the nano- and micro-scales of reverse osmosis membranes--A comprehensive characterization of physiochemical properties of uncoated and coated membranes by XPS, TEM, ATR-FTIR, and streaming potential measurements. *Journal of Membrane Science* 2007; **287**: 146-156.
- [2] Dalwani M, Benes NE, Bargeman G, Stamatialis D, Wessling M. A method for characterizing membranes during nanofiltration at extreme pH. *Journal of Membrane Science* 2011; **363**: 188-194.
- [3] Teixeira MR, Rosa MJ, Nyström M. The role of membrane charge on nanofiltration performance. *Journal of Membrane Science* 2005; **265**: 160-166.
- [4] Nghiem LD, Schäfer AI, Elimelech M. Removal of natural hormones by nanofiltration membranes: Measurement, modeling, and mechanisms. *Environmental Science & Technology* 2004; **38**: 1888-1896.
- [5] Bowen WR, Mukhtar H. Characterisation and prediction of separation performance of nanofiltration membranes. *Journal of Membrane Science* 1996; **112**: 263-274.
- [6] Childress AE, Elimelech M. Effect of solution chemistry on the surface charge of polymeric reverse osmosis and nanofiltration membranes. *Journal of Membrane Science* 1996; **119**: 253-268.
- [7] Verliefde ARD, Cornelissen ER, Heijman SGJ, Petrinic I, Luxbacher T, Amy GL, Van der Bruggen B, van Dijk JC. Influence of membrane fouling by (pretreated) surface water on rejection of pharmaceutically active compounds (PhACs) by nanofiltration membranes. *Journal of Membrane Science* 2009; **330**: 90-103.
- [8] Hoek EMV, Bhattacharjee S, Elimelech M. Effect of membrane surface roughness on colloidal-membrane DLVO interactions. *Langmuir* 2003; **19**: 4836-4847.

Appendix 3 – Characterisation of fouled membranes

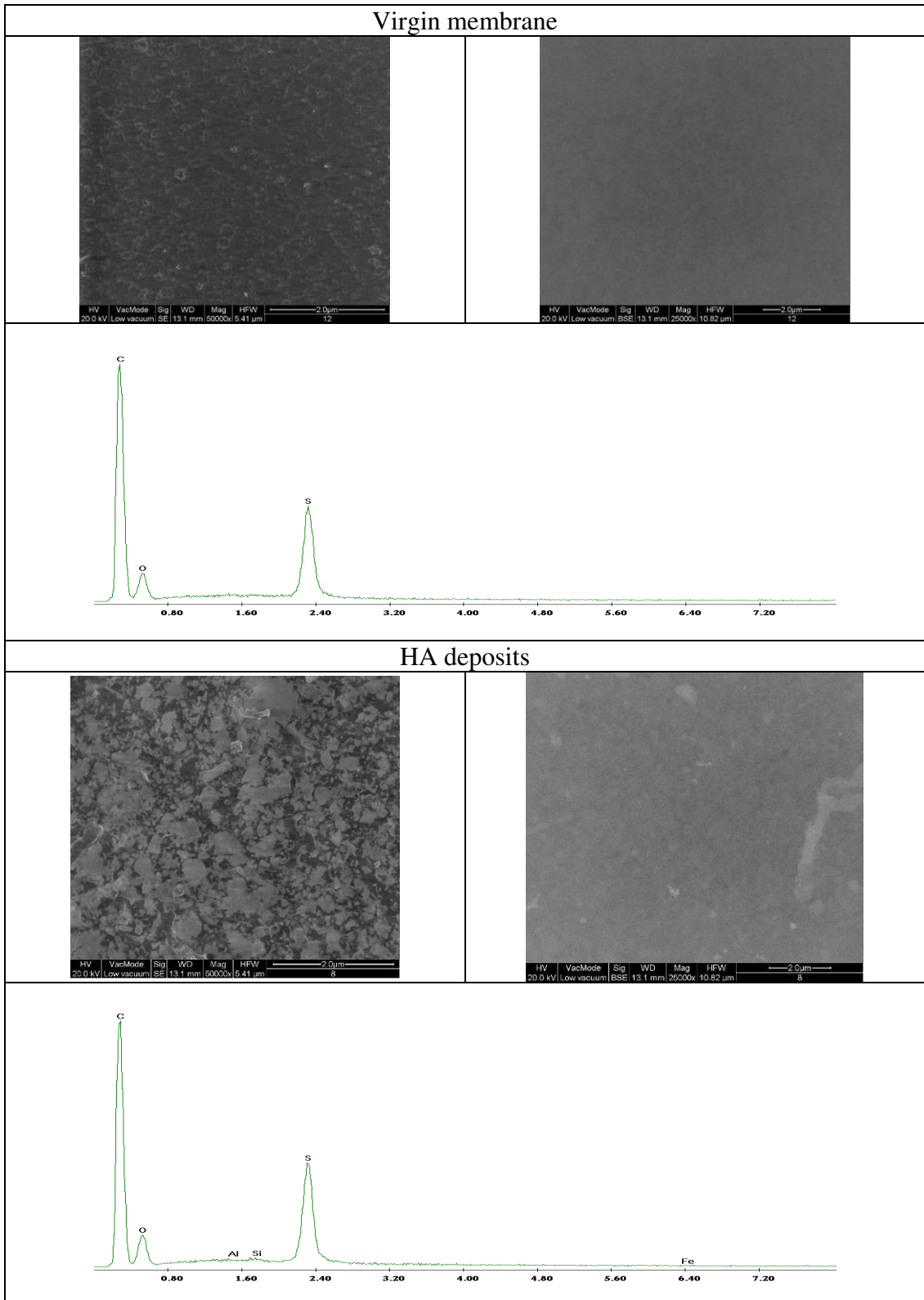
SEM images and ATR-FTIR scans were performed on the membranes employed in the experiments described in Chapter 9.

- (a) membrane compacted with ultrapure water (virgin membranes)
- (b) membrane after filtration of HA (12.5 mgC/L) and background electrolyte
- (c) membrane after filtration of HA (12.5 mgC/L) + Ca (2.5 mM) and background electrolyte
- (d) membrane after filtration of Mn (500 mg/L) and background electrolyte
- (e) membrane after filtration of HA (12.5 mgC/L) + Mn (500 mg/L) and background electrolyte
- (f) membrane after filtration of HA (12.5 mgC/L) + Mn (500 mg/L) + Ca (2.5 mM) and background electrolyte.

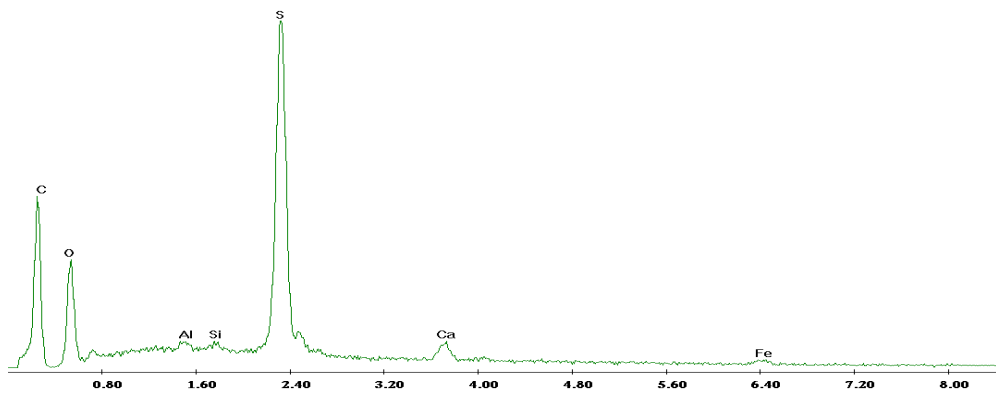
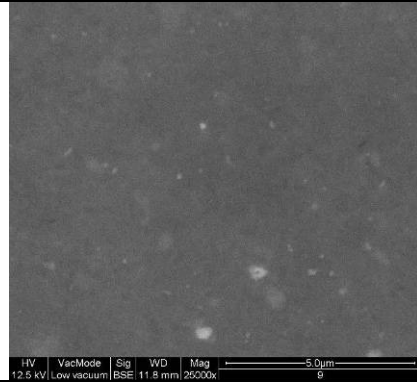
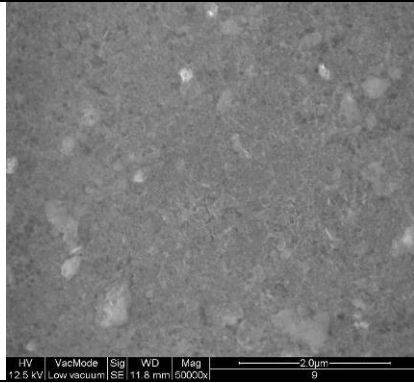
A.3.1 SEM images

SEM images and EDX spectra (Section 4.3.9) of membrane surfaces and cross sections are presented in Tables A.3-1.

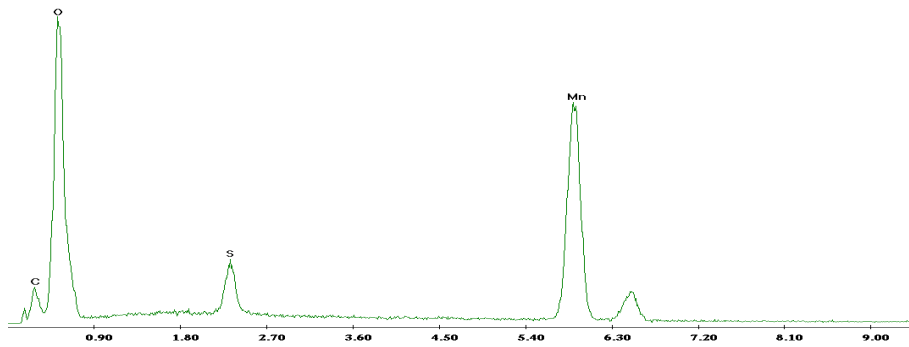
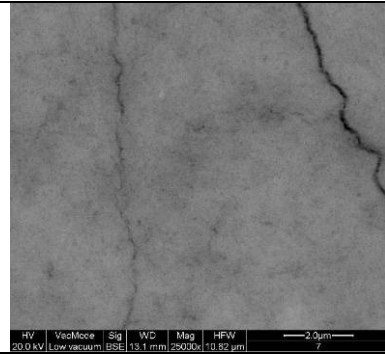
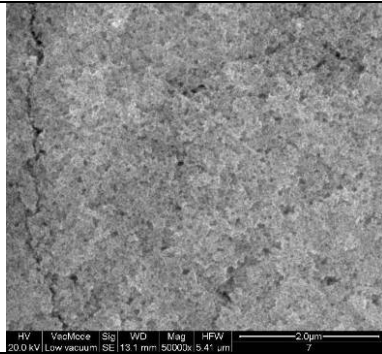
Table A.3-1 Surface SEM images (left side), SEM-BSE images (right side) and EDX spectra for TFC-SR2



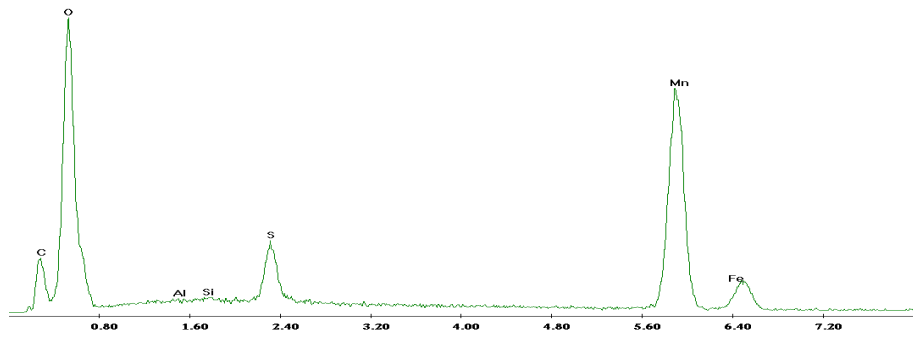
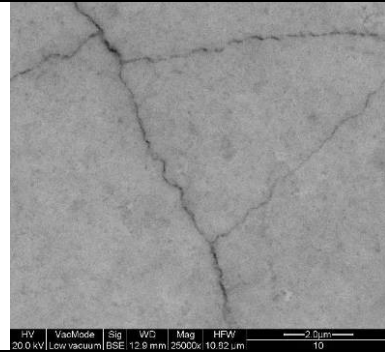
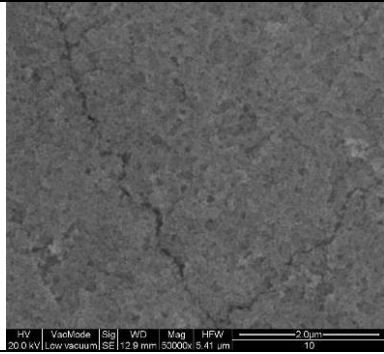
HA + Ca deposits



Mn deposits



HA + Mn deposits



HA + Mn + Ca deposits

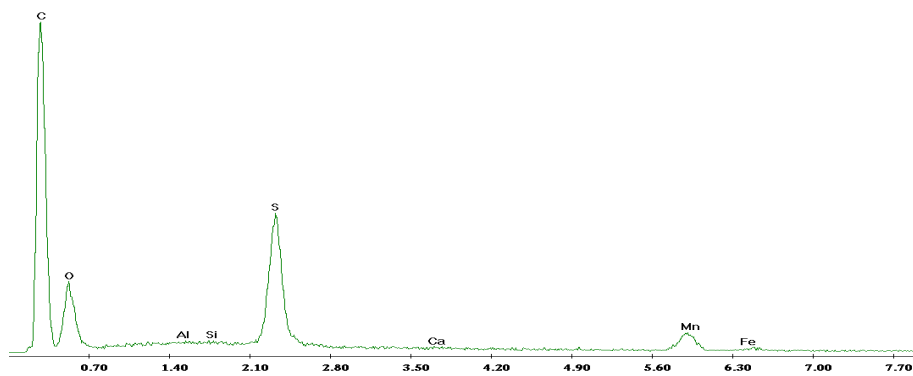
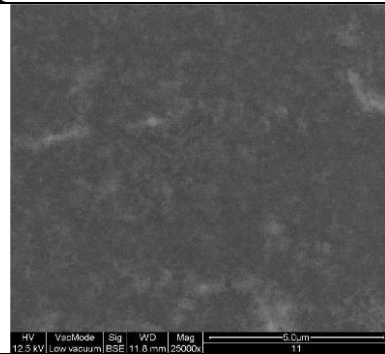
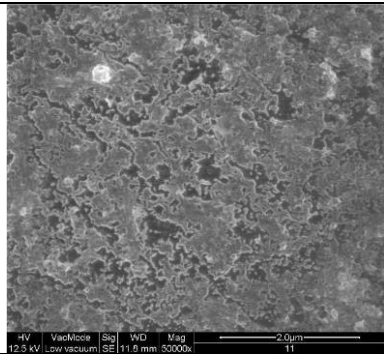
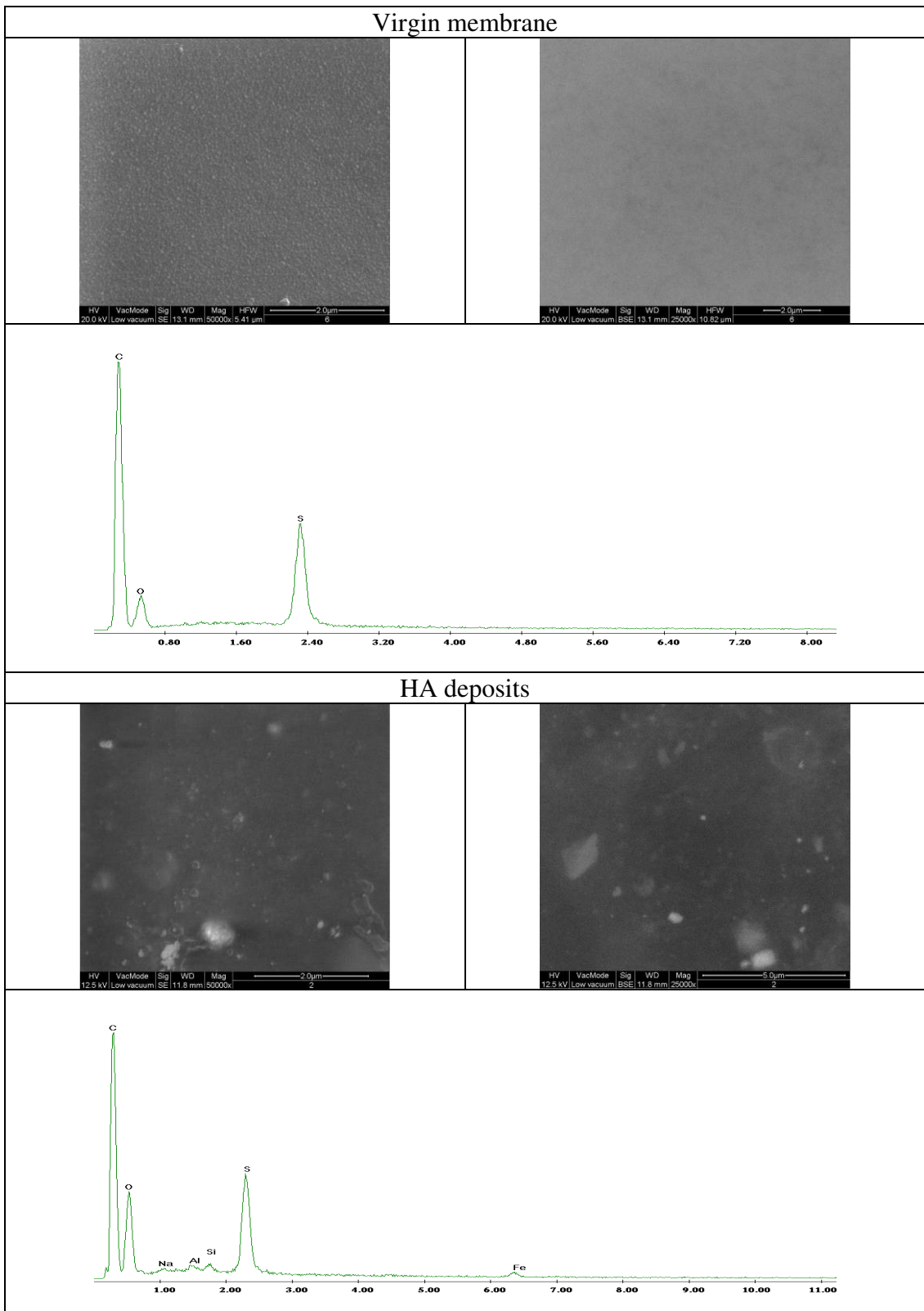
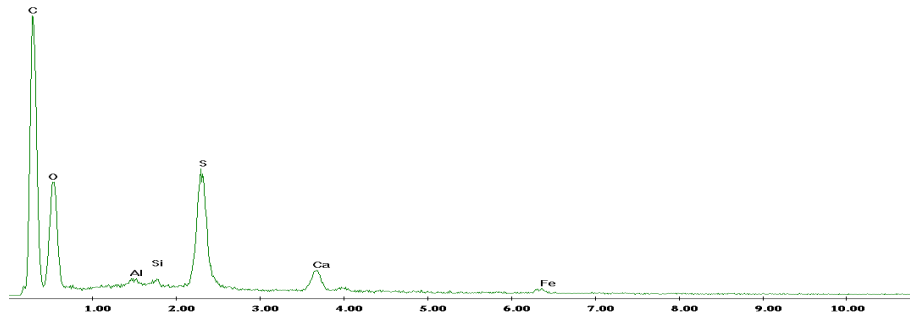
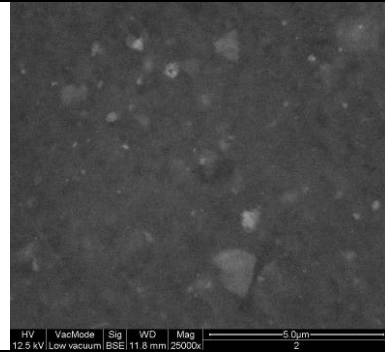
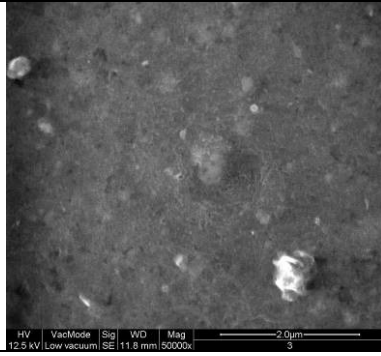


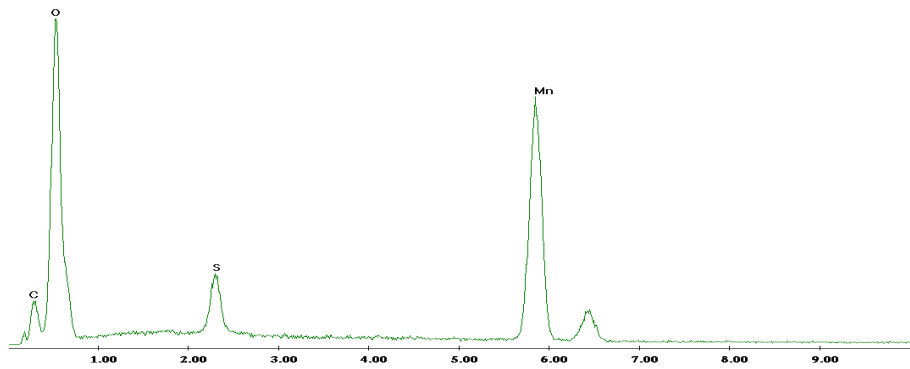
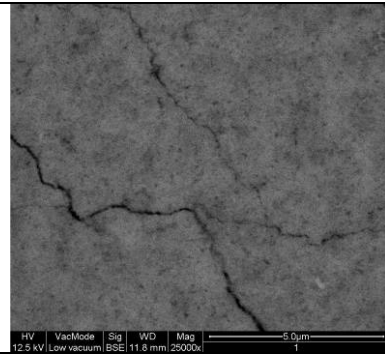
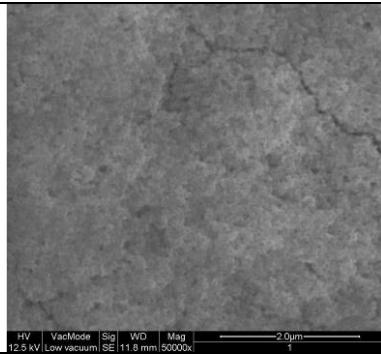
Table A.3-2 Surface SEM images (left side), SEM-BSE images (right side) and EDX spectra for TFC-SR3



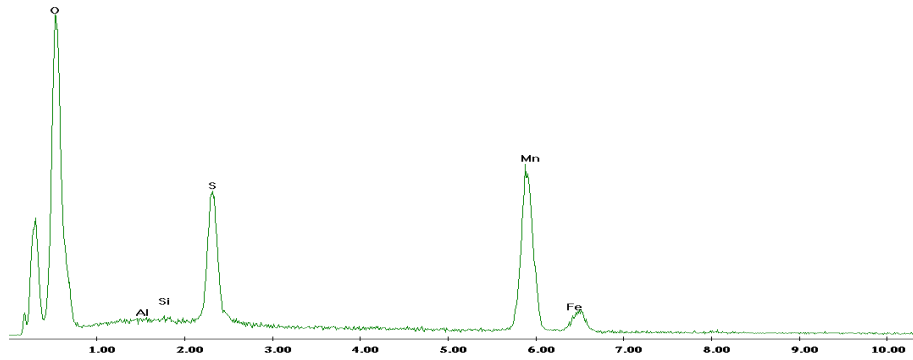
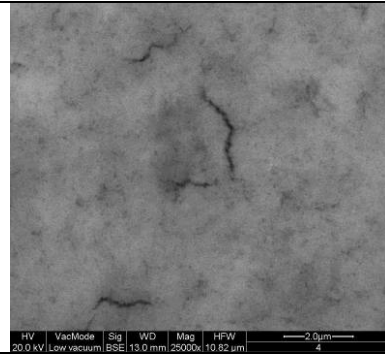
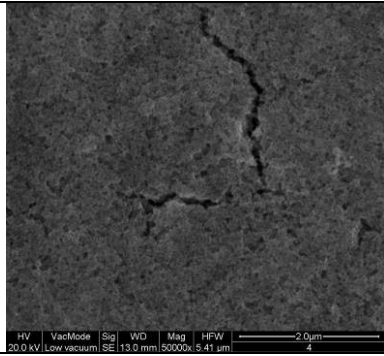
HA + Ca deposits



Mn deposits



HA + Mn deposits



HA + Mn + Ca deposits

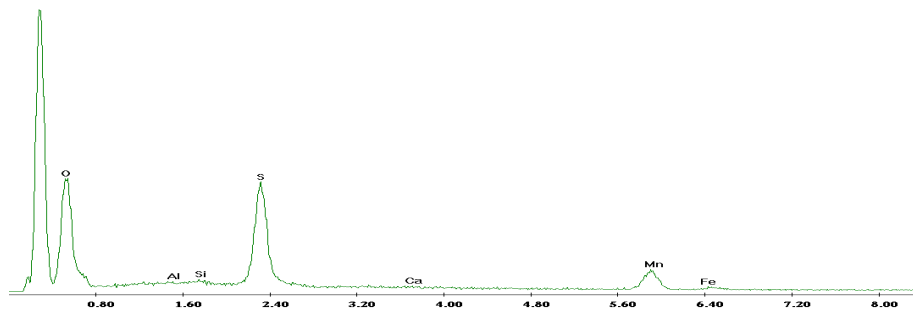
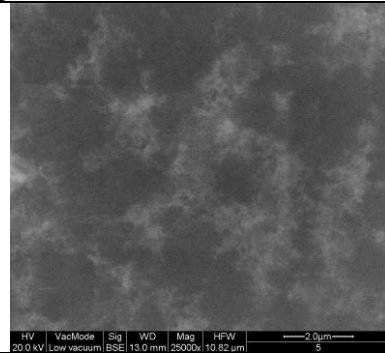
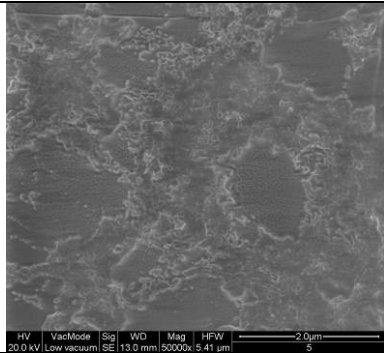
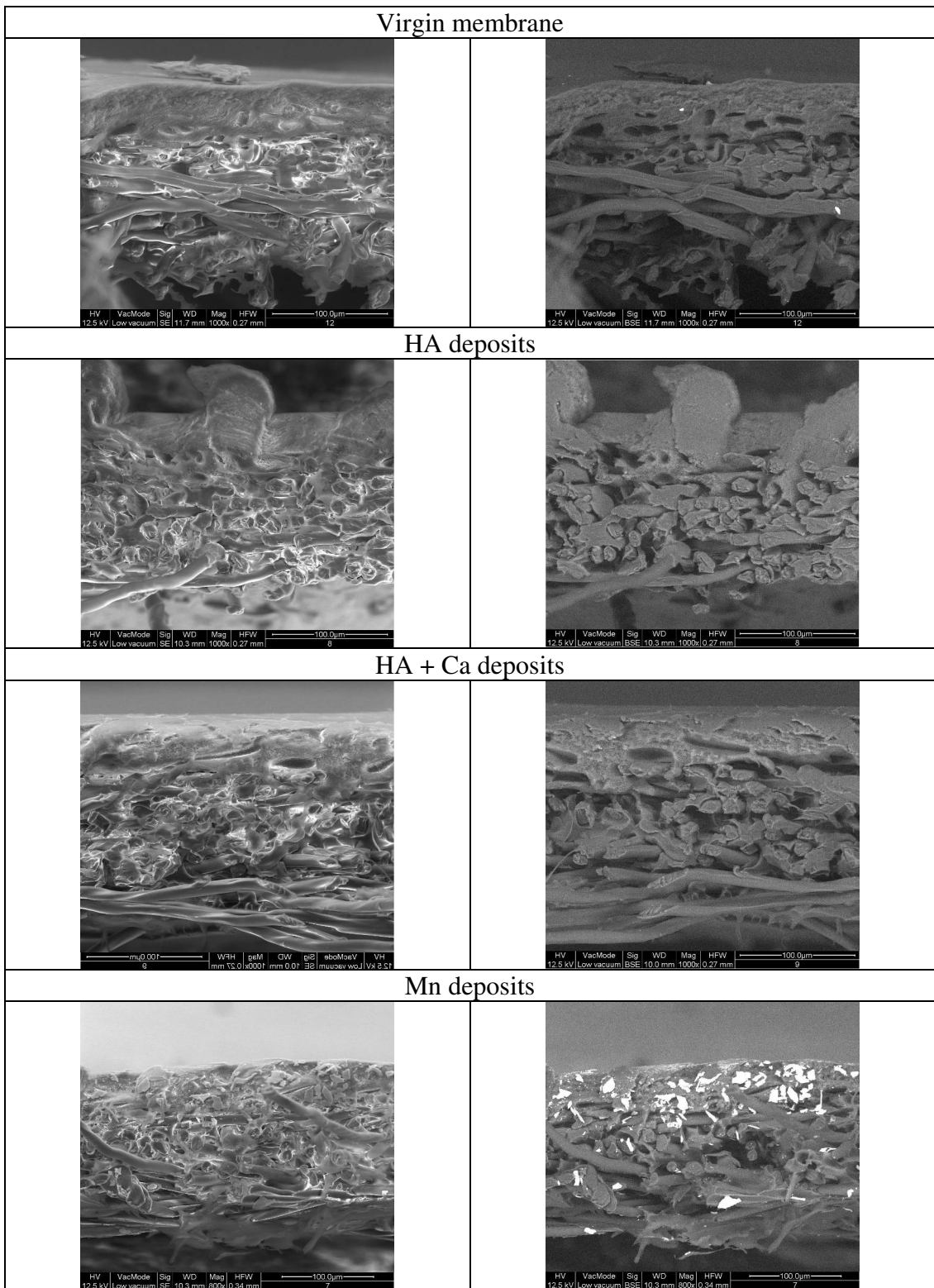
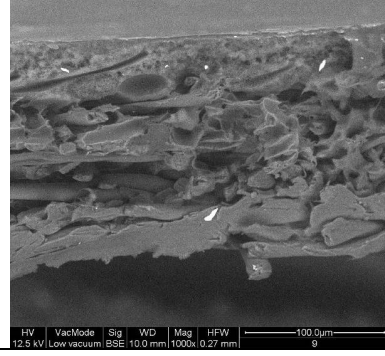
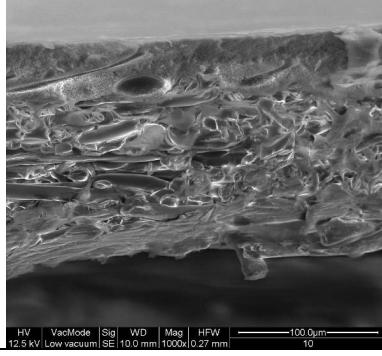


Table A.3-3 Cross-section SEM images (left side), SEM-BSE images (right side) for TFC-SR2



HA + Mn deposits



HA + Mn + Ca deposits

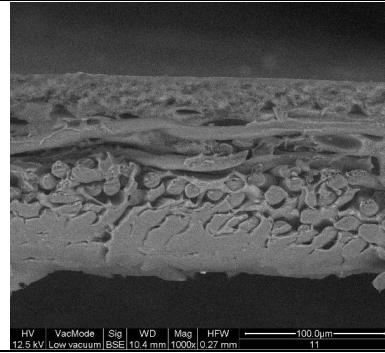
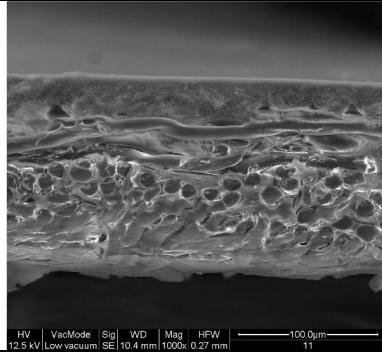
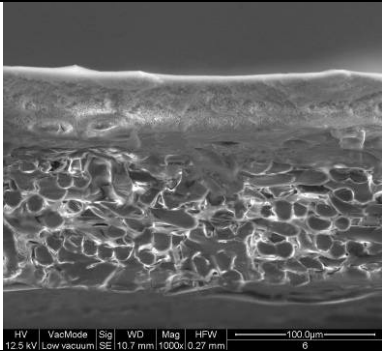
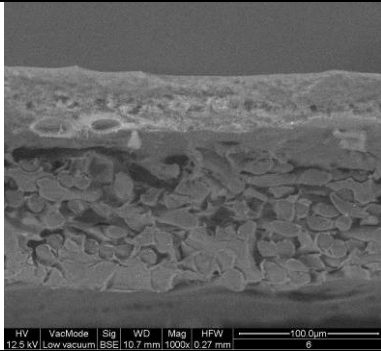
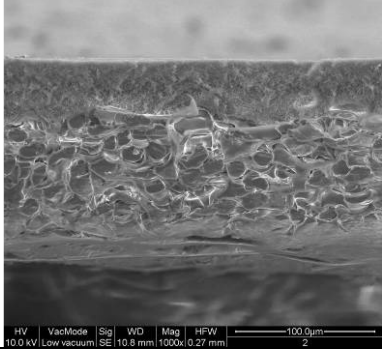
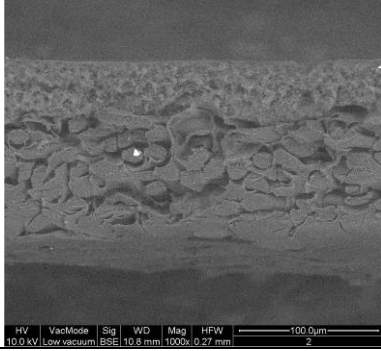
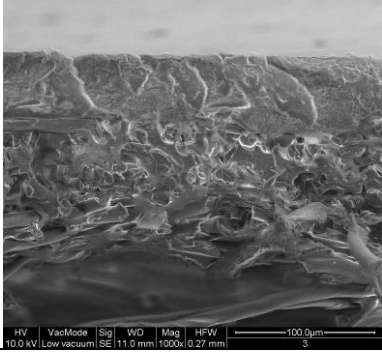
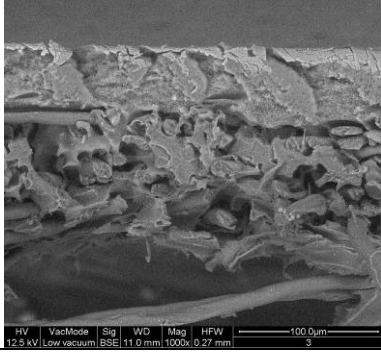
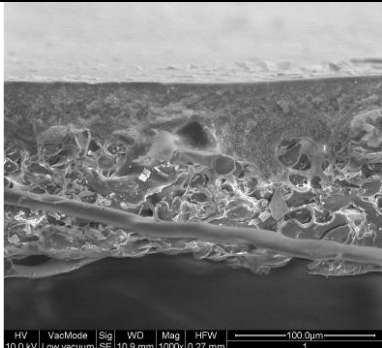
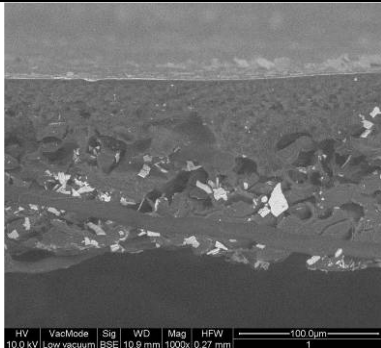
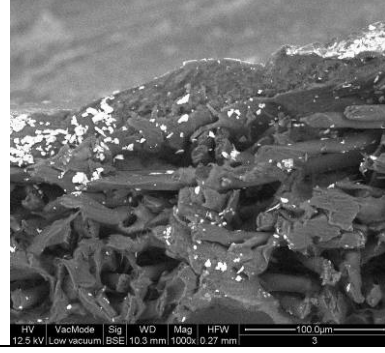
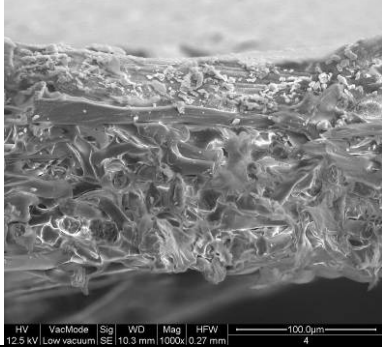


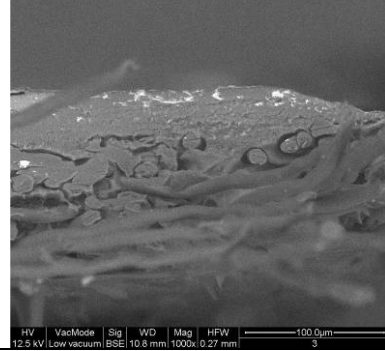
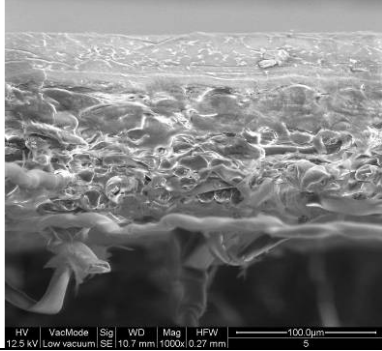
Table A.3-4 Cross-section SEM images (left side), SEM-BSE images (right side) for TFC-SR3

Virgin membrane			
			
HA deposits			
			
HA + Ca deposits			
			
Mn deposits			
			

HA + Mn deposits



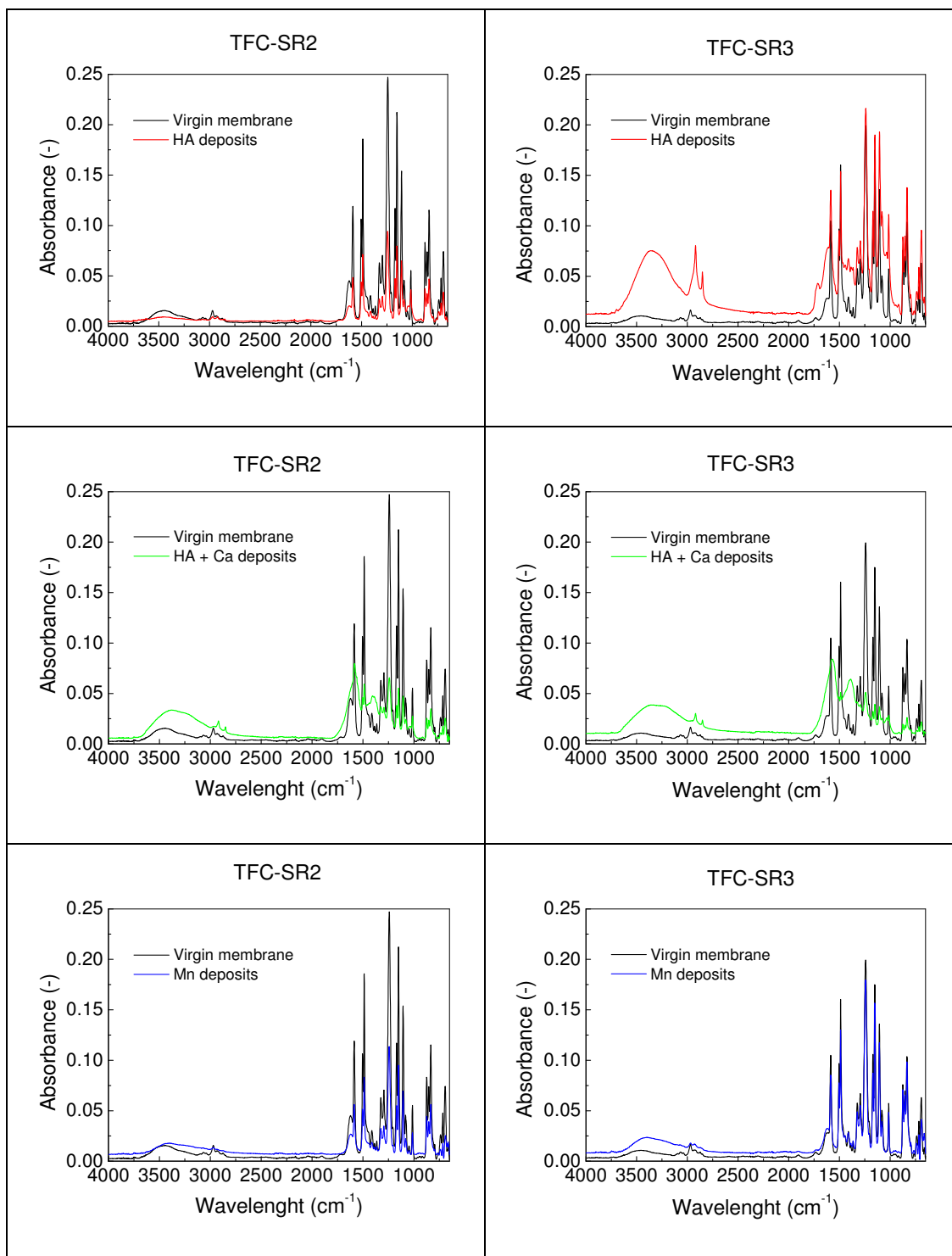
HA + Mn + Ca deposits

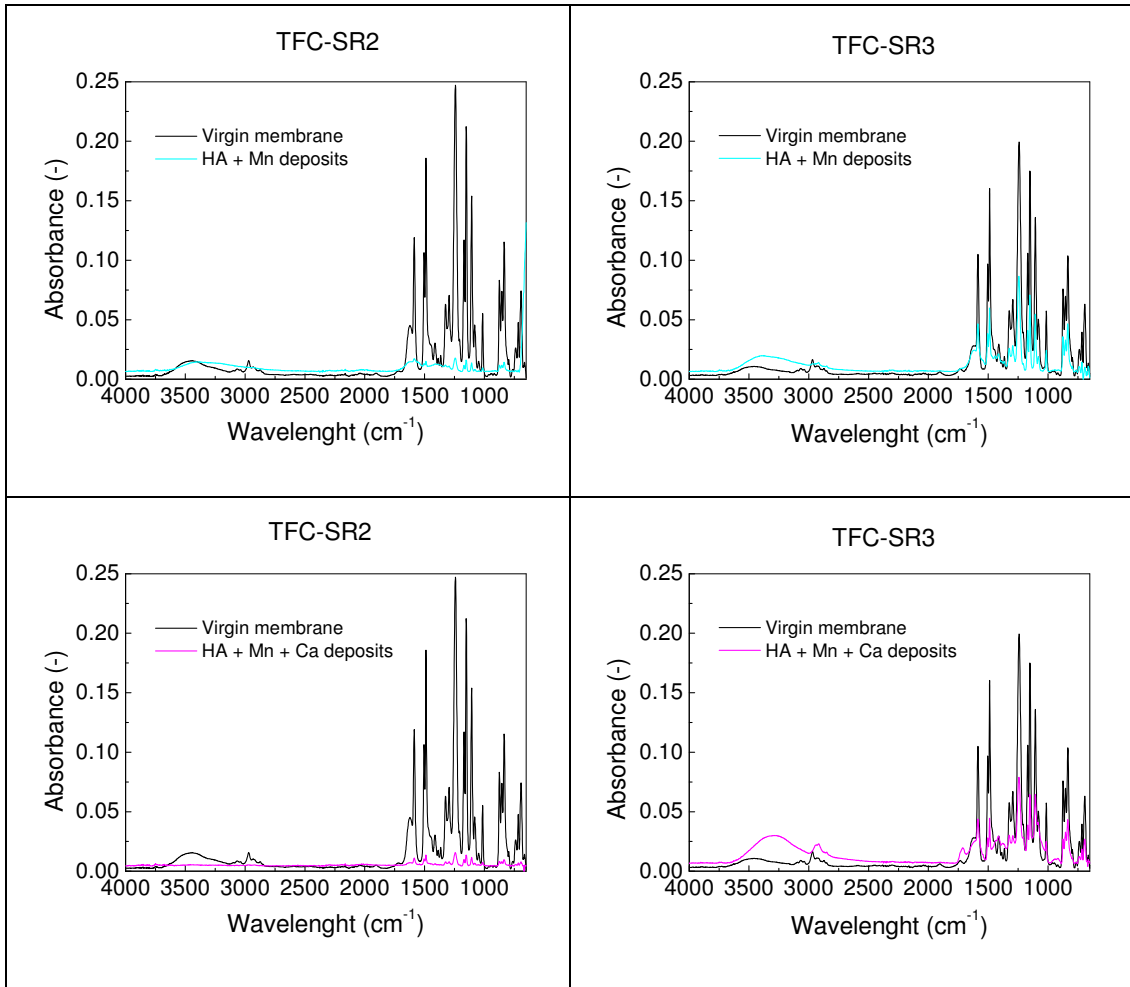


A.3.2 ATR-FTIR spectra

Spectra of virgin membranes were compared with the spectra of the membranes filtered with different solutes.

Table A.3-5 ATR-FTIR spectra of TFC-SR2 (left) and TFC-SR3 (right)





Appendix 4 – Solute removal using membranes powered by renewable energy

A.4.1 Introduction

Appendix 1 showed that in remote areas of Scotland membrane plants successfully produced drinking water delivered to small communities. This is the case even if high energy consumption per volume of produced water, which increases as plant size decreases, remains one of the main drawbacks. The availability of electricity in remote areas is usually limited as many small remote communities are located off-grid. In this content, membrane plants powered by renewable energy (RE) have a huge potential to produce safe drinking water.

To date, several photovoltaic (PV) and wind energy powered membrane systems have been developed, and several big scale desalination plants powered by RE are currently operated worldwide [1-17]. In fact, it has been reported that by 2003 PV panels were already employed to power 43% of the existing big scale RE-RO plants, while only 20% used wind energy [1].

Small scale RE-membrane systems have been developed primarily for research or demonstration purposes [1]. Small scale PV-RO plants have been reported to produce between 0.1 to 45 m³/day of drinking water with SEC between 0.8 kWh/m³ to 4.2 kWh/m³ for brackish water and 4 kWh/m³ and 22.8 kWh/m³ for seawater, depending on the feed water salinity and quantity of produced water [1-5, 18-20]. Less research has been carried out with small wind-RO systems. The capacity of the systems presented in the literature varies between 0.18- 9 m³/day and reported SEC varies between 3.5-10.3 kWh/m³ (only results for seawater available) [7-9, 21-23]. Research on RE-membrane systems employing membranes other than RO and treating water other than seawater and brackish water is scarce.

Small scale RE-membrane systems employ batteries or other energy storage devices to avoid energy fluctuation due to the variability of the RE sources. However, the use

of batteries is not ideal, especially in remote communities and at high temperatures. This is because batteries decrease the system efficiency and increase the system maintenance and operational costs, as they need replacement every 2 to 5 years. RE systems instead are usually designed for a 20 year life time. Additionally, batteries present a higher risk due to potential accidental spillages due to improper battery disposal [24, 25], and therefore associated environmental impact in a life cycle assessment. As a consequence, small scale battery-less membrane systems have been developed, in which RE is directly coupled with the pump used to pressurise water through the membranes [2, 3, 26-31]. Lack of energy storage results in variable operation of the membranes in terms of power, hence pressure and flow, which presents new challenges with regards to the operation of membranes in non-steady conditions. The use of wind energy without battery storage presents a bigger challenge than solar energy as wind energy is more intermittent due to turbulence and gusts over short periods of time (ranging from seconds to minutes) [32].

Membranes have been designed to operate at stable pressure and flux, so fluctuating operation has been inferred to cause mechanical fatigue to membranes, shorten membrane lifetime and increase fouling and scaling [1, 2, 7]. However, no membrane damages was observed after 7,000 hours of fluctuating operation of a battery-less wind-RO desalination system [31]. Moreover, fluctuating operation has been shown to disturb the polarisation layer and potentially reduce the effects of fouling and scaling [33-35].

Studies on small scale battery-less RE-membrane systems have mainly employed RO membranes for desalination of seawater and brackish water and they have mainly focused on proving the technical feasibility of the systems in terms of robustness and conductivity removal. Studies on the impact of energy fluctuation on system performance, in terms of pressure, flux, recovery, SEC and studies on the impact of fluctuations on the removal of specific solutes other than conductivity are scarce.

In this work, the performance of a battery-less hybrid UF-NF/RO membrane system powered by solar and wind energy producing around 1 m³/day of drinking water was

evaluated. This system has been previously tested with solar energy during a six week period in six different remote locations of central Australia [25, 36-39]. In Pine Hill, one of the locations selected for the field trials, the system was shown to tolerate large solar fluctuation (500-1,200 W/m²) and treat brackish water to Australian drinking water standards [25]. The impact of fluctuating energy on the retention of inorganic solutes was found to be solute specific. For solutes with large hydrated radius, retention by RO membranes was high (>99.5%) and independent from the change in solar power throughout the day. Retention of smaller inorganics was lower (>85%) and was impacted by solar irradiance [37]. The system has also been previously tested with simulated wind energy in the laboratory using synthetic brackish water and the influence of wind speed, wind turbulence intensity and period of oscillations on the system performance and conductivity removal were evaluated [32]. The system produced good quality permeate unaffected from fluctuations, but significant deterioration of performance was observed during pump switching on and off.

The objectives of this study were to:

- Analyse data collected in Australia during a field trial at Coober Pedy in order to establish the performance of the system for conductivity removal when powered by solar energy.
- Test the system in the laboratory with simulated solar and wind energy in order to evaluate the impact of fluctuating energy on the treatment of real Scottish surface water.

A.4.2 Materials and methods

The battery-less RE-membrane system employed in this work used a RE simulator, PV modules or a wind turbine to power a two-stage membrane process. The first stage consisted of submerged UF membranes, while the second stage consisted of a pressurised NF or RO membrane module (Figure A-4.1). A custom-designed progressive cavity pump (Mono-Pumps Australia, Permanent Magnet Brushless Direct Current Motor) drove the feed through the UF membranes at negative suction

pressure of about -0.5 bar, pressurising the UF permeate through the NF/RO module (maximum 12 bar).

During the Australian field trip at Coober Pedy, six Zenon ZW10 UF membranes connected in parallel and immersed in a 300 L stainless steel tank were employed. A RO membrane, FILMTEC™ BW30 (Dow Water Solutions) was selected for the second stage since it was shown to have a good performance for brackish water [25]. During the laboratory experiments, a cassette of Zenon ZW1000 UF membranes immersed in a 500 L stainless steel tank was used. For the second stage, TFC-SR2 NF membrane (Koch Membrane Systems) was selected to treat Scottish surface water since TFC-SR2 showed high organic matter removal (Chapter 6) and required less energy than the tighter TFC-SR3. Moreover, solute retention for the looser membrane was expected to be more influenced by fluctuating energy, since retention of solutes with smaller hydrated radius (with respect to membrane pore radius) were shown to be impacted by a change in power [37]. The TFC-SR2 module employed in this study had a pure water permeability of 14.4 L/m²hbar, comparable to the pure water permeability obtained from the membrane coupons used in the stirred cells experiments (Table 4-2).

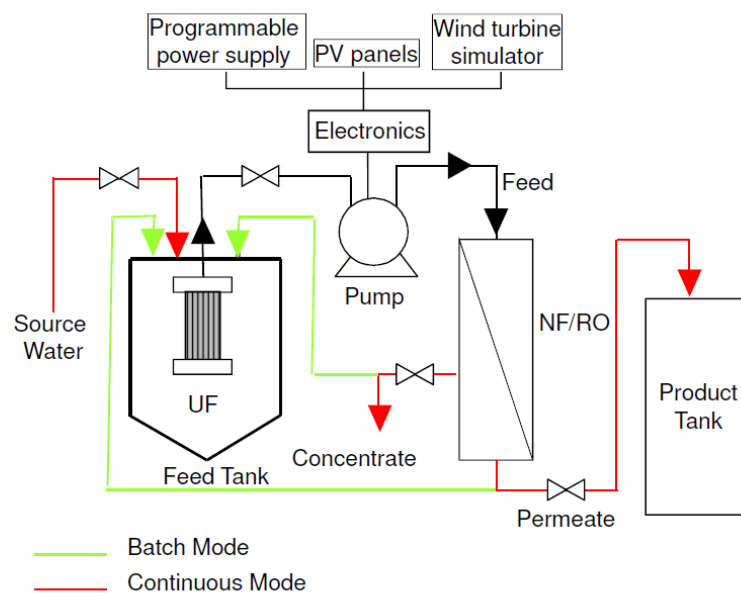


Figure A-4.1 Schematic of the RE-membrane system used in this study.

During the Australian field trial the system was powered by four 24 V_{DC} (nominal) PV modules (BP solar, BP3150S), rated at 150W peak (under laboratory conditions of 1000W/m²). The PV panels were mounted onto a single-axis solar tracker composed by a linear actuator (Mono-pumps Australia) that allowed the modules to follow the sun path from east to west during the day. During the laboratory experiments, the system was powered by a programmable power supply (Agilent Technologies, E4350B) which could simulate constant power inputs (range 0-300W) and solar power. Wind power was simulated in the laboratory using a wind turbine simulator constituted by a wind turbine generator (FuturEnergy) with the blades removed and a geared induction motor (Nord, SK51E-160M/4) controlled using a vector frequency inverter (Nord, SK700E-112-340-A) [40].

During the Australian field trial the power requirements were monitored manually from the electronic interface of the pump. The feed, permeate and concentrate flows were determined manually. Electrical conductivity and temperature for feed, permeate and concentrate were measured with conductivity probes and thermometers. Manual measurements and sampling of process streams were performed every 0.5-1 hour. Pressure was measured at 5s intervals with transducers located upstream and downstream of the pump and on the concentrate stream after the RO membranes. Solar irradiation was measured with a temperature-compensated sensor mounted in the same plane as the PV modules. Pressure and solar irradiation data were supplied to a data logger (DataTaker DT500) and downloaded to a laptop. During laboratory experiments, flow rate, pressure and temperature were taken in the feed, permeate and concentrate stream every second. Voltage and current output from the programmable power supply or the wind simulator were read at rate of 1 Hz. Flow, pressure, temperature, voltage and current were recorded using a data logger (DataTaker DT800) and downloaded to a PC. Feed, permeate and concentrate sample were collected at regular intervals and analysed for pH, TOC and inorganic compounds using the methods described in Section 4.3. The temperature of the feed water was maintained constant at 15 °C by constant circulation through a water chiller system.

Solute retention, membrane recovery and flux were calculated using the expressions provided in Sections 2.2.1 and 2.2.5. Transmembrane pressure (TMP) and SEC were determined as follows:

$$TMP = \frac{p_f + p_c}{2} - p_p \quad (\text{A.1})$$

where p_f , p_c and p_p are the measured pressure of the feed, concentrate and permeate, respectively ($p_p = 0$).

$$SEC = \frac{I_{pump} U_{pump}}{Q_p} \quad (\text{A.2})$$

where I_{pump} is the pump current, U_{pump} is the pump voltage and Q_p is the permeate flow.

A.4.3 Experimental

A.4.3.1 Australian field trial

Field trials were performed in October 2005 by students of the University of Wollongong in Coober Pedy, a very remote town of 3,500 inhabitants (plus about 1,000 tourists during winter) located in central Australia. The town receives a yearly average solar irradiation of 5.8 kWh/m²day (1990-2008), while in the month of October the average daily solar irradiation is 6.78 kWh/m²day (1990-2008) [41]. Drinking water at Coober Pedy is mainly obtained from a sand aquifer, characterized by relatively low salinity water, with conductivity of about 7 mScm⁻¹. Drinking water is treated by two RO plants, a main plant with capacity of 850 m³day⁻¹ that was commissioned in 1985 and a back-up plant built in 2001 of 600 m³day⁻¹ capacity. Both plants are equipped with the BW30 membrane modules used in the trials.

In order to estimate the performance of the PV-RO system for treating Coober Pedy brackish water, two pilot tests were performed using real solar energy:

- First pilot test performed on 26 October 2005 in batch mode, i.e. the permeate and concentrate were continuously recycled back to the feed tank (Figure A-4.1).

-
- Second pilot test performed on 27 October 2005 in a continuous mode, i.e. the feed tank was continuously filled directly from the bore and the permeate and concentrate were discarded (Figure A-4.1).

In both experiments, the feed tank was filled before sunrise and the back-pressure valve was manually set to provide a pressure of 7 bar at feed flow of 300 Lh⁻¹. The system was then left to run powered by solar energy without any further manipulation of the valves until sunset, when the system shut down automatically.

The batch mode experiment allowed testing the system with constant feed water characteristics, while the continuous mode test was aimed to reproduce a more realistic performance of the system over time.

A.4.3.2 Laboratory experiments

Laboratory experiments employed surface water collected from a site located 10 miles from Edinburgh. The raw water was collected from a water reservoir with a clean 1 m³ tank and brought to the laboratory. All experiments were performed within five days of water collection and the water in the tank was continuously stirred with a pump.

In order to evaluate the impact of fluctuating energy on solute removal four experiments were performed:

- Steady state experiments: experiments at constant power held for an hour at steps of 60, 120, 180, 240 and 360 W. Feed, permeate and concentrate samples were collected for each condition. These experiments constituted a baseline for comparison of the results obtained during fluctuating energy experiments.
- Solar energy experiments: solar energy power was simulated using irradiation data recorded at Loughborough (UK) on 09/01/11. Feed, permeate and concentrate samples were collected every half an hour.
- Simulated fluctuation experiments: oscillating power experiments in which the random fluctuations of wind were approximated by a sinusoidal wave and

average power and peak-to-peak amplitude were varied [32]. Average power, corresponding to wind speed, was varied at steps of 60, 120, 180 and 240 W and peak-to-peak amplitude, corresponding to wind turbulence intensity, was varied from 30 to 300 W (extreme turbulence). The period of oscillation was set at 60 seconds, as it was previously shown that system performance was less dependent from this parameter [40]. Each condition was kept for 20 minutes and feed, permeate and concentrate samples were collected for 120 seconds, hence representing the average of two complete oscillating cycles. These experiments allowed evaluating the impact of wind power on solute removal in a controlled manner by eliminating the complexity of real wind fluctuations.

- Wind energy experiments: wind energy power was simulated using wind data obtained from measurements taken near the town of Emden on the North Sea coastline of Germany [40]. A 2.5 hour segment of the wind speed data was chosen as it exhibited a wide range of wind speeds and turbulences. Feed, permeate and concentrate samples were collected every 15 minutes.

For all experiments the back-pressure valve was manually set to provide a pressure of 5 bar at feed flow of 500 Lh^{-1} and the system was then left to run powered by the programmable power supply or the wind turbine simulator.

A.4.4 Impact of real solar energy on conductivity removal

Table A-4.1 shows the daily average performance of the system during the tests performed at Coober Pedy. Both days had similar solar irradiation, resulting in similar average pump power output, which determines the suction pressure at the UF membrane, the RO feed pressure, i.e. the TMP and, in turn, the membrane flux. In both tests, the system showed high conductivity retention, producing from raw water with conductivity of 7.4 mS cm^{-1} and permeate with conductivity of 0.3 mScm^{-1} , below the Australian Drinking Water Guidelines of 0.78 mScm^{-1} [36]. For both batch and continuous tests, the system had a capacity of 764 L per solar day and average SEC of 3.2 kWhm^{-3} , comparable with the results obtained in the literature (Section A.4-1).

Table A.4-1 Daily average results for pilot tests at Coober Pedy

Date	Experiment Mode	Solar irradiation (kWh.m⁻².d⁻¹)	Power (W)	TMP (bar)
26/10/05	batch	10.2	209	10.2
27/10/05	continuous	10.3	210	10.4
Flux (L.m⁻².h⁻¹)	Recovery (%)	Conductivity retention (%)	SEC (kWh.m⁻³)	Total permeate volume (L.d⁻¹)
9.1	17.5	96.3	3.2	764
9.1	17.5	95.9	3.2	764

Figures A-4.2 and A-4.3 show the variation of the system performance when operating with variable energy where: (a) is power; (b) feed flow; (c) TMP; (d) UF (suction) pressure; (e) flux; (f) conductivity of feed, permeate and concentrate; (g) recovery and salt retention; and (h) SEC; while all graphs are overlaid with the solar irradiance.

During clear days, as was the case during those experiments, the fluctuations of irradiance are minimum and the amount of energy received by solar panels is maximum [42]. Solar radiation was at its maximum from about 9 am to 3 pm and increased and decreased sharply before 9 am and after 3 pm, respectively. The system started and ended operation when the available power dropped below the minimum requirement. The system operated for almost 12 hours in this location and month with the maximum power of 254W during the midday plateau.

The feed flow had low variations through the day for both experiments, while the flux followed the evolution of TMP. The feed conductivity was generally constant during the day and the permeate conductivity was higher at the beginning and at the end of the day when less solar radiation and hence power were available to produce flow and pressure. Recovery and retention had low variations throughout the day. The “scattered” points in Figures A-4.2 and A-4.3 represent about 0.3% of all data points in the curve and are thought to be due to sensor problems during the tests.

For the brackish water tested, power variation during clear sky days due to direct use of PV panels without batteries did not affect the permeate conductivity, hence the water quality, and had minimal influence on the permeate production. The PV-membrane system was able to tolerate energy increase and decrease during the solar day. Batch and continuous tests presented similar results and trends, showing that the system performed satisfactorily under variations of feed water characteristics for the brackish water tested.

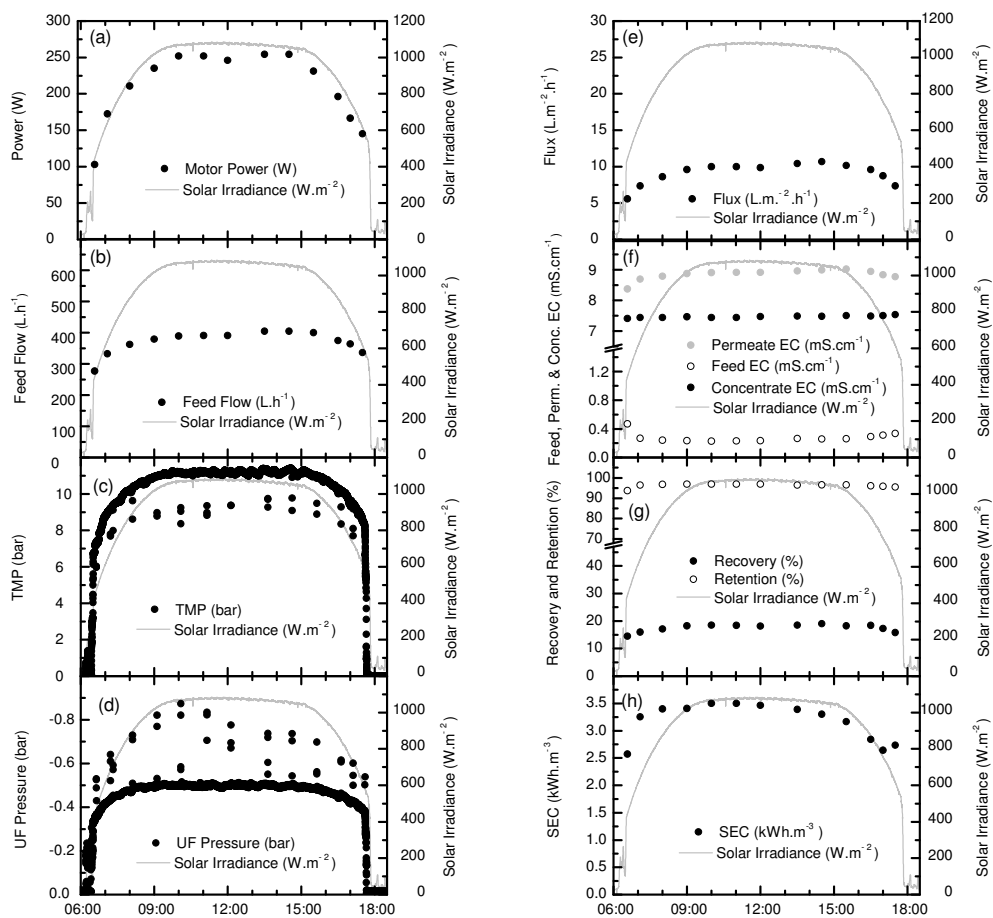


Figure A-4.2 Performance of the PV-RO system tested on 26 October 2005 at Coober Pedy – Batch mode. EC is Electric Conductivity

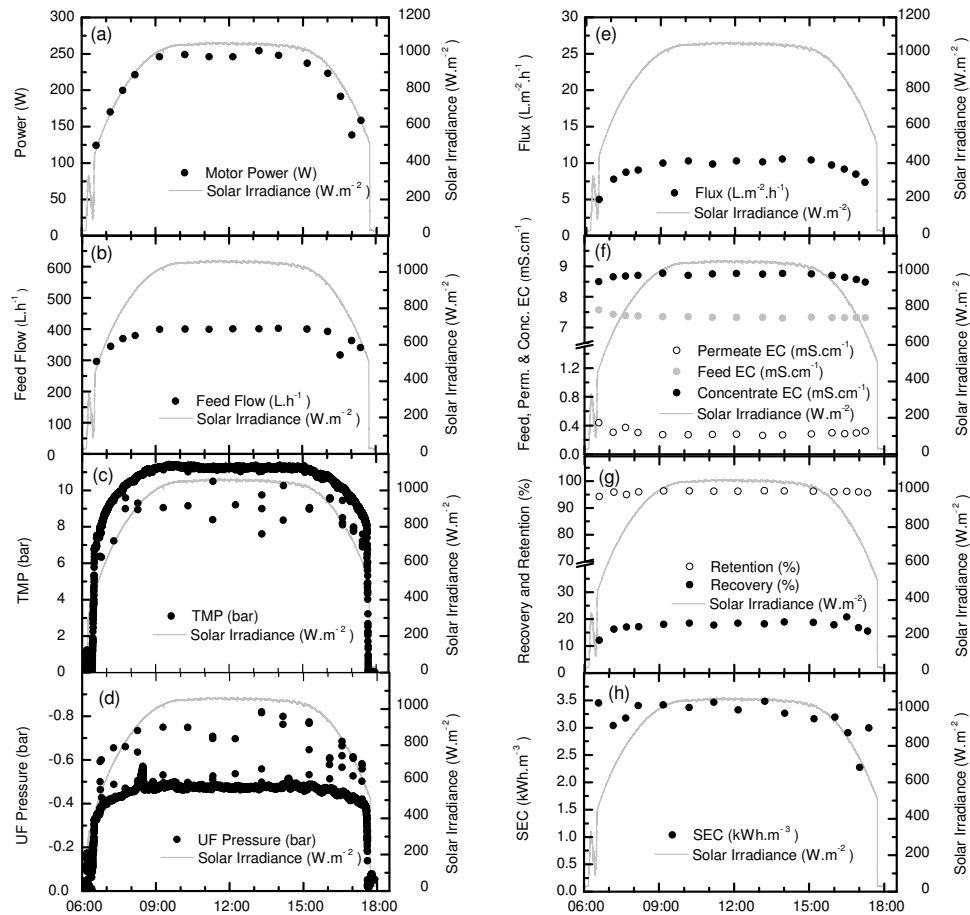


Figure A-4.3 Performance of the PV-RO system tested on 27 October 2005 at Coober Pedy – Continuous mode. EC is Electric Conductivity.

A.4.5 Impact of fluctuating energy on solute removal from real surface water

Table A-4.2 shows the characteristics of the surface water collected 10 miles outside Edinburgh and used in the laboratory experiments. The analysis of the raw water confirmed the soft nature of Scottish water, with low concentration of calcium and magnesium and in general low mineral content (Section 3.2). Apart from iron, all the inorganics were below WHO guidelines [43] and manganese, lead and zinc were below the detection limits. Raw water was very rich in organic matter with a very strong yellow colour.

The Zenon ZW1000 UF membranes, whose scope was to remove bigger particles and prevent fouling of the NF membrane, showed low removal (<60%) of metals and organics. UF permeate was in compliance with WHO guidelines, but the TOC content was still high, leaving the water with a yellow tinge that would not be acceptable to Scottish costumers.

Table A.4-2 Characteristic of Scottish surface water used in the experiments and removal by UF membranes

Parameter	MW (g/mol)	Hydrated radius [44] (nm)	Raw water (mg/L)	UF filtered water (mg/L)	UF Retention (%)	WHO guidelines (mg/L)
Iron	55.8	0.428	0.75	0.31	57.9	0.3
Aluminium	27	0.475	0.19	0.13	32.58	0.2
Calcium	40.1	0.412	11.49	10.73	6.61	100-300
Magnesium	24.3	0.428	1.91	1.85	3.24	100-300
Sodium	22.9	0.358	2.38	2.15	9.95	200
Potassium	39.1	0.331	0.38	0.36	5.42	-
Boron	10.8	NA	0.07	0.06	13.02	0.5
TOC	-	-	40.82	34.71	14.96	0.3

During steady state experiments, TMP, flux and recovery increased almost linearly with the power delivered to the pump (Figure A-4.4), due to the low salinity content of Scottish water. Osmotic pressure of brackish water was shown to level off at high power the curves of TMP, flux and recovery versus power [40], but this effect was highly attenuated with Scottish water. SEC was independent from power, with slightly higher energy consumption at low power, when the flux was also lower, and an average SEC of 1.7 kWh m⁻³ was obtained.

Retention of iron, aluminium and colour (UV) was independent from the pump power while retention of calcium, magnesium, sodium, potassium, boron and TOC increased with increasing pressure (Figure A-4.4c). Solute retention was due to a combination of size exclusion and charge as the order of retention followed the order of hydrated radius and MW and the strength of ion charge. Retention of ions with

higher hydrated radius and higher MW was not affected by change in power, while for smaller ions convection/diffusion dominated retention, confirming what observed in a previous study [37]. TOC retention was also dependent on power, potentially indicating high presence of smaller fractions of organic matter.

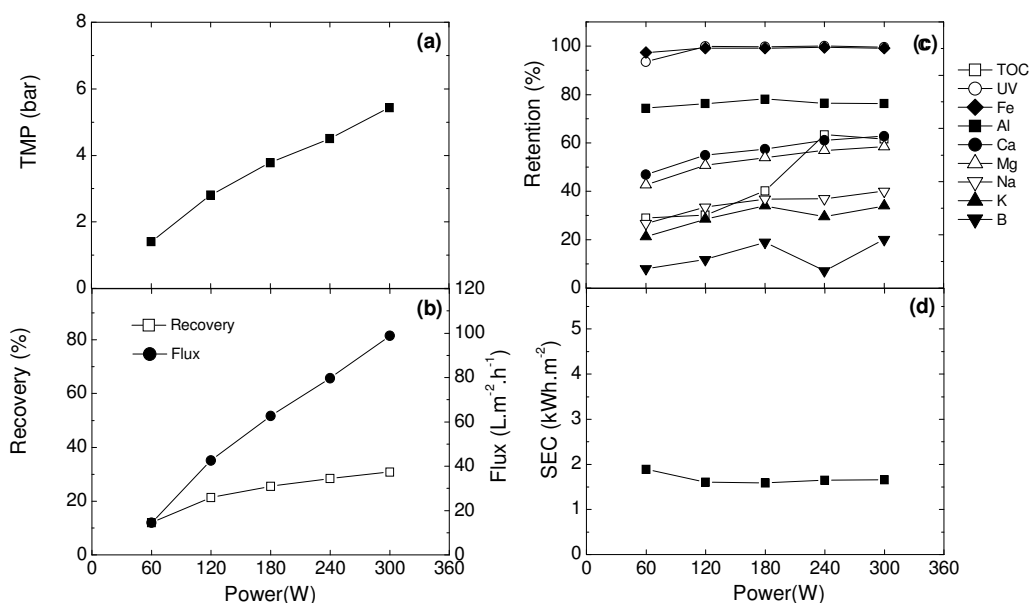


Figure A-4.4 Performance of the system in steady state conditions

Table A-4.3 shows the daily average performance of the system during the tests performed with simulated solar energy. The solar irradiation was lower than in Australia (Table A-4.1), hence the average power delivered to the pump was lower. TFC-SR2, whose MWCO and pore radius are 460 gmol⁻¹ and 0.52 nm respectively, is a looser membrane than BW30, whose MWCO is 88 gmol⁻¹ and pore radius is 0.32 nm [45]. The osmotic pressure of the low salinity Scottish water is considerably lower than the osmotic pressure of the Australian brackish water. As a consequence, the required TMP was lower and the flux and recovery were higher. Under the solar irradiance of the month January in the UK, the system operated for 6 hours, it had maximum power of 290W and produced 668 L per solar day.

The system had average SEC of 0.9 kWhm⁻³, considerably lower than the average SEC obtained during steady-state experiments. Lower SEC was attributed to an increase in permeate flux during solar experiments (average of 65.8 Lm⁻².h⁻¹ for an

average power of 141 W, against 42 Lm⁻²h⁻¹ obtained when the steady state power was 120 W). The increase in permeate flux was also confirmed during experiments with simulated wind energy (Table A-4.3), corroborating the hypothesis that fluctuating energy might reduce the effects of fouling by increasing membrane flux [33-35].

Table A.4-3 Average results for laboratory tests with Scottish surface water

Experiment Mode	Solar irradiation (kWh.m⁻².d⁻¹)	Power (W)	TMP (bar)
solar	0.92	141	3.6
wind	-	121	3.2
Flux (L.m⁻².h⁻¹)	Recovery (%)	SEC (kWh.m⁻³)	Total permeate volume (L.d⁻¹)
65.8	25.9	0.9	668
56.2	25.3	0.4	-

Pump power, TMP, flux and recovery followed the evolution of the solar irradiance, while SEC was constant throughout the solar day (Figure A-4.5), confirming trends obtained in Coober Pedy (Figures A-4.2 and A-4.3). Retention of UV, iron and aluminium was constant during the day, while retention of the other metals and TOC was more variable, with boron having the highest variability and lowest retention. The results confirmed what observed during steady-state experiments. Table A.4-4 shows that the average retention obtained during the solar experiment is comparable with the average retention obtained during steady state experiments. The system achieved 44% retention of TOC and 99% of UV (colour) retention, confirming that TFC-SR2 is an excellent membrane for treating Scottish water.

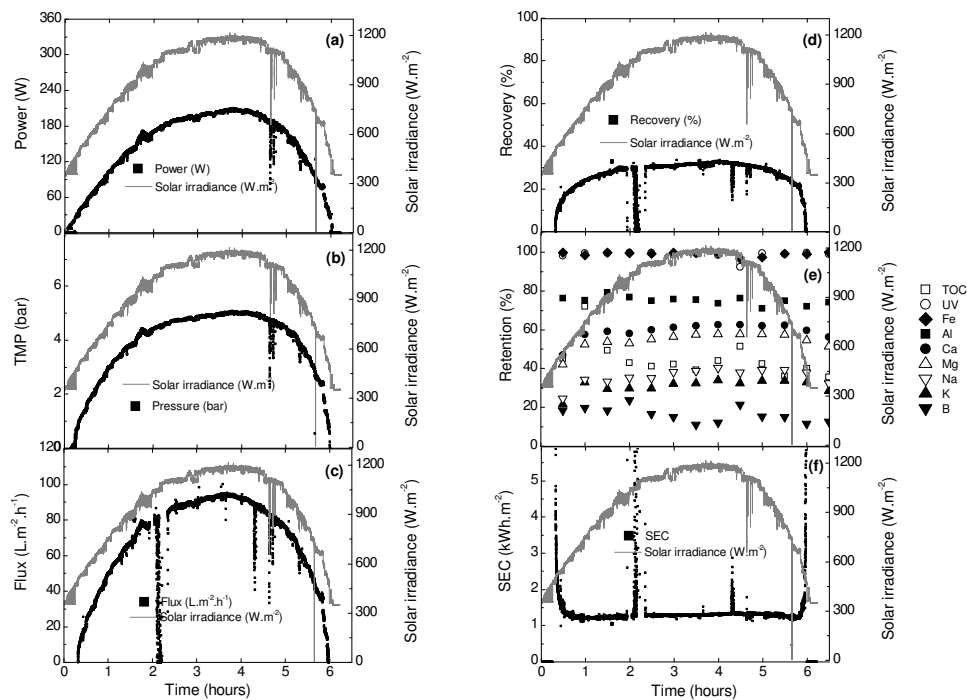


Figure A-4.5 Performance of the system with simulated solar power

Table A.4-4 Average solute retention obtained during laboratory tests with Scottish surface water

Parameter	Retention (%)						
	Steady state	Solar	Wind	Fluctuations			
				60W	120W	180W	240W
Iron	98.9	99.1	98.2	98.3	99.4	99.5	99.4
Aluminium	76.3	75.2	69.1	76.4	77.2	77.4	77.1
Calcium	56.6	59.3	66.1	59.5	60.4	62.9	64.7
Magnesium	52.5	54.5	61.7	55.3	55.8	58.4	60.4
Sodium	34.8	36.1	41.1	31.9	35.7	38.6	41.6
Potassium	29.5	31.1	31.0	30.2	37.1	34.2	37.8
Boron	13.2	15.8	21.3	3.7	0	5.7	15.5
TOC	44.9	44.3	28.1	45.8	43.8	46.2	47.2
UV	98.6	98.7	92.1	98.7	99.3	99.6	98.8

Experiments with oscillating power were conducted to investigate in a controlled manner the impact of wind fluctuations on the system performance. Figures A.4-6

and A.4-7 present the results obtained when average power of 60 and 120 W was employed, corresponding to average wind speed of 3.7 and 5.3 m/s [32]. Experiments with average power of 180 W and 240 W (wind speed of 7.0 and 8.7 m/s [32]) were also performed but they resulted in similar trend and results have not been presented. The effects of different peak-to-peak amplitudes (wind fluctuations) on the system performance are also illustrated.

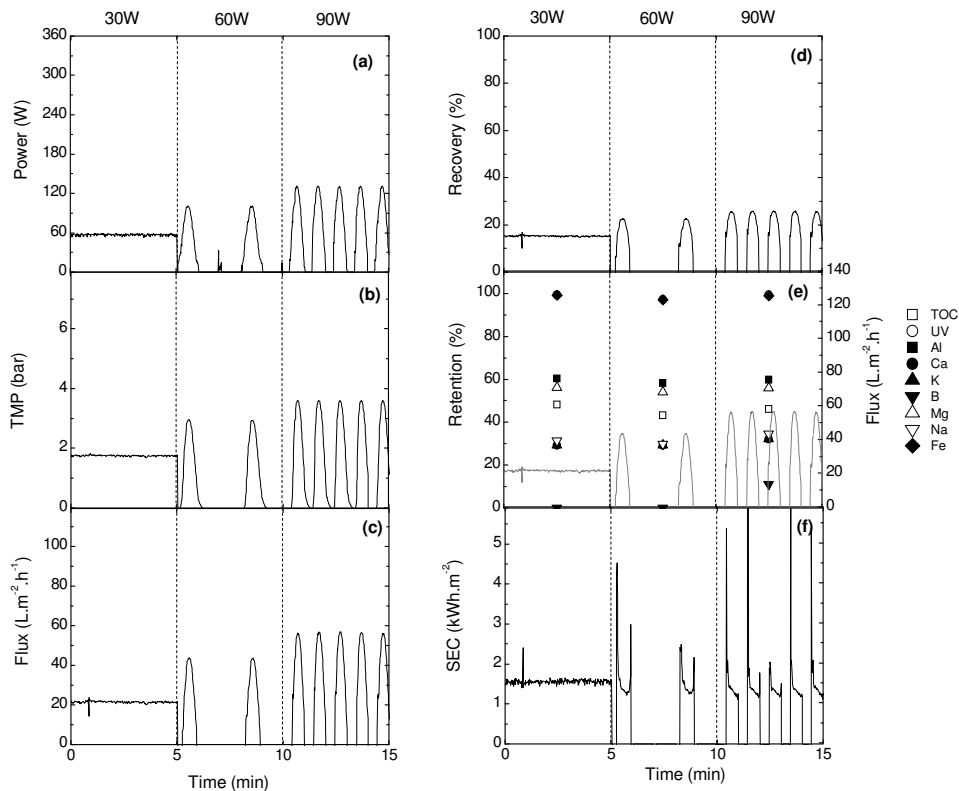


Figure A-4.6 Performance of the system with fluctuating energy- Average power 60W

Oscillating power resulted in oscillating TMP, flux and recovery. When the average power was low (60 W) the system switched on and off for longer periods (Figure A-4.6), but this did not cause deterioration of the average solute retention, in contrast with what observed for conductivity retention [32]. In all studied cases, average solute retention compared well with the retention obtained during steady-state experiments (Table A.4-4). For sodium, potassium and boron retention increased with increasing average power, confirming that ions with smaller hydrated radius and

MW are more influenced by oscillating power. SEC exhibited large spikes when the system was switched on, due to the higher power necessary to achieve the required flux after the system was switched off [40]. Higher average SEC was obtained at 60 W when the system was off for longer periods.

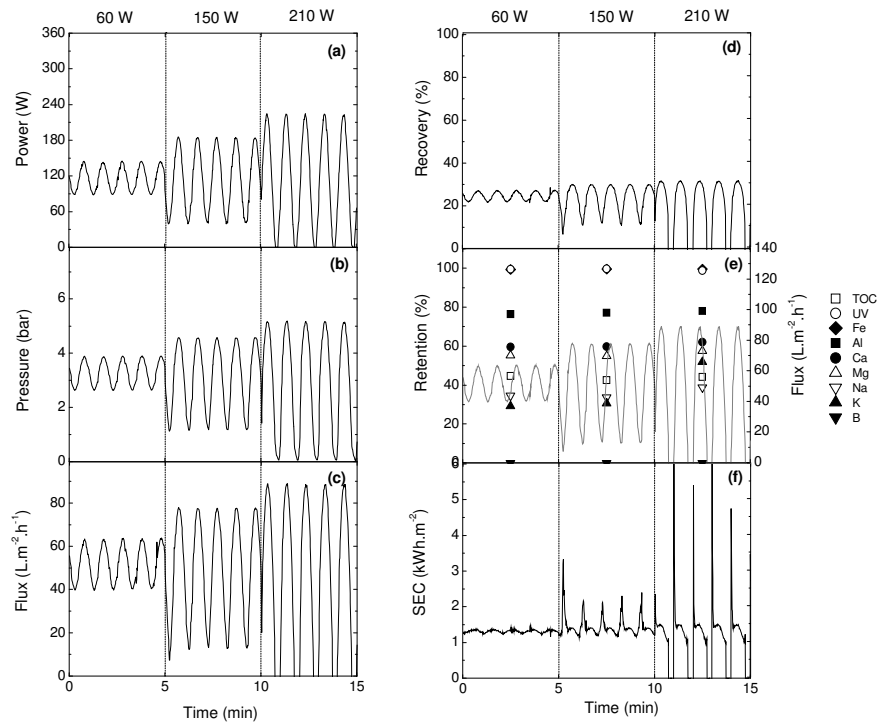


Figure A-4.7 Performance of the system with fluctuating energy- Average power 60W

The experiment with simulated wind energy showed that TMP, flux and recovery did not always follow the pattern of the pump power (Figure A-4.8). Park *et al.* [32] observed that TMP exhibited a decay in order to adsorb the long term fluctuations of wind energy but not the short term ones, resulting in a different pattern from power. Retention of UV, iron, aluminium, calcium and magnesium was constant during the experiments, while retention of TOC, sodium, potassium and boron experienced more variability. These results confirmed what observed during steady-state and solar experiments. Average solute retention compared well with the average retention obtained during the other experiments (Table A.4-4), with the exception of TOC retention which experience deterioration. Since the wind experiments were carried out after 5 days from bringing the raw water from the lab, a change in type of organic

matter might have happened. However, more investigations for explaining this result are required.

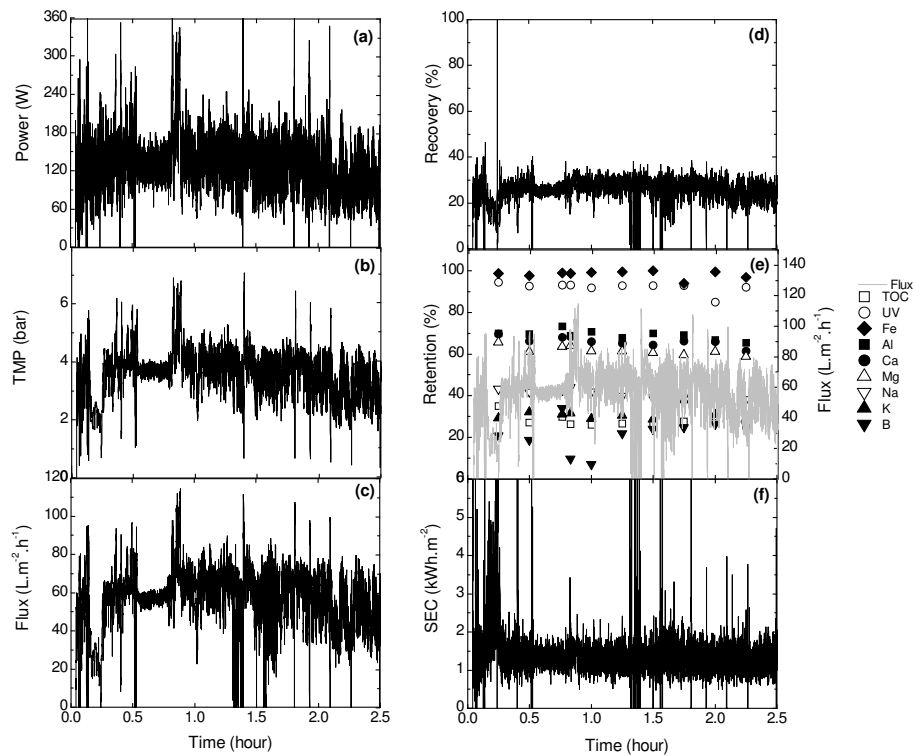


Figure A-4.8 Performance of the system with simulated wind energy

A.4.6 Conclusions

A small scale battery-less hybrid UF-NF/RO membrane system powered by solar and wind energy was tested in the field during trails in Coober Pedy, Australia, where it was powered by real solar energy to treat brackish water, and in the laboratory, where it was powered with simulated solar and wind energy to treat Scottish surface water.

During field tests at Coober Pedy RO membrane BW30 was employed to treat brackish water and remove conductivity to levels below the Australian Drinking Water Guidelines. The system was able to produce 764 L of permeate in a solar day with a SEC of 3.2 kWhm^{-3} . During clear sky days power variation due to direct use of PV panels without batteries did not affect the permeate conductivity, hence the water quality, and had minimal influence on the permeate production. Batch and

continuous tests presented similar results showing that for the treated water variations in feed water characteristics did not affect the system performance.

During experiments with simulated solar and wind energy, the system was able to treat real surface Scottish water to WHO standards, obtaining good removal of TOC and colour. Removal of solutes by fluctuating energy was due to a combination of size exclusion and charge, with larger ions mainly unaffected by fluctuations and smaller ions, whose retention was dominated by convection/diffusion, more influenced by change in power. Fluctuations did not affect the average retention of solutes with respect to the average retention obtained during steady-state experiments. Steady-state experiments can be used to establish the best and worst system performance that can be obtained during operation with RE.

Fluctuating energy increased membrane flux respect to the steady state experiments, potentially indicating that fluctuating energy might reduce the effects of fouling and scaling. Increase in flux resulted in decrease in SEC during operation with solar and wind energy. The system achieved a SEC of 0.9 kWhm^{-3} and 0.4 kWhm^{-3} when operating with solar and wind energy respectively. Further investigations are required to confirm these preliminary results, as these effects could increase the benefits of battery-less RE-membrane systems.

Longer experiments are also required to establish the resilience of the system and of the membranes to fluctuating energy and evaluating the impact of long term operation on the system performance and on the solute retention.

A.4.7 References

- [1] Tzen E, Morris R. Renewable energy sources for desalination. *Solar Energy* 2003; **75**: 375-379.
- [2] Forstmeier M, Feichter W, Mayer O. Photovoltaic powered water purification - challenges and opportunities. *Desalination* 2008; **221**: 23-28.
- [3] Mohamed ES, Papadakis G, Mathioulakis E, Belessiotis V. A direct coupled photovoltaic seawater reverse osmosis desalination system toward battery based systems -- a technical and economical experimental comparative study. *Desalination* 2008; **221**: 17-22.
- [4] Espino T, Peñate B, Piernavieja G, Herold D, Neskakis A. Optimised desalination of seawater by a PV powered reverse osmosis plant for a decentralised coastal water supply. *Desalination* 2003; **156**: 349-350.
- [5] Badreddin E, Gambier A, Aboul-Fotouh F. Laboratory set-up for education and research on automation of reverse osmosis plants employing a sustainable energy source. *Desalination* 2004; **166**: 307-314.
- [6] Koklas PA, Papathanassiou SA. Component sizing for an autonomous wind-driven desalination plant. *Renewable Energy* 2006; **31**: 2122-2139.
- [7] Henderson CR, Manwell JF, McGowan JG. A wind/diesel hybrid system with desalination for Star Island, NH: feasibility study results. *Desalination* 2009; **237**: 318-329.
- [8] Infield D. Performance analysis of a small wind powered reverse osmosis plant. *Solar Energy* 1997; **61**: 415-421.
- [9] Miranda MS, Infield D. A wind-powered seawater reverse-osmosis system without batteries. *Desalination* 2003; **153**: 9-16.
- [10] Witte T, Siegfriedsen S, El-Allawy M. WindDeSalter® Technology Direct use of wind energy for seawater desalination by vapour compression or reverse osmosis. *Desalination* 2003; **156**: 275-279.
- [11] Mohamed ES, Papadakis G. Design, simulation and economic analysis of a stand-alone reverse osmosis desalination unit powered by wind turbines and photovoltaics. *Desalination* 2004; **164**: 87-97.

-
- [12] Carta J, González J, Subiela V. The SDAWES project: an ambitious R&D prototype for wind-powered desalination. *Desalination* 2004; **161**: 33-48.
- [13] Subiela VJ, Carta JA, González J. The SDAWES project: lessons learnt from an innovative project. *Desalination* 2004; **168**: 39-47.
- [14] Carta JA, González J, Subiela V. Operational analysis of an innovative wind powered reverse osmosis system installed in the Canary Islands. *Solar Energy* 2003; **75**: 153-168.
- [15] Moreno F, Pinilla A. Preliminary experimental study of a small reverse osmosis wind-powered desalination plant. *Desalination* 2005; **171**: 257-265.
- [16] Tzen E, Theofiloyianakos D, Sigalas M, Karamanis K. Design and development of a hybrid autonomous system for seawater desalination. *Desalination* 2004; **166**: 267-274.
- [17] Tzen E, Theofiloyianakos D, Kologios Z. Autonomous reverse osmosis units driven by RE sources experiences and lessons learned. *Desalination* 2008; **221**: 29-36.
- [18] Gocht W, Sommerfeld A, Rautenbach R, Melin T, Eilers L, Neskakis A, Herold D, Horstmann V, Kabariti M, Muhaidat A. Decentralized desalination of brackish water by a directly coupled reverse-osmosis-photovoltaic-system - a pilot plant study in Jordan. *Renewable Energy* 1998; **14**: 287-292.
- [19] Ahmad GE, Schmid J. Feasibility study of brackish water desalination in the Egyptian deserts and rural regions using PV systems. *Energy Conversion and Management* 2002; **43**: 2641-2649.
- [20] Laborde HM, Franca KB, Neff H, Lima AMN. Optimization strategy for a small-scale reverse osmosis water desalination system based on solar energy. *Desalination* 2001; **133**: 1-12.
- [21] Petersen G, Fries S, Mohn J, Muller A. Wind and solar powered reverse osmosis desalination units - design, start up, operating experience. *Desalination* 1981; **39**: 125-135.
- [22] McBride R, Morris R, Hanbury W. Wind power a reliable source for desalination. *Desalination* 1987; **67**: 559-564.
- [23] Robinson R, Ho G, Mathew K. Development of a reliable low-cost reverse osmosis desalination unit for remote communities. *Desalination* 1992; **86**: 9-26.

-
- [24] Schäfer AI, Richards BS. Testing of a hybrid membrane system for groundwater desalination in an Australian national park. *Desalination* 2005; **183**: 55-62.
- [25] Richards BS, Capão DPS, Schäfer AI. Renewable energy powered membrane technology. 2 The effect of energy fluctuations on performance of a photovoltaic hybrid membrane system. *Environmental Science & Technology* 2008; **42**: 4563–4569.
- [26] Harrison DG, Ho GE, Mathew K. Desalination using renewable energy in Australia. *Renewable Energy* 1996; **8**: 509-513.
- [27] Joyce A, Loureiro D, Rodrigues C, Castro S. Small reverse osmosis units using PV systems for water purification in rural places. *Desalination* 2001; **137**: 39-44.
- [28] Thomson M, Infield D. A photovoltaic-powered seawater reverse-osmosis system without batteries. *Desalination* 2003; **153**: 1-8.
- [29] Thomson M, Infield D. Laboratory demonstration of a photovoltaic-powered seawater reverse-osmosis system without batteries. *Desalination* 2005; **183**: 105-111.
- [30] Thomson M, Miranda MS, Infield D. A small-scale seawater reverse-osmosis system with excellent energy efficiency over a wide operating range. *Desalination* 2003; **153**: 229-236.
- [31] de la Nuez Pestana I, Javier García Latorre F, Argudo Espinoza C, Gómez Gotor A. Optimization of RO desalination systems powered by renewable energies. Part I: Wind energy. *Desalination* 2004; **160**: 293-299.
- [32] Park GL, Schäfer AI, Richards BS. Renewable energy powered membrane technology: the effect of wind speed fluctuations on the performance of a wind-powered membrane system for brackish water desalination. *Journal of Membrane Science* 2011; **370**: 34-44.
- [33] Kennedy TJ, Merson RL, McCoy BJ. Improving permeate flux by pulsed reverse osmosis. *Chemical Engineering Science* 1973; **29**: 1927-1931.
- [34] Wang Y, Howell JA, Field RW, Wu D. Simulation of cross-flow filtration for baffled tubular channels and pulsatile flow. *Journal of Membrane Science* 1994; **95**: 243-258.

-
- [35] Howell JA, Arnot TC, Chua HC, Godino P, Hatziantoniou D. Controlled flux behaviour in membrane processes. *Macromolecular Symposia* 2002; **188**: 23-35.
- [36] Schäfer AI, Broeckmann A, Richards BS. Renewable energy powered membrane technology. 1 Development and characterization of a photovoltaic hybrid membrane system. *Environmental Science & Technology* 2007; **41**: 998-1003.
- [37] Richards LA, Richards BS, Schäfer AI. Renewable energy powered membrane technology. Salt and inorganic contaminant removal by nanofiltration/reverse osmosis. *Journal of Membrane Science* 2011; **369**: 188-195.
- [38] Rossiter HMA, Graham MC, Schäfer AI. Impact of speciation on behaviour of uranium in a solar powered membrane system for treatment of brackish groundwater. *Separation and Purification Technology* 2010; **71**: 89-96.
- [39] Richards LA, Richards BS, Rossiter HMA, Schäfer AI. Impact of speciation on fluoride, arsenic and magnesium retention by nanofiltration/reverse osmosis in remote Australian communities. *Desalination* 2009; **248**: 177-183.
- [40] Park GL. Wind-powered membrane desalination for brackish water, PhD Thesis, Heriot-Watt University. 2012.
- [41] Bureau of Meteorology. Climate Statistics for Australian Locations, http://www.bom.gov.au/climate/averages/tables/cw_016007_All.shtml (accessed March 2012).
- [42] Kawasaki N, Oozeki T, Otani K, Kurokawa K. An evaluation method of the fluctuation characteristics of photovoltaic systems by using frequency analysis. *Solar Energy Materials and Solar Cells* 2006; **90**: 3356-3363.
- [43] World Health Organization. *Guidelines for drinking-water quality*. Geneva, 2008.
- [44] Nightingale ER. Phenomenological theory of ion solvation. Effective radii of hydrated ions. *The Journal of Physical Chemistry* 1959; **63**: 1381-1387.
- [45] Semião AJC. Estrogenic micropollutant removal by nanofiltration, PhD Thesis, The University of Edinburgh. 2011.